DISSERTATION

ADVANCING THE UNDERSTANDING OF OSTEOSARCOMA METASTASIS: CHARACTERIZING THE IMPACT OF EXOSOMES ON LUNG FIBROBLASTS AND METASTATIC COLONIZATION

Submitted by

Eric Patrick Palmer

Department of Microbiology, Immunology, and Pathology

In partial fulfillment of the requirements

For the Degree of Doctor of Philosophy

Colorado State University

Fort Collins, Colorado

Summer 2025

Doctoral Committee:

Advisor: Daniel P. Regan

Doug Thamm
Brendan Podell
Elizabeth Redente

ABSTRACT

ADVANCING THE UNDERSTANDING OF OSTEOSARCOMA METASTASIS: CHARACTERIZING THE IMPACT OF EXOSOMES ON LUNG FIBROBLASTS AND METASTATIC COLONIZATION

Osteosarcoma (OS) is the most common malignant bone cancer, typically diagnosed in children and young adults. 30-40% of all OS patients develop tumor recurrence that occurs almost exclusively in the form of lung metastasis, which is associated with a dismal 20% 5-year survival rate. Recent evidence suggests organ specific metastasis, organotropism, may be driven by tumor secreted extracellular vesicles called exosomes. Exosomes have been shown to traffic to specific organs where they are taken up by target cells, releasing their biological cargos, and reprogramming those cells towards tumor-promoting phenotypes that alter the microenvironment in advance of circulating tumor cells, thus creating a pre-metastatic niche. Cancer-associated fibroblasts are a critical cell type within the lung TME, which promote immune suppression, drug resistance, and tumor cell survival. Prior work shows tumor cells can co-opt fibroblasts to a pro-tumorigenic phenotype via exosome mediated intercellular communication. Currently, the mechanisms by which OS exosomes modulate resident lung fibroblast function and promote enhanced metastatic colonization of the lung has not been evaluated.

To investigate this, we isolated exosomes from a panel of 6 OS cell lines. We assessed the uptake and response of human donor-derived primary lung fibroblasts (LF's; n=4) to OS exosome treatment *in vitro* via flow cytometry, confocal fluorescent microscopy, proliferation assays, phospho-kinase array, multiplex cytokine analysis and RNA-sequencing. We observed that LFs efficiently take up OS exosomes, which is associated with induction of MAPK pathway activation, fibroblast proliferation and significantly enhanced secretion of IL-6, CXCL8 and CCL2 compared to untreated LFs. RNA-seq of exosome treated LFs confirmed these responses and revealed significant enrichment of pathways related to cytokine secretion, proliferation, immune cell chemotaxis, migration, proinflammatory and profibrotic mediators. Finally, in an exosome-educated lung fibroblast-OS co-culture model, exosome educated LFs conferred significantly increased OS cell survival and proliferation as compared to untreated fibroblasts.

To evaluate the impact of OS-derived exosomes on metastatic colonization *in vivo*, we sought to develop a highly sensitive mouse model of OS metastasis for detection of OS cells by bioluminescent IVIS imaging and spectral flow cytometry. To overcome the lack of universally expressed and distinguishing cell surface markers on OS cells, we evaluated using fluorescent cell labeling dyes, Cell Trace Yellow and DIR. By using a mouse lung resident cell type antibody panel, we determined these dyes are not restricted to the tumor compartment and therefore are likely not useful for tracking OS cells *in vivo*. Next, using a lentiviral transduction system, we generated a 143b, OS cell line that expressed nuclear red fluorescent protein (RFP) and Luciferase. Here, we demonstrate the use of this reporter system allows for the rapid and highly sensitive detection of OS cells in the lung by bioluminescent imaging and spectral flow cytometry within 24-hours of tumor cell, tail vein injections.

Next, we evaluated the impact of repeated intravenous exosome educations on metastatic colonization of the lung using both human OS cell line, 143b in an immunocompromised xenograft mouse model and mouse OS cell line, K7M2, in an immunocompetent syngeneic mouse model. Bioluminescent intravital imaging 4 days post-tumor cell tail vain injections reveal exosomes derived from 143b OS cells but not K7M2 OS cells promoted enhanced metastatic lung colonization efficiency. Based on these observations, we sought to determine if changes in resident mouse lung cell populations and intracellular cell signaling were associated with increased metastatic lung colonization resulting from exosome treatments. By employing a 9-marker, anti-mouse panel, we show no significant changes to resident mouse lung CD45+ or stromal cell populations. Additionally, we observed no changes to lung concentrations of previously identified IL-6 and CCL2 upon exosome education. However, follow up studies would show tumor cell involvement may be required to stimulate significant changes to cell populations and cell signaling within this model. Finally, despite observations that OS exosomes can induce striking changes to lung fibroblasts in vitro and promote metastatic colonization in vivo, we did not observe any significant differences in overall survival among mice exposed to OS exosomes prior to tumor cell injection.

Taken together, we show OS-derived exosomes can induce lung fibroblasts to shift towards a tumor-promoting phenotype in vitro. Additionally, chronic exosome treatments promote metastatic colonization in an immunocompromised xenograft mouse model. However, these findings were not

correlated to alterations among resident lung cell populations, tumor-promoting intracellular signaling molecules, or overall survival.

ACKNOWLEDGEMENTS

All good things in life start with the love and support of the ones we hold close. First, I'd like to thank my advisor, Dr. Daniel Regan, for his willingness to take a chance on me before he even had a lab of his own. He brought me in and told me about some crazy, off the wall projects he wanted to pursue. This thesis is the culmination of one of those ideas. Dr. Regan is a kindred spirit. I will always admire and respect his intelligence, curiosity, work ethic, and his ability to remember figures from papers published 10 years ago. Thank you for giving me the freedom to find my way, for supporting and encouraging me when I was wondering in the dark at my lowest point, and for celebrating my achievements. I'm forever grateful.

I'd also like to thank my committee members, Drs. Doug Thamm, Brendan Podell, and Elizabeth Redente. You are among the smartest and kindest people I have ever met. Thank you for being such great role models, for offering your knowledge, providing guidance, and for being so quick to respond to my calendar invites. You are truly inspirational.

I offer many thanks to the other members of the FACC, for their invaluable leadership, mentorship, and willingness to hear me complain about whatever was bothering me at the time, even when they were busy. An extra shout out goes to Dr. Gustavson. Thank you for making sure I never take things too seriously, for all our random chit chats about every topic under the sun, but especially over our shared love of the great game of golf. I'd also like to that Guffy for not hiring me when I interviewed for a job in your lab all those years ago. My life would be much different if you had.

I'd especially like to thank the members of the Regan lab who have been there through thick and thin. We've been deep in the trenches together and it's been one of the great honors of my life to grow up with you all. Laurel Haines, for embarking on the exosome journey with me. You've been there from the beginning and you're a much better scientist than I could ever hope to be. I don't know where I'd be without your flow cytometry skills. Katie Cronise, always willing to talk about sports or politics, always there with an encouraging word after taking time to hear me complain, and the best bowler I know. Marika Klosowski, the smartest and most driven member of the group, had a miraculous way of seeing the silver lining and telling me, I'm doing fine. That will always mean a lot to me. Becca Makii, for being light-hearted and having that cool, climber vibe that always helps me through the day, and through the stats

class we took together. I'd also like to thank other lab mates that have come and gone. Aaron, Sofie, Alex, and Carina.

I'd like to acknowledge my family. My mother and father, Sharen and Don Palmer, for supporting me when I was a total troublemaker. Thank you for imparting the value of education on me, and for allowing me to take the risks that let me find myself and become the person I am today. To my sister, Kim. Thank you for exposing me to good music and to the alternative lifestyle and ways of thinking about the world that followed. To my sister, Shelly. Thank you for always being available to chat and for being supportive when things were tough. Thank you for dropping everything to come help take care of me when I had a climbing accident and for buying me a bed when mine was completely falling apart. I'm sorry I head bunted you when I was a baby. To Fran and Steve. You've both been so supportive and encouraging. You've been willing to go out of your way and go above and beyond, doing whatever was necessary to make sure Sarah and I were doing OK. For that, I'm eternally grateful.

Perhaps most deservingly, I'd like to thank my beautiful wife, Sarah. Sarah is without a doubt the kindest and most generous person I've ever met. I can only hope to attain a small part of her intelligence and drive. Without her encouragement, support, and patience with my antics and craziness, I can't imagine where I'd be. Her presence genuinely makes me a better person and for that, I thank you.

DEDICATION

For Sarah and Elouise

TABLE OF CONTENTS

CHAPTER 1

Review of the Literature

Osteosarcoma

Osteosarcoma (OS) is the most common malignant primary bone cancer. OS is typically diagnosed in children and young adults as the disease peaks in adolescence coinciding with the growth spurts associated with puberty. Although this is the most common form of bone cancer, the disease is still relatively rare, with incidence rates of 4.4 cases per million individuals. (Mirabello et al., 2009; Ottaviani & Jaffe, 2009) OS typically presents as a primary tumor located in the metaphysis of the long bones with most tumors arising at the distal femur near the knee joint, at the proximal tibia, or the proximal humerus. Evidence suggests the location of the primary tumor may be an important and distinguishing feature associated with survival outcomes. For instance, a retroactive study among 1,700 patients concluded the site of the primary tumor at diagnosis (axial vs. limb) along with the sex of the individual significantly influenced event-free and 10-year survival rates, as well as response to chemotherapy and extent of surgery. (Cole et al., 2022) For patients diagnosed with only localized disease, the 5-year survival rates using the current standard of care therapeutic approaches is ~65%. However, for the roughly 20% of patients that present with clinically detectable metastatic disease most frequently observed in the lung (>75% of cases), the 5-year survival average is dramatically reduced to less than 30%, a figure that has not improved in decades. This matter is made worse, as it is estimated that another 60% of patients likely have undetectable micrometastatic disease at the time of primary tumor diagnosis. (Bielack et al., 2002; Durfee et al., 2016)

OS can be divided into 7 distinct pathological subtypes differentiated based on histological analysis. These include fibroblastic, chondroblastic, epithelioid, giant-cell rich, small-cell rich, telangiectatic and the most common subtype, osteoblastic. Although over 60% of OS cases are classified as osteoblastic, identified through the presence of transformed osteoblastic cells that produce osteoid matrix, the identity of the cell of origin of OS is currently unknown. However, there is mounting evidence indicating mesenchymal stem/stromal cells (MSC's) or committed osteoblastic precursors can initiate OS

pathogenesis. (Gaebler et al., 2017; Mutsaers & Walkley, 2014) MSC's are osteoblastic progenitors present primarily in the bone marrow. MSC's can differentiate into osteoblasts, chondroblasts, myoblasts, and adipocytes when specific transcription factors are initiated. A complex series of proliferation and differentiation steps involving the transcription factors RUNX2 and Osterix initiate MSC differentiation into pre-osteoblasts or differentiation of pre-osteoblasts into functionally mature osteoblasts. (Nishimura et al., 2012) These transcription factors play and crucial role in bone development by responding to upstream signal transduction cascades activated by growth factors and cytokines heavily implicated in OS tumor development. The role BM-MSCs play in OS initiation was further supported by studies investigating BM-MSCs derived from 4 healthy donors. They show Rb knockdown and c-Myc overexpression promoted MSC differentiation into a phenotype characterized by increased proliferation and decreased cell senescence. These KO cells became capable of forming OS-like tumors in xenograft mouse models, suggesting the most common genetic aberrations identified across OS patients can promote OS-like traits in MSCs. (J. Y. Wang et al., 2017) Similarly, other studies demonstrate knockouts of the tumor suppressor genes, TP53 and Rb, in MSCs derived from bone marrow (BM-MSC) or adipose tissue (ASC) only induced osteogenic commitment in BM-MSCs and not ASC's, which gave rise to transplantable OS-like tumor generation. (Rubio et al., 2013) These results suggest the tissue source of MSCs is also important for promoting the phenotypes associated with OS development and further points to BM-MSCs as a possible progenitor cell type of OS.

Current Standard of Care and the Development of Novel Targeted Inhibitors

The current standard of care for patients presenting with OS was established in the early 1980's and involves a combination of surgical resection, radiotherapy, and a chemotherapy regime comprised of high-dose methotrexate, doxorubicin (Adriamycin) and cisplatin (platinol). The development of surgical interventions that replaced amputations employ the combination of advanced limb-salvage techniques with reconstruction options like allografts, autografts, rotationplasty, and megaprosthesis. Advancements in imaging, pre-operative planning, inoperative precision, and novel approaches to prosthesis design have steadily improved tumor resection margins and patient quality of life. The efficacy of novel surgical approaches like individualized resection blades, the use of robotics, and 3D printed implants is difficult to

ascertain, as the implementation of these methods is hindered by small sample sizes and the high cost associated with the use of these technologies. (Bläsius et al., 2022; Brookes et al., 2021) The most common radiotherapy method used to combat OS, called external beam radiation therapy (ERBT), delivers high-energy subatomic particles to the tumor, damaging the DNA and inducing cell death. The use of ERBT alone is not an effective treatment strategy for OS, however, when used in combination with surgery and chemotherapy has been shown to provide better local and systemic control of OS progression.(Chen et al., 2020; Spałek et al., 2021) The efficacy of radiotherapy as a treatment strategy for OS is limited to several factors. First, OS cells are inherently resistant to the effects of radiation compared to other cancer cell types. Although it is believed the reasons for the high degree of radioresistance may be due to efficient DNA damage repair mechanisms, or activation of specific molecular pathways involved in survival, the exact mechanisms are not completely understood. Other factors that limit the efficacy of radiotherapy are largely dose dependent. OS tumors can become large, often developing in sensitive and anatomically complex regions close to critical organs or vasculature, therefore, achieving high enough doses of radiation can become unfeasible. (Sole et al., 2016) Other factors such as intratumor heterogeneity, OS's high propensity for lung metastasis, the effect of radiation on the host anti-tumor immune responses, and delays in diagnosis and treatment also contribute to the usefulness of radiotherapy. New radiotherapy treatment methods like hypofractionation and stereotactic body radiotherapy (SBRT), that use higher doses of radiation per fraction over shorter periods, have shown promising results. Other methods under development include the use Carbon-ion radiotherapy (CIRT), and combining radiotherapy with novel chemotherapies, targeted agents, and compounds that sensitize cancer cells to radiation, called radiosensitizers. (Landau et al., 2023)

The standard of care chemotherapy regime, referred to as MAP, was introduced decades ago and demonstrated efficacy in improving survival outcomes for patients presenting with localized disease. These therapies are administered prior to (neoadjuvant) and/or after (adjuvant) surgical resection. The development of novel chemotherapeutic agents has been limited since the introduction of the MAP treatment regime, however, two other agents showing promising preclinical results, ifosfamide and etoposide, have gone through several clinical trials in various combinations with limited success. For instance, an open-label, international, randomized control trial, known as EURAMOS-1, compared the

addition of ifosfamide and etoposide to MAP (MAP-IE) to MAP used alone among newly diagnosed patients presenting with resectable, high-grade OS. These trials concluded that substituting a frontline chemotherapeutic agent in the MAP standard of care regime had little to no effect on event-free survival and the addition of ifosfamide or etoposide was associated with increased toxicity. (Ferrari et al., 2012; Marina et al., 2016) Other insights from a recent network meta-analysis of randomized controlled trials concluded the use of compounds like bleomycin and cyclophosphamide, have shown effects in prolonging progression free survival when combined with ifosfamide or vincristine. (X. Wang et al., 2017)

Due to the limited development of novel and effective chemotherapies, the efficacy of more targeted therapies using Multi-Kinase Inhibitors (MKIs) has been investigated for the treatment of OS. MKIs are molecules that exert anti-cancer activity by targeting kinases involved in signal transduction activation of key tumor-promoting pathways identified as being upregulated in cancers, including OS. The clinical efficacy of sorafenib, the first MKI shown to target several key components of the OS TME (RAF, KIT, RET, VEGFR1-3, PDGFR-B), was assessed in OS patients with inoperable, high-grade OS that were unresponsive to frontline, standard of care chemotherapies. Results of this study were promising, as sorafenib showed activity as a further-line treatment for patients with advanced or unresectable OS. However, several adverse events due to toxicity were reported leading to dose reductions or treatment interruptions that ultimately limited the effective usefulness of sorafenib, as it was determined the use of this MKI inhibitor did not improve 6-month progression-free survival of >50%. (Grignani et al., 2015) Another small molecule MKI, anlotinib, showed promising clinical results when treating other cancers like NSLCC and soft tissue sarcoma. In preclinical evaluation, anlotinib was shown to suppress tumor growth, inhibit migration and invasion, and increase the sensitivity of OS to chemotherapy *in vitro* and *in vivo*. A phospho-RTK antibody array of anlotinib treated OS cells confirmed suppression of vascular endothelial growth factor (VEGF) induced angiogenesis and phosphorylation of c-MET, a receptor tyrosine kinase involved in proliferation, migration and invasion that is frequently aberrantly activated in many solid tumors. (Peruzzi & Bottaro, 2006; Wang et al., 2019) Another small-molecule inhibitor of c-MET, cabozantinib, was shown to prolong progression free survival in castration-resistant prostate cancer and metastatic renal carcinoma. Studies demonstrated cabozantinib blocked proliferation of OS cells via autophagy associated mechanisms and significantly down regulated expression of osteoclast marker

genes characteristic of osteoclast differentiation and OS progression, including Receptor Activator of Nuclear Factor k B (RANK). (Fioramonti et al., 2017) Another small-molecule MKI shown to target angiogenic factors (VEGFR1-3, TIE-2), as well as the stromal compartment of the TME (PDGFR-B, FGFR), and the oncogenic kinases (KIT, RET, RAF), regorafenib, was shown to significantly extend progression-free survival in 2 clinical trials conducted on patients with recurrent, progressive, metastatic OS that failed to respond to conventional standard of care chemotherapy. (Davis et al., 2019; Duffaud et al., 2019) Efforts to identify MKIs that are therapeutically efficacious in the treatment of OS are ongoing and several clinical trials evaluating these molecules are currently underway.

Intrinsic Mediators of OS Pathogenesis and Progression

The identification and recognition common genetic alterations occur in tumor-suppressor genes among patients with cancer predisposition syndromes, such as Li-Fraumeni syndrome and hereditary retinoblastoma, led to the identification that somatic mutations of TP53 and RB1 also occurred frequently in OS. The approach of characterizing individual recurrently altered genes in OS as a means to identify prognostic biomarkers, determine drug sensitivity, or discover targetable mechanisms of pathogenesis led to tissue banking initiatives and large genetic and molecular profiling studies that have thus far, failed to identify a reproducible prognostic factor. (Strauss SJ, 2018) These results underpin the highly complex, heterogenous, and unstable nature of the OS genome that is characterized by somatic copy number alterations and rearrangements. For instance, the Cancer Genome Atlas (TCGA) and International Cancer Genome Consortium (ICGC) showed OS displays a relatively high number of somatic point mutations, and a high frequency of structural variants compared to other human cancer types. ("Pan-cancer analysis of whole genomes," 2020) Recently, a common oncogenic event described as chromosomal shattering results in numerous and simultaneous chromosomal rearrangements, called chromothripsis, and is recognized to further promote chromosomal instability that is commonly observed in OS. (Cortés-Ciriano et al., 2020) OS can also undergo whole-genome doubling (WGD) or alternative lengthening of telomeres (ATL), further permitting the survival and expansion of OS cells containing hyper mutated and highly unstable genomes. WGD has been shown to generate unstable tetraploid cells that accumulate numerical and structural chromosomal abnormalities so rapidly, they are able to buffer the

negative effects of deleterious mutations and chromosomal instability. (Quinton et al., 2021) A whole genome sequencing study analyzing DNA from 20 OS tumor samples matched to normal tissue identified a localized hypermutation pattern of single-nucleotide variations, known as kataegis, in 50% of OS tumors tested. This study identified lesions in the TP53 pathway among all tumors in the discovery cohort and recurrent somatic alterations to other common genes associated with OS including RB1, ATRX, and DLG2. (Chen et al., 2014) TP53 is a tumor suppressor gene encoding a protein with a highly diverse functional repertoire that includes responding to cellular stress through induction of senescence, apoptosis, DNA repair and cell cycle arrest. Somatic alterations to TP53, most typically missense substitutions, are frequently altered across many human cancers, and whole genome sequencing studies of OS have led investigators to suspect between 75-90% of OS has TP53 mutations. (Petitjean et al., 2007) The second most altered gene in OS behind TP53, Retinoblastoma transcriptional corepressor 1 (RB1), is a key regulator of cell cycle progression responsible for controlling the transition through G1/S phase. Mutations to this regulator and its subsequent pathways can cause dysfunctional cell cycle progression, allowing cells with DNA damage to avoid the typical cell cycle arrest response, ultimately allowing propagation of altered cell types, thereby promoting oncogenesis. (Schott et al., 2020)

Because mutational alterations to the tumor-suppressor genes frequently associated with OS pathogenesis result in a loss of protein function, successful development of therapeutic approaches addressing these individual mutations are unlikely to be successful. More recently, a shift towards characterizing and classifying the broader landscape of pathways and genomic signatures of OS has been used to identify novel and potentially targetable molecular profiles. One such study aimed to develop an Immune-related gene (IRG) signature among sample gene expression profiles from the Therapeutically Applicable Research to Generative Effective Treatments (TARGET) databases. Among the 604 differentially enriched IRGs identified, a 13 IRG signature was successfully constructed that correlated with OS patient overall survival and metastatic recurrence. (Wu et al., 2020) Using whole-genome and whole-exosome sequencing (WGS, WES) of 112 childhood and adult OS tumors, investigators discovered alterations in the insulin-like growth factor (IGF) signaling genes and components of their downstream signaling pathways in 27% of cases with specific alterations in IGF1, IGF1R, IGF2R and IGFBP5. An additional 87 OS tumors were confirmed to have IGF mutations using

fluorescence in situ hybridization in 14% of cases. (Behjati et al., 2017) A similar sequencing study that evaluated RNA-sequencing data from 59 OS tumor/normal tissue pairs only identified TP53 mutations as occurring at a significant frequency across samples. Using pathway analysis, heuristic analytical algorithms, a comparative oncology approach, and shRNA screen, the same study identified phosphatidylinositol 3-kinase/mammalian target of rapamycin (PI3K/mTOR) pathway as a possible therapeutic vulnerability in OS, later confirmed both *in vitro* and *in vivo*. (Perry et al., 2014) Borrowing an approach used to classify and organize Medulloblastoma into 4 distinct molecular variants (Northcott et al., 2011), copy-number amplification and changes in gene expression among patient-derived (PDX) tumor xenografts was categorized and separated into 6 distinct groups based on activation of key signaling pathways including cyclinE1/CDK2, Myc/CDK9, CDK4/CDk6/FOXM1, PTEN/PI3K/AKT1/mTOR, AURKb and VEGFA/R. Using a chemotherapeutic scheme designed specifically to target OS tumors belonging to each of the 6 classified categories led to improved responses for “genome-matched” therapies in their PDX xenograft mouse models. (Sayles et al., 2019) However, a follow up study conducted by the NCI Pediatric Preclinical Testing Consortium (PPTC) demonstrated there was a considerable amount of overlap with many OS PDX tumors belonging to multiple groups based on their respected pathway alterations, making it difficult to clearly classify those samples into any one category. A current, large-scale international prospective precision medicine study referred to as MAPPYACTS, set out to define tumor molecular profiles with recurrent metastatic disease that included a large sample set of 787 patients. Investigators discovered at least 1 genetic alteration that led to a targeted treatment suggestion in 436 patients (69%). 107 of 356 (30%) patients that had follow-up beyond 12 months received one or more matched targeted therapies with over half belonging to the AcSe-ESMART platform clinical trial. This targeted and personalized treatment strategy resulted in a 17% objective response rate. (Berlanga et al., 2022) Another study used whole exome sequencing of 31 tumors to decipher the OS mutational evolutionary landscape by inferring clonality of individual mutation events. Many of the 14 genes identified as pathogenic drivers were previously unknown in the context of OS. In 80% of OS tumors analyzed in this study, these 14 genes exhibited a specific combination of single-base substitutions, LOH, or large-scale genomic instability signatures that typically characterize BRCA1/2-deficient tumors, suggesting chromosomal instability results in a BRCA-like genomic instability signature

that may be targetable using poly-(ADP)-ribose polymerase (PARP) inhibitors. (Kovac et al., 2015) Indeed, OS cell lines identified as having disruptive gains in PTEN or losses of ATM, BARD1 or CHEK2 associated with homologous recombination (HR) repair deficiency indicative of “BRCAness” were sensitive to the PARP inhibitor, temozolomide (TMZ) alone and in combination with standard of care chemotherapies *in vitro*. (Engert et al., 2017) (Quinton et al., 2021) These recent approaches aiming to categorize OS patient samples based on a milieu of genomic and molecular alterations in the hopes of developing personalized and targeted therapies are promising. However, these methods largely overlook the inter and intra-tumoral heterogeneity of a given tumor, a critical component of OS that reduces the effectiveness of targeted therapies. This was highlighted by a study that used a de novo-induced murine OS model paired with an RGB-based single-cell tracking system. Although OS cells within the primary tumor were shown to present polyclonal dynamics initially, this phase of tumorigenesis was subsequently followed by clonal dominance associated with adaptations to the local microenvironment. However, this study also found that individual micro-metastases arising spontaneously were clonal, but interestingly, had a different cellular origin than the dominant clones in the primary tumors. (Gambera et al., 2018) This suggests OS pathogenesis and metastatic colonization can occur as cancer clones that potentially display differential therapy response profiles coexist simultaneously and propagate in parallel. This further underscores the genomic heterogeneity of OS observed between patients as well as intratumorally. Furthermore, it appears as though there exists a continuum from intra-tumoral heterogeneity to clonal dominance within phases of initial primary tumor progression and metastatic outgrowth. These results substantially complicate attempts to classify the intrinsic characteristics of OS aimed to stratify patients based on predicted therapy response or to identify novel therapeutic targets as these defining criteria are evolving and dynamic.

Extrinsic mediators of the OS tumor microenvironment

Osteosarcoma develops in a highly dynamic, specialized, and complex bone microenvironment composed of mineralized extracellular matrix (ECM), bone cells (osteoclasts, osteoblasts, osteocytes), stromal cells (MSCs, fibroblasts), vascular cells (endothelial cells and pericytes), and immune cells (macrophages, lymphocytes). Within the bone microenvironment, intense paracrine and cellular

communication networks are used to maintain tissue homeostasis under normal conditions. However, OS co-opts normal bone physiological pathways through crosstalk between OS and the complex web of matrix proteins and cellular components by inducing expression of environmental signals like cytokines, chemokines, soluble growth factors, and extracellular vesicles (EVs).

The extracellular tissue architecture and normal remodeling functions within the bone microenvironment during tissue homeostasis involve a balance between bone desorption and deposition facilitated by osteoclasts and osteoblasts, respectively. On one side of this coin, these events can become highly dysregulated as OS can stimulate focal bone deposition. For example, expression profiling studies characterizing bone regulator genes among 30 OS patients demonstrated tartrate-resistant acid phosphatase (ACP5), bone morphogenetic protein 7 (BMP7), collagen type XI, alpha 2 (COL11A2), and protein tyrosine phosphatases zeta 1 (PTPRZ1) genes significantly correlated with OS biology and clinical features, with COL11A2 mRNA levels correlating with worse overall and event free survival. (Toledo et al., 2010) *In vivo* studies seeking to recapitulate events in OS pathogenesis that lead to the hallmark radiographic feature of OS, periosteal sunburst spiculation, identified bone morphogenetic protein-4 (BMP-4), a protein produced by OS cells capable of inducing reactive ossification and ectopic bone formation from osteoblast activity. (Yoshikawa et al., 1994) The other side of the coin typically associated with normal tissue homeostasis involves bone resorption, which also becomes highly dysregulated in the OS TME. For instance, the aggressiveness of OS has been associated with para-tumor osteolysis and detection of osteolytic markers induced by the binding of Receptor Activator of Nuclear Factor kappa B Ligand (RANKL) to its receptor (RANK). In a cyclical, feedforward signaling mechanism that drives OS cell proliferation and bone degradation, osteocytes responsible for maintaining homeostasis embedded in the bone, were shown to produce RANKL in the OS TME, while bone resorbing osteoclast precursors expressed RANK on their cell surface. The upregulation and activation of this signaling axis then leads to increased osteoclast activity that induces the release of tumor-promoting factors like transforming growth factor-β (TGF-β) and insulin-like growth factor-1 (IGF-1) from the degrading bone matrix. (Avnet et al., 2008) (Lamora et al., 2016; Nakashima et al., 2011) The importance of osteolysis mediated by RANKL signaling in OS progression was highlighted by studies that sought to determine the prevalence of RNAKL and RANK expression among primary human OS patients using immunohistochemistry or flow cytometry

observed upregulation of the receptor/ ligand pair in 68% of samples assessed, although only 37% (29/79) samples exhibited >10% RNAKL positive OS tumor cells. (Branstetter et al., 2015) Furthermore, in a retrospective, immunohistochemical study using samples from 40 OS patients, RANKL expression was correlated to clinical characteristics related to a poor preoperative chemotherapy response and the 5-year event-free survival of patients with RANKL score >4 was 17.8 +/- 10% compared to RANKL scores 1-3 or 0 (50.0 +/- 15.8%, 56.0 +/- 13.7%, respectively). (Lee et al., 2011) Therefore, the RANK/RANKL signaling pathway was observed to be upregulated across a large percent of human OS primary tumor samples and is associated with worse patient outcomes. These results suggest the importance of this signaling axis in tissue remodeling dysregulation and OS progression. However, the low percent of OS cells within a given tumor identified as upregulating RANK signaling, indicate this may not be an ideal target for novel anti-tumor therapeutic development.

Other signal transduction pathways associated with OS progression within the primary TME include TGF-β, fibroblast growth factors (FGFs) and wingless and Int-1 (Wnt). FGF's can regulate normal skeletal development by inducing proliferation and maturation of pre-osteoblasts. (Ornitz & Marie, 2019) Targeting FGF receptors using the receptor tyrosine kinase inhibitor, AZD4547, was shown to decrease lung metastasis *in vivo*, indicating the potential role and therapeutic vulnerability for FGF receptors in OS progression. (Weekes et al., 2016)

The Wnt signaling pathway is highly regulated and involved in cellular processes such as proliferation, migration, polarization, and cellular differentiation. Mutations causing dysregulation of the Wnt signaling pathway are often associated with tumor development and chemoresistance across many cancers, including OS. Aberrant activation of Wnt/β-Catenin signaling in bone sarcomas requires an autocrine Wnt signaling loop that induces upregulation of specific Wnt ligands and receptors that further drive OS proliferation. (C. Chen et al., 2015) Wnt signaling promotes the invasive capacity of cancer cells though the regulation of transcription factors like Snail-1, Snail-2, Zeb-1, Zeb-2 or Twist. These factors increase the epithelial-mesenchymal transition (EMT), a step considered essential for OS cell invasion into adjacent tissues and vasculature. EMT functions by repressing key components of intercellular junctions, such as E-cadherin, while increasing mesenchymal markers like N-cadherin, vimentin, and fibronectin.(Lei et al., 2015; Sharili et al., 2011) In TP53 and Rb knockout BM-MSCs, it was shown that

tumoral bone formation and increased tumoral osteoid matrix resulting from stimulation with the osteoinductive factor, bone morphogenetic protein-2 (BMP-2), occurred in a Wnt signaling dependent manner, further highlighting the importance of Wnt signaling in OS development and progression. (Rubio et al., 2014) Although mounting evidence supports a key role for Wnt//β-Catenin signaling in OS tumorigenesis, other studies have reported conflicting observations showing inactivation of the Wnt/β-Catenin signaling pathway also played a key role in OS progression. Furthermore, OS patient samples often display frequent deletions among critical genes involved in the Wnt signaling pathway. (Cai et al., 2010; Cleton-Jansen et al., 2009; Du et al., 2014) Despite these potential contradictions, efforts to develop therapeutic interventions that disrupt Wnt signaling in OS using monoclonal antibodies, small molecule inhibitors, and targeted long, non-coding RNAs (lnc-RNAs) identified to promote OS stemness, are currently under investigation. For instance, preclinical models demonstrate the effective inhibition of OS metastatic phenotypes using a monoclonal antibody targeting the Wnt signaling inhibitor, dickkopf-1. (Chu et al., 2021) Similar preclinical results show the small molecule inhibitor, salinomycin, can inhibit OS stem cell proliferation by selectively downregulating the Wnt-B-catenin pathway, however, the development of this inhibitor has been hindered by difficulties in effective delivery to the tumor. (Irmak et al., 2020) Finally, efforts to develop methods to target the lncRNA, DLX6 (AS1), shown to promote stemness in OS cells via the micro RNA-129-5p are also being evaluated. (Zhang et al., 2018)

TGF-β signaling is one of the most important factors in the bone environment as it helps to retain homeostasis between bone resorption and formation by signaling to both osteoblasts and osteoclasts. (Janssens et al., 2005; Tang & Alliston, 2013) TGF-β also regulates components of the metastatic cascade, such as the epithelial-mesenchymal transition (EMT), tumor cell invasion, angiogenesis, and immunosuppression. (Juárez & Guise, 2011) To the cells of the mesenchymal osteoblastic lineage during OS progression, TGF-β plays a complicated role in bone remodeling as MSC's are stimulated to proliferate and migrate during the earliest stages of osteoblastogenesis but inhibits MSC differentiation into osteoblasts during the late stages of osteoblastogenesis. (Maeda et al., 2004) The importance of this signaling axis involvement in OS progression cannot be understated, and as such, efforts to develop therapeutic strategies that inhibit TGF-β signaling are ongoing. Small molecule inhibitors that target the upstream kinase, TβRI/ALK5, antisense oligonucleotides that have been shown to suppress the

transcription of TGF-β expression, and the use of soluble receptor decoys, called ligand traps, prevent TGF-β from binding to its cognate receptor, have recently been evaluated.(Ge & Huang, 2023; Wang et al., 2020) Additionally, therapeutic strategies combining TGF-β signaling inhibition with chemotherapies like rapamycin and doxorubicin, or immune checkpoint inhibitors have also been investigated. The development of inhibitors that disrupt TGF-β signaling within the OS TME has been met with mixed results due to the pleiotropic nature of this pathway, as its activation has been associated with both tumor promoting and tumor suppressing functions.

Immune Cells of the OS Tumor Microenvironment

The complex and highly dynamic network of immune cells, their activation states, and the soluble signaling molecules that mediate the extent of their function within the OS TME, is increasingly being recognized for its prognostic value and potential as a therapeutic target. For instance, a recent study sought to evaluate relationships between peripheral immune cells among 327 OS patients undergoing treatment for use as a prognostic indicator. In this study, the lymphocyte-to-monocyte ratio (LMR) was calculated from pre-operative blood cell counts and plotted against overall and event-free survival. Using a predictive model, results from this study demonstrate elevated alkaline phosphatase, metastasis at diagnosis, and therapy response were significantly associated with the LMR. Furthermore, a low LMR was associated with a significantly shorter overall and event-free survival, demonstrating the importance of deciphering the immune landscape in OS, and pointing to the role of monocyte recruitment in survival outcomes. (Liu et al., 2015) These observations are in alignment with studies that used IHC to determine the presence and quantity of CD45+ leukocytes among 56 primary bone sarcomas. Their results identified the CD45+ immune cell type that primarily composes the OS tumor microenvironment as being tumor-associated macrophages (TAMs), followed by dendritic, lymphoid and myeloid cells to a lesser extent. (Inagaki et al., 2016) Adding to this, pre-therapeutic biopsies of 124 patients with OS, researchers observed the percent of CD68/CD163 tumor-infiltrating macrophages (TAMs) and their respective polarization state described in the classical sense (M1/M2 defined by pSTAT1/CMAF staining, respectively), the number of CD8+ lymphocytes, osteoclasts, and the expression of PD1/PDL-1 immune

checkpoint receptor/ligand cognates, significantly correlated with clinical outcomes. Additionally, high CD163 levels as being determined by greater than 50% of cells (43.8% of patients) associated with CMAF nuclear expression significantly correlated with better overall survival and longer metastasis progression-free survival independent of metastatic status. (Bousquet et al., 2016) The importance of TAMs and their functional state within the OS TME was further highlighted by studies using tissue microarrays to characterize the TME by IHC, as well as genome-wide expression profiling among pre-therapy OS biopsies, which confirmed “M1” TAM infiltration was associated with reduced metastasis and improved survival in high-grade OS. (Buddingh et al., 2011; Dumars et al., 2016) It should be noted the classical and simplified interpretation of M1/M2 macrophage polarization has more recently been updated to describe these immune cells existing within a functional and phenotypic continuum. Regardless, these studies reveal the importance of TAM infiltration and polarization state within the OS TME cannot be understated, as they provide a potential immune cell-based prognostic indicator for clinical outcomes and rationale for the development of macrophage activating agents like mifamurtide (muramyl tripeptide). Indeed, studies aiming to evaluate the immunomodulatory effects of mifamurtide used in combination with ifosfamide have been promising, as *ex vivo* monocyte-mediated tumoricidal activity was elevated 24 and 72-hours post therapy administration. (Kleinerman et al., 1995) Compared to conventional treatment alone, Mifamurtide has also been shown to improve the probability of acquiring distant metastasis with patient groups having positive surgical margins (7 and 20 months, respectively) and was associated with a 1-year and 2-year survival rate of 71.7% and 45.9%, respectively. (Anderson et al., 2014; Taçyıldız et al., 2020) Currently, a phase II, multicenter, randomized clinical trial (SARCOME13) using mifamurtide in combination with standard post-operative care is currently underway (NCT03643133).

Due to a lack of tumor-neoantigens and minimal immune cytotoxic lymphocyte (CD8+) infiltrates, OS is typically characterized as being a an immunogenically “cold” solid tumor. (Casey & Cheung, 2020) Despite this, lymphocyte population dynamics have been evaluated within the OS TME and have been shown to play an important role in OS progression. For instance, whole-slide imaging and IHC validated by methylation of specific gene analysis revealed among OS biopsies that CD8+ T cell infiltration into the OS TME as well as the cytotoxic CD8+ to regulatory T Cell ratio (CD8+/FOXP3+) was significantly associated with lower rates of metastasis. (Fritzsching et al., 2015) Additionally, the ratio of cytotoxic

CD8+ cells to immunosuppressive FOXP3+ cells was also capable of acting as a prognostic indicator of overall survival. (Gomez-Brouchet et al., 2017) Another study examined the expression level of Programmed Death Ligand 1 (PD-L1) and found PD-L1 expression correlated with immune cell infiltration and event-free survival. (Koirala et al., 2016) PD-1, the cognate receptor for PD-L1, is expressed on the surface of activated CD8+ T lymphocytes and Natural Killer cells, and when bound decreases the effective cytotoxicity of CD8+ T lymphocytes and NK cells against many cancer types, including OS. Compounds that block the PD-1/PD-L1 interaction been shown to dramatically improve the function of OS-reactive CD8+ T lymphocytes *in vitro* and in *in vivo* mouse models of OS. (Lussier et al., 2015) Additionally, multiplex immunofluorescence panels comparing pretreatment and 8-week on-treatment responses to the anti-PD-1/PD-L1 monoclonal antibody, pembrolizumab, determined treatment responders had an increase in the density of activated T cells (CD8+, CD3+, PD-1+) and a decrease in PD-L1 expressing TAMS, which correlated with progression-free survival. (Keung et al., 2020) Due to the success of ICIs in other cancer types, 14 eligible studies comprising 868 patients, pooled hazard ratios that indicated a statistically significant association between PD-L1 expression and overall and event-free survival, suggesting a an important role for PD-L1 as a prognostic indicator. (Zhu et al., 2017) These results also provide rationale for the targeting of ICs in OS, however, trials investigating the clinical efficacy of 3 anti-PD-L1 monoclonal antibodies, avelumab (NCT03006848), pembrolizumab (NCT02301039), or nivolumab (NCT02304458) are currently no longer recruiting or have been suspended due to several factors, including lack of clinical efficacy.

Bone marrow-derived mesenchymal stem cells (BM-MSCs) are another critical cell type considered to be one of the most important factors that promote OS tumorigenesis and metastasis. BM-MSCs are capable of dramatic influence over the OS TME. acting as sensors that respond to stimuli by expressing cytokines, chemokines, and growth factors highly implicated in OS developmental biology. MSC's are non-hematopoietic precursors that can self-renew and differentiate into many different mesenchymal cell lineages like osteocytes, chondrocytes, and adipocytes. (Dominici et al., 2006) Once stimulated with the inflammatory cytokines, interleukin 1beta (IL1beta) and tumor necrosis factor alpha (TNF-a), MSCs that express a variety of tyrosine kinase receptors were shown to significantly increase migration toward the extracellular signaling molecules secreted by OS tumor cells, monocyte

chemoattractant protein 1 (MCP-1/CCL2), growth-related oncogene-alpha (GRO-a), and transforming growth factor B(TGF-B). (Ponte et al., 2007) Thus, BM-MSCs display a strong tropism toward OS cells and as discussed earlier, may be the progenitor cell type of OS. BM-MSCs in the OS TME can also respond to oxidative stress induced by OS cells undergoing metabolic reprogramming by producing lactate through upregulation of lactate monocarboxylate transporters. (Bonuccelli et al., 2014) As increasing lactate concentrations acidify the OS TME, MSCs respond by secreting mitogenic, and chemotactic factors associated with NF-kB pathway activation, which function in a feedback loop promoting the invasion and migration of OS into adjacent tissues. (Avnet et al., 2017) As an example, under normal conditions the loss of cell adhesion molecules induces a form of apoptotic cell death called anoikis. The acidic OS TME has been shown to stimulate IL-8 secretion by MSCs, causing anoikis resistance associated with the promotion of OS pulmonary metastasis via the IL-8/CXCR1/AKT pathway. (Du et al., 2018) It is now well recognized that expression of genes induced under hypoxic conditions, most notably hypoxia-inducible factor (HIF), promote OS metastasis and overexpression of HIF is associated with therapy resistance, poor survival and a malignant phenotype. Recently, the SUMO-specific protease 1 (SENP1) was shown to be highly upregulated in OS cells and through a feedback loop, stimulated HIF-1a expression associated with upregulation of EMT genes, suggesting a role for this feedback loop in promoting OS invasiveness. (Wang et al., 2018) To further demonstrate the importance of the OS cell/MSC interaction in the primary TME, it was shown co-culturing MSCs with OS cells *in vitro* stimulated the migratory capacity and increased proliferation of OS cells via TGF-B and IL-6 secretion, effects impaired by the introduction of an anti-IL-6 neutralizing antibody. (Cortini et al., 2016) Additionally, co-injection of human MSCs and the OS cell line, F5M2, in nude mice significantly increased the number of tumor nodules per lung compared to control groups at 6 weeks post injection, highlighting the importance of OS tumor cell/MSC interactions across several aspects of OS tumorigenesis. (Zhang et al., 2013)

The crosstalk between OS cells and BM-MSCs in the primary TME also promotes MSC trans-differentiation into cancer-associated fibroblasts (CAFs). As OS cells secrete MCP-1 (CCL2), TGF-B, and GRO-a into the OS TME, MCS are recruited into contact with OS cells facilitating their trans-differentiation. CAFs alter the composition of the TME's extracellular matrix, and secrete a large variety of

mitogenic growth factors, cytokines, chemokines and metalloproteinases. Importantly, CAFs within the OS TME significantly increase levels of the signaling molecules, MCP-1, GRO-a, IL-6, and IL-8, further promoting the mesenchymal to amoeboid transition (MAT) in OS cells, thereby increasing their invasiveness and metastatic potential. (Pietrovito et al., 2018)

Osteosarcoma exosomes and the pre-metastatic niche

Many cancer types exhibit a high predilection for organ specific metastasis referred to as "organotropism," and the high incidence of recurrent metastasis of OS to the lung is particularly exceptional. Metastasis is the leading cause of cancer-related deaths and requires a complex series of events culminating in dissemination of cancer cells from the primary site of tumorigenesis to distal organs capable of supporting circulating tumor cells in an otherwise hostile environment. (Massagué & Obenauf, 2016) In 1889, Dr. Stephen Paget proposed the "seed and soil" hypothesis to account for his observations of organotropism, which proposed metastatic tumor cells (seeds) require a suitable and hospitable environment (soil) for metastatic dissemination and colonization. (Paget, 1989) Dr. Paget's hypothesis was revisited over 100 years later, and a growing and substantial body of evidence now supports several key aspects of the theory. (Fidler & Poste, 2008) A great body of work emphasized investigating the role of tumor intrinsic properties in driving organ specific metastasis, however, these approaches failed to account for the impact of molecular events in distant tissues occurring in advance of metastatic colonization. More recently, seminal work in the field demonstrated primary tumor-secreted factors promote vascular leakiness and the upregulation of extracellular matrix components in site-specific distal organs. These factors were associated with alterations and the reprogramming of resident stromal cell populations and upregulation of pro-inflammatory mediators, thus creating an immune-suppressive, hospitable microenvironment capable of supporting the extravasation, colonialization, and metastatic outgrowth of incoming circulating tumor cells. This organ specific establishment of a favorable microenvironment was coined the pre-metastatic niche (PMN). (Peinado et al., 2011)

Dr. Paget's "seed and soil" hypothesis stated distant organs were inherently receptive to metastatic colonization, however, further studies identified several tumor-derived soluble factors that included growth factors, cytokines, chemokines and small (80-150 nm) tumor-secreted extracellular

vesicles, called exosomes, can remodel distal organs and contribute to PMN formation. Exosomes are secreted by both tumor cells and tumor-associated stromal cells. They contain a variety of biological "cargoes," like lipids, proteins, and nucleic acids, that were shown to remotely reprogram target cells within the PMN. (Peinado et al., 2011) Initial evidence highlighting the potential role of exosome involvement in driving organotropism through PMN formation showed exosomes derived from highly metastatic melanomas increased the metastatic behavior of primary tumors by "educating" bone marrow progenitors through the receptor tyrosine kinase, MET, inducing hallmark and organ specific PMN characteristics. It was also shown that along with MET expression, regulators of membrane trafficking and exosome formation were highly expressed in melanoma cells from individuals with metastatic disease. (Peinado et al., 2012) In another seminal study, it was shown that exosomes derived from highly metastatic pancreatic ductal adenocarcinomas (PDAC) were taken up by Kupffer cells in the liver inducing secretion of TGF-B and fibronectin production by hepatic stellate cells. Furthermore, PDAC-derived exosomes enhanced recruitment of bone marrow-derived macrophages through macrophage migration inhibitory factor (MIF) that was highly expressed on PDAC-derived exosomes, and blockade of MIF prevented liver PMN formation and metastasis. (Costa-Silva et al., 2015) Finally, it was shown that exosomes derived from mouse and human lung, liver, and brain-tropic tumor cells preferentially target resident lung fibroblasts and epithelial cells, Kupffer cells and brain endothelial cells, respectively, according to their preferred destination via exosome/tissue specific integrin repertoires that are capable of facilitating PMN formation. (Hoshino et al., 2015) In summary, these seminal works undertaken primarily by the Lyden group demonstrated tumor-derived exosomes were trafficked to organs associated with the matched tumor-type's organotropism via specific integrin repertoires, were taken up by target cells within those organs, reprogramming them to a tumor-promoting phenotype thereby facilitating PMN formation and enhancing metastatic potential among different cancer types. (Hu et al., 2023) In the context of OS metastasis specifically, EVs derived from highly metastatic OS clonal variants been shown to preferentially localize to the lungs, suggesting their potential role in OS metastatic lung tropism. (Khoo et al., 2024) More recently, OS exosomes have been shown to promote mechanisms associated with lung specific metastasis and PMN formation by remodeling the extracellular matrix, creating vascular instability

and promotion of angiogenesis, creating both an immunosuppressive and pro-inflammatory microenvironment and metabolically reprogramming lung resident cell types.

The extracellular matrix (ECM) is a highly dynamic three-dimensional structural network of macromolecules consisting of collagens, laminins, elastin and elastic fibers, glycoproteins, and proteoglycans. The composition of the ECM's structural molecules is unique to each tissue and interact by binding to each other as well as tissue resident cell adhesion receptors, forming a matrix structure into which cells reside and function within all tissues and organs. (Theocharis et al., 2016) The ECM is continuously being remodeled to modify ECM composition or stiffness through a balance of resident cell secreted enzymes that can degrade or cross-link extracellular matrix proteins, like matrix metalloproteinases (MMPs) and lysyloxidases (LOX), respectively. (Piperigkou et al., 2021; Ye et al., 2020) Through interactions with the ECM, cell surface receptors like integrins, syndecans and discoidin domain receptors (DDRs) respond to the continuously evolving structural network regulating a diverse repertoire of cellular functions such as survival, growth, migration, and differentiation. (Manou et al., 2019) Dysregulation of the processes and signaling that maintain structural and cellular homeostasis within a given tissue are associated with the development and progression of several pathological conditions, including cancer.

Signaling primarily occurs through interactions between the ECM and a combination of 24 non-covalently paired alpha/beta subunits generating 24 transmembrane heterodimers that facilitate bi-directional signaling, called integrins. Ligand-bound integrins engage the ECM network via talin and other cytoskeletal linker proteins leading to activation of focal adhesion kinases, Src-family protein tyrosine kinases, integrin-linked kinase, as well as other pathways heavily implicated in cancer biology, such as Ras-ERK, PI3K/AKT, and YAP/TAZ. (Hynes, 2002) Additionally, altered integrin expression is commonly detected in tumors and is associated with growth factor receptor (GFR), GFR-dependent cancer cell migration and invasion, and can determine colonization of metastatic sites through facilitation of anchorage-independent survival of circulating tumor cells.

The importance of ECM remodeling in OS metastatic progression is highlighted by a study comparing genes and micro-RNAs between primary and metastatic tissue that identified ~160 differentially expressed genes with an enrichment profile that predicted matrix metallopeptidase 3 (MMP3)

and vascular endothelial growth factor B (VEGFB) as being critical to OS metastasis. (Fan et al., 2019) When comparing the high and low metastatic isogenic commercial cell lines, 143b and HOS, respectively, it was identified that miR-143 was the most downregulated miRNA found in 143b. MiR-143b reduced MMP-13 expression thereby reducing invasiveness in mouse models of OS, further supporting the role ECM remodeling in OS metastasis. (Osaki et al., 2011) Finally, the proteolytic MMP-1, which targets a major component of the ECM, collagen type 1, was shown to be highly expressed in 143b cells compared to HOS and normal human bone cells. Stable downregulation of MMP-1 impaired adhesion and anchorage-independent growth of 143b cells in vitro and reduced the size and number of metastatic colonies in mouse models compared to empty vector transduced control cells. (Husmann et al., 2013)

Fibroblasts are a cell type responsible for maintaining tissue homeostasis through ECM remodeling during normal physiology and tissue repair. During the wound healing process, platelets form provisional clots made up of the matrix proteins fibrin and fibronectin. Platelets then recruit macrophages by releasing soluble mediators, which in turn release TGF-B and platelet-derived growth factor (PDGFR) that recruit and activate fibroblasts, directing them to take on pro-fibrotic and myofibroblastic phenotypes characterized by production of MMPs capable of degrading the provisional platelet formed clot, and deposition of collagen fibrils, elastin, proteoglycans, and other ECM components. Under normal conditions, fibroblasts become apoptotic as the wound healing process comes to completion. However, cancer, often referred to as a “wound that never heals,” promotes prolonged myofibroblast activity contributing to pre-metastatic niche formation through continued ECM modification that promotes tumor cell survival. These “activated” myofibroblasts, called cancer associated fibroblasts (CAFs) are a critical cell type within the TME and significantly contribute to PMN formation.

CAFs are considered one of the primary target cells of EVs in the lung and can be reprogrammed via EV transfer of miRNAs and proteins. Tumor derived EVs have been shown to convert normal, quiescent fibroblasts into CAFs that then modify the local ECM, promoting metastasis. (Rana et al., 2013) Recently, it was shown OS derived EVs can drive myofibroblast/cancer-associated fibroblast differentiation through exosomal TGF-B, characterized by increased invasive capacity, increased alpha-smooth muscle actin expression (A-SMA), and fibronectin production. (Mazumdar et al., 2020) Additionally, the collagen subtype COL6A1 was shown to be upregulated in OS metastatic tissues in the

lung, and OS EVs highly enriched with COL6A1were capable of converting normal fibroblasts to CAFs capable of promoting OS cell invasion and migration by mediating the TGF-B/COL6A1 signaling pathway. (Zhang et al., 2021)

Angiogenesis is the normal physiological process of neovascularization that occurs as tissues increase demand for oxygen and nutrients. As tumors require a dense vascular network to supply their growing needs, disruptions in the normal angiogenic processes are a key aspect of tumor growth, invasion, and metastasis. Tumor tissues can respond to hypoxia by producing angiogenic growth factors like vasculo-endothelial growth factor (VEGF), acidic and basic growth factors (aFGF and bFGF), and platelet-derived endothelial cell growth factor (PD-ECGF) that recruit these cell types to form new blood vessels. (Niu & Chen, 2010) The lung is comprised of a highly vascular tissue structure and dense capillary network formed by endothelial and epithelial cells in tight junctions creating the air-blood interface necessary for oxygen exchange. (Aslan et al., 2019) The OS lung PMN is characterized by increased angiogenesis, and vascular permeability resulting from disruptions to cell-cell junctions, and increased resident lung cell adhesion molecule expression, providing improved opportunities for extravasation of circulating tumor cells to seed and colonize the lung. The importance of angiogenesis in PMN formation is underscored by studies demonstrating primary tumors are capable of inducing formation of discrete foci of vascular hyper-permeability in the lungs, leading to preferential homing of metastatic cancer cells to these foci. It was shown this process was due to upregulation of MMP-9 expression and E-selectin, a cell adhesion molecule expressed by endothelial cells activated by pro-inflammatory cytokines like TNF-A and IL-1B, mediated by endothelial cell-focal adhesion kinase (FAK) activity. (Hiratsuka et al., 2011) In the context of OS, it has been shown that vascular permeability is increased in the OS lung PMN and intratumoral microvessel density, an index of tumor angiogenesis, is considered a prognostic risk factor among OS patients, further supporting the importance of OS tumor induced angiogenesis in OS metastatic progression. Due to the critical nature of angiogenesis in primary tumor and metastatic progression, several trials utilizing small molecule inhibitors and monoclonal antibodies to specifically and non-specifically target VEGF and other angiogenic factors in other cancer types have been assessed to varying degrees of success. (Agulnik et al., 2013; Ciardiello et al., 2003; Watanabe et al., 2004)

EVs from other cancer types have been identified as cargo carriers of pro-angiogenic mediators, such as proteins, miRNAs and long non-coding RNAs, shown to stimulate endothelial cells and disrupt cell-to-cell junctions, thereby increasing vascular instability to promote metastatic colonization in the lung. In OS, specifically, EVs can induce increased endothelial cell tube formation *in vitro*, and *in vivo* using chicken chorioallantois membranes, which was associated with specific EV miRNA and protein cargoes, providing evidence human OS EVs can act as carriers of angiogenic factors. (Perut et al., 2019) Recently, long non-coding RNAs have gained attention in OS-exosome mediated angiogenesis of the PMN. It was identified OS cell-derived EVs had elevated levels of long non-coding RNA (lnc-RNA) OIP5-AS1, which promoted proliferation, migration, and invasion of OS cells. It was shown exosomal lnc-RNA OIP5-AS1 increased endothelial tubule formation *in vitro* and significantly correlated with autophagy-related protein 5 (ATG5) expression, shown to play a role in angiogenesis as decreased ATG5 expression in endothelial cells reduced phosphorylation of the VEGF2 receptor. (Y. Li et al., 2021) Additionally, studies show the long non-coding RNA Ewing sarcoma associated transcript 1 (lnc-EWSAT1) promotes OS progression by enhancing proliferation, migration, and invasion through MEG3, a gene shown to regulate p53, RB1, Myc, and TGF-B expression, as well as Wnt-B-catenin signaling. (Shen et al., 2021; Sun et al., 2016) It was recently identified that OS-derived exosomes carry EWSAT1 as cargo and could increase the sensitivity/reactivity of vascular endothelial cells and promoted the secretion of pro-angiogenic soluble factors. (Tao et al., 2020) Another study identified OS-derived exosomal lnc-metastasis-associated lung adenocarcinoma transcript-1 (lnc-MALAT1) to be functionally similar to lnc-EWSAT1, upregulating expression of many of the same genes and pathways leading to increased OS induced PMN angiogenesis. (F. Li et al., 2021) Additionally, lnc-MALAT1 has been shown to induce pro-angiogenic effects through a MALAT1/mechanistic target of rapamycin (mTOR)/hypoxia inducible factor -1a (HIF-1a) signaling axis. Disruption of lnc-MALAT1 signaling using chemically modified small interfering RNAs (siMALAT1) inhibited this signaling axis and reduced the angiogenic effect of MALAT1, indicating an important role for exosomal lnc-RNAs in promoting OS angiogenesis and that targeting their signaling axes may have implications for the development of alternative anti-angiogenic therapies. (Zhang et al., 2017)

A hallmark of the OS lung PMN is the release of pro-inflammatory cytokines and chemokines that direct the infiltration and activation of inflammatory cells known to facilitate OS lung metastatic progression, like bone marrow-derived cells (BMDCs), neutrophils, macrophages and regulatory T lymphocytes (Tregs). An inflammatory microenvironment is also characterized by the induction of leaky blood vessels, revival of dormant circulating tumor cells and promotion of malignant phenotypes of tumor cells, all of which have been shown to be facilitated by tumor-derived EVs from other cancer types. (Wang et al., 2021) In addition to ECM modulation mentioned previously, fibroblasts are also capable of modulating the inflammatory state of the lung pre-metastatic niche. Once viewed as a monolith, the advent of single-cell sequencing technologies has shed light on the diverse range of distinct transcriptional and functional characteristics of CAFs, including those that promote wound-healing, myofibroblastic (myCAF), immunosuppressive antigen presenting (apCAF), and highly secretory, inflammatory (iCAF) phenotypes. (Luo et al., 2022; Peyser et al., 2019) Upon induction by OS-derived EVs, fibroblasts taking on the characteristic iCAF phenotype specifically, have been shown to secrete pro-inflammatory cytokines, chemokines, and growth factors such as IL-6, IL-8, and CCL2. Among the numerous signaling molecules involved in tumorigenesis and PMN formation, these 3 have been demonstrated to be heavily implicated in OS biology. For instance, IL-6 has been shown to directly promote tumor cell proliferation and survival through the JAK/STAT3 signaling axis. IL-6 signaling is also capable of recruiting pro-angiogenic bone marrow-derived progenitor cells and generate monocytic myeloid-derived suppressor cells to the PMN, further promoting an immunosuppressive PMN phenotype. (Karakasheva et al., 2018) IL-8 signaling within the PMN has been shown to be a chemoattractant capable of recruiting several cell types including MSCs as well as neutrophils to the PMN, where they modulate the microenvironment through the release neutrophil extracellular traps (NETs). IL-8 has also been shown to directly interact with tumor cells to promote proliferation, migration, angiogenesis, stemness and EMT. (Bakouny & Choueiri, 2020; Gross et al., 2018) Like IL-8, CCL2 is another chemoattractant, however, CCL2 signaling is primarily responsible for recruiting monocytes and macrophages to the PMN where they exert their immunosuppressive effects that further promote immune evasion and survival of metastatic circulating tumor cells. (Q. Chen et al., 2015; Gok Yavuz et al., 2019; Regan et al., 2022)

Models of OS

Over the past decades, many therapeutic interventions have been developed that showed promising results in a preclinical setting. However, most of these therapies fail to provide a clinical benefit and never gain approval through the trials phase for widespread adoption as a treatment option. The disconnect between preclinical and clinical results is partly due to a lack of models that fully recapitulate the complex milieu of molecular and cellular events that promote OS progression and metastasis in human patients. Systems and models that more accurately reflect the events and interactions that occur within the OS TME are being developed to optimize and streamline the selection process for candidate therapies.

The evaluation of potential therapeutic interventions has traditionally been dependent on the use of 2D monocultures. (Shoieb et al., 1998) OS cell lines derived from different progenitor cell types were identified to possess distinct functional characteristics such as immune attraction, promotion of angiogenesis and metastasis, and a host of other tumorigenic properties. (Mohseny et al., 2011) Additionally, it was discovered the use of an iterative process involving tumor cell injections into mice followed by selection of metastatic clones, led to isogenic subtypes (HOS/143b) capable of rapid metastatic colonization. (Fidler, 2003) These efforts resulted in an accelerated drug discovery process that identified potential therapies like afatinib. (Cruz-Ramos et al., 2020) Interestingly, the widespread use of these now commercially available OS cell lines for therapeutic development is being disputed, as studies indicated their genetic and molecular profiles are substantially altered compared to their original states. Recently, this has raised questions about the validity of findings derived from the use of these cell lines, implying these differences may contribute to the discrepancies observed between preclinical results and clinical efficacy of novel therapies. (Ottaviano et al., 2010) With these limitations in mind, investigators have begun to implement the use of patient-derived OS cell lines (PDX) for preclinical drug evaluations, as molecular and genomic profiling studies indicate even after several passages, PDX cell lines more accurately reflect the matched primary OS tumor. The profiling of PDX cell lines and their use in evaluating novel therapeutic approaches paves the way for the adoption of “personalized” treatment strategies (Schott et al., 2020; Schott et al., 2024)

More recently, a shift towards 3D in vitro models that more accurately mimic the cellular interactions and architectural environment that occur in the OS TME are being developed. Many of the 3D in vitro models employ techniques such as hanging drop, high density collagen, PLMA-based hydrogels and liquid overlay to explore various ECM structural characteristics and their role in the assembly of self-organized OS structures called spheroids. These models have been shown to successfully mimic microenvironments within OS tumors, such as anoxic, hypoxic and oxic niches, and have been used to screen compounds on OS cells alone or in co-culture with cell types commonly observed to interact with and influence OS cell progression in the TME and PMN, such as lung fibroblasts. (Chow et al., 2021; Guan & Huang, 2022; Nunes et al., 2019; Roy et al., 2023)

The addition of *ex vivo* models of OS metastasis have been developed. One such model takes advantage of the highly vascularized chick chorioallantoic membrane (CAM) to xenograft tumor cells onto for the evaluation of angiogenesis, migration and invasion. This method is high throughput, allows for live cell in vivo imaging, and is relatively inexpensive. However, a limitation with this model is the lack of tumor/host immune cell interactions that occur within the OS TME resulting from the immunodeficiency of the chicks. Another ex vivo pulmonary metastasis (PuMA) model overlays thin sections of mouse lung tissue containing previously injected and fluorescently nuclear labeled OS tumor cells onto a gel-foam sponge bathed in complete cell culture media. This method allows for live cell imaging and analysis of OS cell metastatic progression in living tissue comprised of the full complement of microenvironmental factors like ECM and host cell interactions.

Currently, several in vivo mouse models of OS metastasis are regularly employed and decisions about which model to use are dependent upon the questions being asked. For instance, the method by which OS tumor cells can be introduced into mice each have various advantages and disadvantages. These include the use of subcutaneous, intraosseous, para-tibial, and intravenously injections of OS cells. Subcutaneous injections of OS cells heterotopically is simple, allows for noninvasive visualization and measurement of tumor growth, and easy biopsies of tumors for downstream analysis. However, subcutaneous injections do not capture cellular interactions that typically occur in the tumor microenvironment, grow more slowly than other injection methods, and rarely metastasize. Intraosseous, orthotopic injection of OS cells is accomplished along the proximal tibia or distal femur, sites of

introduction that allow OS cells to interact with a native microenvironment, more accurately recapitulating OS tumor progression and spontaneous metastatic lung colonization. However, intraosseous tumor cell injections can result in difficulty measuring increases in tumor volume, a high degree of variation in the establishment of primary OS tumors, and OS cells may be deposited within the bone marrow, a highly vascular region that allows OS cells to rapidly get to the lung and form metastatic colonies. Para-tibial injection of OS cells occurs in the caudal gastrocnemius muscle along the tibial periosteum. This approach has been demonstrated to provide consistent primary tumor growth and lung metastasis and more accurately captures the events of the metastatic cascade; however, metastasis may develop slowly depending on the cell lines being evaluated. Finally, tail-vein injections of OS cells allow for the rapid introduction of tumor cells into the mouse, that are then trafficked directly to the lung. This method causes the rapid development of lung metastasis but fails to capture many of the events that typically occur during the metastatic cascade. The choice of how OS cells are introduced into mice is accompanied by which methods will be employed to monitor and quantify tumor growth and metastasis in vivo or ex vivo. One method now commonly employed transduces OS cells with lentiviral constructs containing the gene encoding an enzyme found in fireflies, luciferase, that produces a bioluminescent signal when exposed to its substrate, luciferin. Highly sensitive IVIS imaging systems can detect the bioluminescent signal from dozens of cells, the signal is restricted to the tumor compartment and is directly proportional to the number of cells expressing the enzyme in the model system. These characteristics make the monitoring of OS progression and metastasis using bioluminescent detection of luciferase expressing OS cells an incredibly valuable tool for OS investigators. (Garimella et al., 2013) The development of “micro” positron emission tomography/computed tomography (PET-CT) and nuclear magnetic resonance imaging (MRI) instruments has allowed OS investigators additional non-invasive and quantitative methods to evaluate various aspects metastatic development in OS mouse models. (Vormoor et al., 2014)

Evaluating the introduction of human OS cells in mouse models requires mice to be severely immunocompromised (SCID). These mice often have one or more immune deficiencies. For instance, mice commonly used in tumor xenograft studies often develop without a functional thymus, causing mice to lack a T lymphocyte response. Although mouse models are meant to accurately mimic OS development observed in humans, discrepancies between in vivo preclinical and clinical anti-tumor

responses may be partially due to the lack of a completely functional immune cell repertoire in mouse models, thereby failing to fully recapitulate all cellular interactions involved in OS development and therapy response. One method recently employed to sidestep this limitation utilizes the generation of humanized mice (NSG) that carry human immune systems through the engraftment of human CD34+ hematopoietic stem cells. (Ko et al., 2021) Another approach to address limitations in evaluating human OS in vivo uses genetically modified mouse models (GEMs). Investigators knockout (KO) genes whose disfunction is most observed in OS patients, such as TP53 and RB1, which results in “spontaneous” OS tumor initiation and metastasis. Interestingly, the tumor latency, time to tumor development or detection of metastatic colonization, and the location of primary tumor development (skull, femur, non-bone tissues) is dependent upon the specific combination of genes being knocked out or silenced. (Mutsaers et al., 2013; Walkley et al., 2008) The spontaneous development of OS in GEM models allow investigators to evaluate the genetic and molecular events that promote the OS tumor initiation, however, many of the genes that are knocked out or silenced are also shared across many cancers, and tumors from cancer types other than OS, such as lymphomas and hemangiosarcomas, often develop.(Donehower et al., 1992) Although mouse models will continue to be viewed as the workhorse for in vivo OS investigations, several other obstacles remain when using mouse models to evaluate human OS, such as the genetic homogeneity of mouse lines, dramatic differences in drug metabolism kinetics, and a lack of “true” spontaneous OS tumor development observed outside of genetic manipulation.

Canines and Pet dogs have increasingly been recognized as a complimentary and translational model for human OS. The use of pet dogs as a model comes with advantages that overcome many of the limitations observed in mouse models. First, dogs are one of the most genetically heterogenous species, dogs spontaneously develop OS at a higher frequency than in humans (10,000 cases per year in the US) and OS develops in dogs that possess competent and intact immune systems. Several studies and clinical trials investigating the efficacy of novel chemotherapeutic and host-directed immune based approaches are currently underway. (Beck et al., 2022)

Concluding Remarks and Project Rationale

As OS is typically diagnosed among children and young adults, the disproportionate number of life years lost resulting from this disease is sobering. Metastasis remains the greatest challenge to improving survival outcomes, and the high predilection of OS to specifically metastasize to the lungs paired with stalled efforts to develop new and effective therapies results in patient outcomes that have not improved in nearly half a century. Substantial efforts have been made to characterize the tumor cell intrinsic and microenvironmental determinates of OS tumorigenesis in the hopes of identifying new avenues to address these challenges. One of the more recent paradigms in this regard involves intracellular signaling facilitated by tumor-derived extracellular vesicles, called exosomes. In other cancer types, exosomes have been shown to traffic to specific organs where upon uptake by several target cell types, release their biological cargoes, reprogramming those cells towards phenotypes that alter the microenvironment in favor of circulating tumor cells, called the pre-metastatic niche. Activated fibroblasts within the tumor microenvironment, referred to as cancer associated fibroblasts, have been increasingly recognized for their contribution to several key, tumor promoting functions including extracellular matrix remodeling, and intracellular signaling facilitated by the secretion of cytokines, chemokines, and growth factors. The role of CAFs in the tumor microenvironment along with the high predilection for lung specific metastasis observed among OS patients led to the hypothesis that exosomes secreted from the OS primary tumor may be targeting lung fibroblasts, remotely inducing CAF-like phenotypes characterized by secretion of tumor promoting cytokines and chemokines. Thus, the overarching goal of this dissertation was to characterize the functional and transcriptional response of lung fibroblasts to OS-derived exosomes *in vitro*, their impact on metastatic lung colonization, and their effect on resident lung cell population dynamics and intracellular signaling *in vivo*.

In Chapter 2, we developed reliable methods to purify and characterize tumor-derived exosomes. Using flow cytometry and fluorescent microscopy, we demonstrate fluorescently labeled OS exosomes purified from 6 OS cell lines are efficiently taken up across several primary, donor-derived lung fibroblast cell lines. This exosome uptake was accompanied by a significant increase in the secretion of IL-6, CXCL8, and CCL2, signaling molecules highly implicated in OS tumorigenesis. We show OS exosomes induce significant proliferation of lung fibroblasts, which was associated with MAPK and STAT3 signal

transduction pathway activation. RNA-sequencing of OS exosome educated fibroblasts and subsequent pathway analysis of differentially expressed genes revealed enrichment for gene sets associated with hallmark CAF phenotypes. Finally, using an *in vitro* co-culture model developed as a simplified representation of the exosome educated lung PMN, we show human OS cells proliferate significantly faster in co-culture with OS-exosome educated lung fibroblasts compared to untreated controls.

Based on these data, we hypothesized that repeated OS exosome treatments would enhance OS cell lung colonization efficiency *in vivo*. To determine this, highly sensitive orthogonal analytical detection methods were developed to identify and quantify OS cells in the lung during the earliest stages of OS lung colonization. In Chapter 3, we evaluated two fluorescent cell labeling dyes, Cell Trace Yellow and DIR, and lentiviral transduction of OS cells to express nuclear RFP for detection and quantification using spectral flow cytometry. Pairing these cell labeling approaches with IVIS imaging and a mouse specific lung cell antibody panel, we show Cell Trace Yellow and DIR dyes are not effective methods for tracking OS cells in the lung as these dyes are not restricted to the tumor compartment. However, along with optimized lung digestion protocols, we demonstrate spectral flow cytometry and *ex vivo* IVIS imaging can be used to track and quantify luciferase and RFP expressing OS cells in the lung within 24 hours of tumor cell injections. Using these approaches to model OS lung colonization represents a promising method to rapidly evaluate tumor cell intrinsic and microenvironmental influences on OS lung metastasis.

In Chapter 4, using *in vivo* IVIS imaging, we show repeated retroorbital OS exosome treatments enhanced the colonization efficiency of OS cells in the lung in two models of OS. Although, we hypothesized exosome treatments would also be associated with changes in cytokine signaling and alterations to cell mouse lung cell populations, we did not observe significant changes in response to OS exosome treatment when OS cells are excluded from the lung. Under the same exosome treatment conditions that also included the introduction of OS cells into the system, we observed trends suggesting OS cell involvement may be required to stimulate detectable changes to mouse lung cell populations and differences between treatment conditions among the cytokines and chemokines we profiled. Furthermore, we did not observe any significant differences in survival outcomes between exosome treatment groups in this model.

Taken together, the work presented in this dissertation suggests OS exosomes may be influential in promoting lung specific OS metastasis and represents promising first steps in identifying an intracellular signaling mechanisms that may be exploited to develop novel anti-metastatic therapies and improve outcomes for OS patients.

References

Alspach, E., K. C. Flanagan, X. Luo, M. K. Ruhland, H. Huang, E. Pazolli, M. J. Donlin, T. Marsh, D. Piwnica-Worms, J. Monahan, D. V. Novack, S. S. McAllister and S. A. Stewart (2014). "p38MAPK plays a crucial role in stromal-mediated tumorigenesis." Cancer Discov **4**(6): 716-729.

Asif, P. J., C. Longobardi, M. Hahne and J. P. Medema (2021). "The Role of Cancer-Associated Fibroblasts in Cancer Invasion and Metastasis." Cancers (Basel) **13**(18).

Asokan, S. and O. R. Bandapalli (2021). "CXCL8 Signaling in the Tumor Microenvironment." Adv Exp Med Biol **1302**: 25-39.

Baglio, S. R., T. Lagerweij, M. Pérez-Lanzón, X. D. Ho, N. Léveillé, S. A. Melo, A. M. Cleton-Jansen, E. S. Jordanova, L. Roncuzzi, M. Greco, M. A. J. van Eijndhoven, G. Grisendi, M. Dominici, R. Bonafede, S. M. Lougheed, T. D. de Gruijl, N. Zini, S. Cervo, A. Steffan, V. Canzonieri, A. Martson, K. Maasalu, S. Köks, T. Wurdinger, N. Baldini and D. M. Pegtel (2017). "Blocking Tumor-Educated MSC Paracrine Activity Halts Osteosarcoma Progression." Clin Cancer Res **23**(14): 3721-3733.

Becker, A., B. K. Thakur, J. M. Weiss, H. S. Kim, H. Peinado and D. Lyden (2016). "Extracellular Vesicles in Cancer: Cell-to-Cell Mediators of Metastasis." Cancer Cell **30**(6): 836-848.

Brichkina, A., T. Bertero, H. M. Loh, N. T. Nguyen, A. Emelyanov, S. Rigade, M. Ilie, P. Hofman, C. Gaggioli and D. V. Bulavin (2016). "p38MAPK builds a hyaluronan cancer niche to drive lung tumorigenesis." Genes Dev **30**(23): 2623-2636.

Bussard, K. M., L. Mutkus, K. Stumpf, C. Gomez-Manzano and F. C. Marini (2016). "Tumor-associated stromal cells as key contributors to the tumor microenvironment." Breast Cancer Res **18**(1): 84.

Cardeñes, B., I. Clares, V. Toribio, L. Pascual, S. López-Martín, A. Torres-Gomez, R. Sainz de la Cuesta, E. M. Lafuente, M. López-Cabrera, M. Yáñez-Mó and C. Cabañas (2021). "Cellular Integrin α5β1 and Exosomal ADAM17 Mediate the Binding and Uptake of Exosomes Produced by Colorectal Carcinoma Cells." Int J Mol Sci **22**(18): integrin.

Chen, C., L. Xie, T. Ren, Y. Huang, J. Xu and W. Guo (2021). "Immunotherapy for osteosarcoma: Fundamental mechanism, rationale, and recent breakthroughs." Cancer Lett **500**: 1-10.

Chen, L., P. Guo, Y. He, Z. Chen, L. Chen, Y. Luo, L. Qi, Y. Liu, Q. Wu, Y. Cui, F. Fang, X. Zhang, T. Song and H. Guo (2018). "HCC-derived exosomes elicit HCC progression and recurrence by epithelial-mesenchymal transition through MAPK/ERK signalling pathway." Cell Death Dis **9**(5): 513.

Chen, Q., W. Sun, Y. Liao, H. Zeng, L. Shan, F. Yin, Z. Wang, Z. Zhou, Y. Hua and Z. Cai (2015). "Monocyte chemotactic protein-1 promotes the proliferation and invasion of osteosarcoma cells and upregulates the expression of AKT." Mol Med Rep **12**(1): 219-225.

Chen, Z., L. Zhou, L. Liu, Y. Hou, M. Xiong, Y. Yang, J. Hu and K. Chen (2020). "Single-cell RNA sequencing highlights the role of inflammatory cancer-associated fibroblasts in bladder urothelial carcinoma." Nat Commun **11**(1): fibroblasts in TME.

Chhoy, P., C. W. Brown, J. J. Amante and A. M. Mercurio (2021). "Protocol for the separation of extracellular vesicles by ultracentrifugation from in vitro cell culture models." STAR Protoc **2**(1): 100303.

Christianson, H. C., K. J. Svensson, T. H. van Kuppevelt, J. P. Li and M. Belting (2013). "Cancer cell exosomes depend on cell-surface heparan sulfate proteoglycans for their internalization and functional activity." Proc Natl Acad Sci U S A **110**(43): 17380-17385.

Cole, S., D. M. Gianferante, B. Zhu and L. Mirabello (2022). "Osteosarcoma: A Surveillance, Epidemiology, and End Results program-based analysis from 1975 to 2017." Cancer **128**(11): 2107-2118.

Costa-Silva, B., N. M. Aiello, A. J. Ocean, S. Singh, H. Zhang, B. K. Thakur, A. Becker, A. Hoshino, M. T. Mark, H. Molina, J. Xiang, T. Zhang, T. M. Theilen, G. García-Santos, C. Williams, Y. Ararso, Y. Huang, G. Rodrigues, T. L. Shen, K. J. Labori, I. M. Lothe, E. H. Kure, J. Hernandez, A. Doussot, S. H. Ebbesen, P. M. Grandgenett, M. A. Hollingsworth, M. Jain, K. Mallya, S. K. Batra, W. R. Jarnagin, R. E. Schwartz, I. Matei, H. Peinado, B. Z. Stanger, J. Bromberg and D. Lyden (2015). "Pancreatic cancer exosomes initiate pre-metastatic niche formation in the liver." Nat Cell Biol **17**(6): 816-826.

Dror, S., L. Sander, H. Schwartz, D. Sheinboim, A. Barzilai, Y. Dishon, S. Apcher, T. Golan, S. Greenberger, I. Barshack, H. Malcov, A. Zilberberg, L. Levin, M. Nessling, Y. Friedmann, V. Igras, O. Barzilay, H. Vaknine, R. Brenner, A. Zinger, A. Schroeder, P. Gonen, M. Khaled, N. Erez, J. D. Hoheisel and C. Levy (2016). "Melanoma miRNA trafficking controls tumour primary niche formation." Nat Cell Biol **18**(9): 1006-1017.

Elyada, E., M. Bolisetty, P. Laise, W. F. Flynn, E. T. Courtois, R. A. Burkhart, J. A. Teinor, P. Belleau, G. Biffi, M. S. Lucito, S. Sivajothi, T. D. Armstrong, D. D. Engle, K. H. Yu, Y. Hao, C. L. Wolfgang, Y. Park, J. Preall, E. M. Jaffee, A. Califano, P. Robson and D. A. Tuveson (2019). "Cross-Species Single-Cell Analysis of Pancreatic Ductal Adenocarcinoma Reveals Antigen-Presenting Cancer-Associated Fibroblasts." Cancer Discov **9**(8): 1102-1123.

Feng, W., D. C. Dean, F. J. Hornicek, H. Shi and Z. Duan (2019). "Exosomes promote pre-metastatic niche formation in ovarian cancer." Mol Cancer **18**(1): 124.

Gong, Z., Q. Li, J. Shi, J. Wei, P. Li, C. H. Chang, L. D. Shultz and G. Ren (2022). "Lung fibroblasts facilitate pre-metastatic niche formation by remodeling the local immune microenvironment." Immunity **55**(8): 1483-1500.e1489.

Gross, A. C., H. Cam, D. A. Phelps, A. J. Saraf, H. K. Bid, M. Cam, C. A. London, S. A. Winget, M. A. Arnold, L. Brandolini, X. Mo, J. M. Hinckley, P. J. Houghton and R. D. Roberts (2018). "IL-6 and CXCL8 mediate osteosarcoma-lung interactions critical to metastasis." JCI Insight **3**(16).

Hoang, B. H., T. Kubo, J. H. Healey, R. Sowers, B. Mazza, R. Yang, A. G. Huvos, P. A. Meyers and R. Gorlick (2004). "Expression of LDL receptor-related protein 5 (LRP5) as a novel marker for disease progression in high-grade osteosarcoma." Int J Cancer **109**(1): 106-111.

Hoshino, A., B. Costa-Silva, T. L. Shen, G. Rodrigues, A. Hashimoto, M. Tesic Mark, H. Molina, S. Kohsaka, A. Di Giannatale, S. Ceder, S. Singh, C. Williams, N. Soplop, K. Uryu, L. Pharmer, T. King, L. Bojmar, A. E. Davies, Y. Ararso, T. Zhang, H. Zhang, J. Hernandez, J. M. Weiss, V. D. Dumont-Cole, K. Kramer, L. H. Wexler, A. Narendran, G. K. Schwartz, J. H. Healey, P. Sandstrom, K. J. Labori, E. H. Kure, P. M. Grandgenett, M. A. Hollingsworth, M. de Sousa, S. Kaur, M. Jain, K. Mallya, S. K. Batra, W. R. Jarnagin, M. S. Brady, O. Fodstad, V. Muller, K. Pantel, A. J. Minn, M. J. Bissell, B. A. Garcia, Y. Kang, V. K. Rajasekhar, C. M. Ghajar, I. Matei, H. Peinado, J. Bromberg and D. Lyden (2015). "Tumour exosome integrins determine organotropic metastasis." Nature **527**(7578): integrins.

Itoh, H., T. Kadomatsu, H. Tanoue, M. Yugami, K. Miyata, M. Endo, J. Morinaga, E. Kobayashi, T. Miyamoto, R. Kurahashi, K. Terada, H. Mizuta and Y. Oike (2018). "TET2-dependent IL-6 induction mediated by the tumor microenvironment promotes tumor metastasis in osteosarcoma." Oncogene **37**(22): 2903-2920.

Kalluri, R. and V. S. LeBleu (2020). "The biology, function, and biomedical applications of exosomes." Science **367**(6478).

Kansara, M., M. W. Teng, M. J. Smyth and D. M. Thomas (2014). "Translational biology of osteosarcoma." Nat Rev Cancer **14**(11): 722-735.

Karakasheva, T. A., E. W. Lin, Q. Tang, E. Qiao, T. J. Waldron, M. Soni, A. J. Klein-Szanto, V. Sahu, D. Basu, S. Ohashi, K. Baba, Z. T. Giaccone, S. R. Walker, D. A. Frank, E. P. Wileyto, Q. Long, M. C. Dunagin, A. Raj, J. A. Diehl, K. K. Wong, A. J. Bass and A. K. Rustgi (2018). "IL-6 Mediates Cross-Talk between Tumor Cells and Activated Fibroblasts in the Tumor Microenvironment." Cancer Res **78**(17): 4957-4970.

Kovac, M., C. Blattmann, S. Ribi, J. Smida, N. S. Mueller, F. Engert, F. Castro-Giner, J. Weischenfeldt, M. Kovacova, A. Krieg, D. Andreou, P. U. Tunn, H. R. Dürr, H. Rechl, K. D. Schaser, I. Melcher, S. Burdach, A. Kulozik, K. Specht, K. Heinimann, S. Fulda, S. Bielack, G. Jundt, I. Tomlinson, J. O. Korbel, M. Nathrath and D. Baumhoer (2015). "Exome sequencing of osteosarcoma reveals mutation signatures reminiscent of BRCA deficiency." Nat Commun **6**: 8940.

Liao, Z., Z. W. Tan, P. Zhu and N. S. Tan (2019). "Cancer-associated fibroblasts in tumor microenvironment - Accomplices in tumor malignancy." Cell Immunol **343**: Review.

Liu, J., S. Wu, X. Zheng, P. Zheng, Y. Fu, C. Wu, B. Lu, J. Ju and J. Jiang (2020). "Immune suppressed tumor microenvironment by exosomes derived from gastric cancer cells via modulating immune functions." Sci Rep **10**(1): 14749.

Liu, Q., A. Li, Y. Tian, J. D. Wu, Y. Liu, T. Li, Y. Chen, X. Han and K. Wu (2016). "The CXCL8-CXCR1/2 pathways in cancer." Cytokine Growth Factor Rev **31**: 61-71.

Lobb, R. J., L. G. Lima and A. Möller (2017). "Exosomes: Key mediators of metastasis and pre-metastatic niche formation." Semin Cell Dev Biol **67**: 3-10.

Luo, H., X. Xia, L. B. Huang, H. An, M. Cao, G. D. Kim, H. N. Chen, W. H. Zhang, Y. Shu, X. Kong, Z. Ren, P. H. Li, Y. Liu, H. Tang, R. Sun, C. Li, B. Bai, W. Jia, Y. Liu, W. Zhang, L. Yang, Y. Peng, L. Dai, H. Hu, Y. Jiang, Y. Hu, J. Zhu, H. Jiang, Z. Li, C. Caulin, J. Park and H. Xu (2022). "Pan-cancer single-cell analysis reveals the heterogeneity and plasticity of cancer-associated fibroblasts in the tumor microenvironment." Nat Commun **13**(1): 6619.

Lussier, D. M., J. L. Johnson, P. Hingorani and J. N. Blattman (2015). "Combination immunotherapy with α-CTLA-4 and α-PD-L1 antibody blockade prevents immune escape and leads to complete control of metastatic osteosarcoma." J Immunother Cancer **3**: 21.

Lussier, D. M., L. O'Neill, L. M. Nieves, M. S. McAfee, S. A. Holechek, A. W. Collins, P. Dickman, J. Jacobsen, P. Hingorani and J. N. Blattman (2015). "Enhanced T-cell immunity to osteosarcoma through antibody blockade of PD-1/PD-L1 interactions." J Immunother **38**(3): 96-106.

Malanchi, I., A. Santamaria-Martínez, E. Susanto, H. Peng, H. A. Lehr, J. F. Delaloye and J. Huelsken (2011). "Interactions between cancer stem cells and their niche govern metastatic colonization." Nature **481**(7379): 85-89.

Man, T. K., X. Y. Lu, K. Jaeweon, L. Perlaky, C. P. Harris, S. Shah, M. Ladanyi, R. Gorlick, C. C. Lau and P. H. Rao (2004). "Genome-wide array comparative genomic hybridization analysis reveals distinct amplifications in osteosarcoma." BMC Cancer **4**: 45.

Mao, X., J. Xu, W. Wang, C. Liang, J. Hua, J. Liu, B. Zhang, Q. Meng, X. Yu and S. Shi (2021). "Crosstalk between cancer-associated fibroblasts and immune cells in the tumor microenvironment: new findings and future perspectives." Mol Cancer **20**(1): 131.

Marra, F., W. Delogu, I. Petrai, S. Pastacaldi, A. Bonacchi, E. Efsen, S. Aleffi, C. Bertolani, M. Pinzani and P. Gentilini (2004). "Differential requirement of members of the MAPK family for CCL2 expression by hepatic stellate cells." Am J Physiol Gastrointest Liver Physiol **287**(1): G18-26.

Massaro, C., H. N. Sensoy, M. Mulders, C. De Schrijver, C. Gómez-Martín, J. Simon Nieto, T. Lagerweij, A. Atmopawiro, J. Pérez-Boza, M. Bebelman, L. Bosch, S. Foderaro, M. Neves Ferreira, M. A. J. van Eijndhoven, J. R. T. van Weering, C. Dell'Aversana, L. Altucci, C. D. Savci-Heijink, N. van de Donk, C. Giorgio, L. Brandolini, M. Allegretti, D. M. Pegtel and S. R. Baglio (2024). "Tumor-Secreted Extracellular Vesicles Counteract Therapy Response by Triggering Inflammatory Mesenchymal Stem Cell Development." Clin Cancer Res **30**(20): 4714-4728.

Mazumdar, A., J. Urdinez, A. Boro, J. Migliavacca, M. J. E. Arlt, R. Muff, B. Fuchs, J. G. Snedeker and A. Gvozdenovic (2020). "Osteosarcoma-Derived Extracellular Vesicles Induce Lung Fibroblast Reprogramming." Int J Mol Sci **21**(15).

Meltzer, P. S. and L. J. Helman (2021). "New Horizons in the Treatment of Osteosarcoma." N Engl J Med **385**(22): 2066-2076.

Milane, L., A. Singh, G. Mattheolabakis, M. Suresh and M. M. Amiji (2015). "Exosome mediated communication within the tumor microenvironment." J Control Release **219**: 278-294.

Nirala, B. K., T. Yamamichi, D. I. Petrescu, T. N. Shafin and J. T. Yustein (2023). "Decoding the Impact of Tumor Microenvironment in Osteosarcoma Progression and Metastasis." Cancers (Basel) **15**(20).

Peinado, H., M. Alečković, S. Lavotshkin, I. Matei, B. Costa-Silva, G. Moreno-Bueno, M. Hergueta-Redondo, C. Williams, G. García-Santos, C. Ghajar, A. Nitadori-Hoshino, C. Hoffman, K. Badal, B. A. Garcia, M. K. Callahan, J. Yuan, V. R. Martins, J. Skog, R. N. Kaplan, M. S. Brady, J. D. Wolchok, P. B. Chapman, Y. Kang, J. Bromberg and D. Lyden (2012). "Melanoma exosomes educate bone marrow progenitor cells toward a pro-metastatic phenotype through MET." Nat Med **18**(6): 883-891.

Pols, M. S. and J. Klumperman (2009). "Trafficking and function of the tetraspanin CD63." Exp Cell Res **315**(9): 1584-1592.

Regan, D. P., L. Chow, S. Das, L. Haines, E. Palmer, J. N. Kurihara, J. W. Coy, A. Mathias, D. H. Thamm, D. L. Gustafson and S. W. Dow (2022). "Losartan Blocks Osteosarcoma-Elicited Monocyte Recruitment, and Combined With the Kinase Inhibitor Toceranib, Exerts Significant Clinical Benefit in Canine Metastatic Osteosarcoma." Clin Cancer Res **28**(4): 662-676.

Regan, D. P., J. W. Coy, K. K. Chahal, L. Chow, J. N. Kurihara, A. M. Guth, I. Kufareva and S. W. Dow (2019). "The Angiotensin Receptor Blocker Losartan Suppresses Growth of Pulmonary Metastases via AT1R-Independent Inhibition of CCR2 Signaling and Monocyte Recruitment." J Immunol **202**(10): 3087-3102.

Ristorcelli, E., E. Beraud, S. Mathieu, D. Lombardo and A. Verine (2009). "Essential role of Notch signaling in apoptosis of human pancreatic tumoral cells mediated by exosomal nanoparticles." Int J Cancer **125**(5): 1016-1026.

Ritter, J. and S. S. Bielack (2010). "Osteosarcoma." Ann Oncol **21 Suppl 7**: vii320-325.

Salunkhe, S., Dheeraj, M. Basak, D. Chitkara and A. Mittal (2020). "Surface functionalization of exosomes for target-specific delivery and in vivo imaging & tracking: Strategies and significance." J Control Release **326**: 599-614.

Skog, J., T. Würdinger, S. van Rijn, D. H. Meijer, L. Gainche, M. Sena-Esteves, W. T. Curry, Jr., B. S. Carter, A. M. Krichevsky and X. O. Breakefield (2008). "Glioblastoma microvesicles transport RNA and proteins that promote tumour growth and provide diagnostic biomarkers." Nat Cell Biol **10**(12): 1470-1476.

Suzuki, M., T. Tetsuka, S. Yoshida, N. Watanabe, M. Kobayashi, N. Matsui and T. Okamoto (2000). "The role of p38 mitogen-activated protein kinase in IL-6 and IL-8 production from the TNF-alpha- or IL-1beta-stimulated rheumatoid synovial fibroblasts." FEBS Lett **465**(1): 23-27.

Takahashi, Y., T. Yasui, K. Tamari, K. Minami, K. Otani, F. Isohashi, Y. Seo, R. Kambe, M. Koizumi and K. Ogawa (2017). "Radiation enhanced the local and distant anti-tumor efficacy in dual immune checkpoint blockade therapy in osteosarcoma." PLoS One **12**(12): e0189697.

Talbott, H. E., S. Mascharak, M. Griffin, D. C. Wan and M. T. Longaker (2022). "Wound healing, fibroblast heterogeneity, and fibrosis." Cell Stem Cell **29**(8): 1161-1180.

Tsukamoto, H., K. Fujieda, S. Senju, T. Ikeda, H. Oshiumi and Y. Nishimura (2018). "Immune-suppressive effects of interleukin-6 on T-cell-mediated anti-tumor immunity." Cancer Sci **109**(3): 523-530.

Umezu, T., H. Tadokoro, K. Azuma, S. Yoshizawa, K. Ohyashiki and J. H. Ohyashiki (2014). "Exosomal miR-135b shed from hypoxic multiple myeloma cells enhances angiogenesis by targeting factor-inhibiting HIF-1." Blood **124**(25): 3748-3757.

Viñas, J. L., M. Spence, A. Gutsol, W. Knoll, D. Burger, J. Zimpelmann, D. S. Allan and K. D. Burns (2018). "Receptor-Ligand Interaction Mediates Targeting of Endothelial Colony Forming Cell-derived Exosomes to the Kidney after Ischemic Injury." Sci Rep **8**(1): 16320.

Wan, Y., Y. Zhao, M. Cao, J. Wang, S. V. Tran, Z. Song, B. W. Hsueh and S. E. Wang (2024). "Lung Fibroblasts Take up Breast Cancer Cell-derived Extracellular Vesicles Partially Through MEK2-dependent Macropinocytosis." Cancer Res Commun **4**(1): 170-181.

Wang, Y. C., L. H. Zheng, B. A. Ma, Y. Zhou, M. H. Zhang, D. Z. Zhang and Q. Y. Fan (2011). "Clinical value of signal transducers and activators of transcription 3 (STAT3) gene expression in human osteosarcoma." Acta Histochem **113**(4): 402-408.

Wei, K., H. N. Nguyen and M. B. Brenner (2021). "Fibroblast pathology in inflammatory diseases." J Clin Invest **131**(20).

Wortzel, I., S. Dror, C. M. Kenific and D. Lyden (2019). "Exosome-Mediated Metastasis: Communication from a Distance." Dev Cell **49**(3): 347-360.

Wu, C. C., H. C. Beird, J. Andrew Livingston, S. Advani, A. Mitra, S. Cao, A. Reuben, D. Ingram, W. L. Wang, Z. Ju, C. Hong Leung, H. Lin, Y. Zheng, J. Roszik, W. Wang, S. Patel, R. S. Benjamin, N. Somaiah, A. P. Conley, G. B. Mills, P. Hwu, R. Gorlick, A. Lazar, N. C. Daw, V. Lewis and P. A. Futreal (2020). "Immuno-genomic landscape of osteosarcoma." Nat Commun **11**(1): 1008.

Wu, F., J. Yang, J. Liu, Y. Wang, J. Mu, Q. Zeng, S. Deng and H. Zhou (2021). "Signaling pathways in cancer-associated fibroblasts and targeted therapy for cancer." Signal Transduct Target Ther **6**(1): 218.

Yang, L., X. Huang, H. Guo, L. Wang, W. Yang, W. Wu, D. Jing and Z. Shao (2021). "Exosomes as Efficient Nanocarriers in Osteosarcoma: Biological Functions and Potential Clinical Applications." Front Cell Dev Biol **9**: 737314.

Zou, S., Q. Tong, B. Liu, W. Huang, Y. Tian and X. Fu (2020). "Targeting STAT3 in Cancer Immunotherapy." Mol Cancer **19**(1): 145.

CHAPTER 2

Osteosarcoma exosome priming of primary human lung fibroblasts induces an immune modulatory and pro-tumorigenic phenotype[1]

Abstract

Osteosarcoma (OS) is the most common malignant bone cancer. 30-40% of all OS patients develop tumor recurrence, almost exclusively in the form of lung metastasis, which is associated with a dismal 20% 5-year survival rate. Cancer-associated fibroblasts are a critical cell type within the lung TME, which promote immune suppression, drug resistance, and tumor cell survival. Prior work shows tumor cells can [1]co-opt fibroblasts to a pro-tumorigenic phenotype via exosome mediated intercellular communication. Currently, the mechanisms by which OS exosomes modulate resident lung fibroblast function has not been evaluated. To investigate this, we isolated exosomes from a panel of 6 OS cell lines. We assessed the uptake and response of human donor-derived primary lung fibroblasts (LF's; n=4) to OS exosome treatment *in vitro* via flow cytometry, confocal fluorescent microscopy, proliferation assays, phospho-kinase array, multiplex cytokine analysis and RNA-sequencing. We observed that LFs efficiently take up OS exosomes, which is associated with induction of MAPK pathway activation, fibroblast proliferation and significantly enhanced secretion of IL-6, CXCL8 and CCL2 compared to untreated LFs. RNA-seq of exosome treated LFs confirmed these responses and revealed significant enrichment of pathways related to cytokine secretion, proliferation, immune cell chemotaxis, migration, proinflammatory and profibrotic mediators. Finally, in an exosome-educated lung fibroblast-OS co-culture model, exosome educated LFs conferred significantly increased OS cell survival and proliferation as compared to untreated fibroblasts. Together, these data suggest OS-derived exosomes can induce a hallmark, CAF-like inflammatory phenotype in lung fibroblasts providing valuable insights into mechanisms that may promote recurrent OS lung metastasis. These findings provide a critical first step in

[1] Thank you to the many people who contributed to this chapter: Daniel Regan, Laurel Haines, Kathryn Cronise, Sunetra Das, Aaron Offerman, Carina Easton

characterizing the capacity of OS-derived exosomes to reprogram primary lung fibroblasts towards a tumor-promoting inflammatory phenotype *in vitro*, offering novel molecular targets for modulation of fibroblasts in the lung microenvironment as potential therapeutic strategies to prevent OS metastasis.

Introduction

Osteosarcoma (OS) is a highly malignant primary bone tumor characterized by its aggressive behavior, predilection for occurrence in children and young adults, and recurrent disease that presents almost exclusively in the form of lung metastasis.(Ritter and Bielack 2010, Kansara, Teng et al. 2014, Cole, Gianferante et al. 2022) Despite the discovery of intrinsic molecular drivers of OS progression and promising pre-clinical studies demonstrating efficacy of immune checkpoint inhibitors and molecular targeted therapies, clinical outcomes for OS patients remain unchanged and patients continue to receive the same multi-drug chemotherapy protocol of methotrexate, doxorubicin, and cisplatin (MAP) developed over three decades ago.(Man, Lu et al. 2004, Kovac, Blattmann et al. 2015, Lussier, Johnson et al. 2015, Lussier, O'Neill et al. 2015, Takahashi, Yasui et al. 2017, Wu, Beird et al. 2020, Chen, Xie et al. 2021, Meltzer and Helman 2021) The disconnect between preclinical models of metastasis and clinical efficacy highlights a failure of current models to fully recapitulate the complexity of key cellular players and signaling mechanisms within the tumor microenvironment (TME), their role in extrinsically driving disease progression and therapy resistance, and the urgent need to develop new models that accelerate progress toward novel therapeutic interventions.(Nirala, Yamamichi et al. 2023)

Among the intricate network of factors that contribute to OS progression, the role of extracellular vesicles, particularly exosomes, has begun to emerge as a key signaling mechanism.(Yang, Huang et al. 2021) Exosomes are nano-sized vesicles secreted by various cell types, including cancer cells, and have garnered considerable attention for their ability to mediate intercellular communication through transfer of bioactive molecules such as proteins, lipids and nucleic acids.(Milane, Singh et al. 2015, Becker, Thakur et al. 2016) Furthermore, evidence suggests cancer derived exosomes are implicated in a myriad of processes within the local tumor microenvironment (TME) that promote tumor growth and metastasis, immune evasion, angiogenesis, and epithelial to mesenchymal transition (EMT).(Skog, Würdinger et al.

2008, Ristorcelli, Beraud et al. 2009, Peinado, Alečković et al. 2012, Umezu, Tadokoro et al. 2014, Kalluri and LeBleu 2020, Liu, Wu et al. 2020) Importantly, exosomes have been shown to traffic to site specific organs and mediate remote priming of resident cells to promote formation of a specialized microenvironment enhancing survival, growth, and colonization of incoming, circulating cancer cells, a key process in conditioning of the premetastatic niche (PMN).(Costa-Silva, Aiello et al. 2015, Hoshino, Costa-Silva et al. 2015, Lobb, Lima et al. 2017, Feng, Dean et al. 2019)

Lung fibroblasts, traditionally viewed as an essential component of the pulmonary stroma for their multifaceted role in maintaining tissue homeostasis and response to injury, are now recognized as regulators of various pathological processes including inflammation, fibrosis and cancer.(Bussard, Mutkus et al. 2016, Liao, Tan et al. 2019, Wei, Nguyen et al. 2021, Talbott, Mascharak et al. 2022) Evidence suggests fibroblasts can undergo dynamic alterations in response to signaling from the primary tumor. Within this context, lung fibroblasts have been identified as a key cellular target of tumor-secreted exosomes, leading to their co-optation as active participants in PMN formation through cellular and molecular events, such as extracellular matrix remodeling, secretion of growth factors and chemokines, and immunomodulation.(Liao, Tan et al. 2019, Mao, Xu et al. 2021, Gong, Li et al. 2022) These “activated,” or cancer-associated fibroblasts (CAF) are comprised of a diverse array of functionally distinct subtypes, each of which exert profound influence over the architectural and biochemical landscape of the lung PMN.(Luo, Xia et al. 2022)

Thus, while mounting evidence has implicated tumor-derived exosomes and non-malignant resident cells as effectors of organ-specific metastasis in multiple cancers such as melanoma, breast, liver and pancreatic,(Peinado, Alečković et al. 2012, Costa-Silva, Aiello et al. 2015, Feng, Dean et al. 2019) the cellular and molecular mechanisms governing osteosarcoma’s striking predilection for metastasis to the lung remain to be fully elucidated. This is a key knowledge gap in osteosarcoma metastasis biology which if addressed could identify novel molecular targets for host-directed anti-metastatic therapies or biomarkers for identifying those OS patients at high-risk for metastasis. Therefore, we investigated the role OS-derived exosome signaling plays in promoting the transition of primary donor-derived, human lung fibroblasts (LFs) toward a tumor promoting phenotype. We show that OS-derived exosomes are efficiently taken up by LFs *in vitro*, inducing enhanced fibroblast proliferation, MAPK signal

transduction, and secretion of cytokines and chemokines previously implicated in OS lung metastasis including IL-6, CXCL8 and CCL2. Additionally, transcriptomic analysis of LF response to OS exosome priming demonstrated significant enrichment of genes associated with a pro-tumorigenic secretory profile and enhanced proliferation, as well as genes associated with the promotion of adhesion, ECM remodeling, and angiogenesis. Furthermore, we show that OS exosome activation elicits pro-tumorigenic functions in LFs including monocyte recruitment and enhanced survival of OS cells in a fibroblast-OS cell co-culture model. These data provide a mechanistic basis for potential molecular targets that may be effective in modulating pro-tumorigenic functions of fibroblasts in the lung microenvironment as a therapeutic strategy for OS metastasis.

Materials and Methods

Cell lines

Human osteosarcoma (OS) cancer cell lines (143b, HOS, MG63.0, MG63.2, U2OS and SAOS-2) and other cancer cell lines (Malme-3M, TCCSUP, and T84) were purchased from the American Type Culture Collection (Manassas, VA USA). Breast cancer cell lines (MDA-MB-231 and MDA-MB-468) were purchased from the University of Colorado Cancer Center Tissue Culture Shared Resource. Normal Human Lung Fibroblasts (NHLF) from n = 4 individual donors were purchased from Lonza Inc. Additional information regarding lung fibroblast donor age and sex are provided in supplementary table S1. All tumor cell lines were validated by short tandem repeat (STR) analysis and all cell lines were routinely tested for mycoplasma contamination using a commercially available assay (Mycoalert from Lonza Inc.). Tumor cells were maintained in DMEM media (Gibco, Grand Island, NY USA) or RPMI (MB231 and MB468) supplemented with 10% fetal bovine serum (FBS; Atlas Biologicals, Fort Collins, CO USA), penicillin (100 U/mL), and streptomycin (100 mg/mL) (All from Gibco). NHLF were maintained in FBM-2 (Lonza Inc.) supplemented with insulin, hFGF, gentamicin, and 2% FBS (complete FGM). Cells were grown sterilely on standard plastic tissue culture flasks (Cell Treat, Shirley, MA), under standard conditions of 37 °C, 5% CO_2, and humidified air. To transduce OS cell lines using Incucyte Nuclight rapid red cell labelling lentivirus constructs (Sartorius, cat# 4771), 5000 OS cells were plated (15-35% confluent) in flat-bottom

96-well plates in complete DMEM media for 24 hours. Media was removed and replaced with complete DMEM media containing Nuclight lentivirus at an MOI of 3 (8 µg/mL) for 72 hours while monitoring for RFP expression using the Incucyte S3 live cell imaging system (Sartorius Inc. Göttingen, Germany). Subsequently, RFP labelled cells were selected for using 1 µg/mL puromycin in complete DMEM media while being monitored for expression selection by Incucyte over the course of three days.

Isolation of Exosomes

Cancer cell lines were seeded in 5-deck multi-flasks (Corning Falcon, cat# 353144) at ~20% confluence (roughly 1 million cells) in their respective media containing 10% FBS for 24 hours. Subsequently, media was removed and replaced with their respective base media containing only 2% exosome depleted FBS for 3 days before harvesting this tumor conditioned media (CM) for exosome isolation. Fetal bovine serum (FBS) was depleted of exosomes by differential ultracentrifugation (Optima Max-XP ultracentrifuge (cat# 393315), MLA-55 rotor (cat# 393203), Beckman-Coulter) at 120,000 xg for 3 hours at 4°C and was confirmed to be depleted of exogenous exosomes by Qnano Gold (Izon) tunable-resistive pulse sensing particle analysis, as described below.(Chhoy, Brown et al. 2021) To isolate tumor-derived exosomes, tumor-CM was first centrifuged at 3,000 xg for 10 minutes at 4°C to remove cellular debris, and then was subjected to ultrafiltration using Amicon Ultra Centrifugal filters (Centricon Plus-70) with a 100 kDa molecular weight cut-off to concentrate EVs. To prepare the centricon plus-70 centrifugal filter (Sigma, cat# UFC710008) for concentration of tumor-CM, 35 mL of PBS was loaded and centrifuged at 3500 xg and 4°C for 10 minutes to remove glycerol from the filter. After discarding the PBS flow through, 70 mL of prepared tumor-CM was loaded onto the filter and centrifuged at 3500 xg for 45 minutes at 4°C. Flow through was discarded followed by addition of 35 mL of PBS to the filter and centrifuged at 3500 xg and 4°C for 15 minutes to wash the column. Flow through was once again discarded and the filters were flipped upside down, placed on the collection cup, and centrifuged at 1000 xg and 4°C for 2 minutes. This concentrated ultrafiltrate of tumor-CM collected from the centrifugal filters was then subjected to size exclusion chromatography to isolate a pure population of tumor-derived exosomes using QeV original 35 nm size exclusion chromatography columns and automatic fraction

collector (Izon Scientific). Samples were eluted with 1x PBS and the void volume as well as all ten 0.5ml eluted fractions were collected and subjected to nanoparticle tracking and microBCA protein analyses for quantification of extracellular vesicle and protein concentrations. Fractions 1-3, identified as the particle rich, protein-poor fractions, as reported in the QeV Original User Manual, were pooled and sterile filtered using 45 µm PES membrane syringe filters (Merck Millipore Ltd., Cat# SLGPR33S) prior to further characterization for exosome purity, as described below. Chromatography columns were reused no more than 5 times per manufacturer recommendation and were washed with PBS 3 times between uses.

Exosome characterization

For transmission electron microscopy (TEM), exosome pellets were loaded onto formvar/carbon-coated EM grids, fixed with 2% paraformaldehyde, and stained with 1% aqueous uranyl acetate. The samples were then examined using a TEM (JEM-1400, JEOL). For nano particle tracking analysis (NTA), particle concentrates were diluted 1/10 in 3x PBS, then examined using a tunable pulse resistant sensing (TPRS) instrument, Qnano Gold (Izon). A nanopore 150 (NP150) at 47nm stretch, 24 V at approximately 100 nA was applied and measured against standard particles of 100 nm in diameter at $1.3e^{13}$ particles per mL.

For western blot analysis of canonical exosome surface proteins, 200 mL of exosome concentrates at 1e10 particles per mL were ultracentrifuged at 100,000 xg on an ultracentrifuge (MAX-XP, Beckman-Coulter) for 1 hour. Pellets were lysed using M-PER lysis buffer (Thermo Scientific cat# 78501) supplemented with protease and phosphatase inhibitor mini tablets (Pierce cat#A32961) prior to addition of 4x laemlli loading buffer with 10% beta-mercaptoethanol followed by boiling at 95°C for 5 min. Proteins were run on SDS-PAGE gel and transferred to PVDF membrane. Membranes were blocked with 5% BSA in TBS with 0.1% Tween 20 then incubated independently with the following primary antibodies: Rabbit anti-CD9 (D801A, Cell Signaling Technologies), rabbit anti-CD81 (D3N2D, Cell Signaling Technologies). For flow cytometry of exosome markers, $1e^{10}$ exosomes/mL were ultracentrifuged at 100xg for 1 hour, pellet was resuspended in 100 mL of FACS buffer containing mouse anti-human CD9-APC (MEM-61, Invitrogen), CD81-FITC (M38, Life Technologies), and CD63-PacBlue (H5C6, BioLegend)

antibodies for 15 minutes before quenching with 1 mL of FACS buffer. Two washing steps of ultracentrifugation with resuspension in 1 mL FACS buffer were performed followed by a final resuspension in 150 ul FACS buffer prior to flow cytometric analysis on a Cytek Aurora 4 laser spectral flow cytometer.

Assessment of tumor exosome uptake by lung fibroblasts

To evaluate OS cell line derived exosome uptake by normal human lung fibroblasts in vitro, 1e10 exosomes per mL were ultracentrifuged at 100,000 xg for 1 hour to pellet the exosomes, further concentrating them and allowing for the removal of PBS supernatant. Pellets were resuspended in 100 mL of diluent C then labeled with the lipophilic membrane dye PKH26 (Sigma, PKH26GL) at 1 mM for 5 minutes prior to the addition of 200 mL water. Labeled exosomes or equimolar dye only vehicle controls were centrifuged again at 100,000 xg for 1 hour to pellet the exosomes and separate them from unwanted, unincorporated dye particles. Supernatants containing unincorporated dye were removed and the labeled exosome pellets or dye only controls were resuspended in 100 μL PBS and 800 μL serum free DMEM for use in the following NHLF exosome uptake experiments.

NHLF were either plated in flat-bottom 96-well plates at 20,000 cells per well for flow cytometry, or in chamber slides (Thermo, Cat# 177445) at 5,000 cells per well (fluorescence microscopy) in complete FGM and allowed to adhere overnight. The next day, media was removed and replaced with 200 μL of serum-free media containing PKH-26 labeled OS-derived exosomes at $1e^9$ exomes per mL and incubated at 37°C for 4 hours. For flow cytometric analysis of OS exosome uptake, NHLF cells were washed with PBS, trypsinized, then treated with zombie NIR (BioLegend, cat# 423105) viability dye in PBS containing 5 μM EDTA for 15 minutes. Cells were then washed twice in FACS buffer prior to being analyzed by a Cytek aurora, 4 laser, flow cytometer. For confocal microscopy of NHLF after the 4 hr exosome incubation, cells were washed twice with PBS then fixed using 4% paraformaldehyde (Thermo, Cat# J19943.K2) diluted 1:1 with PBS for 10 minutes prior to imaging. Fixed cells were stained with actingreen (Invitrogen cat# R37110) following recommended protocols, then chamber slides were cover slipped with DAPI containing ProLong diamond antifade mountant (Invitrogen) and allowed to dry

overnight prior to imaging. Confocal fluorescence imaging was performed using an Olympus IX83 spinning disc microscope, Hamamatsu ORCA-R2 digital camera, and CellSense software (Olympus, V4.2, USA), and both high magnification single field and low magnification whole slide images were captured using standardized exposure times across vehicle control and PKH26 exosome-treated NHLF slides.

Phospho-kinase analysis of lung fibroblasts

Kinase activation in exosome-treated lung fibroblasts was assessed using the proteome profiler human phospho-kinase array kit (R&D systems, Cat# ARY003). 300,000 NHLF (n=2 biologically independent donors, F62, M12; see Table S1) were plated in 25cm^2 tissue culture flasks for each treatment condition overnight in complete FGM. After 24 hours, media was replaced with either 5 mL of OS-derived exosomes (143b) at 5e^9 OS exosomes/mL in serum free DMEM (sf-DMEM) or sf-DMEM alone (control). Subsequently, fibroblasts received two additional exosome treatments at 24 and 72 hours, removing 2.5 mL of the conditioned media and replacing with 2.5 mL of 5e^9 OS exosomes/mL in sf-DMEM or serum-free DMEM only for control wells. 4 hours after the last exosome-treatment, cells were washed with PBS and lysed using the lysis buffer provided in the array kit. Protein concentration was measured using a Pierce BCA assay kit (ThermoFisher Inc.) and equal amounts of control and exosome-treated lung fibroblast protein lysates were analyzed by immunoblotting according to the kit manufacturer protocol. Membranes were imaged on a ChemiDoc imaging system (BioRad Inc.) at equivalent exposure times (5 minutes) to maximize signal to noise ratio. Using ImageJ image analysis software to quantify phospho-protein abundance, membrane images were analyzed for integrated pixel density. The average signal (pixel density) of the pair of duplicate spots representing each phosphorylated kinase protein was determined and then an averaged background signal, generated from a clear array of the array membrane, was subtracted from each spot. These values were then compared between control and exosome-treated NHLF to determine the relative change in phosphorylated kinase proteins between samples.

Additionally, OS exosome-induced kinase activation in human lung fibroblasts was quantitatively assessed using Milliplex MAPK/SAPK and Akt/mTOR phospho-protein magnetic bead-based assays (Sigma Aldrich, catalog #48-660MAG, #48-611MAG) and a MagPix instrument (Luminex, Austin, TX). For these assays, 10,000 NHLF were plated per well in 96-well flat-bottom plates and allowed to adhere overnight in complete FGM. 24 hours post-plating, media was removed and NHLF were treated with either sf-DMEM containing $5e^9$ OS exosomes/mL (N=5 OS cell lines) or sf-DMEM alone. OS exosome education was then repeated 72 hours post-plating. At 96 hours post-plating, NHLF were washed with 200 µl PBS, and lysed using M-PER buffer (ThermoFisher Inc.) containing Pierce protease/phosphatase inhibitor cocktail (ThermoFisher Inc.). Lysates were processed and analyzed for phospho-protein relative abundance according to the manufacturers protocol. Samples were analyzed using the Luminex MagPix instrument. Quality control and initial processing of data was performed with Luminex xPONENT software, prior to export and further analysis with GraphPad Prism version 10.0.1 (La Jolla, CA USA).

RNA-seq analysis of OS exosome treated primary human donor lung fibroblasts

NHLF from a single donor (M48) were plated in triplicate at 100,000 cells/well in 24-well plates in complete FGM and allowed to adhere overnight. Cells were then treated with HOS, 143B, MG63.0 or MG63.2 OS exosomes at 5e9 particles/mL the next day (~24h post-plating) and again at 72h post plating. 24h following the last exosome treatment, RNA was extracted using a Qiagen RNeasy mini kit. Extracted RNA was sent to Novogene Corp Ltd. for sequencing. Samples were tested for quality control by Agilent 2100 Bioanalyzer system and by agarose gel electrophoresis. Libraries were run on a NovaSeq 6000 to generate 150 bp paired-end reads to a target depth of 40M raw reads/sample. Following quality control (FASTQC v0.11.8) and adaptor removal (Trimmomatic v0.39), FASTQ reads were aligned to the human reference genome GRCh38 (Ensembl release 107) using STAR alignment tool (v2.7.10a).

Following alignment, the remainder of downstream analyses were performed using R statistical software (v4.2.3). Unexpressed or lowly expressed genes were filtered out by required a minimum count of 10 in at least 3 samples. Normalization and identification of differentially expressed genes between control and exosome-primed fibroblasts were performed using the DESeq2 package (v1.38.3) requiring

an fdr < 0.05 and a fold change cutoff of 2. Differentially expressed genes were analyzed for enrichment of pathways/processes by screening against curated gene sets within the Molecular Signatures Database (Hallmarks, CP: BioCarta, CP: PID, CP: Reactome, CP: WikiPathways, GO:BP and GO:MF collections) using the "enricher" function within the clusterProfiler (v4.6.2) package (fdr < 0.05). Graphical representations of gene expression analyses were created using ggplot2 (v3.4.4), EnhancedVolcano (v1.16.0), and ComplexHeatmap (2.14.0).

Multiplex cytokine analysis of lung fibroblasts

Multiplex cytokine analysis of control and OS-exosome treated lung fibroblasts was performed using a human cytokine/chemokine/growth factor 45-Plex Panel (Invitrogen, EPXR450-12171-901). Both male and female donor NHLF (M29, F62) were treated by OS-exosomes from n=4 cell lines that were sex matched to the fibroblast donor. Male were MG63.0 and MG63.2 and female were 143B and HOS. For exosome treatment, 10,000 NHLF were plated in triplicate in 96-well plates and allowed to adhere overnight in complete FGM. At 24- and 72-hours post-plating, NHLF were treated with either sf-DMEM alone (control) or OS-derived exosomes at 5e+9 exosomes/mL in sf-DMEM. Twenty-four hours after the last exosome treatment, conditioned media was harvested, and supernatant obtained by centrifugation at 10,000 xg to remove cell debris. Cytokine concentration in NHLF supernatant was then measured according to the kit manufacturer's protocol. In a second set of independent experiments, 10,000 NHLF (n=3 donors; F62, M29, M12) were plated in the same manner and underwent the same tumor-derived exosome treatment protocol as described above. Exosome treatment conditions included: 1) OS exosomes (n=5 cell lines), other tumor histotype exosomes (n=5; MB231, MB468, Malme-3M, T84, TCCSUP), or untreated control (sf-DMEM). Conditioned media from these conditions as well as tumor-derived exosome preparations alone (n=10) were analyzed for cytokine secretion using the same kit and protocol as described above. Samples were run on a Luminex MagPix instrument. Quality control and initial processing of data was performed with Luminex xPONENT software, prior to export and further analysis with GraphPad Prism version 10.0.1 (La Jolla, CA USA).

Primary human lung fibroblast-osteosarcoma cell co-culture experiments

10,000 NHLF were plated in triplicate in flat-bottom 96-well plates and allowed to adhere overnight in complete FGM. The next day, media was removed and NHLF were then treated with either sf-DMEM alone (vehicle) or sf-DMEM containing OS exosomes (n=4) at $5e^9$ exosomes/mL every 48 hours for 3 total treatments. 24 hours after the 3rd exosome treatment, Nuclight Red-labeled OS cells in sf-DMEM were seeded in triplicate at 100 cells/well either alone (control), or in wells containing 'uneducated' NHLF, or NHLF 'educated' with OS exosomes matched to that respective OS cell line. RFP+ OS cell survival/proliferation was monitored and quantified using the Incucyte S3 live cell imaging system for 7 days. During this 7-day culture period, OS-NHLF co-culture wells either received no additional exosome treatment or received 3 additional OS exosome treatments ($5e^9$ exosomes/mL every 48 hours). Nuclear labeled (RFP) OS cell survival and proliferation was assessed every 24 hours for 7 days using the Incucyte S3 live imaging system (Sartorius Inc, Göttingen, Germany). RFP+ OS cells/well were quantified using the Incucyte Image Analysis software and OS cell survival/proliferation was quantified as the fold change in RFP+ cell count per well by dividing day 7 RFP+ OS cell counts by post-plating baseline RFP+ OS cell counts.

NHLF cell survival/proliferation assays

7500 NHLF were plated in 96-well plates in triplicate overnight in complete FGM. NHLF were treated with $1e^9$ exosomes per mL (n=4) 24 and 72 hours post plating. At 96 hours post-plating, NHLF were fixed using 2% paraformaldehyde for 10 min prior to being fluorescently labeled using NucSpot live cell nuclear labeling (Biotium) following manufacturer's protocols, then imaged using the Incucyte S3 live cell imaging system (Sartorius Inc. Göttingen, Germany). Cell survival/proliferation was quantified as an endpoint change in RFP+ cell count per well.

Western blot analysis of exosome treated NHLF

Changes in canonical CAF marker expression by NHLF in response to OS exosome treatment were assessed by western blot analysis. NHLF were treated with exosomes as previously described,

lysates were generated using M-PER buffer (Thermo) supplemented with phosphatase and protease inhibitors (Pierce), and protein concentration was measured by BCA. 10 μg of protein was loaded into each well in a 10-well mini-Protean TGX gel 4-20% (BioRad, Cat# 4561094) run in 1x loading buffer (Bio-Rad, Cat#10026938) at 180 V for 40 min. on a PowerPac basic power supply (BioRad, Cat# 1645050) prior to transfer to PVDF membrane (BioRad, Cat# 1620174) using the TransBlot turbo transfer system (BioRad, Cat# 17001915) for 7 min. Membranes were blocked for 1 hour in 5% BSA in TBST prior to overnight incubation at 4°C with, anti-human, rabbit FAP and α-SMA antibodies diluted 1:1000 in 5% BSA in TBST (Invitrogen, CAT# PA5-32765, Proteintech, Cat# 55135). Membranes were washed 3x for 5 in each using TBST prior application of secondary anti-rabbit HRP conjugated antibody (Cell Signaling Technologies, Cat#7074) diluted to 1:5000 in 5% BSA in TBST for 1 hour prior to 3x additional 5 min washing steps in TBST. Membranes were imaged using the Chemidoc XRS+ imaging system (Bio-Rad) using the Clarity Max Western ECL substrate (Bio-Rad, Cat# 170562). Densitometry analysis was performed using ImageJ software, and adjusted band volume was normalized to loading control (GAPDH).

Migration Assay

Normal human lung fibroblasts (M48) were plated in triplicate in 12-well plates at 150,000 cells per well for 24 hours in FGM. After which, media was removed and replaced with sf-DMEM alone as vehicle control or with 1E9 exosomes per mL in sf-DMEM at 0.5 mL with full media replacement per well at 24- and 72-hours post-plating. Supernatants were collected, centrifuged at 10,000 xg to remove cell debris, and validated for IL-6, CXCL8, and CCL2 concentrations by ELISA. 150 µL of exosome treated fibroblast supernatants, sf-DMEM as negative control, 10% serum complete DMEM, and sf-DMEM containing 1ng/mL recombinant CCL2 (Peprotech, Cat# 300-04) as positive controls were loaded into the bottom chamber of a 5 µm HTS Trans-well 96-well support (Corning, Cat# 3387). Prior, THP-1 cells (ATCC, Cat# TIB-202) were grown in complete serum RPMI until reaching desired concentration. Cells were counted and plated in the upper chamber of the trans-well support in 50 µL at 50,000 cells per well for 4 hours followed by image analysis using confocal microscopy.

Statistical analyses

Samples were not randomly assigned to experimental groups, and experimenters were not blind to group assignment and outcome assessment. For the comparison of mean values between three or more groups, a one-way ANOVA with Tukey's post-test was performed. For comparison of means between two groups, or comparison of repeated measures between two groups, a two-tailed, unpaired Students' *t* test or Wilcoxon matched-pairs t test was used, respectively. All statistical analyses were performed using Graph Pad Prism software, version 10 (La Jolla, CA, USA). Unless otherwise specified, all data are representative of at least three independent experiments, and all results are expressed as the mean ± standard deviation, with each dot representing individual measurements.

Data Availability Statement

All data generated in this study are available within the article and its supplementary data files and are available upon request from the corresponding author. Raw RNA sequencing data from this study are publicly available for download from the Sequence Read Archive under BioProject PRJNA1231444.

Results

Isolation and characterization of osteosarcoma cell-derived exosomes

To first confirm our ability to effectively isolate a pure population of exosomes from human osteosarcoma (OS) cell lines, we characterized exosome production from the paired isogenic high and low metastatic cell lines 143B/HOS and MG63.2/ MG63.0, respectively, as well as U2OS and SAOS-2 cells. Extracellular vesicles enriched from OS cell-conditioned media by ultrafiltration and size exclusion chromatography were of high concentration and of the expected size range for exosomes based on particle analysis by tunable resistive pulse sensing (TRPS), with a mean particle diameter ranging from 125-138 nM and mode particle diameter ranging from 86-116 nM (Fig. 2.1A). Additionally, 143B and SAOS-2 exosomes were imaged using transmission electron microscopy, which also demonstrated the expected size and sphere-shaped morphology of exosomes (Figure 2.1B). Moreover, flow cytometric analysis of these particles demonstrated high expression of the putative exosome markers CD9, CD63, and CD81 (Fig. 2.1C), which was also confirmed by western blot analysis (Fig. 2.1D).

Primary human donor-derived NHLF efficiently internalize OS exosomes in vitro

To determine if healthy human lung fibroblasts (NHLF) are capable of internalizing OS-derived exosomes in vitro, NHLF from both male and female donors (n=4 independent donors, supplementary table S1) were treated with equal numbers of PKH26-labeled OS exosomes from n = 6 OS cell lines for 4 hours prior to flow cytometric analysis. PKH26 labeled exosomes from all 6 OS cell lines were efficiently taken up by all 4 independent donor NHLF cell lines *in vitro*, with over 90 percent uptake compared to the unstained exosomes and dye only controls. (Fig. 2.1E-G, Supplementary Table S2). Evaluation of PKH26+ exosome geometric mean fluorescent intensity (gMFI) across fibroblast donors and OS cell lines demonstrated differences in exosome uptake according to fibroblast donor and OS cell line, with the high metastatic cell line 143b demonstrating the greatest mean uptake of exosomes across all donors and M54 NHLF internalizing more PKH26+ exosomes compared to other donors. (Fig. 2.1F, G). Confocal fluorescent microscopy of NHLF (donor F62) treated for 4 hours with PKH26 labeled exosomes also

confirmed intracellular uptake of OS-derived exosomes (Fig. 2.1H). These data demonstrate that primary human lung fibroblasts are capable of robust internalization of OS exosomes, and that this exosome uptake is conserved across a panel OS cell lines and multiple independent male and female donor lung fibroblasts.

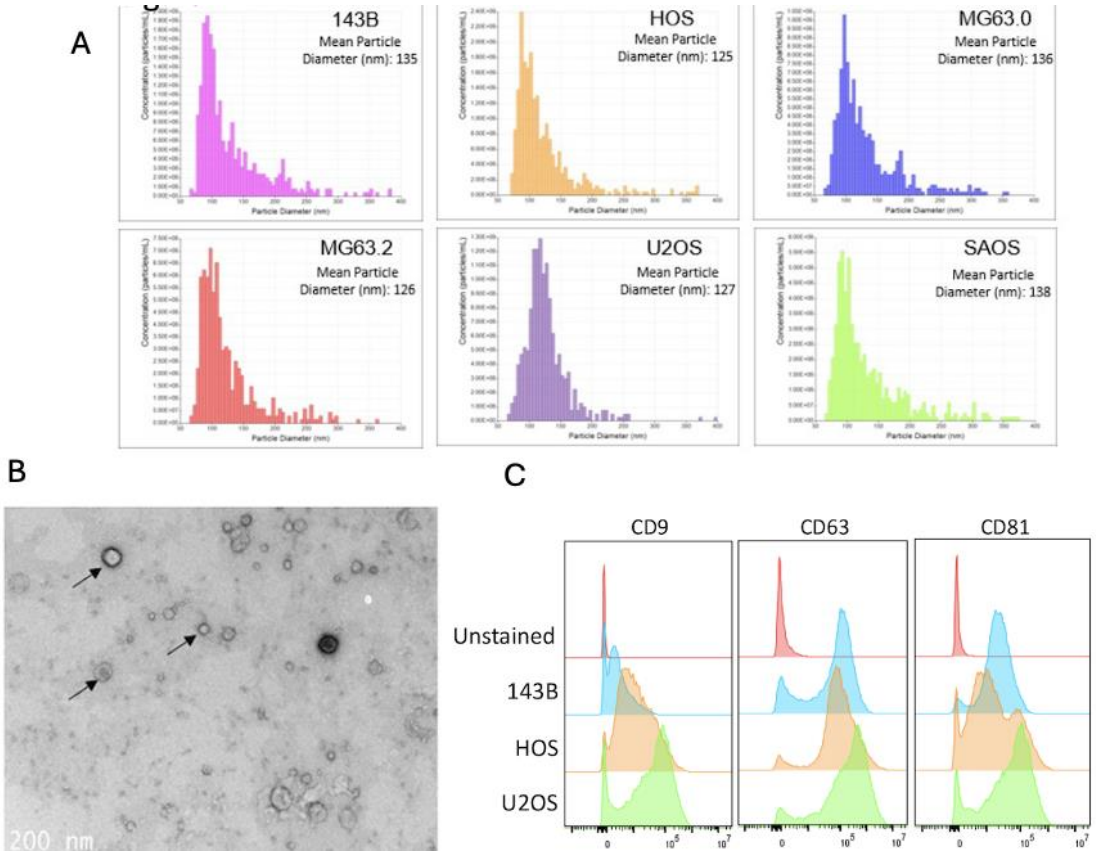

Figure 2.1. Characterization of isolated OS-derived exosomes and quantification of OS exosome uptake in NHLF a) Tunable pulse resistance sensing analysis (TRPS, Qnano) of exosomes isolated from OS cells lines (n=6) represent median and mode particle diameter and particle counts per mL. **b)** Transmission election micrograph of 2% uranyl acetate negative staining of 143B exosomes captured on carbon coated microgrids. Scale bar = 200 nm. **c)** Flow cytometry analysis of exosome markers CD9, CD63, and CD81 on OS cell lines (n=3).

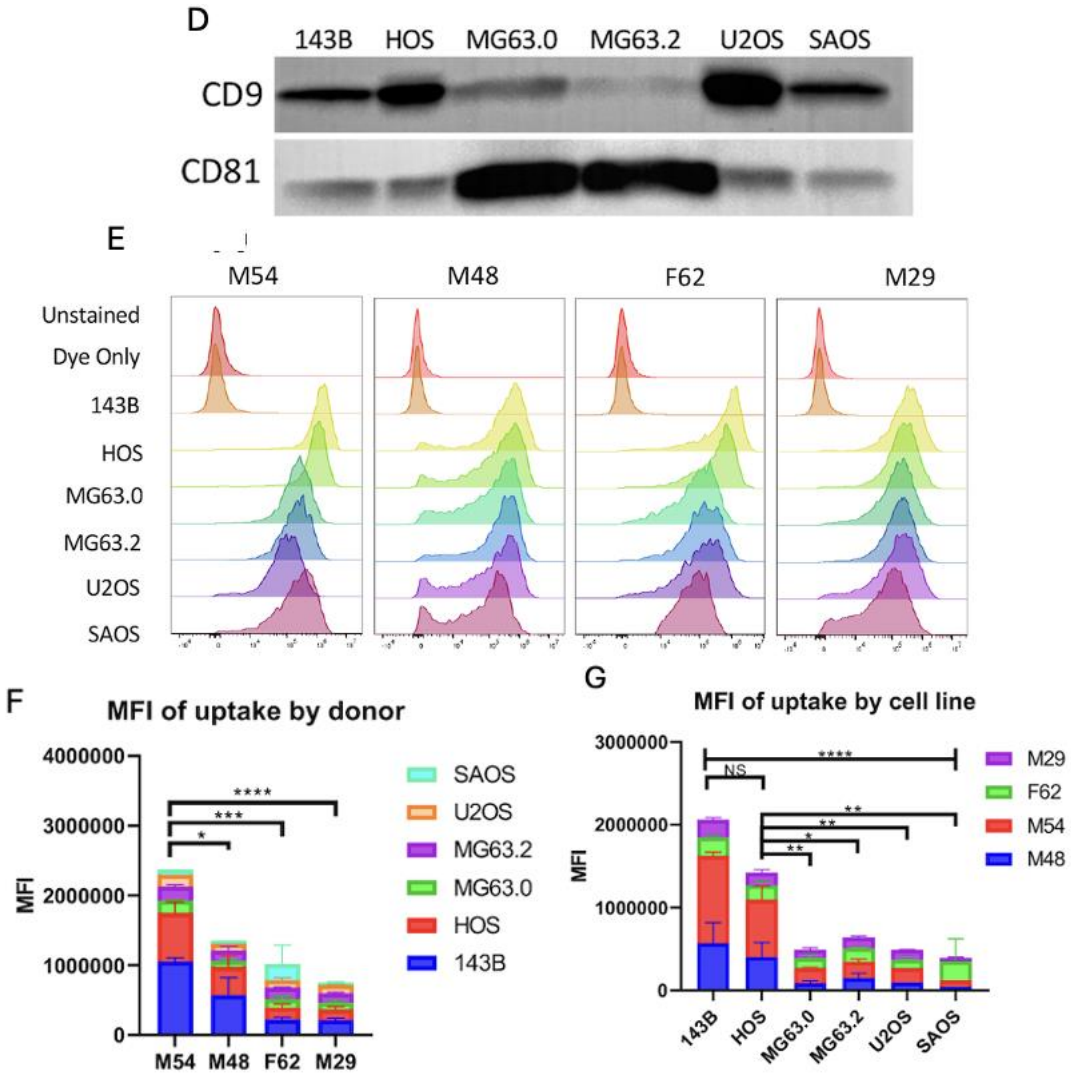

Figure 2.1. Characterization of isolated OS-derived exosomes and quantification of OS exosome uptake in NHLF D) Western blot analysis of exosome markers CD9 and CD81 on OS-derived exosomes (n=6). **E)** Flow cytometry analysis of internalized fluorescently labeled (PKH26) exosomes from 6 OS cell lines, dye only control, and 143B unstained control across 4 donor-derived NHLF cell lines. **F)** Mean fluorescent intensity (gMFI) of PKH26-OS exosome uptake (n=6) separated by donor NHLF (n=4) g) gMFI of PKH26-OS exosome uptake separated by OS cell line. Results from technical replicates.

)

H

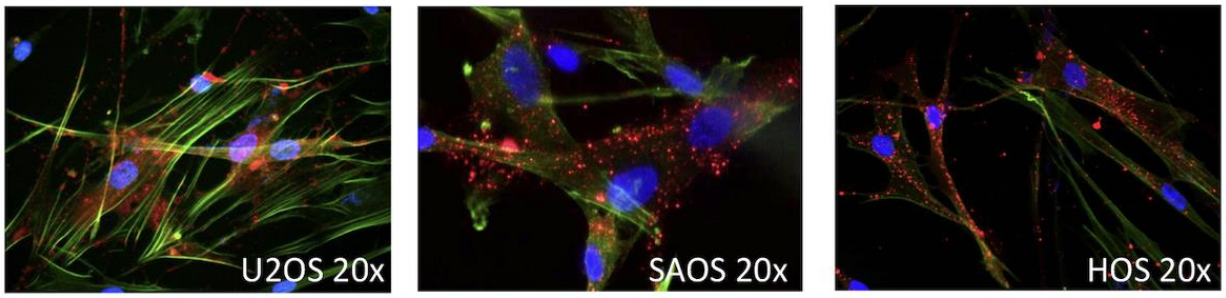

Figure 2.1. Characterization of isolated OS-derived exosomes and quantification of OS exosome uptake in NHLF H) Fluorescent confocal microscopy images of PKH26-OS exosomes (n=3) internalized by actin green (green) and DAPI (blue) counter stained F62, donor-derived NHLF. 2-way ANOVA and Tukey's multiple comparisons * < 0.05 ** < 0.01 *** < 0.001 **** < 0.0001

RNA sequencing of OS exosome treated fibroblasts reveals gene signatures associated with hallmark CAF phenotypes

Given efficient internalization of OS-derived exosomes by lung fibroblasts, we sought to identify transcriptomic responses indicative of possible exosome mediated phenotypic or functional changes in lung fibroblasts. RNA sequencing of lung fibroblasts in response to OS-derived exosome treatment revealed 488 significantly differentially expressed genes, with 347 upregulated and 141 downregulated genes (Fig. 2.2A). Of the top 50 differentially expressed genes (Fig. 2.2B), many were associated with hallmark CAF phenotypes, including upregulation of cytokine and chemokine expression (CXCL-1, 3, 6,10, IL-6, CCL2), extracellular matrix remodeling (MMP3, periostin, elastin, collagens type 1,4), angiogenesis (angiopoietin like 1, bradykinin receptor B1), and proliferation (E2F1, GTSE1). Pathway analysis of differentially expressed genes in response to exosome priming revealed enrichment of gene sets related to previously documented biologically relevant CAF subsets including inflammatory CAFs (iCAFs) and myofibroblastic CAFs (myCAFs). Enriched gene sets included pathways involved in cytokine and chemokine activity, immune suppression, myeloid cell chemotaxis, as well as proliferation, epithelial to mesenchymal transition, and collagen production/fibrosis (Fig. 2C, D). Furthermore, genes enriched in the gene set "proinflammatory and profibrotic mediators" (Fig. 2.2D) consist of upregulation of molecules previously implicated in OS lung metastasis, such as IL-6, CCL2, and CXCL8,(Itoh, Kadomatsu et al. 2018) or reported to be upregulated in metastasis-associated fibroblasts (MAFs) in other cancers.(Asif,

Longobardi et al. 2021) Together, these transcriptional changes suggest that OS exosomes can promote rapid transition of normal lung fibroblasts into a metastasis-associated fibroblast phenotype.

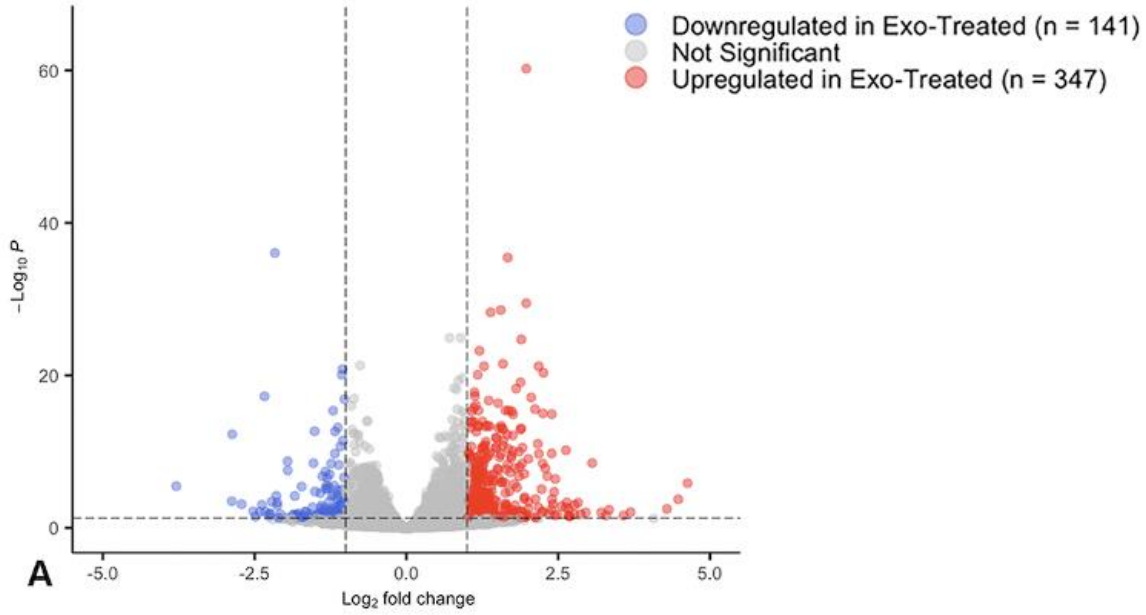

Fig 2.2 OS-derived exosomes induce differential expression of genes associated with hallmark CAF phenotypes A) Volcano plot of differentially expressed genes in NHLF in response to OS exosome treatment (n = 4 human OS cell lines). 347 upregulated genes (red) and 141 downregulated genes (blue) at adjusted p value < 0.05 and fold change cutoff of 2.

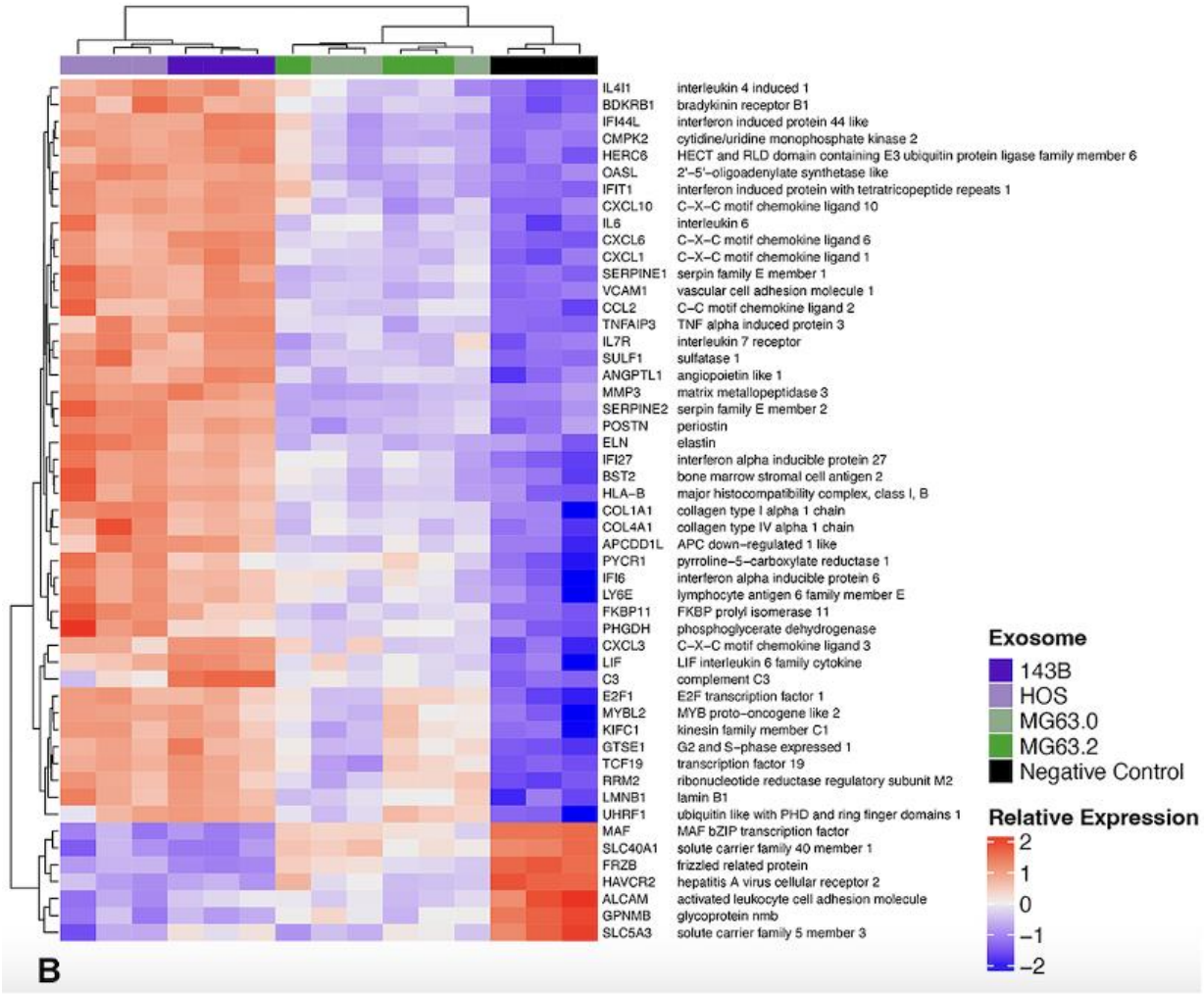

Fig 2.2. OS-derived exosomes induce differential expression of genes associated with hallmark CAF phenotypes B) Heatmap of the 50 most significant differentially expressed genes comparing OS exosome treatment (143b, HOS, MG63.0, MG63.2) and untreated control.

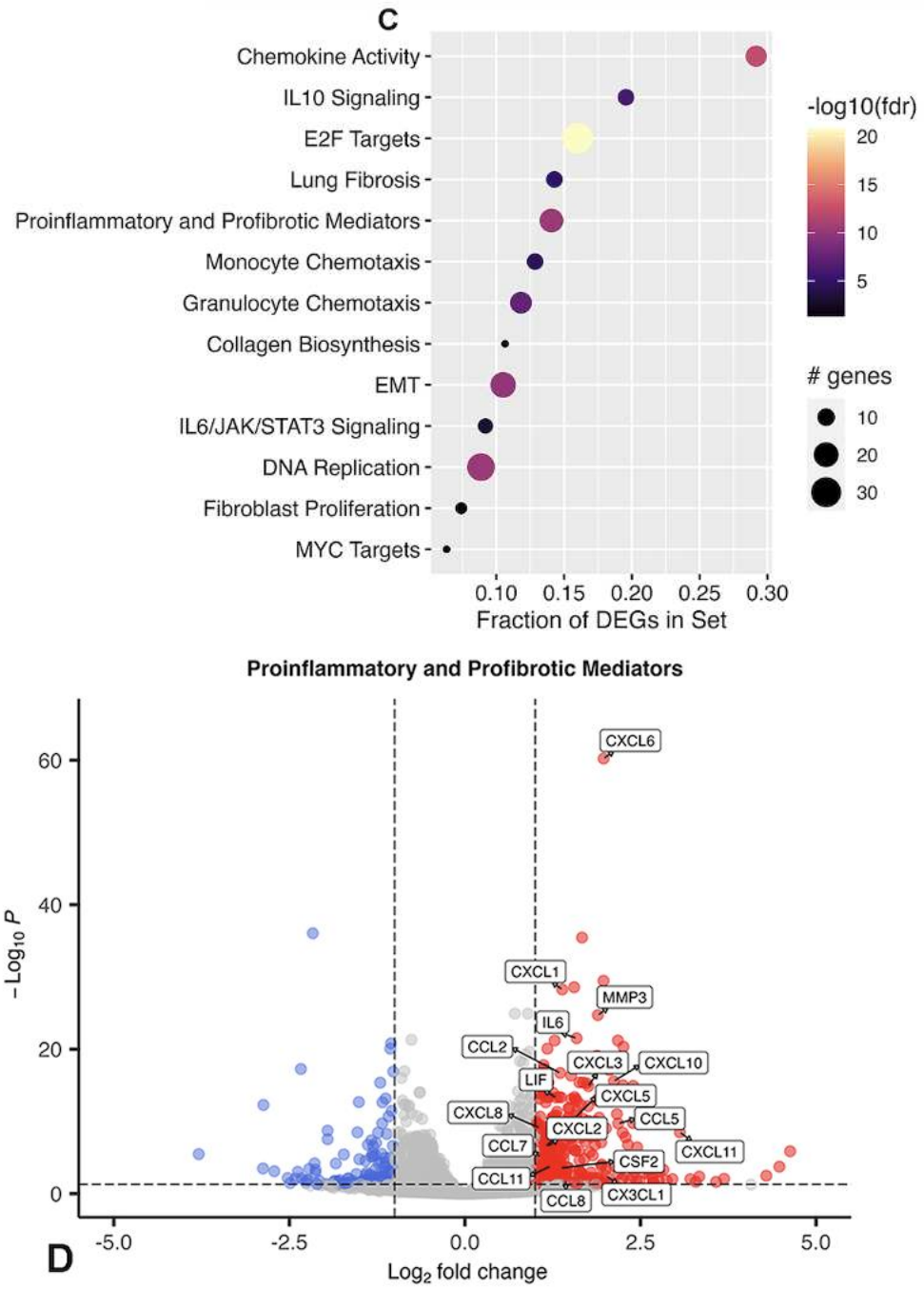

Fig 2.2 OS-derived exosomes induce differential expression of genes associated with hallmark CAF phenotypes C) dot plot of selected enriched pathways/processes from the cluster profiler gene enrichment tool. **D)** volcano plot of differentially expressed genes within the proinflammatory and profibrotic mediator's gene set.

OS exosomes promote proliferation and differential kinase activation in lung fibroblasts

Tumor exosome internalization has been shown to modulate recipient target cell phenotype through activation of a host of signal transduction pathways.(Chen, Guo et al. 2018) As a first step to identify potential molecularly targetable pathways mediating OS exosome-induced activation of lung fibroblasts, we semi-quantitatively analyzed phosphorylation changes in 46 different kinases across four separate donor lung fibroblasts following 4 days of 'education' with 143B OS exosomes (F62, M12, M48 and M54). Focusing only on those kinases which were detectable across all four donor lung fibroblasts,143B exosome treatment induced variably increased phosphorylation of 7 different kinases relative to donor-matched untreated control fibroblasts, including HSP27, GSK-3b, PLC-g1, STAT5a/b, WNK1, PRAS40, and STAT3 with significantly increased phosphorylation of HSP27, PRAS40, and STAT3 across all four donors (Fig. 2.3A, B).

As all three of these molecules represent either substrates or upstream activators of the MAPK and Akt/mTOR pathways, we next sought to analyze activation of these specific pathways using a quantitative bead-based phospho-protein assay. For these assays, we treated F62 donor lung fibroblasts with exosomes derived from a larger panel of OS cell lines (n=5; 143B, HOS, MG63.0, MG63.2, SAOS), and compared OS exosome induced kinase activation in LFs to that observed for exosomes derived from a panel of five other highly lung metastatic, non-OS, human tumor cell lines. Indeed, similar to results observed with the immunoblot kinase array, F62 NHLF relative phosphorylation levels across treatment with all n = 5 OS cells demonstrated significant increases in HSP27, p38 and ERK1/2 phosphorylation relative to NHLF treatment with exosomes derived from non-OS tumor cell lines (Fig. 2.3C); however, no statistically significant phospho-proteins were upregulated in the AKT/mTOR pathway. These data identify key intracellular signal transduction pathways whose activation in response to OS-derived exosomes is conserved across multiple OS cell lines and donor fibroblasts.

Given that OS-exosome treatment of lung fibroblasts induced 1) enrichment of gene signatures associated with cell proliferation, and 2) phosphorylation of pro-proliferation/survival signal transduction pathways which have been implicated in transition of resident fibroblasts to a canonical CAF phenotype in primary tumors,(Wu, Yang et al. 2021) we hypothesized that OS exosomes may be mediating a similar global transition in cell state from a quiescent lung fibroblast to a cancer-associated fibroblast (CAF) phenotype. To investigate this, NHLF survival and proliferation in response to OS exosome treatment was evaluated with live cell imaging. Compared to untreated control NHLF, we observed statistically significant increases in NHLF survival/proliferation in response to treatment with HOS, MG63.0, and MG63.2 exosomes across 3 independent fibroblast donors (Fig. 3D). Additionally, we evaluated the expression of canonical CAF markers, a-smooth muscle actin (a-SMA) and fibroblast activated protein (FAP) by western blot analysis of OS-exosome treated NHLFs; however, no significant upregulation of these markers in response to OS exosome treatment was observed (Fig. 3E).

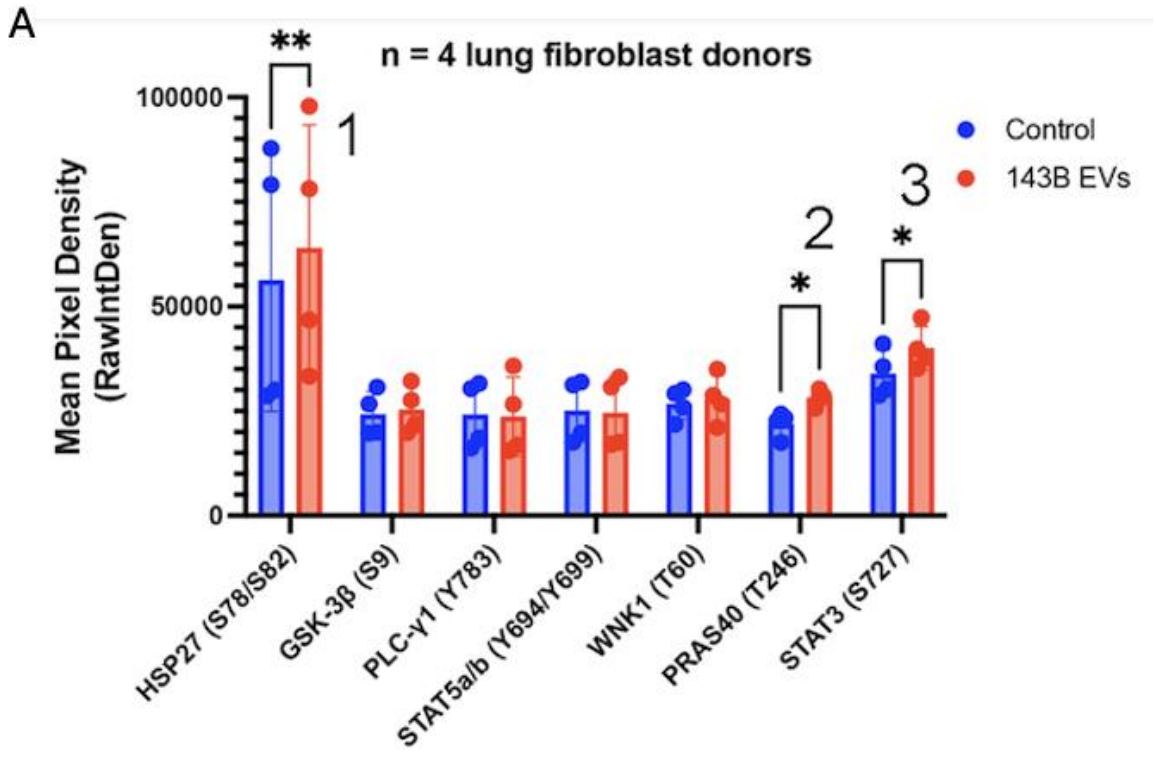

Figure 2.3 OS-derived exosomes induce signal transduction pathways, enhance proliferation, but do not induce expression of canonical CAF markers in NHLF, *in vitro* A) Bar graph of normalized fold-change integrated intensity from human phospho-protein array depicting the most upregulated phospho-proteins in NHLF (n=4) after 143b exosome treatment across 39 analytes.

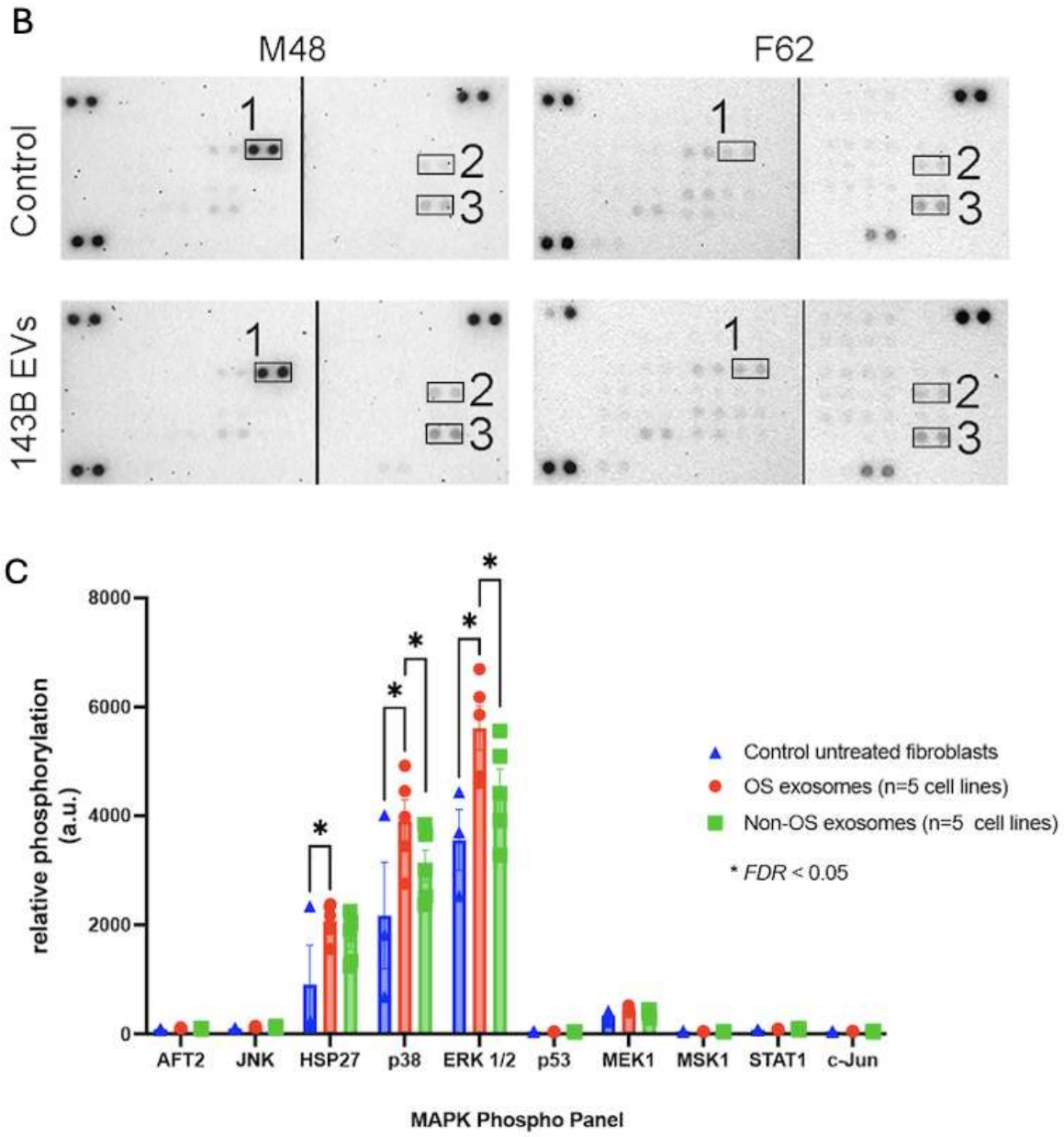

Figure 2.3 OS-derived exosomes induce signal transduction pathways, enhance proliferation, but do not induce expression of canonical CAF markers in NHLF, *in vitro* B) Representative images of untreated and 143B treated F62 and M48 NHLF phospho-protein array. **C)** Analysis of MAPK pathway activity comparing untreated control and pooled, OS-exosome treated (n=5) F62 NHLF measured by bead-based phospho-protein array. 2-way ANOVA and Sidak's multiple comparisons test were used to analyze bead-based assays, * < 0.05

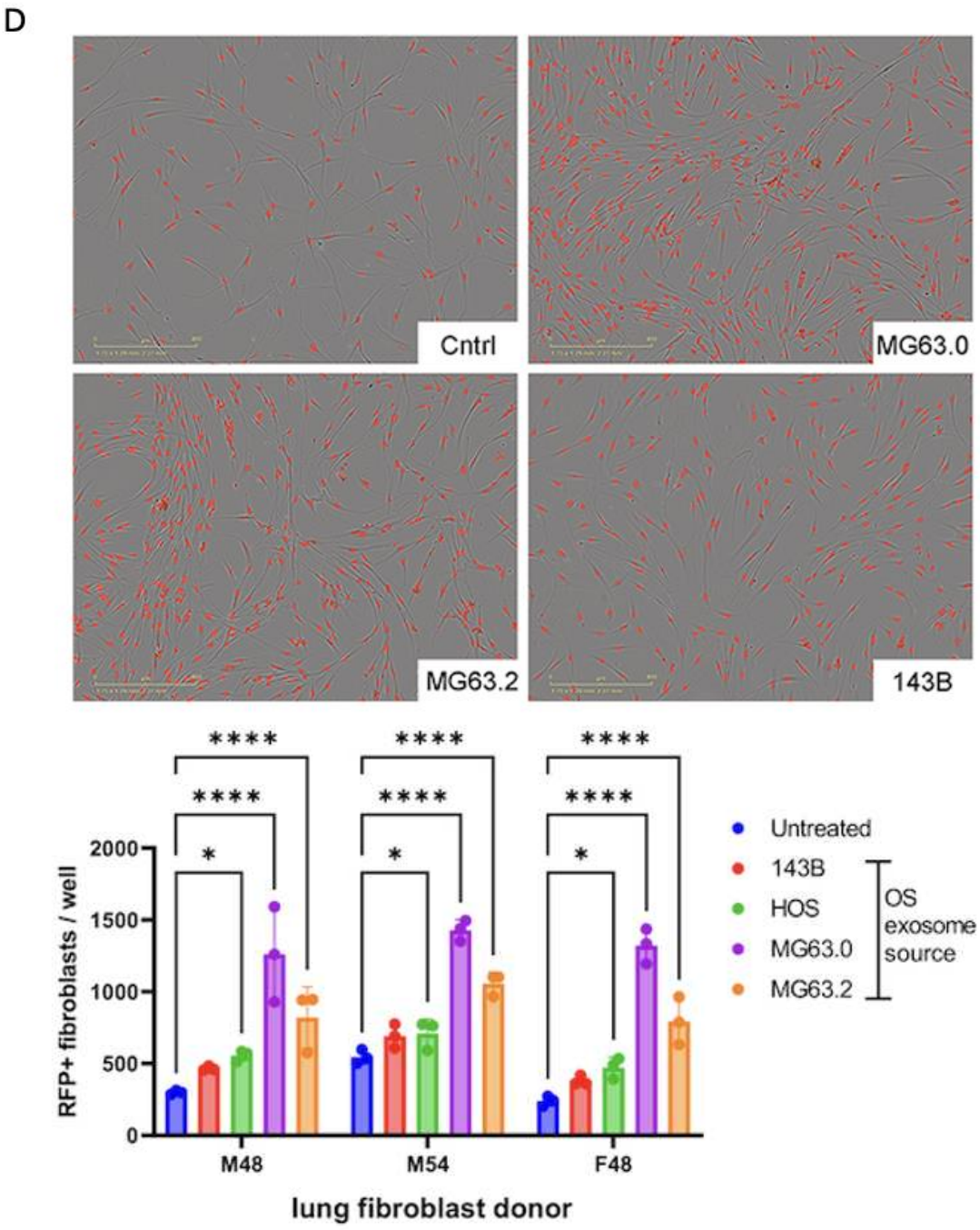

Figure 2.3 OS-derived exosomes induce signal transduction pathways, enhance proliferation, but do not induce expression of canonical CAF markers in NHLF, *in* d) End-point fibroblast proliferation across 3 independent donors comparing untreated, serum-free control and OS-exosome (n=4) treated fibroblasts and corresponding representative live cell imaging. Results show mean +/- SD of technical replicates. 2-way ANOVA and Tukey's multiple comparisons * < 0.05 ** < 0.01 *** < 0.001 **** < 0.0001

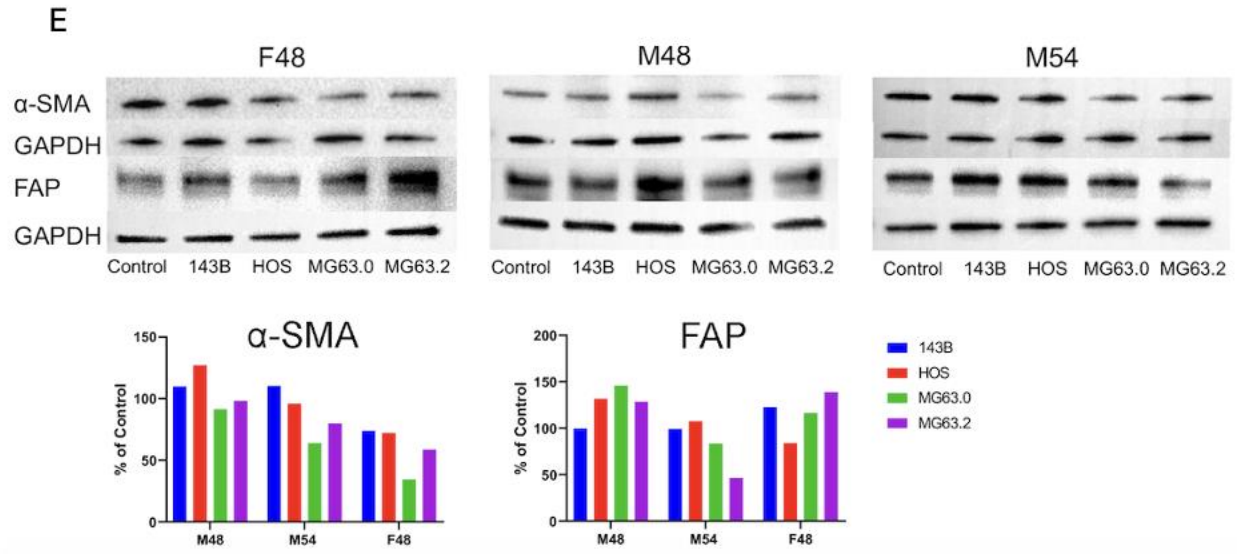

Figure 2.3 OS-derived exosomes induce signal transduction pathways, enhance proliferation, but do not induce expression of canonical CAF markers in NHLF, *in vitro* **E)** Western blot analysis of lysates generated from untreated, serum-free control and exosome (n=4) treated NHLF (n=3) to determine expression of canonical CAF markers alpha smooth muscle actin (α-SMA) and fibroblast activated protein (FAP) followed by densitometry analysis.

OS-exosomes induces an inflammatory, pro-tumorigenic secretome in primary human lung fibroblasts

Cancer-associated fibroblasts (CAFs) within the primary tumor microenvironment (TME) have been shown to mediate their pro-tumorigenic functions through secretion of a variety of soluble mediators, including growth factors, cytokines, and chemokines. As our transcriptomic analysis of OS exosome treated lung fibroblasts suggested enrichment of a similar iCAF-like phenotype, we hypothesized that normal lung fibroblasts would respond to priming with OS-derived exosomes in a similar manner, upregulating secretion of known pro-metastatic cytokines. To characterize the secretory phenotype of NHLF in response to OS exosome 'education', conditioned media from OS-exosome treated fibroblasts were assessed using a bead-based, 45-plex cytokine array. Analysis of pooled triplicate means from n = 2 NHLF donors (1 male and 1 female) treated with OS exosomes derived from n = 4 cell lines (MG63.0, MG63.2, HOS, and 143B) demonstrated significantly (adj $P < 0.05$) increased secretion of IL-6, CXCL8 and CCL2 in conditioned media of OS exosome 'educated' lung fibroblasts as compared to untreated

NHLF (Fig. 2.4A;), with mean increases in OS exosome educated vs. control NHLF of 10,876 pg/mL, 6,446 pg/mL, and 6,077 pg/mL for IL-6, CCL2, and CXCL8, respectively. Additionally, analysis of this data using NHLF from both female (F62) and male (M12) donors sex matched and paired to isogenic low and high-metastatic respective male (MG63.0/MG63.2) and female (143B/HOS) OS cell lines demonstrated that while secretion of these molecules does not appear to be dependent on the sex of OS exosome donor or recipient fibroblast cell line, there was significantly increased fibroblast secretion of IL-6, CCL2, and CXCL8 in response to exosomes derived from the high metastatic 143B clone, and increased CCL2 secretion in response to exosomes from the high metastatic MG63.2 clone, as compared to the low metastatic subclones (Fig. 2.4B).

Next, to determine if this OS-exosome induced secretory profile in NHLF was a unique response to OS cells, given their high metastatic tropism for the lung, or conserved across other highly metastatic tumor types, we also isolated exosomes from the same panel of five cell lines utilized in the phosphokinase arrays and representing a variety of other tumor histotypes which also display enhanced proclivity for lung metastasis, including: melanoma (Malme-3M), colorectal carcinoma (T84), urothelial carcinoma (TCC-Sup) and two triple negative breast cancer cell lines (MB-231, MB-468). Utilizing the same 45-plex bead-based cytokine array, analysis of supernatants from control untreated NHLF (n=3 independent donors), or NHLF 'educated' with exosomes derived from OS cells (n=5) or tumor cells of other non-OS histotypes (n=5) demonstrated significant (adj $P < 0.05$) differential upregulated secretion of 27 cytokines/chemokines/growth factors in OS-exosome primed lung fibroblasts as compared to priming of NHLF with exosomes of non-OS tumor histotypes (Fig. 2.4C, D), with IL-6, CXCL8 and CCL2 again demonstrating the greatest mean difference between OS exosome treated NHLFs vs non-OS exosome treated NHLFs (Fig. 2.4D, E). Lastly, these same purified exosome preparations used for fibroblast education were also analyzed to determine whether these observations were the result of these cytokines being uniquely present within the exosomes themselves or possibly through their concentration during the exosome isolation process; however, minimal to no detectable levels of these cytokines were observed in the exosome preparations (Fig. 2.4C, E). Together, these data demonstrate that OS exosome treatment of primary human lung fibroblasts *in vitro* significantly upregulates secretion of known pro-metastatic cytokines and chemokines, including molecules previously demonstrated by us and others to be

implicated in OS lung metastasis or metastasis-associated fibroblast function (Gross, Cam et al. 2018). Moreover, these data also demonstrate that this effect is both conserved across multiple biologically independent fibroblast donors and is greater in response to OS exosomes as compared to exosomes isolated from other highly lung metastatic tumor histotypes.

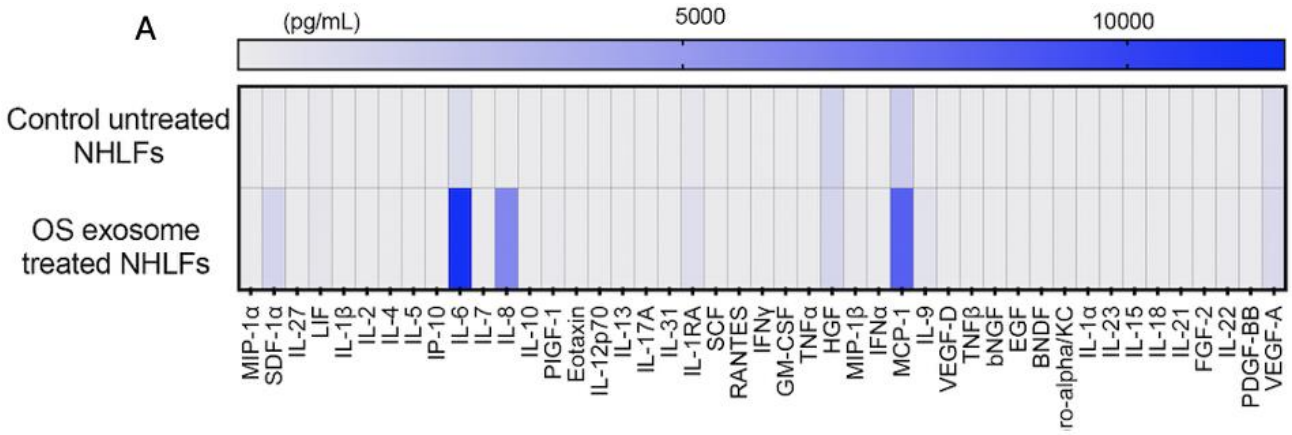

Figure 2.4. OS Exosomes induce pro-tumorigenic secretory profile in NHLF A) Heatmap depicting cytokine secretion in supernatants of pooled OS-educated (n=4) NHLF (n=2) assessed by 45-plex, bead-based cytokine panel. Multiple t tests male and female combined, mean values (pg/mL) **** < 0.0001

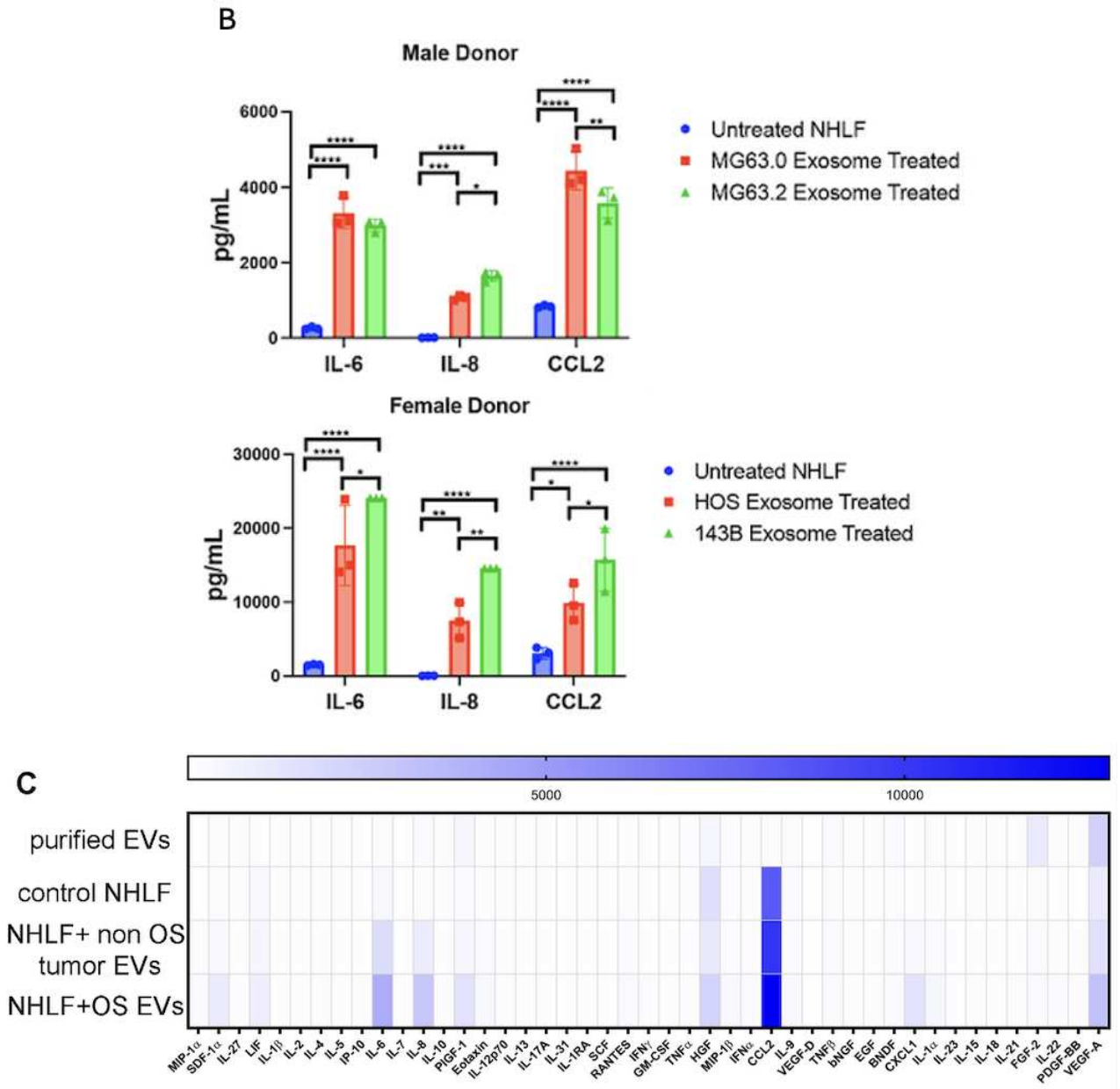

Figure 2.4. OS Exosomes induce pro-tumorigenic secretory profile in NHLF B) Significantly upregulated cytokines from panel a., IL-6, IL-8, and CCL2, with sex matched NHLF donor to OS exosome cell line (Male, MG63.0/MG63.2) (Female, 143b/HOS) 2-Way ANOVA and Tukey's multiple comparisons * < 0.05 ** < 0.01 *** < 0.001 **** < 0.0001 **C)** Heatmap depicting cytokines in pooled exosome preps alone form OS and other cell types (n=10), supernatants of pooled untreated fibroblasts (n=3), pooled exosome treated NHLF from histotypes other than OS (n=5), and OS exosome treated (n=5) NHLF (n=3)

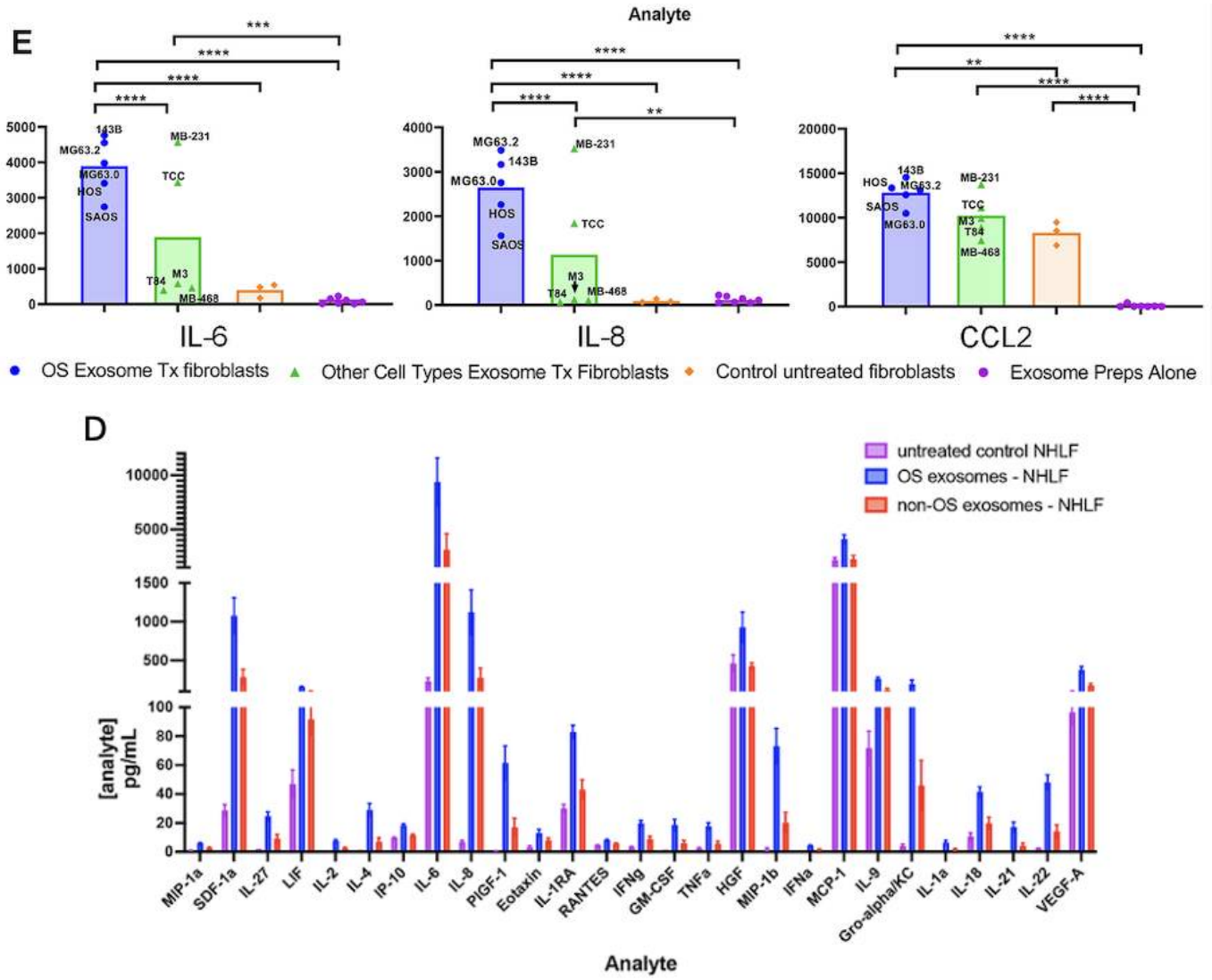

Figure 2.4. OS Exosomes induce pro-tumorigenic secretory profile in NHLF. D) Bar graph showing significant differential cytokine expression across 27 analytes when comparing NHFL (n=3) treated with OS exosomes (n=5) and other cell types (n=5) **E)** Bar graphs depicting mean cytokine concentrations (pg/mL) from the 3 most significantly upregulated cytokines from panel c., IL-6, IL-8, and CCL2 and the respective cell lines' cytokine concentration. 2-way ANOVA and Tukey's multiple comparisons * < 0.05 ** < 0.01 *** < 0.001 **** < 0.0001.

Priming of NHLF with OS-derived exosomes enhances OS cell survival in a primary human lung fibroblast-OS cell co-culture model

Given that OS exosome treatment significantly changed the secretome of lung fibroblasts, including upregulation of cytokines known to have paracrine growth promoting actions on tumor cells, we sought to determine the functional impact of OS-exosome primed NHLF on OS cell proliferation and survival. To do this, we designed a NHLF-OS cell co-culture assay to mimic early tumor cell dissemination to the lung. NHLFs were either pre-treated or continuously primed with OS-derived exosomes before and after low-density seeding (100 cells/well) of matched RFP+ OS cell lines in serum free media onto either a monolayer of exosome primed NHLF, untreated NHLF, or in monoculture control wells (Fig. 2.5A). Growth curves comparing fold change of 143B RFP cell growth/survival over time within the 4 treatment conditions demonstrates significantly enhanced growth within exosome primed NHLF across 3 donors compared to unprimed NHLFs or OS-cells in monoculture (Fig. 2.5B). Importantly, this growth advantage occurred whether NHLFs are treated with exosomes prior to OS-cell seeding only or continuously throughout the duration of culture, and was not observed for OS exosome treatment of OS cell monocultures, suggesting that OS exosomes themselves have no direct effect on OS cell proliferation, either in the presence or absence of lung fibroblasts (Fig. 2.5B) Representative images show the growth advantage conferred to 143B RFP cells by OS-exosome primed NHLF compared to NHLF that did not receive exosome treatments (Fig. 2.5C). Moreover, OS-cell survival was significantly enhanced across multiple NHLF donors and OS cell lines when LFs were primed with exosomes from that respective OS cell line. Exosome priming of all 3 NHLF donors enhanced 143B growth/survival, while 2 NHLF donors (M48 and M54) enhanced MG63.0 cell survival/proliferation, and 1 NHLF donor (M54) significantly increased MG63.2 cell survival/proliferation (Fig. 2.5D, E). As OS exosome treatment of lung fibroblasts promotes significant secretion of CCL2, a chemokine implicated in the recruitment of inflammatory monocytes to early metastatic sites, we sought to determine the functional impact of OS exosome induced NHLF CCL2 production on the chemotactic potential of human THP-1 monocytes. We observed significantly increased THP-1 migration to OS-exosome treated NHLF supernatants, with significant migration in 143B treated NHLF supernatants, as compared to the negative control and untreated

fibroblast supernatants (Fig. 2.5F).

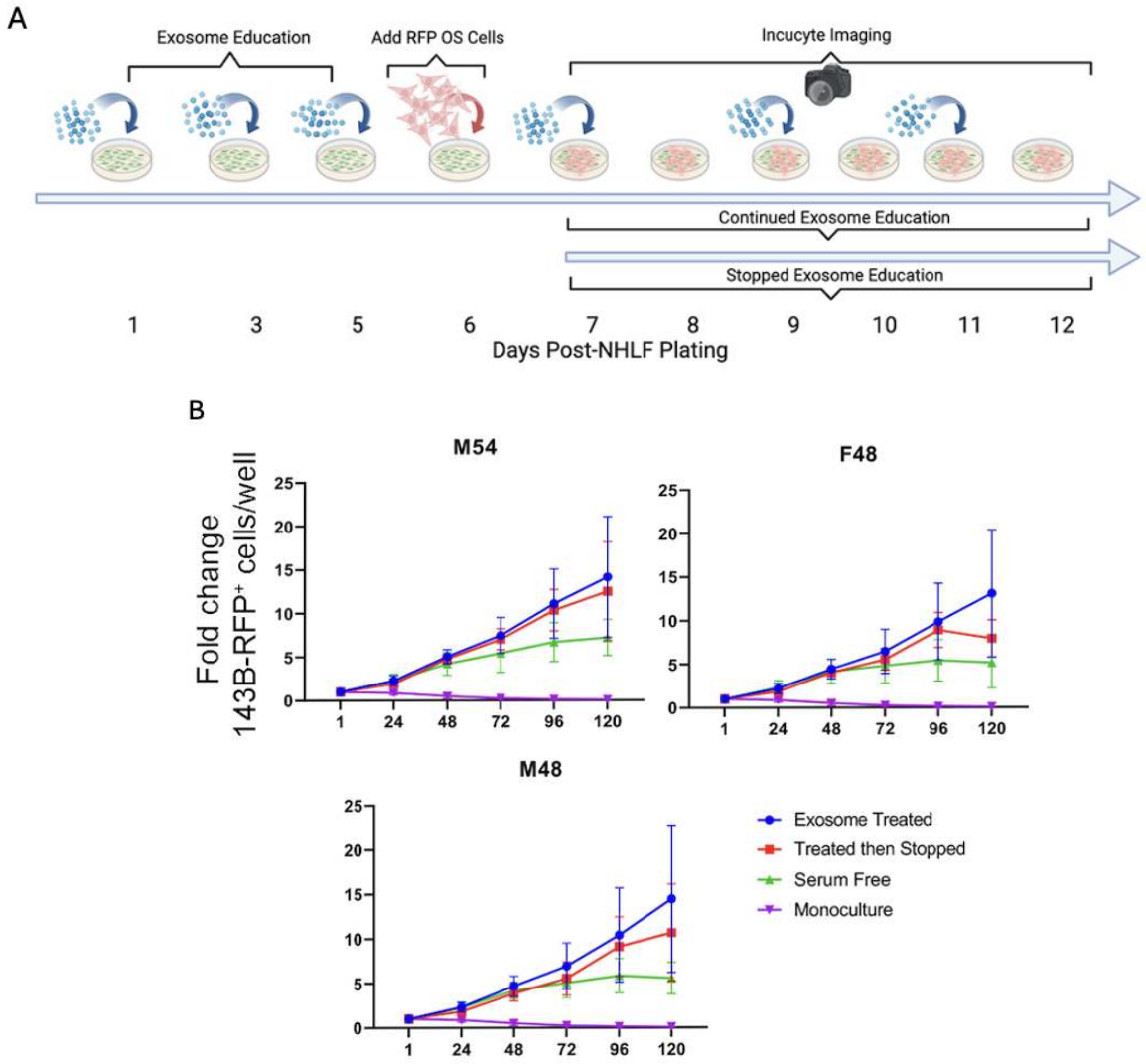

Figure 2.5. Exosome priming of NHLF promotes increased OS survival in an *in vitro* co-culture model and exosome treated fibroblast supernatants promote monocyte migration A) schematic depicting OS-cell, NHLF co-culture model. **B)** fold change growth curves of RFP-labeled 143b OS cells in co-culture with 3 independent NHLF donors that were treated with 143b exosomes throughout the experiment, only prior to OS-cell seeding, serum free untreated control or OS cells in monoculture.

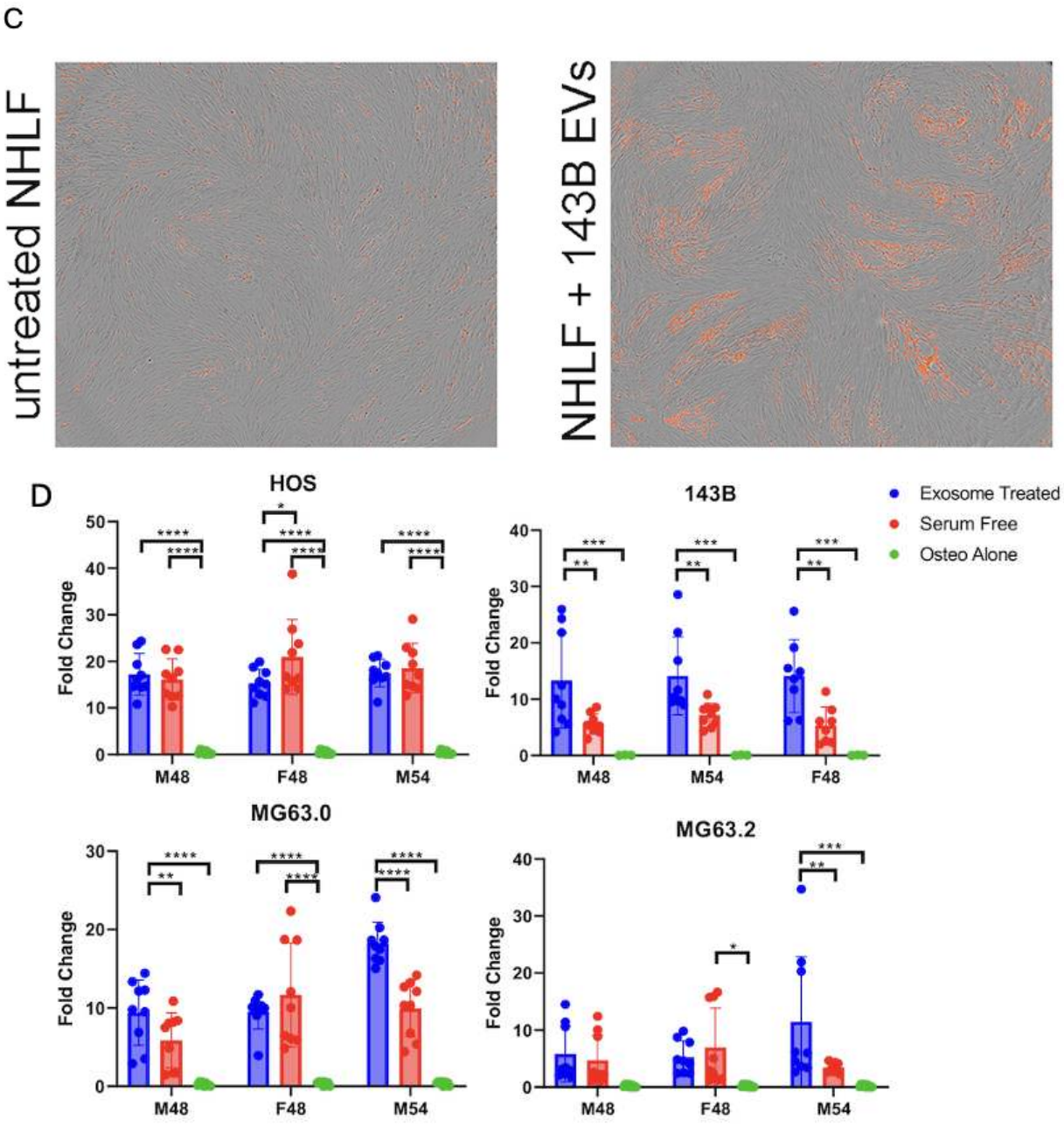

Figure 2.5. Exosome priming of NHLF promotes increased OS survival in an *in vitro* co-culture model and exosome treated fibroblast supernatants promote monocyte migration c) representative images of RFP-labeled 143b cells (Red) in co-culture with NHLF in untreated serum free control or 143b exosome treated conditions. Means of 3 biological replicates +/- SD. d) End-point fold change from co-culture experiments across 3 independent NHLF donors comparing exosome treated, untreated serum free control, and OS cells in mono-culture from 4 OS cell lines. Means of 3 biological replicates +/- SD

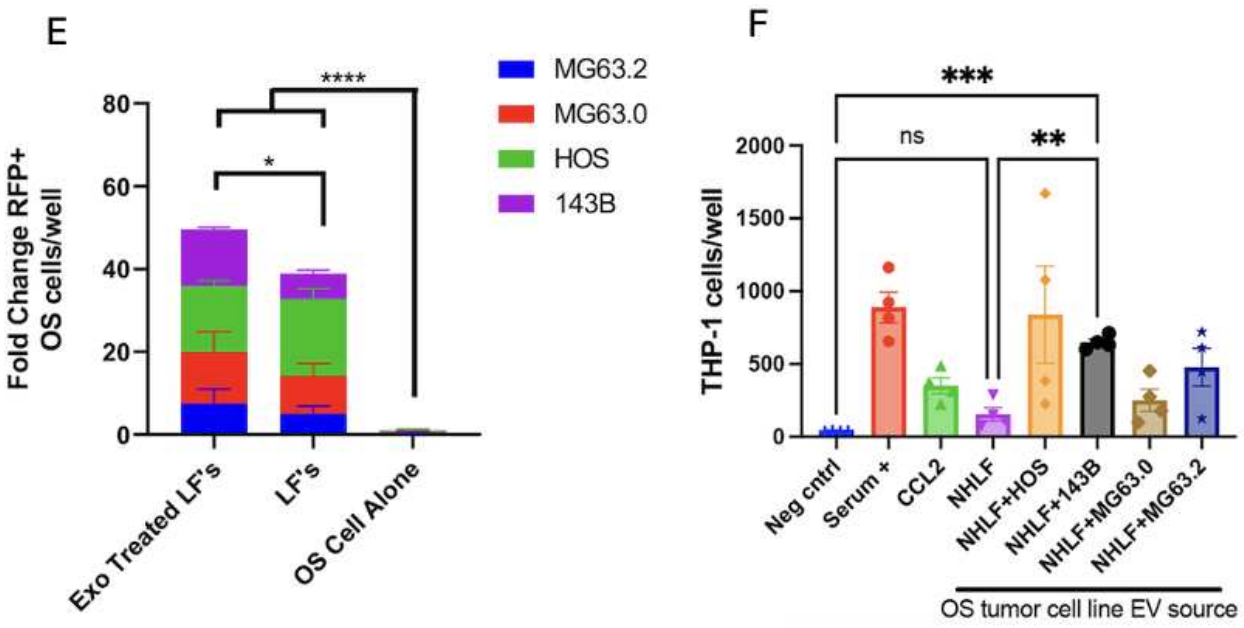

Figure 2.5. Exosome priming of NHLF promotes increased OS survival in an *in vitro* co-culture model and exosome treated fibroblast supernatants promote monocyte migration E) Pooled end-point fold change comparing exosome treated, untreated serum free control and OS cells in monoculture across 3 independent NHLF and 4 OS cell lines. **F)** Migration of THP-1 monocytes toward untreated fibroblast supernatants and OS-exosome treated (n=4) supernatants. 2-way ANOVA and Tukey's multiple comparisons * < 0.05 ** < 0.01 *** < 0.001 **** < 0.0001.

Discussion

In 1889, Stephen Paget first postulated his “seed and soil” hypothesis seeking to explain why certain cancers are predisposed to metastasize to specific distant organs, inciting research into the non-random pattern of cancer metastasis. Over a century later, research investigating extrinsic factors of cancer cells that contribute to metastatic dissemination have identified small, tumor-derived extracellular vesicles as important mediators of this process in multiple cancers with distinct metastatic organ predilections such as melanoma, pancreatic, and breast cancers. (Wortzel, Dror et al. 2019) However, despite osteosarcoma’s striking predilection for lung metastasis, there have been limited investigations into OS tumor-derived extracellular vesicles and their ability to interact with non-malignant resident cell types of the lung. Here, we demonstrate that normal lung fibroblasts rapidly and efficiently internalize OS exosomes across a panel of OS cell lines and fibroblast donors. This OS exosome priming induces distinct transcriptomic changes in lung fibroblasts including upregulation of genes and pathways of canonical cancer-associated fibroblast phenotypes including both myofibroblastic (myCAF) and inflammatory (iCAF) subsets. Moreover, we provide in vitro evidence of OS exosomes’ ability to drive normal lung fibroblasts toward pro-tumorigenic CAF functions including OS exosome mediated fibroblast proliferation, induction of fibroblast secretion of key cytokines and chemokines previously implicated in OS lung metastasis progression, and promotion of OS cell survival in a fibroblast OS cell co-culture model. These data suggest that OS exosomes can promote transition of normal lung fibroblasts into metastasis-associated fibroblast phenotypes with pro-tumorigenic functional consequences, providing rationale for future pre-clinical investigations testing genomic or pharmacologic approaches to interrupt this intercellular signaling as potential anti-metastatic strategies for OS.

Although uptake of exosomes from all 6 OS cell lines occurred in more than 90% of LFs and across all four donor fibroblast cell lines, the degree to which uptake occurred was not equal, both in terms of OS cell line source exosomes and between LF donors. This difference in uptake may simply be the result of inherent biological variability across human donors, or a more specific lock-and-key mechanism based on unique exosome and cell surface ligand-receptor interactions. Indeed, prior studies have demonstrated a dependency on specific cognate integrin receptor repertoires between exosome

and target cells in directing organ specific homing (Pols and Klumperman 2009, Christianson, Svensson et al. 2013, Hoshino, Costa-Silva et al. 2015, Viñas, Spence et al. 2018, Salunkhe, Dheeraj et al. 2020, Cardeñes, Clares et al. 2021); however, these mechanisms have not been described specifically for lung fibroblasts. While the molecular machinery mediating OS exosome uptake by lung fibroblasts was not specifically evaluated in this study, we did identify MAPK/ERK pathway activation in lung fibroblasts in response to OS exosome priming. Importantly, signaling components of the MAPK pathway have been previously reported to mediate uptake of breast cancer EVs by lung fibroblasts. In a high-content screen of FDA-approved anticancer drugs, Wan et al. identified MEK2-dependent micropinocytosis as a requirement for lung fibroblast uptake of MDA-MB-231 breast cancer EVs.(Wan, Zhao et al. 2024)

In addition to MAPK/ERK pathway activation, kinase profiling of lung fibroblasts in response to OS exosome priming also identified significant activation of p38/MAPK, and the upstream activator of ERK1/2, STAT3. ERK1/2, p38 MAPK and STAT3 signaling cascades have all been shown to mediate the transition from a quiescent fibroblast phenotype to a characteristic CAF phenotype associated with CAF induced cancer progression, chemoresistance, and immune suppression.(Alspach, Flanagan et al. 2014, Brichkina, Bertero et al. 2016, Dror, Sander et al. 2016, Karakasheva, Lin et al. 2018, Zou, Tong et al. 2020) Notably, STAT3 has been shown to be overexpressed in OS patient tumor tissues and high STAT3 protein level was associated with increased metastasis and reduced disease-free and overall survival. However, whether STAT3 overexpression in these OS patient tissues was purely restricted to the tumor compartment or was also a result of cancer-associated fibroblast contribution remains unclear, as co-immunolabeling for STAT3 and tumor or fibroblast specific cell phenotype markers was not performed in this study.(Wang, Zheng et al. 2011)

These protein kinases we identified to be activated in OS EV primed lung fibroblasts are also known drivers of secretion of key tumor promoting cytokines and chemokines such as IL-6, IL-8, and CCL2 across a range of cell types, including in fibroblasts.(Suzuki, Tetsuka et al. 2000, Marra, Delogu et al. 2004) In line with these observations, of the 45 cytokines, chemokines, and growth factors assessed in the supernatants of OS exosome treated fibroblasts, IL-6, CXCL8, and CCL2 were the most significantly upregulated proteins, all canonical CAF-secreted cytokines.(Chen, Sun et al. 2015, Chen, Zhou et al. 2020) In the context of premetastatic niche formation, IL-6 can elicit both direct intrinsic effects on cancer

cells, such as cell cycle progression, invasion and metastasis, and indirect, cell-extrinsic effects on the TME, including promotion of angiogenesis, tumor-promoting inflammation, and immune suppression. (Tsukamoto, Fujieda et al. 2018) CXCL8 is a pleiotropic signaling molecule known to mediate CAF-promotion of angiogenesis, epithelial mesenchymal transition (EMT), and recruitment of MDSC's and tumor-associated neutrophils (TANs).(Liu, Li et al. 2016, Asokan and Bandapalli 2021) Specifically in the context of OS, IL-6, CXCL8 and CCL2 have all been linked to promotion of OS lung metastatic progression. Gross et al demonstrated that both IL-6 and CXCL8 secretion by OS cell lines correlated strongly with lung colonization efficiency in murine xenograft models, and that combined blockade of these molecules prevented metastatic growth. (Gross, Cam et al. 2018) Moreover, they demonstrated that both IL-6 and CXCL8 mRNA and protein expression was significantly upregulated in human OS patient lung metastases as compared to matched primary tumors. Intriguingly, IL-6 and CXCL8 immunolabeling was localized along the tumor-lung interface of these metastases, a microanatomical region often spatially enriched for CAFs, suggesting lung fibroblasts may be contributing to this IL-6 and CXCL8 expression given that dual labeling for tumor or fibroblast cell specific phenotype markers was also not performed in this study.

Similarly, targeting of the CCL2-CCR2 signaling axis in OS has also emerged as a potential avenue for antimetastatic immunotherapy. Prior work has demonstrated that both human and canine OS cell lines overexpress CCL2, which is correlated with increased monocyte migration in vitro and monocyte enrichment in patient lung metastases. These studies also showed that losartan, an angiotensin II receptor (AT1R) antagonist used in the treatment of hypertension, can block in vitro CCL2- and OS cell-elicited monocyte recruitment through non-competitive inhibition of CCL2 induced ERK1/2 activation, independent of AT1R signaling. In multiple preclinical mouse models, losartan suppressed lung metastasis via blockade of CCL2-CCR2 monocyte recruitment, and in a clinical trial in dogs with spontaneous lung metastatic OS, losartan in combination with the multi-kinase inhibitor toceranib, was associated with modulation of CCL2-CCR2 pharmacodynamic endpoints and a clinical benefit rate of 50%.(Regan, Coy et al. 2019, Regan, Chow et al. 2022) As a result of this promising pre-clinical data, a clinical trial evaluating losartan in combination with sunitinib as an antimetastatic therapy human pediatric and adult patients with relapsed or refractory OS is currently underway [ClinicalTrials.gov NCT03900793].

Thus, our data suggest that lung fibroblast targeting within the OS TME may represent another potential strategy to block CCL2-mediated monocyte recruitment to lung metastases.

Recent advances in single cell multi-omic technologies have shed light on the spatial, transcriptomic, and functional heterogeneity of CAF subpopulations. CAFs have been subclassified into at least 3 highly plastic subtypes that share several common characteristics while diverging in others. These subtypes have been described as myofibroblast, antigen-presenting, and inflammatory CAFs, or myCAF, apCAF, and iCAF respectively.(Luo, Xia et al. 2022) Our transcriptomic profiling of lung fibroblasts in response to OS exosome education revealed nearly 500 significant differentially expressed genes including many associated with cytokine/chemokine expression, interferon expression, and complement, all genes typical of the iCAF phenotype. Moreover, genes associated with the myCAF phenotype that regulate ECM remodeling, such as various types of collagens, matrix metalloproteases, elastin, and periostin were also highly upregulated upon OS exosome treatment. While fibroblast mediated remodeling or secretion of ECM components within metastatic sites is known to promote circulating tumor cell seeding and outgrowth, the specific upregulation of periostin by LFs in response to OS EVs is intriguing. Specifically, tumor cell induced expression of periostin by resident fibroblasts was shown to be essential for breast cancer lung metastasis through periostin-mediated enrichment of Wnt ligands, and Wnt receptor expression in OS has been associated with OS metastasis in rodent models and worse event-free survival in patients.(Hoang, Kubo et al. 2004) (Malanchi, Santamaria-Martínez et al. 2011) In contrast, genes typically associated with the apCAF phenotype like Serum Amyloid A3, Secretory Leukocyte Pepdidase and Major Histocompatibility complex 2, were not differentially expressed in response to OS exosome education.(Elyada, Bolisetty et al. 2019) In addition to upregulation of genes that partition CAFs into their respective subtypes, pathway analysis revealed gene sets that promote other hallmark CAF functions including angiogenesis, adhesion, and proliferation.

These results, when viewed from the lens of the CAF subtype framework, suggest that OS-derived exosomes may have the capacity to promote transition of normal lung resident fibroblasts towards metastasis-associated fibroblasts exhibiting both myCAF and iCAF phenotypes, providing a rationale for future *in vivo* studies evaluating this mechanism within the context of OS lung pre-metastatic niche formation. These findings parallel those of two other studies evaluating the molecular and functional

changes of fibroblastic cell types in response to human OS cell-derived EV treatment in vitro. Adipose-derived mesenchymal stem cells (MSCs) were also observed to efficiently internalize 143B OS cell EVs, which induced MSC proliferation and IL-6 secretion,(Baglio, Lagerweij et al. 2017) just like the inflammatory and proliferative phenotypes we observed in our EV-educated primary lung fibroblasts. Similarly, investigation of the effects of human OS cell-derived EVs on fetal lung fibroblast cell lines WI-38 and MRC-5 demonstrated that 143B OS-derived EVs drive myCAF differentiation of normal fetal lung fibroblasts characterized by increased invasion, a-SMA expression, and fibronectin production,(Mazumdar, Urdinez et al. 2020) analogous to the myCAF gene signature enrichment we observed in our RNAseq analysis of OS EV-educated lung fibroblasts.

While these various CAF subtypes are associated with defined mechanisms of tumor promotion in other cancer types, limited evidence regarding the role of CAFs in mediating pro-tumorigenic functional responses in OS cells, such as changes in cell survival or proliferation, exists. Given that OS exosome priming of lung fibroblasts induced many of the phenotypes seen in previously described CAF subtypes, we sought to leverage this response to develop a simplistic and scalable *in vitro* co-culture model which attempts to recapitulate the early lung metastatic microenvironment and the impact of OS cell-lung fibroblast crosstalk on OS cell survival. Under conditions of cellular stress induced by serum deprivation and low seeding density, OS cells were fully dependent on lung fibroblasts to sustain their proliferation. Although OS cells can typically survive under serum starved conditions when plated at higher densities, OS cells seeded at low densities like those used as controls have difficulty attaching to the well bottom, and after 24 hours they appear to bleb, begin to die, and fully lift off the plastic of the well. The same OS cells seeded in wells that contain fibroblasts quickly embed themselves within the fibroblast monolayer and begin to proliferate. Proliferation of OS cells embedded within the fibroblast monolayer was significantly more pronounced upon OS exosome activation of these lung fibroblasts and was characterized by multifocal, clustered outgrowths indicative of OS lung metastasis demonstrated in Fig.5C. Interestingly, 2 to 3 fold higher OS cell proliferation occurred whether fibroblasts were primed by exosomes prior OS cell seeding alone or exosome educations continued after seeding throughout the remainder of the experiment compared to “uneducated” fibroblasts in the serum-free condition, where OS cell proliferation leveled off as demonstrated in Fig.5B. This suggests exosome priming is sufficient to

induce phenotypic changes in fibroblasts that are conducive for enhanced OS cell proliferation and continued exosome educations are not required to observe this effect. However, the mechanism by which OS EV-primed lung fibroblasts promote the enhanced OS cell growth advantage observed in this model remains to be defined, whether that be ECM outside-in signaling, cytokine-mediated paracrine effects, or juxtracrine signaling through cell-to-cell contact with exosome primed fibroblasts. To our knowledge, only two other studies have evaluated the functional effects of OS EV-primed fibroblastic cell interactions with OS cells, which demonstrated that human OS EV-primed MSCs can promote OS primary tumor growth, metastasis, and drug resistance in murine xenograft models.(Baglio, Lagerweij et al. 2017, Massaro, Sensoy et al. 2024) These studies demonstrated that EV-associated TGFβ induced IL-6 secretion in MSCs, which drove tumor progression through paracrine STAT3 activation in OS cells, suggesting that the increased IL-6 secretion we observed in response to OS EV treatment of primary lung fibroblasts may be mediating this enhancement of OS cell survival and proliferation in our model. Thus, our data also support the notion that exosome priming and reprogramming of lung fibroblasts may be a critical first step to reorganizing the lung microenvironment in preparation of supporting circulating OS cell seeding and outgrowth and warrant future in vivo investigation of these phenomena.

In conclusion, we demonstrate that OS-derived exosomes have significant functional impacts on normal lung fibroblasts, inducing a rapid transition in phenotype following exosome uptake including distinct kinase activation, increased fibroblast proliferation, and enhanced secretion of known pro-metastatic cytokines and chemokines previously implicated in OS lung metastasis. Transcriptomic profiling of OS exosome primed lung fibroblasts confirmed significant enrichment of canonical myofibroblastic and inflammatory CAF gene signatures. Importantly, this OS exosome mediated transition of LFs into CAFs was associated with increased monocyte recruitment and promotion of OS cell survival and proliferation under conditions of cellular stress in vitro. Collectively, these data suggest that an OS exosome - lung fibroblast signaling circuit may represent an important event in orchestrating the establishment of a metastasis permissive microenvironment in the lung. Thus, these data provide a foundation for future in vivo studies investigating these mechanisms within preclinical murine models of OS metastasis to determine whether this intercellular communication network may represent a novel therapeutic target for interrupting the premetastatic microenvironment in OS.

Acknowledgements

The work for this projected was supported by the Boettcher Foundation and NIH grants 5T32GM136628 (LAH), 1K01OD022982 (DPR), R03OD028265 (DPR), and P30 CA046934 (University of Colorado Cancer Center Support Grant).

References

Alspach, E., K. C. Flanagan, X. Luo, M. K. Ruhland, H. Huang, E. Pazolli, M. J. Donlin, T. Marsh, D. Piwnica-Worms, J. Monahan, D. V. Novack, S. S. McAllister and S. A. Stewart (2014). "p38MAPK plays a crucial role in stromal-mediated tumorigenesis." Cancer Discov **4**(6): 716-729.

Asif, P. J., C. Longobardi, M. Hahne and J. P. Medema (2021). "The Role of Cancer-Associated Fibroblasts in Cancer Invasion and Metastasis." Cancers (Basel) **13**(18).

Asokan, S. and O. R. Bandapalli (2021). "CXCL8 Signaling in the Tumor Microenvironment." Adv Exp Med Biol **1302**: 25-39.

Baglio, S. R., T. Lagerweij, M. Pérez-Lanzón, X. D. Ho, N. Léveillé, S. A. Melo, A. M. Cleton-Jansen, E. S. Jordanova, L. Roncuzzi, M. Greco, M. A. J. van Eijndhoven, G. Grisendi, M. Dominici, R. Bonafede, S. M. Lougheed, T. D. de Gruijl, N. Zini, S. Cervo, A. Steffan, V. Canzonieri, A. Martson, K. Maasalu, S. Köks, T. Wurdinger, N. Baldini and D. M. Pegtel (2017). "Blocking Tumor-Educated MSC Paracrine Activity Halts Osteosarcoma Progression." Clin Cancer Res **23**(14): 3721-3733.

Becker, A., B. K. Thakur, J. M. Weiss, H. S. Kim, H. Peinado and D. Lyden (2016). "Extracellular Vesicles in Cancer: Cell-to-Cell Mediators of Metastasis." Cancer Cell **30**(6): 836-848.

Brichkina, A., T. Bertero, H. M. Loh, N. T. Nguyen, A. Emelyanov, S. Rigade, M. Ilie, P. Hofman, C. Gaggioli and D. V. Bulavin (2016). "p38MAPK builds a hyaluronan cancer niche to drive lung tumorigenesis." Genes Dev **30**(23): 2623-2636.

Bussard, K. M., L. Mutkus, K. Stumpf, C. Gomez-Manzano and F. C. Marini (2016). "Tumor-associated stromal cells as key contributors to the tumor microenvironment." Breast Cancer Res **18**(1): 84.

Cardeñes, B., I. Clares, V. Toribio, L. Pascual, S. López-Martín, A. Torres-Gomez, R. Sainz de la Cuesta, E. M. Lafuente, M. López-Cabrera, M. Yáñez-Mó and C. Cabañas (2021). "Cellular Integrin α5β1 and Exosomal ADAM17 Mediate the Binding and Uptake of Exosomes Produced by Colorectal Carcinoma Cells." Int J Mol Sci **22**(18): integrin.

Chen, C., L. Xie, T. Ren, Y. Huang, J. Xu and W. Guo (2021). "Immunotherapy for osteosarcoma: Fundamental mechanism, rationale, and recent breakthroughs." Cancer Lett **500**: 1-10.

Chen, L., P. Guo, Y. He, Z. Chen, L. Chen, Y. Luo, L. Qi, Y. Liu, Q. Wu, Y. Cui, F. Fang, X. Zhang, T. Song and H. Guo (2018). "HCC-derived exosomes elicit HCC progression and recurrence by epithelial-mesenchymal transition through MAPK/ERK signalling pathway." Cell Death Dis **9**(5): 513.

Chen, Q., W. Sun, Y. Liao, H. Zeng, L. Shan, F. Yin, Z. Wang, Z. Zhou, Y. Hua and Z. Cai (2015). "Monocyte chemotactic protein-1 promotes the proliferation and invasion of osteosarcoma cells and upregulates the expression of AKT." Mol Med Rep **12**(1): 219-225.

Chen, Z., L. Zhou, L. Liu, Y. Hou, M. Xiong, Y. Yang, J. Hu and K. Chen (2020). "Single-cell RNA sequencing highlights the role of inflammatory cancer-associated fibroblasts in bladder urothelial carcinoma." Nat Commun **11**(1): fibroblasts in TME.

Chhoy, P., C. W. Brown, J. J. Amante and A. M. Mercurio (2021). "Protocol for the separation of extracellular vesicles by ultracentrifugation from in vitro cell culture models." STAR Protoc **2**(1): 100303.

Christianson, H. C., K. J. Svensson, T. H. van Kuppevelt, J. P. Li and M. Belting (2013). "Cancer cell exosomes depend on cell-surface heparan sulfate proteoglycans for their internalization and functional activity." Proc Natl Acad Sci U S A **110**(43): 17380-17385.

Cole, S., D. M. Gianferante, B. Zhu and L. Mirabello (2022). "Osteosarcoma: A Surveillance, Epidemiology, and End Results program-based analysis from 1975 to 2017." Cancer **128**(11): 2107-2118.

Costa-Silva, B., N. M. Aiello, A. J. Ocean, S. Singh, H. Zhang, B. K. Thakur, A. Becker, A. Hoshino, M. T. Mark, H. Molina, J. Xiang, T. Zhang, T. M. Theilen, G. García-Santos, C. Williams, Y. Ararso, Y. Huang, G. Rodrigues, T. L. Shen, K. J. Labori, I. M. Lothe, E. H. Kure, J. Hernandez, A. Doussot, S. H. Ebbesen, P. M. Grandgenett, M. A. Hollingsworth, M. Jain, K. Mallya, S. K. Batra, W. R. Jarnagin, R. E. Schwartz, I. Matei, H. Peinado, B. Z. Stanger, J. Bromberg and D. Lyden (2015). "Pancreatic cancer exosomes initiate pre-metastatic niche formation in the liver." Nat Cell Biol **17**(6): 816-826.

Dror, S., L. Sander, H. Schwartz, D. Sheinboim, A. Barzilai, Y. Dishon, S. Apcher, T. Golan, S. Greenberger, I. Barshack, H. Malcov, A. Zilberberg, L. Levin, M. Nessling, Y. Friedmann, V. Igras, O. Barzilay, H. Vaknine, R. Brenner, A. Zinger, A. Schroeder, P. Gonen, M. Khaled, N. Erez, J. D. Hoheisel and C. Levy (2016). "Melanoma miRNA trafficking controls tumour primary niche formation." Nat Cell Biol **18**(9): 1006-1017.

Elyada, E., M. Bolisetty, P. Laise, W. F. Flynn, E. T. Courtois, R. A. Burkhart, J. A. Teinor, P. Belleau, G. Biffi, M. S. Lucito, S. Sivajothi, T. D. Armstrong, D. D. Engle, K. H. Yu, Y. Hao, C. L. Wolfgang, Y. Park, J. Preall, E. M. Jaffee, A. Califano, P. Robson and D. A. Tuveson (2019). "Cross-Species Single-Cell Analysis of Pancreatic Ductal Adenocarcinoma Reveals Antigen-Presenting Cancer-Associated Fibroblasts." Cancer Discov **9**(8): 1102-1123.

Feng, W., D. C. Dean, F. J. Hornicek, H. Shi and Z. Duan (2019). "Exosomes promote pre-metastatic niche formation in ovarian cancer." Mol Cancer **18**(1): 124.

Gong, Z., Q. Li, J. Shi, J. Wei, P. Li, C. H. Chang, L. D. Shultz and G. Ren (2022). "Lung fibroblasts facilitate pre-metastatic niche formation by remodeling the local immune microenvironment." Immunity **55**(8): 1483-1500.e1489.

Gross, A. C., H. Cam, D. A. Phelps, A. J. Saraf, H. K. Bid, M. Cam, C. A. London, S. A. Winget, M. A. Arnold, L. Brandolini, X. Mo, J. M. Hinckley, P. J. Houghton and R. D. Roberts (2018). "IL-6 and CXCL8 mediate osteosarcoma-lung interactions critical to metastasis." JCI Insight **3**(16).

Hoang, B. H., T. Kubo, J. H. Healey, R. Sowers, B. Mazza, R. Yang, A. G. Huvos, P. A. Meyers and R. Gorlick (2004). "Expression of LDL receptor-related protein 5 (LRP5) as a novel marker for disease progression in high-grade osteosarcoma." Int J Cancer **109**(1): 106-111.

Hoshino, A., B. Costa-Silva, T. L. Shen, G. Rodrigues, A. Hashimoto, M. Tesic Mark, H. Molina, S. Kohsaka, A. Di Giannatale, S. Ceder, S. Singh, C. Williams, N. Soplop, K. Uryu, L. Pharmer, T. King, L. Bojmar, A. E. Davies, Y. Ararso, T. Zhang, H. Zhang, J. Hernandez, J. M. Weiss, V. D. Dumont-Cole, K. Kramer, L. H. Wexler, A. Narendran, G. K. Schwartz, J. H. Healey, P. Sandstrom, K. J. Labori, E. H. Kure, P. M. Grandgenett, M. A. Hollingsworth, M. de Sousa, S. Kaur, M. Jain, K. Mallya, S. K. Batra, W. R. Jarnagin, M. S. Brady, O. Fodstad, V. Muller, K. Pantel, A. J. Minn, M. J. Bissell, B. A. Garcia, Y. Kang, V. K. Rajasekhar, C. M. Ghajar, I. Matei, H. Peinado, J. Bromberg and D. Lyden (2015). "Tumour exosome integrins determine organotropic metastasis." Nature **527**(7578): integrins.

Itoh, H., T. Kadomatsu, H. Tanoue, M. Yugami, K. Miyata, M. Endo, J. Morinaga, E. Kobayashi, T. Miyamoto, R. Kurahashi, K. Terada, H. Mizuta and Y. Oike (2018). "TET2-dependent IL-6 induction mediated by the tumor microenvironment promotes tumor metastasis in osteosarcoma." Oncogene **37**(22): 2903-2920.

Kalluri, R. and V. S. LeBleu (2020). "The biology, function, and biomedical applications of exosomes." Science **367**(6478).

Kansara, M., M. W. Teng, M. J. Smyth and D. M. Thomas (2014). "Translational biology of osteosarcoma." Nat Rev Cancer **14**(11): 722-735.

Karakasheva, T. A., E. W. Lin, Q. Tang, E. Qiao, T. J. Waldron, M. Soni, A. J. Klein-Szanto, V. Sahu, D. Basu, S. Ohashi, K. Baba, Z. T. Giaccone, S. R. Walker, D. A. Frank, E. P. Wileyto, Q. Long, M. C. Dunagin, A. Raj, J. A. Diehl, K. K. Wong, A. J. Bass and A. K. Rustgi (2018). "IL-6 Mediates Cross-Talk between Tumor Cells and Activated Fibroblasts in the Tumor Microenvironment." Cancer Res **78**(17): 4957-4970.

Kovac, M., C. Blattmann, S. Ribi, J. Smida, N. S. Mueller, F. Engert, F. Castro-Giner, J. Weischenfeldt, M. Kovacova, A. Krieg, D. Andreou, P. U. Tunn, H. R. Dürr, H. Rechl, K. D. Schaser, I. Melcher, S. Burdach, A. Kulozik, K. Specht, K. Heinimann, S. Fulda, S. Bielack, G. Jundt, I. Tomlinson, J. O. Korbel, M. Nathrath and D. Baumhoer (2015). "Exome sequencing of osteosarcoma reveals mutation signatures reminiscent of BRCA deficiency." Nat Commun **6**: 8940.

Liao, Z., Z. W. Tan, P. Zhu and N. S. Tan (2019). "Cancer-associated fibroblasts in tumor microenvironment - Accomplices in tumor malignancy." Cell Immunol **343**: Review.

Liu, J., S. Wu, X. Zheng, P. Zheng, Y. Fu, C. Wu, B. Lu, J. Ju and J. Jiang (2020). "Immune suppressed tumor microenvironment by exosomes derived from gastric cancer cells via modulating immune functions." Sci Rep **10**(1): 14749.

Liu, Q., A. Li, Y. Tian, J. D. Wu, Y. Liu, T. Li, Y. Chen, X. Han and K. Wu (2016). "The CXCL8-CXCR1/2 pathways in cancer." Cytokine Growth Factor Rev **31**: 61-71.

Lobb, R. J., L. G. Lima and A. Möller (2017). "Exosomes: Key mediators of metastasis and pre-metastatic niche formation." Semin Cell Dev Biol **67**: 3-10.

Luo, H., X. Xia, L. B. Huang, H. An, M. Cao, G. D. Kim, H. N. Chen, W. H. Zhang, Y. Shu, X. Kong, Z. Ren, P. H. Li, Y. Liu, H. Tang, R. Sun, C. Li, B. Bai, W. Jia, Y. Liu, W. Zhang, L. Yang, Y. Peng, L. Dai, H. Hu, Y. Jiang, Y. Hu, J. Zhu, H. Jiang, Z. Li, C. Caulin, J. Park and H. Xu (2022). "Pan-cancer single-cell analysis reveals the heterogeneity and plasticity of cancer-associated fibroblasts in the tumor microenvironment." Nat Commun **13**(1): 6619.

Lussier, D. M., J. L. Johnson, P. Hingorani and J. N. Blattman (2015). "Combination immunotherapy with α-CTLA-4 and α-PD-L1 antibody blockade prevents immune escape and leads to complete control of metastatic osteosarcoma." J Immunother Cancer **3**: 21.

Lussier, D. M., L. O'Neill, L. M. Nieves, M. S. McAfee, S. A. Holechek, A. W. Collins, P. Dickman, J. Jacobsen, P. Hingorani and J. N. Blattman (2015). "Enhanced T-cell immunity to osteosarcoma through antibody blockade of PD-1/PD-L1 interactions." J Immunother **38**(3): 96-106.

Malanchi, I., A. Santamaria-Martínez, E. Susanto, H. Peng, H. A. Lehr, J. F. Delaloye and J. Huelsken (2011). "Interactions between cancer stem cells and their niche govern metastatic colonization." Nature **481**(7379): 85-89.

Man, T. K., X. Y. Lu, K. Jaeweon, L. Perlaky, C. P. Harris, S. Shah, M. Ladanyi, R. Gorlick, C. C. Lau and P. H. Rao (2004). "Genome-wide array comparative genomic hybridization analysis reveals distinct amplifications in osteosarcoma." BMC Cancer **4**: 45.

Mao, X., J. Xu, W. Wang, C. Liang, J. Hua, J. Liu, B. Zhang, Q. Meng, X. Yu and S. Shi (2021). "Crosstalk between cancer-associated fibroblasts and immune cells in the tumor microenvironment: new findings and future perspectives." Mol Cancer **20**(1): 131.

Marra, F., W. Delogu, I. Petrai, S. Pastacaldi, A. Bonacchi, E. Efsen, S. Aleffi, C. Bertolani, M. Pinzani and P. Gentilini (2004). "Differential requirement of members of the MAPK family for CCL2 expression by hepatic stellate cells." Am J Physiol Gastrointest Liver Physiol **287**(1): G18-26.

Massaro, C., H. N. Sensoy, M. Mulders, C. De Schrijver, C. Gómez-Martín, J. Simon Nieto, T. Lagerweij, A. Atmopawiro, J. Pérez-Boza, M. Bebelman, L. Bosch, S. Foderaro, M. Neves Ferreira, M. A. J. van Eijndhoven, J. R. T. van Weering, C. Dell'Aversana, L. Altucci, C. D. Savci-Heijink, N. van de Donk, C. Giorgio, L. Brandolini, M. Allegretti, D. M. Pegtel and S. R. Baglio (2024). "Tumor-Secreted Extracellular Vesicles Counteract Therapy Response by Triggering Inflammatory Mesenchymal Stem Cell Development." Clin Cancer Res **30**(20): 4714-4728.

Mazumdar, A., J. Urdinez, A. Boro, J. Migliavacca, M. J. E. Arlt, R. Muff, B. Fuchs, J. G. Snedeker and A. Gvozdenovic (2020). "Osteosarcoma-Derived Extracellular Vesicles Induce Lung Fibroblast Reprogramming." Int J Mol Sci **21**(15).

Meltzer, P. S. and L. J. Helman (2021). "New Horizons in the Treatment of Osteosarcoma." N Engl J Med **385**(22): 2066-2076.

Milane, L., A. Singh, G. Mattheolabakis, M. Suresh and M. M. Amiji (2015). "Exosome mediated communication within the tumor microenvironment." J Control Release **219**: 278-294.

Nirala, B. K., T. Yamamichi, D. I. Petrescu, T. N. Shafin and J. T. Yustein (2023). "Decoding the Impact of Tumor Microenvironment in Osteosarcoma Progression and Metastasis." Cancers (Basel) **15**(20).

Peinado, H., M. Alečković, S. Lavotshkin, I. Matei, B. Costa-Silva, G. Moreno-Bueno, M. Hergueta-Redondo, C. Williams, G. García-Santos, C. Ghajar, A. Nitadori-Hoshino, C. Hoffman, K. Badal, B. A. Garcia, M. K. Callahan, J. Yuan, V. R. Martins, J. Skog, R. N. Kaplan, M. S. Brady, J. D. Wolchok, P. B. Chapman, Y. Kang, J. Bromberg and D. Lyden (2012). "Melanoma exosomes educate bone marrow progenitor cells toward a pro-metastatic phenotype through MET." Nat Med **18**(6): 883-891.

Pols, M. S. and J. Klumperman (2009). "Trafficking and function of the tetraspanin CD63." Exp Cell Res **315**(9): 1584-1592.

Regan, D. P., L. Chow, S. Das, L. Haines, E. Palmer, J. N. Kurihara, J. W. Coy, A. Mathias, D. H. Thamm, D. L. Gustafson and S. W. Dow (2022). "Losartan Blocks Osteosarcoma-Elicited Monocyte Recruitment, and Combined With the Kinase Inhibitor Toceranib, Exerts Significant Clinical Benefit in Canine Metastatic Osteosarcoma." Clin Cancer Res **28**(4): 662-676.

Regan, D. P., J. W. Coy, K. K. Chahal, L. Chow, J. N. Kurihara, A. M. Guth, I. Kufareva and S. W. Dow (2019). "The Angiotensin Receptor Blocker Losartan Suppresses Growth of Pulmonary Metastases via AT1R-Independent Inhibition of CCR2 Signaling and Monocyte Recruitment." J Immunol **202**(10): 3087-3102.

Ristorcelli, E., E. Beraud, S. Mathieu, D. Lombardo and A. Verine (2009). "Essential role of Notch signaling in apoptosis of human pancreatic tumoral cells mediated by exosomal nanoparticles." Int J Cancer **125**(5): 1016-1026.

Ritter, J. and S. S. Bielack (2010). "Osteosarcoma." Ann Oncol **21 Suppl 7**: vii320-325.

Salunkhe, S., Dheeraj, M. Basak, D. Chitkara and A. Mittal (2020). "Surface functionalization of exosomes for target-specific delivery and in vivo imaging & tracking: Strategies and significance." J Control Release **326**: 599-614.

Skog, J., T. Würdinger, S. van Rijn, D. H. Meijer, L. Gainche, M. Sena-Esteves, W. T. Curry, Jr., B. S. Carter, A. M. Krichevsky and X. O. Breakefield (2008). "Glioblastoma microvesicles transport RNA and proteins that promote tumour growth and provide diagnostic biomarkers." Nat Cell Biol **10**(12): 1470-1476.

Suzuki, M., T. Tetsuka, S. Yoshida, N. Watanabe, M. Kobayashi, N. Matsui and T. Okamoto (2000). "The role of p38 mitogen-activated protein kinase in IL-6 and IL-8 production from the TNF-alpha- or IL-1beta-stimulated rheumatoid synovial fibroblasts." FEBS Lett **465**(1): 23-27.

Takahashi, Y., T. Yasui, K. Tamari, K. Minami, K. Otani, F. Isohashi, Y. Seo, R. Kambe, M. Koizumi and K. Ogawa (2017). "Radiation enhanced the local and distant anti-tumor efficacy in dual immune checkpoint blockade therapy in osteosarcoma." PLoS One **12**(12): e0189697.

Talbott, H. E., S. Mascharak, M. Griffin, D. C. Wan and M. T. Longaker (2022). "Wound healing, fibroblast heterogeneity, and fibrosis." Cell Stem Cell **29**(8): 1161-1180.

Tsukamoto, H., K. Fujieda, S. Senju, T. Ikeda, H. Oshiumi and Y. Nishimura (2018). "Immune-suppressive effects of interleukin-6 on T-cell-mediated anti-tumor immunity." Cancer Sci **109**(3): 523-530.

Umezu, T., H. Tadokoro, K. Azuma, S. Yoshizawa, K. Ohyashiki and J. H. Ohyashiki (2014). "Exosomal miR-135b shed from hypoxic multiple myeloma cells enhances angiogenesis by targeting factor-inhibiting HIF-1." Blood **124**(25): 3748-3757.

Viñas, J. L., M. Spence, A. Gutsol, W. Knoll, D. Burger, J. Zimpelmann, D. S. Allan and K. D. Burns (2018). "Receptor-Ligand Interaction Mediates Targeting of Endothelial Colony Forming Cell-derived Exosomes to the Kidney after Ischemic Injury." Sci Rep **8**(1): 16320.

Wan, Y., Y. Zhao, M. Cao, J. Wang, S. V. Tran, Z. Song, B. W. Hsueh and S. E. Wang (2024). "Lung Fibroblasts Take up Breast Cancer Cell-derived Extracellular Vesicles Partially Through MEK2-dependent Macropinocytosis." Cancer Res Commun **4**(1): 170-181.

Wang, Y. C., L. H. Zheng, B. A. Ma, Y. Zhou, M. H. Zhang, D. Z. Zhang and Q. Y. Fan (2011). "Clinical value of signal transducers and activators of transcription 3 (STAT3) gene expression in human osteosarcoma." Acta Histochem **113**(4): 402-408.

Wei, K., H. N. Nguyen and M. B. Brenner (2021). "Fibroblast pathology in inflammatory diseases." J Clin Invest **131**(20).

Wortzel, I., S. Dror, C. M. Kenific and D. Lyden (2019). "Exosome-Mediated Metastasis: Communication from a Distance." Dev Cell **49**(3): 347-360.

Wu, C. C., H. C. Beird, J. Andrew Livingston, S. Advani, A. Mitra, S. Cao, A. Reuben, D. Ingram, W. L. Wang, Z. Ju, C. Hong Leung, H. Lin, Y. Zheng, J. Roszik, W. Wang, S. Patel, R. S. Benjamin, N. Somaiah, A. P. Conley, G. B. Mills, P. Hwu, R. Gorlick, A. Lazar, N. C. Daw, V. Lewis and P. A. Futreal (2020). "Immuno-genomic landscape of osteosarcoma." Nat Commun **11**(1): 1008.

Wu, F., J. Yang, J. Liu, Y. Wang, J. Mu, Q. Zeng, S. Deng and H. Zhou (2021). "Signaling pathways in cancer-associated fibroblasts and targeted therapy for cancer." Signal Transduct Target Ther **6**(1): 218.

Yang, L., X. Huang, H. Guo, L. Wang, W. Yang, W. Wu, D. Jing and Z. Shao (2021). "Exosomes as Efficient Nanocarriers in Osteosarcoma: Biological Functions and Potential Clinical Applications." Front Cell Dev Biol **9**: 737314.

Zou, S., Q. Tong, B. Liu, W. Huang, Y. Tian and X. Fu (2020). "Targeting STAT3 in Cancer Immunotherapy." Mol Cancer **19**(1): 145.

Supplemental Data

A

Cat# CC-2512	Sex	Age	Lot#
M29	Male	29	Unknown
M12	Male	12	H0000615568
F62	Female	62	18TL057581
F48	Female	48	20TL356516
M48	Male	48	21TL088250
M54	Male	54	21TL076039

B

% exosome uptake				
	M54	**M48**	**F62**	**M29**
143b	98.3	96.3	90	97.5
HOS	99.2	97.7	85.4	97.2
MG63.0	98.1	91.3	80.5	96.6
MG63.2	98	95	88.1	97.7
U2OS	94.6	93.4	79.1	94.7
SAOS	93.4	89.7	71.4	86.3

Supplementary Fig. 1, 2 A) Fibroblast naming convention, sex and age of donor, and lot number from the supplier (Lonza) **B)** % uptake of PKH26 labeled exosomes by fibroblast donor derived from each OS cell line evaluated as measured by mean fluorescence intensity

CHAPTER 3

Development of a highly sensitive and quantitative *in vivo* model of OS metastatic lung colonization

Abstract

Osteosarcoma (OS) is the most common malignant cancer of the bone, which is typically diagnosed in children and young adults. Metastatic dissemination occurs almost exclusively to the lung and represents the greatest obstacle to improving the dismal survival outcomes in patients that develop recurrent disease. The current standard of care includes a combination of surgical resection, radiotherapy and a decade's old multi-drug chemotherapeutic treatment strategy. The successful deployment of targeted small molecule and cell based therapeutic interventions that emerged from the identification of specific intrinsic tumor-promoting characteristics among other cancer types, have thus far proven to be substantially less useful in developing therapies for OS. As a result, survival outcomes have not substantially improved for almost half a century. Several compounds and cell-based therapies have displayed promising *in vitro* and *in vivo* preclinical results in recent years. However, there remains a substantial disconnect between the outcomes of these studies and clinical efficacy, and many of these therapies ultimately fail the approval process for widespread use. This may be due to the use of current preclinical models of OS that often fail to fully recapitulate the molecular and cellular events that promote OS metastatic progression in the lung, resulting in a considerable knowledge gap in our understanding of these critical processes. To address the need for preclinical models to further our understanding of the mechanisms of OS lung specific metastasis, we sought to develop a highly sensitive and quantitative method to detect and quantify OS cells during the rate limiting step of the metastatic cascade, at the earliest stages of metastatic colonization. To accomplish this, we evaluated the use of OS cell fluorescent labeling using compounds that function under distinct mechanisms, including intracellular (Cell Trace Yellow), membrane intercalating (DIR), and nuclear restricted (RFP). We determine the optimal cell labeling methods for detection of OS cells by spectral flow cytometry *in vitro* and *ex vivo*. We then employ a luciferase expression system in lentiviral transduced OS cells, allowing for the parallel detection of an

OS specific bioluminescent signal detected by IVIS imaging systems. Here, we show fluorescently labeling OS cells using Cell Trace and DIR allows for the detection of a fluorescent signature in tumor cell injected mouse lung, single cell suspensions using spectral flow cytometry. However, by using a mouse, resident lung cell flow cytometry antibody panel, we determine the signal from these fluorescent dyes are not restricted to the tumor compartment. Finally, using a dual-reporter, RFP-Luciferase expression system, we show human OS cells can be quantified using correlative detection methods run in parallel in a mouse lung within 24 hours of tumor cell injection. Taken together, these data demonstrate the viability of using spectral flow cytometry in tandem with IVIS imaging to detect RFP-Luciferase expressing OS cells at the earliest stages of OS lung colonization *in vivo*, thus allowing for a novel, highly sensitive and quantitative method for evaluating mechanisms that may drive lung specific metastasis.

Introduction

Osteosarcoma (OS) is a highly malignant cancer of the bone. The onset and diagnosis of this rare disease primarily occurs in adolescence, typically presenting as a primary tumor localized in the metaphysis of the long bones, often accompanied by metastatic lesions in the lung. (Mirabello, Troisi et al. 2009, Ottaviani and Jaffe 2009) Surgical resection, radiotherapy, and a combinatorial chemotherapy regime comprised of high dose Methotrexate, Adriamycin, and Cisplatin are the current standard of care. This treatment strategy substantially improved survival outcomes among OS patients when these approaches gained widespread adoption over 40 years ago.(Isakoff, Bielack et al. 2015) Since then, however, the approval of effective and novel therapies has stalled along with improvements in clinical outcomes. Although, the standard of care is relatively effective at improving the chances of progression-free survival when addressing a primary tumor alone, the predilection for lung specific metastasis displayed by OS paired with the high rate of recurrence substantially reduces the effectiveness of current treatment strategies, and is associated with a dismal 20%, 5-year survival rate. (Kempf-Bielack, Bielack et al. 2005) The approaches used to identify and target the genomic alterations and intrinsic mediators responsible for driving tumorigenesis successfully employed in the development of therapies used to treat other cancer types has largely failed to materialize for OS. (Takahashi, Yasui et al. 2017, Zhang, Tan et al.

2022) This is due in large part to the relatively high degree of genomic instability and heterogeneity, both intratumorally and between OS patients, as well as an inability to successfully target the most commonly observed genomic alterations that were identified, including p53, RB1, and c-MYC. (Berman, Calo et al. 2008, Bousquet, Noirot et al. 2016) Additionally, the identification of tumor-cell extrinsic mediators capable of downregulating the host's anti-tumor immune responses, called immune checkpoints, led to the development of cell-based therapies that block the signaling responsible for driving this immunomodulatory effect. This class of therapies designed to target receptors like Cytotoxic T-lymphocyte associated protein 4 (CTLA-4) and ligands like Programmed Death-ligand 1 (PDL-1), were proven effective in reversing the downregulation of anti-tumor immune responses, thereby improving survival outcomes in other cancer types, like melanoma. (Cranmer and Hersh 2007, Jiang, Shi et al. 2019, Wu, Beird et al. 2020) However, the clinical benefits of including ICIs as part of the treatment strategy were not observed among OS patients resulting from the heterogenous characteristics and immunologically "cold" OS TME. (Zhang, Tan et al. 2022) Since then, several other compounds and therapeutic approaches that showed promising preclinical results have also failed to demonstrate efficacy and improve outcomes for OS patients in a clinical setting. (Lilienthal and Herold 2020)

The striking disconnect between successful preclinical studies and clinical outcomes partly stems from a lack of models that can fully recapitulate the cellular and molecular events that occur during OS tumorigenesis and metastatic progression. The continual development of novel molecular and genomic based tools has allowed investigators to gain new insights into the intrinsic and extrinsic drivers that promote OS tumorigenesis within the TME, and the events that initialize OS metastatic behavior. However, there remains a considerable knowledge gap in our understanding of perhaps the most critical events that occur during the earliest stages of OS lung specific metastatic colonization. If addressed, discoveries in this area may be useful in identifying novel prognostic indicators, or gain insights into the cellular and molecular drivers of metastatic colonization that could be exploited for the development of novel anti-metastatic therapeutic approaches.

Therefore, we sought to develop an in vivo model that would allow investigators to probe events that occur during the earliest stages of OS cell lung colonization using highly sensitive and quantitative methods such as spectral flow cytometry and bioluminescent imaging. To achieve this and overcome the

lack of OS cell specific surface markers typically used to detect cell populations using flow cytometry, we evaluated several florescent cell labeling methods including membrane intercalating (DIR) and intracellular (Cell Trace Yellow) dyes, and transduced expression of nuclear restricted red fluorescent protein (RFP). Here, we show the optimization of fluorescent cell labeling dyes substantially reduces signal blead-over to unlabeled cells, while maintaining the highest signal intensity, thereby allowing for the separation of distinct populations when evaluated by spectral flow cytometry *in vitro* and *ex vivo*. However, by employing a six-marker flow cytometry panel, we determine the fluorescent signal associated with OS cell labeling dyes are transferred to resident cell populations in the lung, providing evidence the use of these dyes is likely not an effective tool for *in vivo* tracking of OS cells in the lung. Finally, we evaluate the efficacy of a dual reporter nuclear red fluorescent protein, luciferase expression system for tracking and quantifying human 143b cells *in vivo*. We show RFP positive cells are detected in mouse lung single cell suspensions using spectral flow cytometry within 24-hours of tumor cell tail vein injections. The results herein, describing our observations of dual RFP-Luciferase expressing OS cells *in vivo,* suggest the use of spectral flow cytometry paired with bioluminescent IVIS imaging could be used to detect and quantify OS cells at the earliest stages of metastatic lung colonization. This mouse model of OS offers a potential window to better understand the cellular and molecular events that may promote OS metastatic lung colonization and explore methods for developing and evaluating novel anti-metastatic therapeutic strategies.

Methods and Materials

Mice

6–8-week-old, female BALB/cJ and BALB/c-severely compromised immuno-deficient (SCID) mice were purchased from Jackson Laboratory (Bar Harbor, Maine, #000651, #001803, respectively). All animals were housed in microisolator cages in groups of 5 in the Bay Laboratory Animal Facility at Colorado State University. All procedures were approved by the Institutional Animal Care and Use Committee (IACUC, protocol #4874) at Colorado State University, Fort Collins, CO.

Cell Lines

The human osteosarcoma (OS) cell line 143b was purchased from the American Type Culture Collection (ATCC, Manassas, VA USA). The murine OS cell line K7M2 was generously provided to our group by Dr. Dawn Duval (Flint Animal Cancer Center, Fort Collins, CO). All tumor cell lines were validated by short tandem repeat (STR) analysis and were routinely tested for mycoplasma contamination using a commercially available assay (Mycoalert, Lonza Inc.). Tumor cells were maintained in DMEM media (Gibco, Grand Island, NY USA) supplemented with 10% fetal bovine serum (FBS; Atlas Biologicals, Fort Collins, CO USA), penicillin (100 U/mL), and streptomycin (100 mg/mL) (All from Gibco). Cells were grown sterilely on standard plastic tissue culture flasks (Cell Treat, Shirley, MA), under standard conditions of 37 °C, 5% CO_2, and humidified air. For transduction using RFP and Luciferase (firefly 3) lentiviral constructs (GenTarget, San Diego, CA, #LVP674-PBS), 5k K7M2 or 143b cells were plated in 24-well, flat-bottom plates in 1 mL complete DMEM containing 10% fetal bovine serum and 1U/mL penicillin, 100 ug/mL streptomycin for 24 hours in an incubator at 37C, 5% CO2, 5% humidity, respectively. Media was removed from each well, and replaced with 1 mL complete DMEM media and 50 uL commercial lentiviral particle stock preparation. Cells were allowed to grow for 3 days in an incubator followed by fluorescent live cell imaging of adhered, RFP positive tumor cells using Incucyte S3 live imaging system (Sartorius Inc. Göttingen, Germany) to confirm successful transduction efficiency. Additionally, transduced wells were given a final concentration of 150 ug/mL D-Luciferin salt (200x was 30 mg/mL in DMSO, LUCK-1G, GoldBio, St. Louis, MO), and bioluminescent intensity was measured using the Spectrum Intravital Imaging System (IVIS) (Perkin Elmer, Waltham, MA). Media was removed and replaced with complete DMEM with 5 ug/mL Puromycin as antibiotic selection. Cells were monitored daily for RFP expression using the Incucyte live cell imaging until >99% of cells were RFP positive. Cells were then grown in complete DMEM media under standard conditions.

Fluorescent Labeling of OS Cells

For Cell Trace Yellow (Thermofisher, Waltham, MA, #C34573), a stock concentration of 2.5 mM was generated by reconstituting Cell Trace Yellow dye in 80 uL DMSO. OS cells were grown in 225 cm2 tissue culture flasks standard conditions in complete DMEM media. Once ~80% confluent, media was

removed, cells were washed with 10 mL 1x PBS, then 3 mL Trypsin was added to the flask for 5 min. at 37degrees. 10 mL of complete DMEM were added to the flask to wash any remaining adhered cells from the bottom of the flask. All media was removed, and cells were centrifuged at 1200 rpm and 22 degrees C for 5 minutes. Supernatant was removed and cells were resuspended in 2 mL PBS. 20 uL of cell suspension was removed for counting using the T4 Cellometer (Nexcelom, Lawrence, MA). Cells were brought to a final concentration of 1e6 OS cells per mL followed by addition of Cell Trace Yellow stock solution of 2.5 mM at between 2.5 uM and 0.625 uM. The cell suspension was then incubated at 37 degrees in standard conditions for 10 minutes. Cells were removed and 2x volume complete DMEM media was added to absorb unincorporated dye. This cell suspension was then centrifuged at 1200 rpm and 22 degrees C for 5 minutes. Supernatant was removed and replaced with the initial volume of complete DMEM media to bring the cell pellet back to 1e6 cells per mL. This suspension was allowed to sit at room temperature in the dark for 10 minutes to allow for incorporated dye to esterify within the cells. This suspension was then centrifuged at 1200 rpm and 22 degrees C for 5 minutes. For in vivo studies, supernatant was removed and pelleted cells were resuspended in enough 1x PBS to bring cell suspension to a concentration of 2e7 cells per mL.

For DiOC18(7)(DIR) (Thermofisher, Waltham, MA, #D12731), a stock concentration of 2.46 mM was generated by reconstituting 10 mg DIR (1,1'-Dioctadecyl-3,3,3',3'-Tetramethylindotricarbocyanine Iodide) in 4 mL DMSO. OS cells were trypsonized and counted as noted above. DIR dye was added to a 10 mL cell suspension of OS cells in complete DMEM at a cell density of 1e6 cells per mL at concentrations between ~2.5 uM and 625 nM. The cell suspension containing DIR dye was gently vortexed then incubated for 20 min. at 37C in standard conditions. The suspension was pelleted by centrifugation at 1200 rpm for 4 min. at 22C. The supernatant was removed, and the cells were washed by gently resuspending in complete DMEM. This washing step was repeated 2X before cells were resuspended in 1x sterile PBS.

In Vitro Evaluation of Fluorescent Cellular Labeling Dyes

For mixing of labeled and unstained human OS, 143b cells in a 1:1 ratio prior to flow cytometry analysis: 143b cells were trypsonized, counted, and brought up to 1e6 cells/mL in 1X sterile PBS then incubated with Cell Trace or DIR fluorescent dyes at either 5 uM, 2.5 uM, 1.25 uM, 833 nM, or 625 nM concentrations, respectively. The cell labeling process was quenched and fluorescently labeled cells were plated at 200,000 live cells per well in a 96-well, clear, flat-bottom plate. Labeled cells were plated individually and in a 1:1 ratio with unstained 143b cells. Unstained 143b cells were also plated individually for use as unstained controls. The plate was incubated at 37C for 4 hours before being transferred to a 96-well, clear, V-bottom plate. The cells were then centrifuged at 1200 rpm for 5 min., supernatants were removed by gently flicking the plate over a sink, then 200 uL FACS buffer was added as a washing step before centrifugation. This final washing step was repeated 3x, cells were then resuspended in a final volume of 150 uL FACs buffer before immediate analysis using the Aurora 4-laser spectral flow cytometer (Cytek, Fremont, CA). For measurement of fluorescent dye stability over time and following the same labeling protocol above, 100,000 143b cells were labeled with Cell Trace or DIR fluorescent dyes at 1.25 uM, respectively, before being plated in 3, separate T-75 tissue culture flasks each. Over consecutive 24-hour periods, labeled cells were harvested from 1 T-75 flasks per day, counted, and plated in 96-well, V-bottom plates. Cells were washed and analyzed using spectral flow cytometry following protocols mentioned above.

Ex Vivo Assessment of Cell Trace Fluorescent Dye

For the harvesting of mouse lungs for digestion and generation of single cell suspensions: 2, 8 to10-week old naïve Balb/C-SCID mice were sacrificed by cervical spine dislocation under isoflurane anesthesia, their lungs were harvested and put on ice for immediate tissue digestion. Briefly, lungs were placed in 1 mL ice cold 2x collagenase D (200 uL 10x per mL) and DNase (0.125 mg/mL or 80 U/mL) in serum free DMEM util all lungs were collected. Lungs were minced with ethanol-cleaned razor blades, then returned to collagenase/DNase media to incubate for 30 min. at 37C. 100 uL of 100 mM pH balanced EDTA is added to top the enzymatic reaction, partially digested lung homogenates were

returned to ice, then triturated using 18-gauge needles to fully break up the tissue. Cell suspensions were run through 100 uM filter into 15 mL conical tubes before being centrifuged at 300xg for 5 min. at 4C. Supernatants were discarded, and cell pellets were resuspended in 1 mL of ACK lysis buffer for 5 min. to lyse red blood cells. 5 mL, ice cold complete DMEM is added to each 15 mL conical tube followed by another centrifugation step. Supernatants were again discarded, and the lung cell pellet was resuspended in 500 uL 1x sterile PBS prior to cell counting and evaluation of viability. During the lung digestion process, luciferase expressing 143b cells (143b-Luc) were labeled with Cell Trace dye at 2.5 uM, 1.25 uM, 833 nM, and 625 nM concentrations. Lung digested single cell suspensions were counted and plated in a 96-well, V-bottom plate either individually, or in 1:5, 1:10, and 1:20 ratios with Cell Trace labeled 143b-luc cells from each labeling concentration. For plating of the standard curve, unstained 143B cells were counted and plated in duplicate, 2-fold serial dilutions starting at 200,000 cells moving down to ~1,562 cells per well. The plate containing the mixtures of Cell Trace labeled 143b-Luc cells, naïve mouse lung cells, and unstained 143b-Luc cells were washed 3x with FACS buffer as mentioned above. Cells were brought up to a volume of 125 uL using FACS buffer. Then 25 uL D-Luciferin salt (200x stock solution in DMSO) at a 33.3:1 dilution was added to each well (final concentration of 150 ug/mL in 150 uL total volume per well) 10 min. prior to the detection of bioluminescent signal using intravital imaging systems (IVIS)(Perkin-Elmer, Waltham, MA). The IVIS was set to read bioluminescence in open filter with automatic detection times under the “C” field of view. This typically results in a 2 min. detection time. After IVIS imaging, the plate was then analyzed on the cytometer as mentioned above. For data analysis, the luminescent signal detected by the IVIS from the standard curve was used to generate a predicted number of 143b-Luc cells based on the bioluminescent signal in each of the wells containing 143b-Luc cells mixed ex vivo with mouse lung cells. The predicted numbers of cells using the IVIS standard curve were then correlated to the number of Cell Trace positive cells identified by spectral flow cytometry.

***In Vivo* Assessment of DIR and Cell Trace Yellow fluorescent dyes**

For both DIR and Cell Trace Yellow in vivo studies, 143b-Luc cells were labeled with 625 nM Cell Trace or DIR dye using the protocols described previously. Following quenching, cells were brought up to 2e7 cells per mL in sterile 1x PBS and briefly kept on ice. Just prior to intravenous, tail vein injection of

labeled 143b-Luc cells into Balb/c-scid mice, D-Luciferin stock solution was added to 143b-Luc cell stock to a final concentration of 150 ug/mL. Each mouse was then injected with 50 uL labeled 143b-Luc cells at 1e6 cells per mL 10 min. prior to the initial *in vivo* post-injection bioluminescent imaging. 4 days post-tumor cell injection, mice were administered 150 mg/kg D-luciferin at a concentration of 30 mg/mL interperitoneally (roughly 100 uL stock d-Luciferin for 20g mouse), 10 min. prior to isoflurane anesthesia and IVIS imaging. The IVIS settings for bioluminescent detection mentioned earlier were altered from "well plate" to "mouse" settings. For the detection of fluorescence, the IVIS was set to detect fluorescence using a 10 second exposure time and filter settings optimized based on the excitation and emission spectra of DIR and Cell Trace Yellow (750-780, 546-579 nm, respectively). Mice were immediately sacrificed by cervical spine dislocation under isoflurane anesthesia and lungs were imaged by IVIS ex vivo before being digested into single cell suspensions using the protocols mentioned previously.

A panel of fluorescently conjugated anti-mouse antibodies and zombie live/dead dye used to identify resident mouse lung cell populations and distinguish live from dead cells was employed for flow cytometry analysis (Supplemental Table 1) Efforts to minimize light exposure should be taken in all steps moving forward. Briefly, after lung cells from each mouse were plated in their respective wells in a 96-well, V-bottom plate, 100 uL of zombie NIR used in Cell Trace Yellow studies or Zombie Yellow for DIR studies was applied to cells at a 1:1000 dilution in 1X PBS + 5mM EDTA for 15 min. at room temp in a dark drawer. The plate was centrifuged at 300 xg for 5 min. at 4C, supernatants were discarded, and cells were resuspended in 150 uL FACS buffer. This was repeated 2x, then following centrifugation and supernatant removal, 10 uL mouse block (Recipe) was added to each well for 5 min. at room temperature to prevent non-specific binding of fluorescent antibodies. Then 50 uL of primary antibodies diluted to their respective concentrations in FACS buffer were added on top of the mouse block, the plate was incubated at room temp. in a dark drawer for 15-20 min. then 100 uL FACS buffer was added directly to each well. The plate was washed 3x with FACS buffer as described previously before being brought to a final volume of 150 uL for flow cytometry analysis. Naïve mice were also sacrificed, and their lungs were processed for flow cytometry at the same time as the experimental mice. Lung cells from these mice are used for single stain unmixing and fluorescence minus one (FMO) controls used for informing gating strategies during down-stream data analysis. For in vivo studies, at the time 143b-Luc cells were labeled,

DIR and Cell Trace Yellow cells not injected into mice were plated in T-75 tissue culture flasks and incubated under standard conditions until mice were sacrificed. These cells were added to the well plate to inform gating strategies during flow cytometry analysis. For in vivo Cell Trace Yellow studies, standard curves of unstained 143b-Luc cells were plated for IVIS imaging.

***In vivo* assessment of red fluorescent protein, luciferase expressing 143b cells**

For K7M2-RFP Time Course Study - 15, 7- to 8-week-old Balb/C mice purchased from Jackson Labs (Bar Harbor, Maine, #000651) were separated into 3 groups of 5. For each group of 5 mice, 4 mice were tail-vein injected with 1e6 nuclear RFP expressing mouse OS cell line, K7M2 (K7M2-RFP) and 1 mouse from each group was left naïve to use as a control for downstream analysis. A group of mice were sacrificed at 4, 8, and 14-days, each, post-tumor cell injection and lungs were harvested. One half of each mouse's lungs were digested for flow cytometry analysis, and the other half of each mouse's lungs were embedded in OTC, snap frozen in aerosolized liquid nitrogen vapor for 3 minutes. Then frozen samples were transferred to storage in the -80C freezer prior to tissue sectioning using a cryostat. Slides were stained with DAPI and Actingreen according to manufacturer protocols. Slides were then images using a fluorescent confocal microscope, and analyzed using Visiopharm software (Horsholm, Denmark). For flow cytometry, lung tissues were digested immediately post-organ harvest using lung digestion protocol mentioned previously. Cell counts and viability of mouse lung single-cell suspensions were performed followed by plating approximately 200,000 live cells per well in a 96-well V-bottom plate. K7M2-RFP cells were also trypsonized from a tissue culture flask and plated in a well with mouse lung cells from naïve, non-tumor bearing mice as a control prior to flow cytometry analysis using the Cytek aurora 4-laser spectral flow cytometer and spectral unmixing of samples. For confocal fluorescent microscopy and visiopharm analysis, OTC embedded and frozen mouse lung tissues were sectioned into 5, 5 um slices using a cryostat tissue sectioning instrument and immediately placed onto microscope slides. Slides were stored in -20C freezer prior to analysis. Slides were stained with the nuclear staining dye, DAPI (Blue) and actin staining dye, Actingreen (green) prior to analysis. Using the Olympus confocal fluorescent microscope – a 10x overview image of each of the 5 lung sections was generated. Using the overview, a

20x focus map was generated to automate a focused and stitched 20x image. Images were analyzed using a visiopharm app we developed to detect and quantify RFP cells.

For 143b-RFP-Luc Study - 3 weeks in advance of the anticipated study completion days, 1e6 143b OS cells transduced with a dual red fluorescent protein-luciferase reporter lentiviral construct (143b-RFP-Luc) were tail vein injected into a Balb/c-scid mouse. This was enough time for the injected OS cells to colonize the lung, forming gross metastases whose bioluminescent signal was easily detected by IVIS imaging *in vivo*. The lungs from this mouse were used as a positive control during the unmixing process and to inform gating strategies during data analysis. For the 1 and 4-day post-tumor cell injection *in vivo* mouse studies, 1e6 143b-RFP-Luc cells were tail vein injected into 3 Balb/c-scid for each timepoint. Mice were imaged using the IVIS immediately post tail vein injection for both timepoints, and again 1 day prior to study completion for only the 4-day study. IVIS imaging of mice was discontinued on the day mice were sacrificed for tissue processing and downstream analysis to reduce the influence the bioluminescent signal from IVIS imaging was having on the spectral unmixing process. Lungs were digested using a protocol determined to be better at liberating RFP cells from within the lung's cellular matrix. Briefly, following euthanasia by cervical dislocation under isoflurane anesthesia, a digestion solution comprised of 500 uL collagenase D (1 mg/mL in 1x PBS), 250 uL Dispase (5 U/mL in 1x PBS), 32 uL Elastase (4 U/mL in 1x PBS), and 500 uL sterile 0.9% saline was instilled in each mouse lung via the trachea. The trachea was tied off using surgical suture, lungs were removed and allowed to sit at room temp for 10 min. in a 12-well flat bottom plate. Lungs were then minced using ethanol-cleaned razor blades followed by incubation at 37C for 30 min. Partially digested lung homogenates were triturated using a P-1000 pipette with tips cut at the end. The lungs were transferred to a 15 mL conical tube and 5 mL complete DMEM media was added before centrifugation at 1500 rpm for 5 min. at 4C. Any floating tissue remaining was gently removed and returned to the cell culture plate. Supernatants were removed from each 15 mL conical tube and cell pellets were resuspended in 1 mL of trypsin solution comprised of 500 uL 0.25% trypsin, 500 uL saline, and 20 uL of DNAse solution per mL before incubation on a rotating plate at 37C for 30 min. Homogenates were again triturated using a P-1000 pipette, returned to a 15 mL conical tube where 3 mL complete DMEM media was added before centrifugation at 1500 rpm for 5 min at 4C. Supernatants were discarded, 5 mL sterile 0.9% saline was added, and using a 10 mL syringe attached to

an 18-gauge needle, the pellet was pipetted in and out several times to form a single cell suspension prior to use of 100 um filters. Cells were then centrifuged at 1200 rpm for 5 min., supernatants were discarded, and cells were resuspended in 500 uL cold 1x sterile PBS. Cell suspensions were counted, and viability was determined before being plated in equal volumes in 2 separate plates. One plate was a clear, 96-well V-bottom plate to be used for spectral flow cytometry analysis, and the other plate was a 96-well clear/flat bottom, black walled plate to be used for IVIS imaging. Additionally, in vitro 143b-RFP-Luc cells were plated in duplicate 2-fold serial dilutions starting at 100,000 cells per well. Cells being prepared for flow cytometry were stained with zombie live/dead following protocols described previously. Following the final washing steps, wells were brought up to 100 uL in FACS buffer, then 100 uL cold 4% paraformaldehyde was added for 10 minutes. This was followed by a final centrifugation step at 1200 rpm for 5 minutes at room temp. before bringing up each well to a final volume of 150 uL for storage in the dark at 4C and eventual flow cytometry analysis. For the plate being used for IVIS imaging, D-luciferin solution (30 mg/mL) was added to a final concentration of 150 ug/mL (200x) 10 min. prior to IVIS imaging using the well plate auto exposure setting described previously.

Results

In vitro evaluation of fluorescent cellular labeling dyes

We set out to develop a sensitive and quantitative method for detecting OS cells during the earliest stages of metastatic lung colonization using spectral flow cytometry. Unlike most other cell types, however, OS has no universally expressed distinguishing cell surface markers that are typically exploited for the identification of cell populations when using flow cytometry. Because of this, we identified two fluorescent cell labeling compounds that function under distinct mechanisms, one membrane intercalating (DIR) and the other intracellular (Cell Trace Yellow). To determine the optimal cell labeling methods and concentrations using these two fluorescent dyes, *in vitro* experiments were conducted using the human OS cell line, 143B, labeled with either ((1,1'-Dioctadecyl-3,3,3',3'-Tetramethylindotricarbocyanine Iodide, (DIR)) or Cell Trace Yellow. Cells were labeled in concentrations ranging from 5 uM to 156 nM, analyzed alone or in a 1:1 ratio mixed with unstained 143b cells, and allowed to incubate together for 4 hours prior to spectral flow cytometric analysis. When mixed with 143b cells labeled with DIR and Cell Trace at 5 uM, unstained 143b cells shift far to the right compared to unstained cells alone as depicted in the representative flow plots for each dye's respective fluorescent channel (Fig. 3.1A). The shift among unstained cells is representative of an increase in signal intensity indicative of a potential transfer of dye to unstained cells. To determine if this effect is dye concentration dependent, 143b cells were labeled at concentrations ranging from 2.5 uM to 625 nM prior to a 4-hour incubation with unstained 143b cells in a 1:1 ratio. Flow plots show a shift among unstained 143b cells associated with increased fluorescent signal intensity; however, this effect is mitigated by reducing concentrations of dye during the labeling process. Of the concentrations tested, a consistent signal intensity distinguishing labeled and unlabeled cells was observed at a dye concentration of 625 nM for both dyes (Fig 3.1B). Furthermore, as the concentration of dye is reduced during the labeling processes, the separation between co-incubated, labeled and unstained 143b cells increases as measured by variance, allowing for the visualization of more distinct and separate populations of cells during data analysis (Fig 3.1C, Supplementary Fig. 3.1A). Additionally, the observed decrease in signal intensity among Cell Trace labeled 143b cells occurred when analyzed alone, indicating the decrease in signal intensity results from lower dye concentrations and not from the

loss of dye to unstained cells (Fig. 3.1D). Despite functioning under different mechanisms, we observed DIR and Cell Trace Yellow labeling of 143b cells results in a shift in fluorescent signal intensity in unstained 143b cells, an effect optimization of labeling techniques improves in a concentration dependent manner. We next sought to determine if this effect was due to proximity of cell populations during co-incubation or from the disruption of cellular membranes during the repeated washing and centrifugation steps typically used prior to flow cytometry analysis. It was determined that minimizing the steps involved in sample preparation reduced the fluorescent signal intensity associated with the transfer of dye to unstained cells, but did not completely abrogate this effect, indicating the fluorescent signal is transferred to unstained cells by multiple mechanisms (Fig. 3.1E, Supplementary 3.1B-C). To determine the stability of these cell labeling dyes over time, we assessed their signal intensity over 3 consecutive days post-labeling. The signal intensity peaks of Cell Trace labeled cells remained less widely distributed compared to DIR dye, indicating a higher degree of stability over time (Fig. 3.1F). These data indicate fluorescently labeled OS cells are detected using flow cytometry, and optimization of cell labeling methods can reduce the spill over of fluorescent signal into unstained cells. These results suggest fluorescent labeling of OS cells may be useful for detecting OS cells in mouse lungs using flow cytometry.

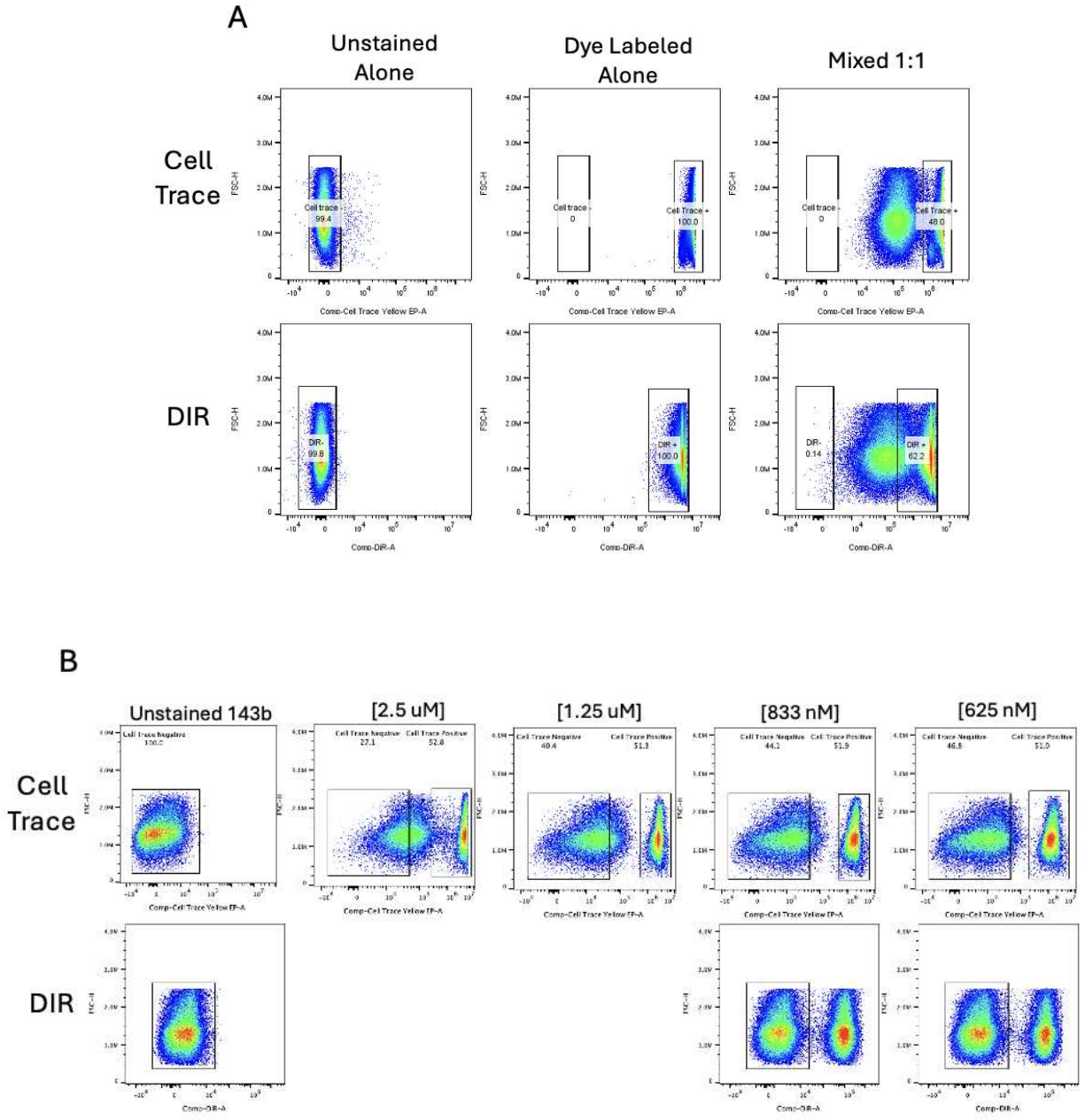

Fig 3.1 In vitro assessment of fluorescent cellular labeling dyes A) Flow plots showing unstained 143b cells, DIR and Cell Trace labeled 143b cells (5 uM for each dye), and labeled and unstained 143b cells mixed in a 1:1 ratio. **B)** Flow plots showing unstained 143b cells alone and mixed in a 1:1 ratio with Cell Trace labeled 143b cells labeled at 4 concentrations (2.5 uM, 1.25 uM, 833 nM, 625 nM) as well as flow plots showing unstained 143b cells mixed in 1:1 ratios with DIR labeled 143b cells labeled at 2 concentrations (833 nM, and 625 nM).

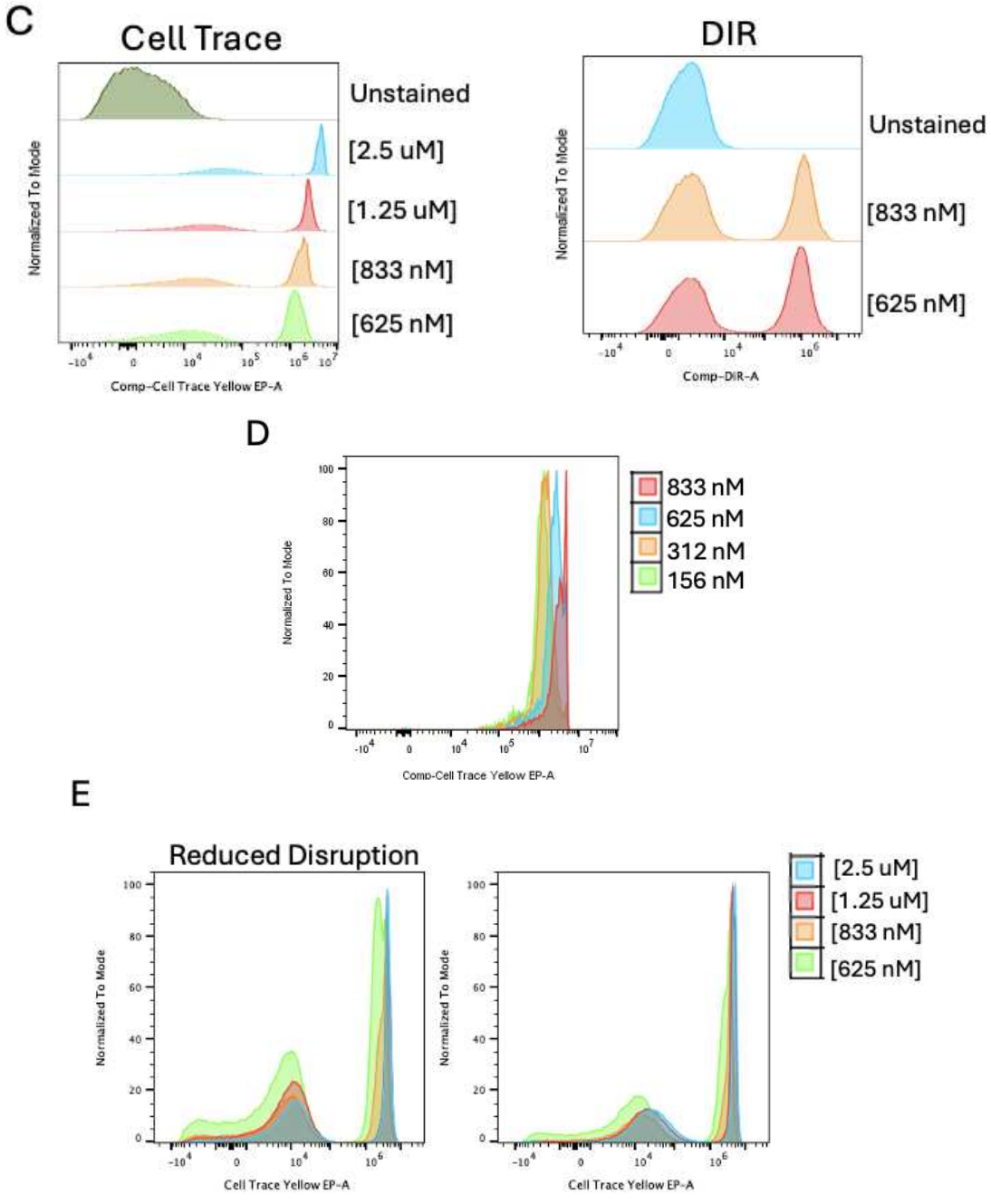

Fig 3.1 In vitro assessment of fluorescent cellular labeling dyes C) Pooled and stacked histograms representing the data from Fig. 1B. **D)** Histogram depicting the fluorescent intensity of 143b cells alone, labeled with Cell Trace at 4 concentrations (2.5 uM, 1.25 uM, 833 nM, 625 nM). **E)** Stacked histogram flow cytometry plots depicting unstained 143b cells mixed in a 1:1 ratio with Cell Trace labeled 143b cells at 4 concentrations (2.5 uM, 1.25 uM, 833 nM, 625 nM) and processed either with minimal or including all washing steps in preparation for flow cytometry analysis.

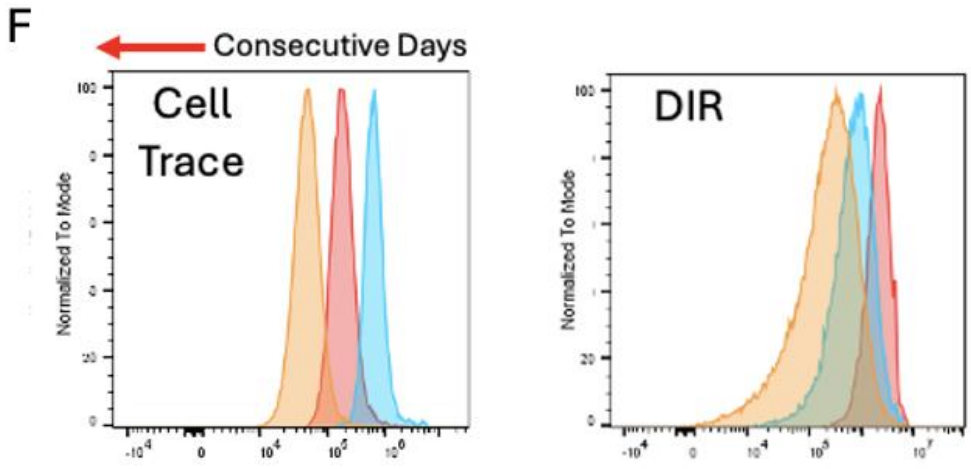

Fig 3.1 In vitro assessment of fluorescent cellular labeling dyes F) Histograms showing pooled peak signal intensity of Cell Trace and DIR labeled 143b cells analyzed on consecutive days. All samples were analyzed using the Cytek Aurora 4-lazer under the same settings and data was analyzed using FlowJo software.

***In vivo* evaluation of DIR labeled 143b cells**

Our initial *in vitro* analysis of fluorescent labeling dyes indicated DIR labeling of 143b OS cells resulted in less dye transfer to unstained cells compared to Cell Trace Yellow. Therefore, we next sought to determine if DIR labeled 143b cells could be detected in the lung post tumor cell injection by flow cytometry. To confirm DIR positivity was restricted to the tumor compartment during lung colonization following intravenous injection of labeled tumor cells, we employed the use of a 6-marker antibody panel developed to label and detect resident mouse lung cell populations by flow cytometry (Supplementary Fig. 2, Table 1). We also sought to validate these results by employing a second detection method to be run in parallel. To accomplish this, we transduced 143b cells with a luciferase expression system (143b-Luc) for the detection and quantification of bioluminescence using an intravital imaging system (IVIS). First, Balb/c-scid mice were tail vein injected with DIR labeled (625 nM) 143b-Luc cells. Mice were imaged for the detection of bioluminescence and fluorescence using the IVIS tuned to the excitation and emission spectra of DIR (750 nm, 780 nm, respectively). Mice were imaged 10 min. post-tumor cell injection to confirm successful injections, and 4-days post tumor-cell injection *in vivo*, and *ex vivo* to confirm the presence of 143b-Luc cell colonies in the lung (Fig. 3.2A). An initial analysis of IVIS imaging

data comparing fluorescent and bioluminescent signal data at each time point demonstrates a lack of correlation between the two measurement modalities (Fig. 3.2B). Representative flow cytometry plots of digested lung single cell suspensions from a tumor cell injected mouse show the detection of live DIR positive cells using gating strategies informed by **1)** naïve, control mouse lung and **2)** DIR labeled 143b-Luc cells allowed to incubate in a tissue culture plate for 4 days prior to analysis (Fig. 3.2C). The lack of significant correlation between the 4-day *ex vivo* bioluminescence and the percent of live DIR+ cells identified using these gating strategies provided further evidence suggesting the fluorescent signal associated with DIR labeled 143b cells may not restricted to the tumor compartment (Fig. 3.2D). We next sought to determine if this was the case. Using gating strategies to identify CD45+ and CD31+ cells, markers associated with the broad class of mouse resident lung cell populations comprising lymphocytes and endothelial cells, respectively, we show a substantial percent of live, DIR positive cells derived from both gating strategies mentioned previously also express CD45 and CD31 (Fig. 3.2E). These results confirm our suspicion of DIR dye "leakiness." However, employing these 2 markers alone to eliminate both DIR+/CD45+ and DIR+/CD31+ cell populations, the volume adjusted cell counts and percent of live DIR+ cell populations remaining substantially increases the correlation of imaging data to *ex vivo* bioluminescence imaging data (Fig 3.2F). Further analysis demonstrates a DIR specific fluorescent signal is detectable in mouse resident lung cell populations that express cell surface markers associated with alveolar macrophages, dendritic cells, and lung fibroblasts (Supplementary Fig. 2A-2D). Taken together, these data show the DIR fluorescent signature from labeled 143b-Luc cells is not restricted to the tumor compartment upon tail-vein injection and subsequent lung colonization of labeled OS cells. Finally, by employing a relatively simple, 2 marker antibody panel, we show the exclusion of DIR positive cells that also express CD45+ and CD31+ substantially improves the correlation between detection methods.

A

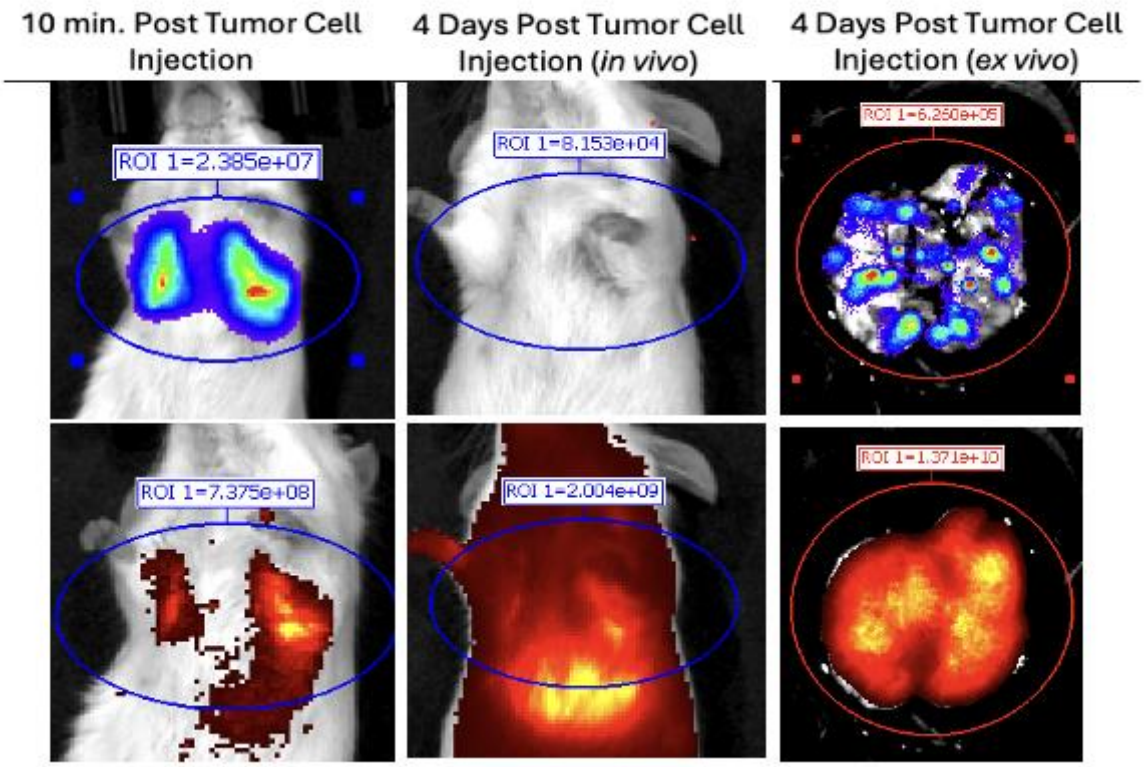

Fig 3.2 In vivo evaluation of DIR labeled 143b cells A) Representative bioluminescent (top) and fluorescent (bottom) IVIS images (mouse #2) taken 10 min. post-tumor cell injection, 4 days post-tumor cell injection in vivo, and ex vivo

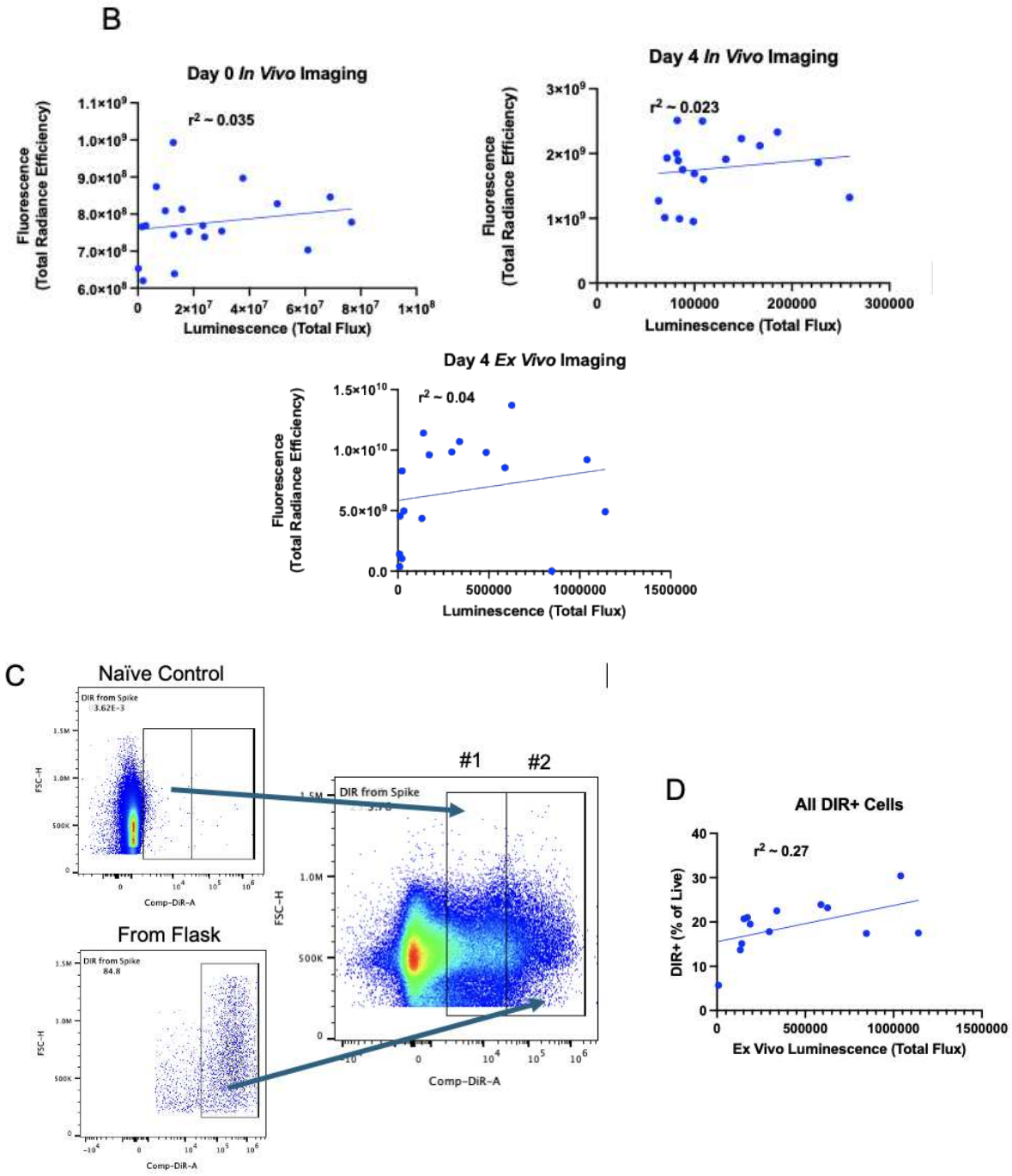

Fig 3.2 In vivo evaluation of DIR labeled 143b cells B) XY plots comparing IVIS detected fluorescent and bioluminescent signal intensities at each time point (10 min. in vivo, 4-day in vivo, 4-day ex vivo) **C)** Flow cytometry plots showing DIR+ gating strategies derived from #1) non-injected, naïve control mouse lung cells (top left),#2) in vitro 143b cells labeled with cell trace at time 0 (bottom left), and application of those gating strategies to identify DIR positive cells in mouse lung single cell suspension (mouse #2). **D)** XY plot comparing DIR+ cells (% of live cells) to ex vivo luminescence (total flux).

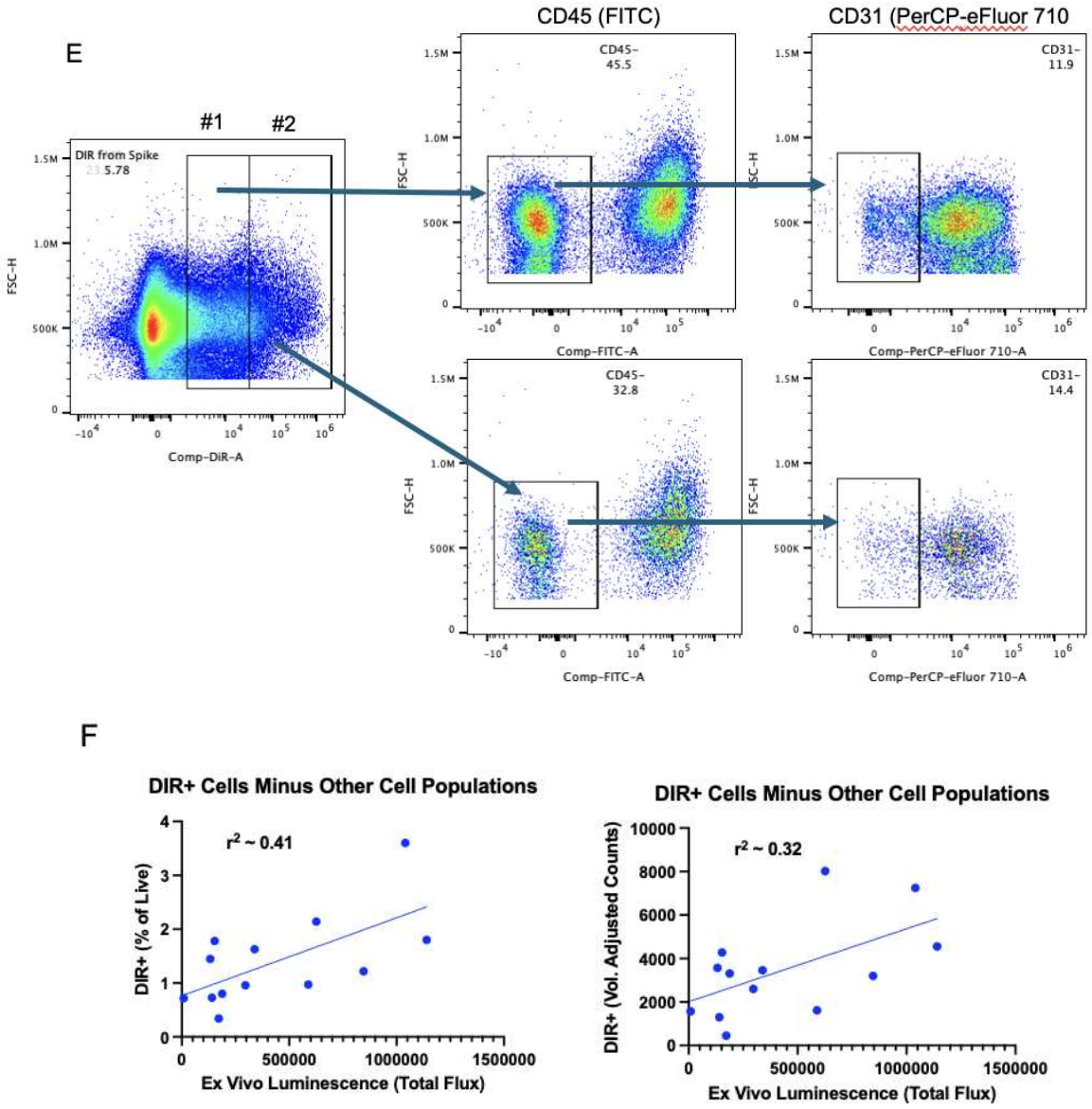

Fig 3.2 In vivo evaluation of DIR labeled 143b cells. E) Flow plots showing all DIR+ cells identified using gates #1 and #2, gating out CD45+ cells (left), and then all CD31+ cells (right). **F)** XY plots comparing ex vivo luminescence (total flux) to DIR+ cells (% of Live, Vol. adjusted counts) after exclusion of CD45+/DIR+ and CD31+/DIR+ cells. Simple linear regressions were used to calculate correlation coefficients in each XY plot

Ex vivo analysis of cell trace dye and comparison to IVIS imaging

It was determined using IVIS imaging paired with a 6-marker flow cytometry panel that DIR labeling of 143b-Luc cells resulted in the transfer of fluorescent signal to resident mouse lung populations upon tail vein injection. We next sought to determine if Cell Trace fluorescent dye could be used as an alternative labeling method to DIR, as they function under different mechanisms. Prior to performing *in vivo* studies, however, we evaluated 143b-Luc cells labeled with Cell Trace using several dye labeling concentrations incubated with naïve mouse lung cells *ex vivo* in several ratios for 4 hours. Flow cytometry analysis shows an improving distinction between Cell Trace labeled 143b-Luc cells and unstained, naïve mouse lung cells as the concentration of dye and the ratio of labeled and unstained cells is decreased (Fig. 3.3A, Supplementary Fig. 3.2A). It should be noted, the final ratios between these cell populations calculated during flow cytometry analysis were less than intended at ~1:13, 1:20, and 1:50, however this difference was consistent across all Cell Trace labeling concentrations (Supplemental Fig. 3.2B). To determine if flow cytometry could be used to detect the potentially small fractions of OS cells within the lung at the earliest stages of metastatic colonization, we sought to assess the lower limits of detection of this detection method. Here, we demonstrate spectral flow cytometry is highly sensitive, capable of detecting fractions of a percent of Cell Trace labeled 143b-Luc cells when mixed with mouse lung cells *ex vivo* (Fig. 3.3B). To further optimize the cross functionality of flow cytometry and IVIS imaging, we plated a standard curve of 143b-Luc cells to be imaged using the IVIS in parallel just prior to the flow cytometry analysis associated with data in Fig 3.3A. By generating a bioluminescent standard curve, we demonstrate the IVIS is highly sensitive, capable of detecting a bioluminescent signal above background associated with hundreds of 143b-Luc cells, and the linearity of the curve shows the bioluminescent signal is proportional to the number of cells in each respective well (Fig. 3.3C). Finally, we determined the IVIS generated standard curve used to predict the number of cells in each well based on their bioluminescent signal was highly correlative with the number of Cell Trace positive cells detected by spectral flow cytometry (Fig. 3D). These data demonstrate lowering the 143b dye labeling concentrations and reducing the ratio of labeled cells to *ex vivo* mouse lung cells further minimizes the transfer of fluorescent signal to unstained cells, thereby increasing the distinction between populations during analysis. Furthermore, as a proof of concept, we show the bioluminescent signal detected using IVIS

imaging is highly correlative to Cell Trace positive cells identified using spectral flow cytometry, even at the lower limits of detection. These results indicate the pairing of IVIS imaging and spectral flow cytometry for the detection of Cell Trace labeled 143B-Luc should be further evaluated *in vivo*.

A

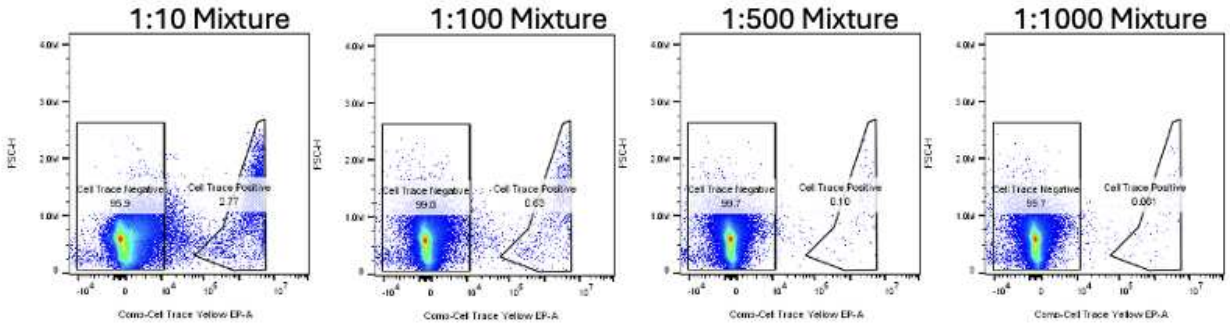

Fig 3.3 Ex vivo analysis of Cell Trace and comparison to IVIS imaging A) Flow plots showing Cell Trace 143b cell labeled at 4 concentrations (2.5 uM, 1.25 uM, 833 nM, 625 nM) alone, or mixed in 3 ratios (1:5, 1:10, 1:20) with unstained mouse lung cells *ex vivo.*

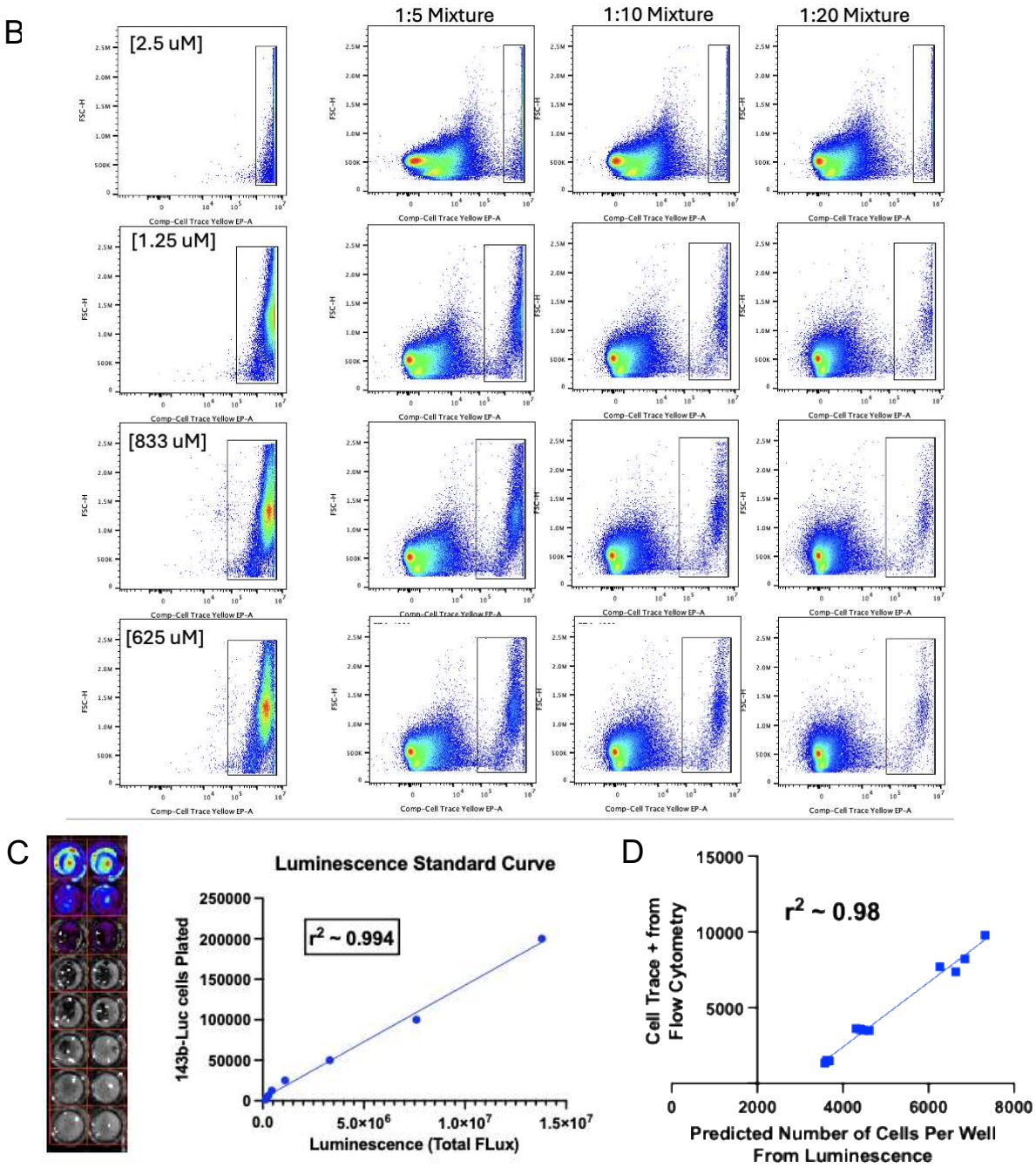

Fig 3.3 Ex vivo analysis of Cell Trace and comparison to IVIS imaging B) Flow plots showing detection of Cell Trace 143b cells (625 nM) mixed at 4 ratios (1:10, 1:100, 1:500, and 1:1000) with unstained mouse lung cells ex vivo. **C)** IVIS image of bioluminescence from the 143b-Luc standard curve (100,000 to 783 143b-Luc cells) and XY plot of cell number plated vs. luminescence (total flux) **D)** XY Plot comparing the counts of Cell Trace+ 143b cells detected by flow cytometry to the predicted number of cells per well using the IVIS standard curve. Simple linear regressions were used to calculate correlation coefficients in each XY plot.

***In vivo* analysis of cell trace cell labeling dye and comparison to IVIS imaging**

Spectral flow cytometry paired with IVIS imaging is a highly sensitive and correlative method for detecting small numbers of Cell Trace labeled cells after incubation with mouse lung cells *ex vivo*. Therefore, we next sought to determine if these methods were effective in detecting Cell Trace labeled cells *in vivo*, and if the fluorescent signal was restricted to the tumor compartment. Previous *in vitro* analysis of Cell Trace stability indicated signal intensity decreases over time. Although results of an *in vivo* cell trace time course study were inconclusive, the data suggests the fluorescent signal associated with Cell Trace had degraded substantially and was not detectable 4-days post-tumor cell injection, despite the detection of a bioluminescent signal (Supplemental Fig. 3.3A). However, the same pilot study detected a substantial *in vivo* and *ex vivo* bioluminescent signal within 24-hours post-tumor cell injection. This observation indicated the potential to use this narrow time window to detect Cell Trace labeled cells by flow cytometry. Following these results, we next set out to determine if Cell Trace dye can be detected 24-hours post-tumor cell injection and if the associated fluorescent signal is restricted to the tumor compartment. This was accomplished by employing the same 6-marker flow cytometry panel used for the *in vivo* DIR analysis previously discussed. This panel was paired with the use of an IVIS standard curve. Briefly, 2 Balb/c-scid mice were tail vein injected with Cell Trace (625nM) labeled 143b-Luc cells and imaged 10 min. post injection and 24-hours post tumor cell injection *in vivo* and *ex vivo* (Fig. 3.4A). To maximize the analysis of correlation between the IVIS standard curve and flow cytometry data, we increased the number of data points for each mouse by plating cells for analysis starting at 1.5 million cells, decreasing stepwise by 250k cells per well until reaching 500k total live cells plated. Using a gating strategy informed from naïve control mouse lung single cell suspensions, we identify Cell Trace positive cells within the tumor bearing mice 24-hours post tumor cell injection using spectral flow cytometry (Fig. 3.4B). We observe a lack of correlation between the percent of live Cell Trace positive cells identified by flow cytometry and the predicted number of 143b-Luc cells within the lung derived from the IVIS standard curve, indicating Cell Trace dye may not be restricted to the tumor compartment (Fig. 3.4C). To probe this result, we employed gating strategies previously used to evaluate DIR dye *in vivo* to exclude live CD45+/Cell Trace+ and CD31+/Cell Trace+ cell populations (Fig. 3.4D). This approach only slightly improved the correlation between the IVIS *ex vivo* bioluminescence and Cell Trace positive cells as a

percent of all live cells, however, a dramatic increase in the correlation was observed when comparing IVIS *ex vivo* bioluminescence Cell Trace positive cells as volume adjusted counts (Fig 3.4E). Again, by using the full panel of anti-mouse antibody markers, we show a Cell Trace fluorescent signal was observed in several other mouse lung resident cell populations identified by their specific repertoire of cell surface markers (Supplemental Fig. 3.4B-E). Taken together, we show labeling 143b-Luc cells with Cell Trace is likely not a useful approach for quantifying metastatic colonization. The signal intensity of Cell Trace labeled cells degrades quickly, and the associated fluorescent signal was detected in several resident lung cells identified by their surface markers. However, we demonstrate a substantial improvement in the correlation of these methods by employing gating strategies that exclude CD45+/Cell Trace+ and CD31+/Cell Trace+ cells. This suggests OS cells can be detected in the lung using flow cytometry, but other approaches are required to distinguish them from resident mouse lung cell populations.

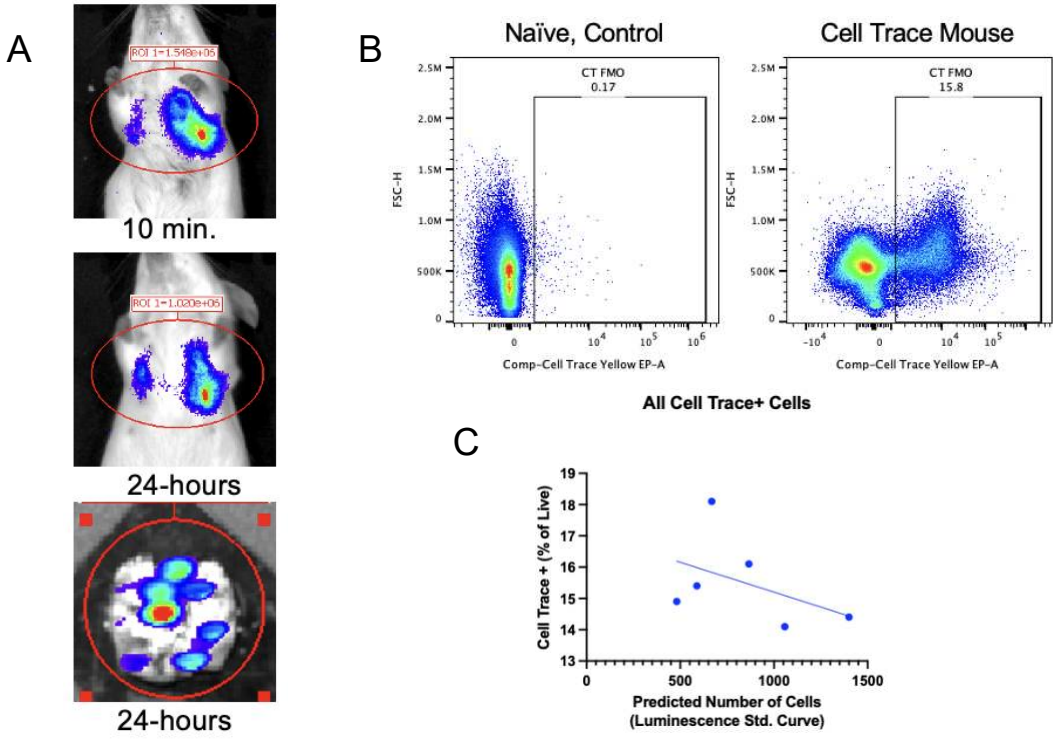

Fig 3.4 In vivo analysis of cell trace labeling dye and comparison to IVIS imaging A) Representative IVIS images 10 min. and 24-hours post-143b-Luc tail vein injection. **B)** Flow plots of naïve and Cell Trace labeled 143b-Luc injected mouse lung cells 24 hours post injection. **C)** XY plot comparing the percent of cell trace positive live cells determined by flow cytometry against the predicted number of cells calculated by the bioluminescent standard curve.

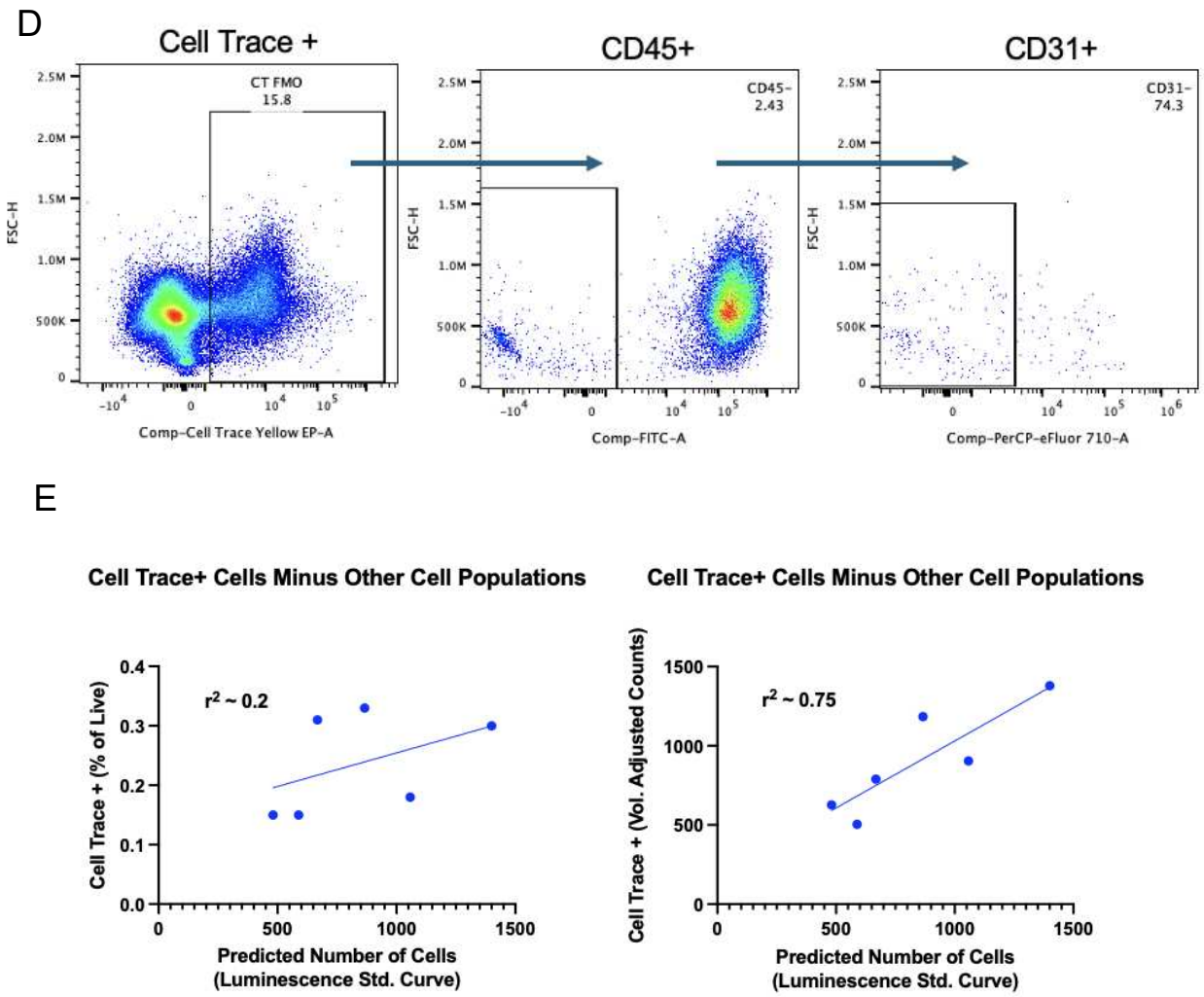

Fig 3.4 In vivo analysis of cell trace labeling dye and comparison to IVIS imaging D) Flow plots depicting the strategy to exclude live, cell trace positive cells by gating out those that are also CD45+ and CD31+ **E)** XY plots comparing Cell Trace positive cells after exclusion of CD45+ and CD31+ cells determined by flow cytometry as percent of live cells (Left) and volume adjusted counts (Right) against the predicted number of cells calculated by the bioluminescent standard curve.

***In vivo* analysis of nuclear labeled RFP K7M2 and 143b OS cells**

Using a mouse lung cell specific antibody panel paired with bioluminescent imaging, we determined the fluorescent signal derived from labeling 143b cells using DIR or Cell Trace Yellow dyes was not restricted to the tumor compartment in the lungs of OS cell injected mice. Previously conducted *in vivo* pilot studies initially aiming to detect and quantify OS cells in the lung in an immunocompetent syngeneic mouse model, used the RFP expressing mouse OS cell line, K7M2 in Balb/C mice. We first conducted time-course studies to determine the optimal timeline conducive for detecting K7M2-RFP cells in the lung. We evaluated mouse lungs 4-, 8-, and 14-days post-K7M2-RFP tail vein injections by flow cytometry paired with confocal fluorescent microscopy and quantitative image analysis of slides generated from fixed, frozen and paraffin embedded lung tissues as depicted in the schematic. (Fig. 3.5A) K7M2-RFP cells grown in a tissue culture flask displayed a fluorescent signal intensity easily detectable by flow cytometry However, the subsequent analysis of K7M2-RFP injected mouse lung single cell digests revealed substantial difficulty in identifying a distinct population of RFP expressing cells by flow cytometry 4- and 8- days post tail vein injection. 2/4 mice had minimally detectable populations of K7M2-RFP cells 14-days post tail vein injection (Fig. 3.5B, C). At this time, we had yet to implement IVIS imaging and sought to use confocal fluorescent microscopy and quantitative image analysis of FFPE sectioned slides as a secondary detection method as seen in representative images and accompanying quantitative analysis (Fig. 3.5D). Flow cytometry and microscopy analysis of mouse lungs 4-days post tail vein injection revealed minimally detectable quantities of K7M2-RFP cells. And although flow cytometry detected a substantial population of K7M2-RFP cells in the lungs of 2/4 mice 14-days post-tail vain injection, follow up image analysis did not detect a quantifiable number of RFP cells in the lungs of those mice, making these results unreliable. However, among mice analyzed 8-days post-tail vein injection, trends observed between flow cytometry and microscopy analysis were correlative (Fig. 3.5E). The potential for introducing unreliable and inconsistent results due to the logistic and methodological complexity involved in image analysis of serial sectioned slides may have contributed to the lack of correlation between flow cytometry and quantitative image analysis observed among K7M2-RFP cells at multiple time-points *in vivo. Ex vivo* IVIS images of luciferase expressing K7M2 cells acquired after the conclusion of this study demonstrate the highly variable localization of metastatic foci often characterized

by either lung wide dispersion or outgrowth of a single, concentrated colony (Fig. 3.5F). This observation further complicates image analysis, as dividing the lungs for use by separate detection methods or imaging slides generated from sections that lack a metastatic foci may result in unreliable imaging results.

To avoid complications arising from the use of fluorescent labeling dyes and the challenges encountered in the detection of K7M2-RFP cells by flow cytometry and microscopy *in vivo,* we revisited the use of nuclear RFP expression as a method for detecting human OS cells in an immunocompromised xenograft model. Prior to this study, evaluation of lung digestion protocols optimized for liberating stromal cell populations, also revealed a significant increase in the number of 143b-RFP cells detected in the lung in mice 3-weeks post-143b-Luc cell tail vein injection (, led us to evaluate 143b cells transduced with lentiviral particles containing a dual, nuclear red fluorescent protein/luciferase construct (143b-RFP-Luc). Transduced cells were tail vein injected into 2 groups of 3 mice each, with a group of mice being sacrificed 24-hours and 4-days post-tumor cell injection (Fig. 3.5G). Flow cytometry plots show that compared to lung cells from a naïve, control mouse, 143b-RFP-Luc cells alone, or spiked in *ex vivo*, display a high fluorescent signal intensity allowing for the separation of distinct populations (Fig. 3.5H). *In vivo* IVIS imaging 10 minutes post 143b-RFP-Luc cell tail vein injections show bioluminescent signal intensities measured as total flux among 3 mice. Flow cytometry plots show the detection of RFP positive cells within mouse lung single-cell suspensions associated with their respective mice shown above within 24-hours of tumor cell injections (Fig. 3.5I). *In vivo* IVIS imaging of 3 tumor bearing mice show a detectable bioluminescent signal 3 days post-tumor cell injection. Flow cytometry plots show the detection of RFP positive cells 24-hours after the IVIS images were taken above, 4 days post-tumor cell injection, respectively (Fig. 3.5J). The bioluminescent signal the IVIS detected from the standard curves of these two experiments was used to predict the number of luciferase expressing cells within each well for a given experiment. Comparing the predicted number of 143b-RFP-Luc cells to the number of cells detected by flow cytometry using a simple linear regression resulted in correlation coefficients of 0.45 for mice 24-hours after tumor cell injections, and 0.78 for mice analyzed 96-hours after tumor cell injections (Fig. 3.5K). These data demonstrate nuclear labeled RFP 143b cells display a fluorescent signal intensity that allows for the detection of dozens of RFP positive OS cells, a tiny fraction of mouse lung cells analyzed using flow cytometry within 24 hours of tumor cell injection. Additionally, IVIS imaging allowed

for the detection of a bioluminescent signal just above background emanating from luciferase expressing 143b cells within the mouse lung samples. The correlation between these two highly sensitive detection methods results in the ability to detect and quantify OS cells at the earliest stages of metastatic colonization, thus providing a high throughput method for further evaluation of mechanisms that drive these events in the hopes of developing novel therapeutic strategies to prevent OS metastasis.

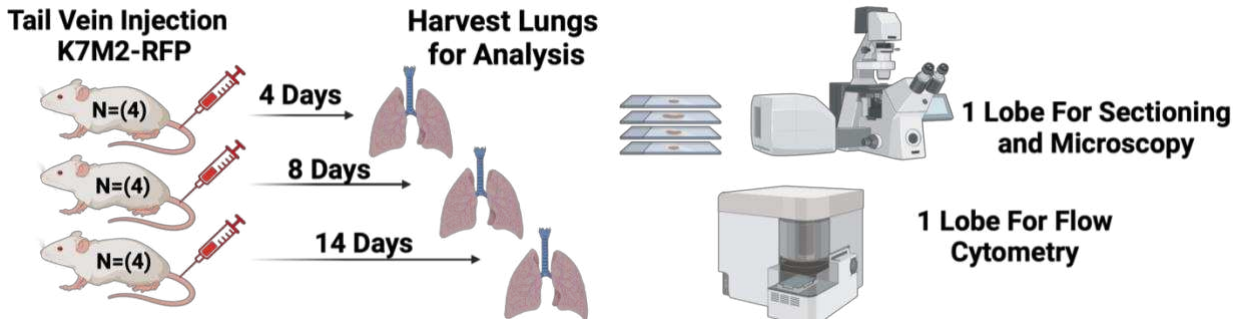

Fig 3.5 In vivo analysis of nuclear labeled 143b-Luc cells A) schematic depicting study methods used to track and quantify K7M2-RFP cells in vivo.

B

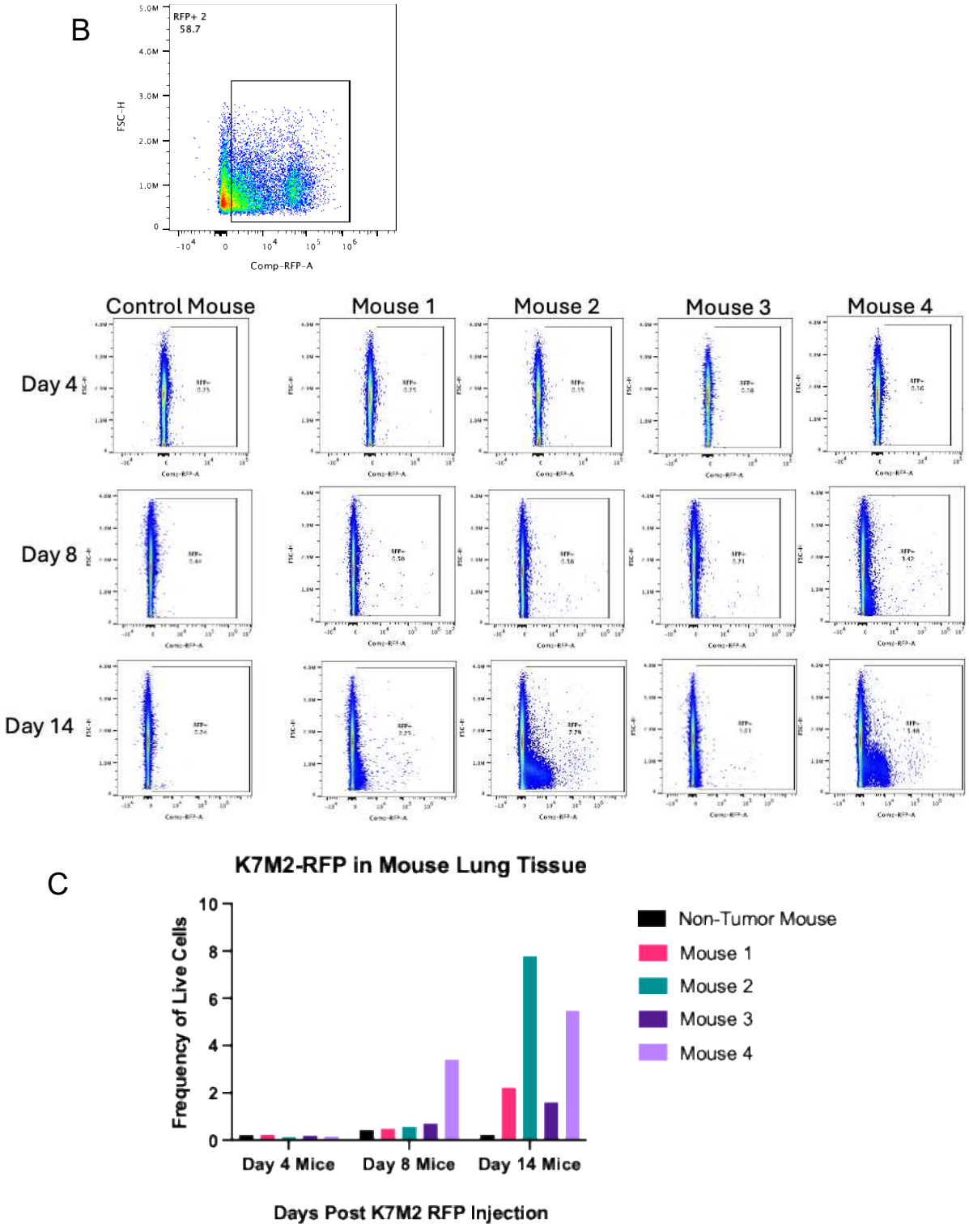

Fig 3.5 In vivo analysis of nuclear labeled 143b-Luc cells B) Flow plots of K7M2-RFP spiked into mouse lung cells ex vivo (Top), and RFP+ cells detected in K7M2-RFP injected mice 4-, and 14-days post-tumor cell injection. **C)** Bar graph of flow cytometry data showing RFP+ cells as a frequency of live cells at 4-, 8-, and 14-days post-tumor cell injection.

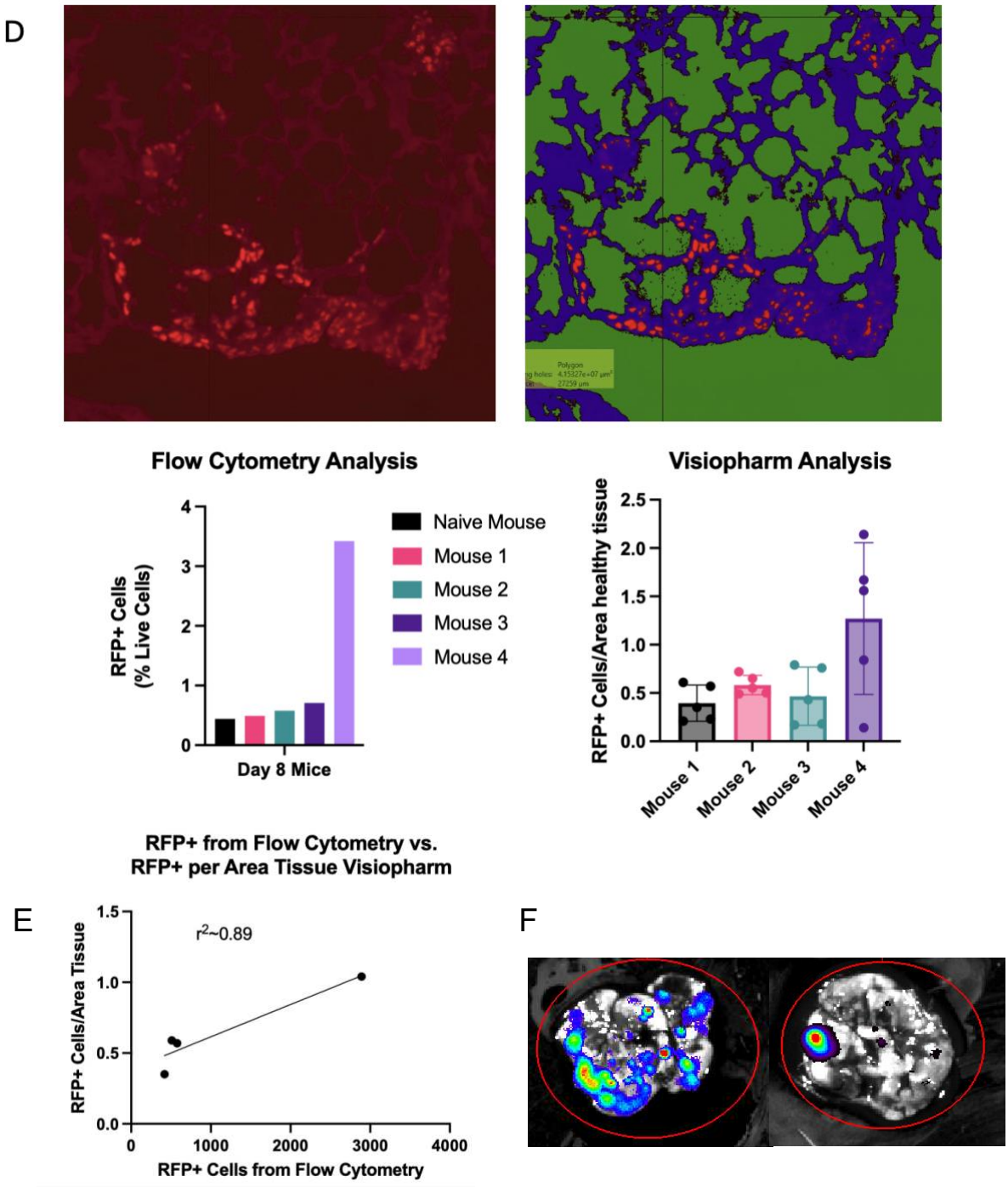

Fig 3.5 In vivo analysis of nuclear labeled 143b-Luc cells D) Rep. Images and quantitative bar graphs of RFP+ cells as percent of live cells measured by flow cytometry (Left) and RFP+ cells as a fraction of healthy tissue (Right) measured by confocal microscopy of sectioned slides and visiopharm analysis of mice 8-days post K7M2-RFP tail vein injection. **E)** XY plot comparing RFP+ cell counts between flow cytometry and microscopy **F)** Representative *ex vivo* IVIS images showing variable metastatic dispersion despite similar bioluminescent signal intensities

G

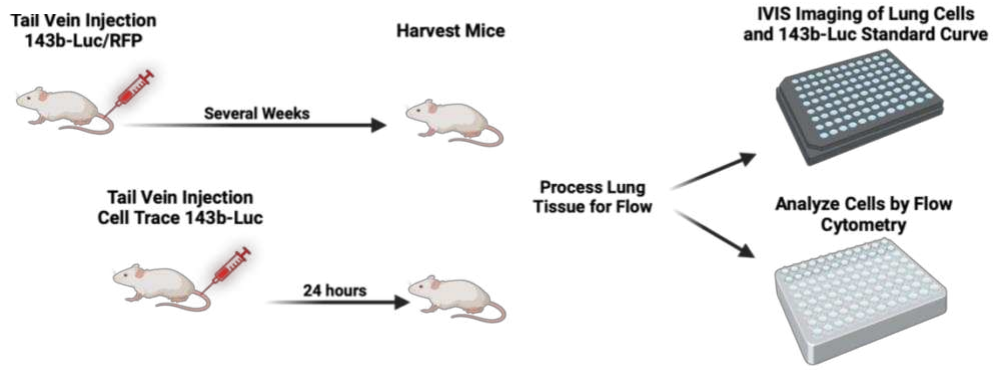

H

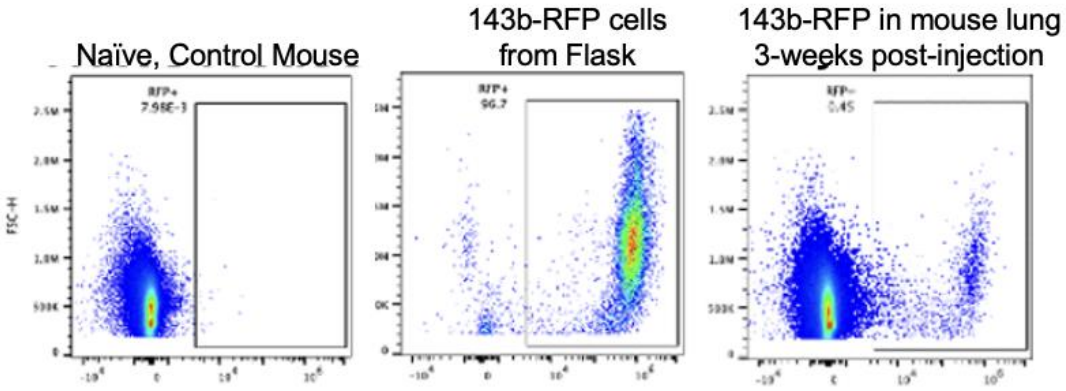

Fig 3.5 In vivo analysis of nuclear labeled 143b-Luc cells G) schematic depicting study methods used to track and quantify K7M2-RFP cells in vivo. **H)** Flow plots depicting RFP signal intensity among naïve, control (Left), 143b-RFP-Luc cells from tissue culture flask (Middle), and 143b-RFP-Luc injected mouse lungs 3-weeks post-tumor cell injection (Right).

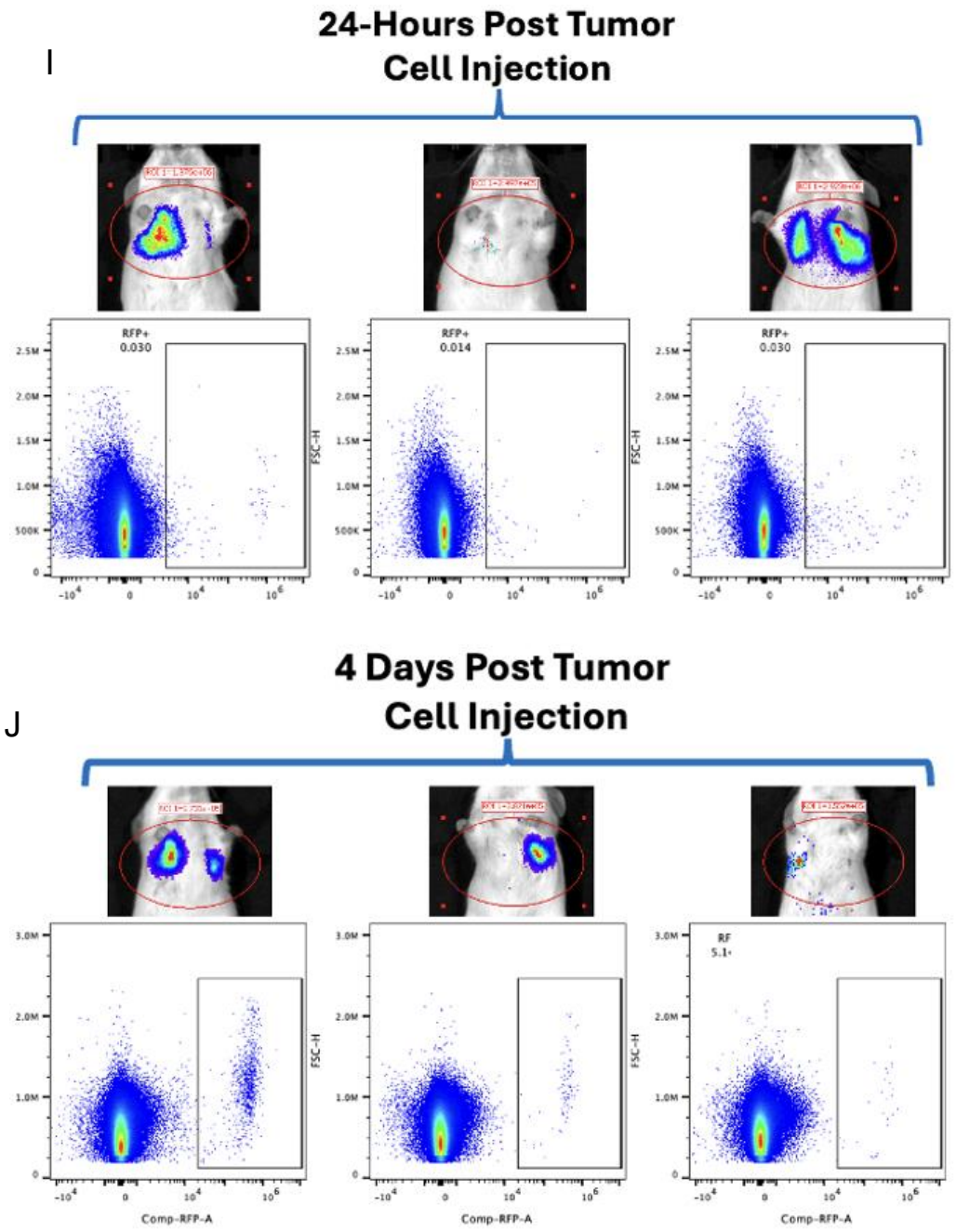

Figure 5 In vivo analysis of nuclear labeled 143b-Luc cells H) In vivo bioluminescent images of 143b-RFP-Luc injected mice 10 min. post-tumor cell injection and flow plots gating on RFP+ cells in the lungs of their respective mice 24-hours post-tumor cell injection. **I)** *In vivo* bioluminescent images of 143b-RFP-Luc injected mice 3 days post-tumor cell injection and flow plots gating on RFP+ cells in the lungs of their respective mice 4 days post-tumor cell injection.

K

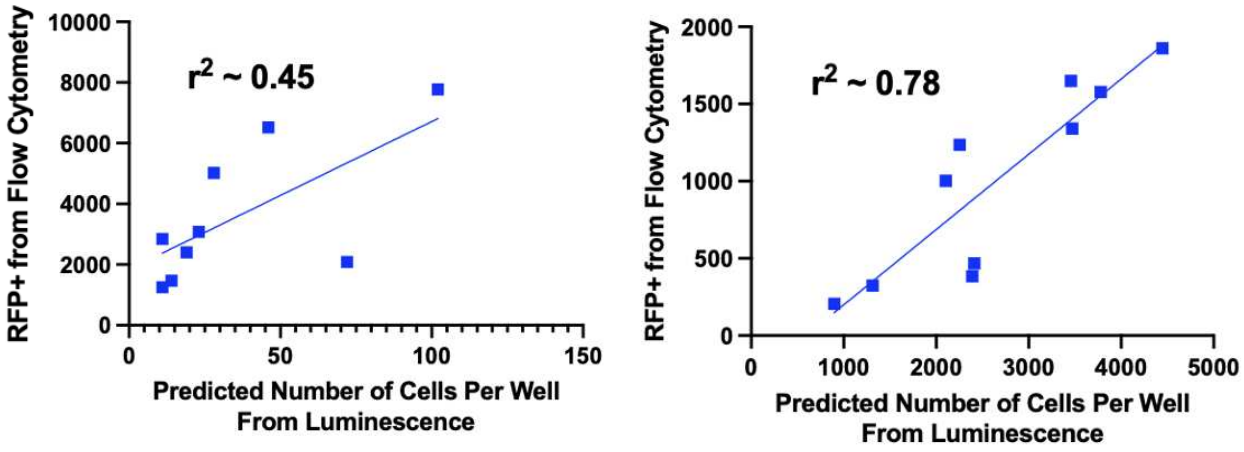

Fig 3.5 In vivo analysis of nuclear labeled 143b-Luc cells. K) XY plots of RFP+ cells (Counts) determined by flow cytometry analysis 24-hours (Left) and 4 days (Right) post-tumor cell injection measured against the predicted number of 143b-Luc cells measured by IVIS imaging and calculated using the standard curve.

Discussion

The development of novel therapeutic strategies targeting OS often stall as they fail to demonstrate clinical efficacy, despite promising preclinical results. (Jiang, Liu et al. 2022) This may be due to inherent biological differences between preclinical animal models and human OS patients as models may not fully recapitulate the milieu of cellular and molecular events that promote the progression of OS within the local or distant metastatic site. (Harris and Hawkins 2022) More recently, investigators have turned towards the development and implementation of novel in vitro and ex vivo methods for evaluating the behavior and biology of OS. These approaches, such as 2D and 3D co-culture models, as well *ex vivo* models like the pulmonary metastasis assay (PUMA), have allowed for studies that probe interactions between OS and the cells commonly found in the OS TME or lung PMN within extracellular structural architecture that more accurately reflects the complexity of the OS TME. (Mendoza, Hong et al. 2010, Nunes, Barros et al. 2019, Schott, Shah et al. 2020, Chow, Wutami et al. 2021, Guan and Huang 2022, Roy, Alix et al. 2023, Schott, Koehne et al. 2024, Yadav, Mahajan et al. 2024) Additionally, the use

of genetically modified mouse models, patient derived xenografts, and novel *in vivo* imaging techniques have increasingly shed light on many key aspects of the metastatic cascade. Despite these innovations, a key knowledge gap in our understanding of the events that occur during the earliest stages of metastatic colonization remain.

To address this challenge, we set out to develop a model of OS metastatic colonization using well established methods like bioluminescent detection by IVIS imaging and flow cytometry. To overcome the limitations associated with the lack of a universally expressed and highly specific OS cell surface marker typically used to discriminate specific cell types using flow cytometry, we evaluated fluorescent cell labeling methods and stable expression of nuclear red fluorescent protein within the highly metastatic human OS cell line 143b. Here, we demonstrate fluorescent cell labeling dyes that function through distinct mechanisms can be optimized to minimize the transfer of their respective fluorescent signal to unstained cell populations *in vitro*. Additionally, we demonstrate a high degree of sensitivity for the detection of labeled OS cells by spectral flow cytometry. Despite this, through a secondary measurement modality and implementation of a mouse resident lung cell antibody panel, we determined these cell labeling dyes were likely not a reliable method for tracking OS cells in the lung, as the fluorescent signal is not restricted to the tumor compartment. Ultimately, the shortcomings resulting from the use of fluorescent labeling dyes were overcome by transducing 143b OS cells with a dual reporter system (RFP, Luciferase) that would allow for detection of OS cells by IVIS imaging and flow cytometry. Using this approach, we demonstrate these two highly sensitive and correlative detection methods are capable of quantifying 143b OS cells in mouse lung, single cell digests within 24 hours of tumor cell tail vein injections.

Several studies have been conducted to characterize the OS cell surface protein expression profile in commercial human OS, canine, and PDX derived cell lines. (Hassan, Bekarev et al. 2011, Gemei, Corbo et al. 2013, Wang, Tian et al. 2022) Many of the markers identified in these studies have been used to develop microfluidic devices, circulating tumor cell capture, CAR-T based therapies, determine OS cellular differentiation states, and biomarker identification for use as prognostic indicators. (Hughes, Thomas et al. 2004, Saini, Hose et al. 2012, Penfornis, Cai et al. 2014, Fasanya, Dopico et al. 2021) However, many of the surface markers identified are also sufficiently expressed on other cell types,

making them difficult to exploit for *in vivo* flow cytometry studies, where the separation of OS cells from mouse tissue resident cell populations is required. To sidestep this, we evaluated the efficacy of 2 fluorescent cell labeling methods. The first, DIR membrane intercalating dye, has been used to label and quantify cancer cells for unconventional *in vitro* 3D spheroid studies, and for *in vivo* studies that used whole body fluorescent imaging. (Carlson, Fujisaki et al. 2013, Osseiran, Austin et al. 2019) The second dye evaluated, Cell Trace Yellow, was designed and primarily used for quantifying cell proliferation, but has also been utilized with some success to track labeled circulating tumor cells *in vivo* using flow cytometry. (Pitsillides, Runnels et al. 2011, Tempany, Zhou et al. 2017)

Labeling 143b cells with these two dyes following the manufacturer recommended cell labeling concentrations and protocols resulted in a fluorescent signal intensity at or past the high limit of detection by the cytometer under “standard” laser settings. Additionally, when incubated in a 1:1 ratio for 4 hours with unstained 143b cells at recommended dye concentrations, we observed a considerable shift in the signal intensity of the unstained cells, indicating a possible transfer of dye to unstained cells. This is an effect observed when using other intracellular amine-reactive fluorescent dyes, such as zombie live/dead. This can result as an artifact of the detection method or, according to the manufacturer of zombie live/dead dyes, Biolegend, is potentially due to a failure to optimize dye concentrations. Accordingly, we determined this effect could be minimized in both a dye concentration dependent manner for DIR and Cell Trace as well as by reducing the ratio of Cell Trace labeled and unstained cells. Another hypothesis was that the sheering forces imposed on labeled cells during the repeated washing and centrifugation steps taken to prepare cells for flow cytometry analysis may be disrupting the integrity of cellular membranes, causing fluorescent dye to escape labeled cells into the extracellular space where it’s taken up by unstained cells. This theory is in line with evidence that circulating tumor cells can experience high fluid shear stresses (60 dynes/cm2). (Regmi, Fu et al. 2017, Moose and Henry 2020) A simple experiment comparing the dye transfer from labeled to unstained cells either with, or without the many washing and centrifugation steps typically used to prepare samples for flow cytometry revealed minimizing these disruptions reduced, but did not completely abrogate dye transfer, suggesting this effect may occur through multiple mechanisms.

Based on *in vitro* evidence that Cell Trace dye signal transfer to other unstained 143b cells could be reduced in a dye concentration dependent manner, we set out to evaluate this effect on populations of cells within the mouse lung *ex vivo* prior to evaluating this dye *in vivo*. We hypothesized the amount of signal transfer may be greater when labeled 143b-Luc cells are incubated with populations of mouse lung cells that have phagocytic functional properties, like macrophages and dendritic cells. (Uribe-Querol and Rosales 2020) Furthermore, as evidence suggests only a tiny fraction of circulating tumor cells derived from a primary tumor, or in our case, via tail vein injection, are likely to survive the sheering stresses of the vasculature and successfully colonize the lung. (M, M et al. 2004, Hanin 2023) Because of this, we incubated mouse lung cells *ex vivo* with incrementally decreasing numbers of Cell Trace labeled 143b cells, which resulted in a further reduction of dye associated signal transfer. By successfully detecting fluorescently labeled OS cells in a system emulating the potentially miniscule number of OS cells likely to successfully colonize the lung, we were able to demonstrate the high degree of sensitivity and potential for using flow cytometry as a method for detecting OS cells at the earliest phases of lung colonization.

Ultimately, though, by benchmarking flow cytometry results with IVIS imaging data and employing a multi-cell mouse lung cell antibody panel, we determined the use of DIR and Cell Trace labeling dyes as a method for *in vivo* detection of tail vein injected OS cells is likely not a reliable approach as we determine both dyes are not restricted to the tumor compartment. However, as a proof of concept, we show using the 6-marker flow cytometry panel to form gating strategies that exclude mouse resident lung cells that were also positive for either dye is a successful strategy for identifying likely OS tumor cells in the lung, as this process substantially improves the correlation between flow cytometry and IVIS imaging data. However, developing, optimizing, and employing a complicated flow cytometry panel is expensive, time consuming, technically challenging and potentially introduces problems with reproducibility. Further adding to this problem is the subjective nature of gating strategies used during data analysis. The use of more than 6 fluorescent markers in single cell suspensions derived from the lung, a highly auto-fluorescent organ, makes the critical process of spectral unmixing flow cytometry data difficult and can influence the resulting analysis. The process of spectral unmixing was made substantially more difficult when combining IVIS imaging with flow cytometry. We would eventually discover the bioluminescent signature used for IVIS imaging increased the fluorescent signal intensity of every channel being

measured by the cytometer, making the complete subtraction of the “auto-fluorescent” signature interfere with every fluorophore used in the panel. This greatly reduced the accuracy and reliability of downstream flow cytometry data analysis. Finally, although these methods and tools were developed to evaluate the earliest stages of metastatic colonization, using fluorescent labeling methods that quickly degrade and therefore, can only be detected for a matter of days, considerably reduces the functional applications of these dyes.

Initial studies investigating *in vivo* metastatic lung colonization employed a syngeneic mouse OS cell line, K7M2, transduced to express nuclear RFP. These studies paired spectral flow cytometry analysis of mouse lung single cell suspensions with a pipeline used to evaluate sectioned frozen lung tissues using confocal fluorescence microscopy and quantitative image analysis. The goal of using a syngeneic metastasis model was appealing as the mice used were immune competent and more faithfully reflected the full complement of cellular interactions that may influence OS metastasis. However, these studies were hampered by complications and setbacks resulting from the relatively weak luminescent and fluorescent signal intensities that made these cells difficult to detect in the lung (Appendix 3A). It may also be likely that compared to the highly metastatic human OS cell line 143b, K7M2 cells may not colonize the lung as successfully. Interestingly, using a human OS cell line transduced to express RFP and Luciferase resulted in a significant increase in signal intensity in RFP signal intensity and bioluminescence detected by flow cytometry and IVIS imaging, respectively. This discrepancy may be the result of variations in vector copy number between cell lines. (Kustikova, Wahlers et al. 2003, Shahar, Landman et al. 2020) Regardless, the increased signal intensity allowed for the detection of 143b cells by flow cytometry and IVIS imaging as early as 24 hours post-tumor cell injection. Additionally, the detection of 143b-RFP-Luc cells *in vivo* was considerably improved by implementing a lung digestion protocol that was shown to be more effective at liberating OS cells from the lung extracellular matrix. To address the concern regarding spectral unmixing interference resulting from the bioluminescent signal, cells from each mouse lung were equally divided between two separate well plates. Each respective plate being specifically designed for their respective data gathering method, which ultimately eliminated this concern.

As a cautionary tale, we conclude the use of the fluorescent cell labeling dyes assessed in these studies are likely not useful for *in vivo* OS metastasis studies, as their signal intensity degrades within several days, and their fluorescent signal is not restricted to the tumor compartment. However, the progressive development and optimization of techniques and methods described herein, has culminated in a high-throughput and highly sensitive system capable of detecting and quantifying the potentially tiny numbers of OS cells within the lung during the earliest stages of metastatic colonization. These findings offer investigators a platform that uses established and relatively accessible instruments to quickly probe the many molecular and cellular drivers of metastasis in the hopes of one day developing novel anti-metastatic therapeutic approaches and improve outcomes for OS patients.

Acknowledgements

The work for this projected was supported by the Boettcher Foundation and NIH grants 5T32GM136628 (LAH), 1K01OD022982 (DPR), R03OD028265 (DPR), and P30 CA046934 (University of Colorado Cancer Center Support Grant).

References

Berman, S. D., E. Calo, A. S. Landman, P. S. Danielian, E. S. Miller, J. C. West, B. D. Fonhoue, A. Caron, R. Bronson, M. L. Bouxsein, S. Mukherjee and J. A. Lees (2008). "Metastatic osteosarcoma induced by inactivation of Rb and p53 in the osteoblast lineage." Proc Natl Acad Sci U S A **105**(33): 11851-11856.

Bousquet, M., C. Noirot, F. Accadbled, J. Sales de Gauzy, M. P. Castex, P. Brousset and A. Gomez-Brouchet (2016). "Whole-exome sequencing in osteosarcoma reveals important heterogeneity of genetic alterations." Ann Oncol **27**(4): 738-744.

Carlson, A. L., J. Fujisaki, J. Wu, J. M. Runnels, R. Turcotte, C. L. Celso, D. T. Scadden, T. B. Strom and C. P. Lin (2013). "Tracking Single Cells in Live Animals Using a Photoconvertible Near-In frared Cell Membrane Label." PLoS ONE **8**(8): e69257.

Chow, T., I. Wutami, E. Lucarelli, P. F. Choong, S. Duchi and C. Di Bella (2021). "Creating In Vitro Three-Dimensional Tumor Models: A Guide for the Biofabrication of a Primary Osteosarcoma Model." Tissue Eng Part B Rev **27**(5): 514-529.

Cranmer, L. D. and E. Hersh (2007). "The role of the CTLA4 blockade in the treatment of malignant melanoma." Cancer Invest **25**(7): 613-631.

Fasanya, H. O., P. J. Dopico, Z. Yeager, Z. H. Fan and D. W. Siemann (2021). "Using a combination of gangliosides and cell surface vimentin as surfa ce biomarkers for isolating osteosarcoma cells in microfluidic devices." Journal of Bone Oncology **28**: 100357.

Gemei, M., C. Corbo, F. D'Alessio, R. Di Noto, R. Vento and L. Del Vecchio (2013). "Surface proteomic analysis of differentiated versus stem-like osteosar coma human cells." PROTEOMICS **13**(22): 3293-3297.

Guan, X. and S. Huang (2022). "Advances in the application of 3D tumor models in precision oncology and drug screening." Front Bioeng Biotechnol **10**: 1021966.

Hanin, L. (2023). "The circulation stage of the metastatic cascade: A mathematical descri ption and its clinical implications." Journal of Theoretical Biology **572**: 111582.

Harris, M. A. and C. J. Hawkins (2022). "Recent and Ongoing Research into Metastatic Osteosarcoma Treatments." International Journal of Molecular Sciences **23**(7): 3817.

Hassan, S. E., M. Bekarev, M. Y. Kim, J. Lin, S. Piperdi, R. Gorlick and D. S. Geller (2011). "Cell surface receptor expression patterns in osteosarcoma." Cancer **118**(3): 740-749.

Hughes, D. P. M., D. G. Thomas, T. J. Giordano, L. H. Baker and K. T. McDonagh (2004). "Cell Surface Expression of Epidermal Growth Factor Receptor and Her-2 with Nuclear Expression of Her-4 in Primary Osteosarcoma." Cancer Research **64**(6): 2047-2053.

Isakoff, M. S., S. S. Bielack, P. Meltzer and R. Gorlick (2015). "Osteosarcoma: Current Treatment and a Collaborative Pathway to Success." J Clin Oncol **33**(27): 3029-3035.

Jiang, T., T. Shi, H. Zhang, J. Hu, Y. Song, J. Wei, S. Ren and C. Zhou (2019). "Tumor neoantigens: from basic research to clinical applications." J Hematol Oncol **12**(1): 93.

Jiang, Z.-Y., J.-B. Liu, X.-F. Wang, Y.-S. Ma and D. Fu (2022). "Current Status and Prospects of Clinical Treatment of Osteosarcoma." Technology in Cancer Research & Treatment **21**.

Kempf-Bielack, B., S. S. Bielack, H. Jürgens, D. Branscheid, W. E. Berdel, G. U. Exner, U. Göbel, K. Helmke, G. Jundt, H. Kabisch, M. Kevric, T. Klingebiel, R. Kotz, R. Maas, R. Schwarz, M. Semik, J. Treuner, A. Zoubek and K. Winkler (2005). "Osteosarcoma relapse after combined modality therapy: an analysis of unselected patients in the Cooperative Osteosarcoma Study Group (COSS)." J Clin Oncol **23**(3): 559-568.

Kustikova, O. S., A. Wahlers, K. Kühlcke, B. Stähle, A. R. Zander, C. Baum and B. Fehse (2003). "Dose finding with retroviral vectors: correlation of retroviral vector copy numbers in single cells with gene transfer efficiency in a cell population." Blood **102**(12): 3934-3937.

Lilienthal, I. and N. Herold (2020). "Targeting Molecular Mechanisms Underlying Treatment Efficacy and Resistance in Osteosarcoma: A Review of Current and Future Strategies." Int J Mol Sci **21**(18).

M, K., N. M, N. R, R. I. J and S. U (2004). "Correlation of circulating tumor cells with tumor size and metastatic load in a spontaneous lung metastasis model." Anticancer Research.

Mendoza, A., S. H. Hong, T. Osborne, M. A. Khan, K. Campbell, J. Briggs, A. Eleswarapu, L. Buquo, L. Ren, S. M. Hewitt, H. Dakir el, S. Garfield, R. Walker, G. Merlino, J. E. Green, K. W. Hunter, L. M. Wakefield and C. Khanna (2010). "Modeling metastasis biology and therapy in real time in the mouse lung." J Clin Invest **120**(8): 2979-2988.

Mirabello, L., R. J. Troisi and S. A. Savage (2009). "Osteosarcoma incidence and survival rates from 1973 to 2004: data from the Surveillance, Epidemiology, and End Results Program." Cancer **115**(7): 1531-1543.

Moose, D. L. and M. D. Henry (2020). "Survival of the resilient: Mechano-adaptation of circulating tumor cells to fluid shear stress." Mol Cell Oncol **7**(4): 1766338.

Nunes, A. S., A. S. Barros, E. C. Costa, A. F. Moreira and I. J. Correia (2019). "3D tumor spheroids as in vitro models to mimic in vivo human solid tumors resistance to therapeutic drugs." Biotechnol Bioeng **116**(1): 206-226.

Osseiran, S., L. A. Austin, T. M. Cannon, C. Yan, D. M. Langenau and C. L. Evans (2019). "Longitudinal monitoring of cancer cell subpopulations in monolayers, 3 D spheroids, and xenografts using the photoconvertible dye DiR." Scientific Reports **9**(1).

Ottaviani, G. and N. Jaffe (2009). "The epidemiology of osteosarcoma." Cancer Treat Res **152**: 3-13.

Penfornis, P., D. Z. Cai, M. R. Harris, R. Walker, D. Licini, J. D. A. Fernandes, G. Orr, T. Koganti, C. Hicks, S. Induru, M. S. Meyer, R. Khokha, J. Barr and R. R. Pochampally (2014). "High CD49f expression is associated with osteosarcoma tumor progressio n: a study using patient-derived primary cell cultures." Cancer Medicine **3**(4): 796-811.

Pitsillides, C. M., J. M. Runnels, J. A. Spencer, L. Zhi, M. X. Wu and C. P. Lin (2011). "Cell labeling approaches for fluorescence-based in vivo flow cytometry." Cytometry Part A **79A**(10): 758-765.

Regmi, S., A. Fu and K. Q. Luo (2017). "High Shear Stresses under Exercise Condition Destroy Circulating Tumor Cells in a Microfluidic System." Sci Rep **7**: 39975.

Roy, M., C. Alix, A. Bouakaz, S. Serrière and J. M. Escoffre (2023). "Tumor Spheroids as Model to Design Acoustically Mediated Drug Therapies: A Review." Pharmaceutics **15**(3).

Saini, V., C. D. Hose, A. Monks, K. Nagashima, B. Han, D. L. Newton, A. Millione, J. Shah, M. G. Hollingshead, K. M. Hite, M. W. Burkett, R. M. Delosh, T. E. Silvers, D. A. Scudiero and R. H. Shoemaker (2012). "Identification of CBX3 and ABCA5 as Putative Biomarkers for Tumor Stem Cells in Osteosarcoma." PLoS ONE **7**(8): e41401.

Schott, C., A. T. Shah and E. A. Sweet-Cordero (2020). Genomic Complexity of Osteosarcoma and Its Implication for Preclinical and Clinical Targeted Therapies. Advances in Experimental Medicine and Biology, Springer International Publishing**:** 1-19.

Schott, C. R., A. L. Koehne, L. C. Sayles, E. P. Young, C. Luck, K. Yu, A. G. Lee, M. R. Breese, S. G. Leung, H. Xu, A. T. Shah, H. Y. Liu, A. Spillinger, I. H. Behroozfard, K. D. Marini, P. T. Dinh, M. V. Pons Ventura, E. N. Vanderboon, F. K. Hazard, S. J. Cho, R. S. Avedian, D. G. Mohler, M. Zimel, R. Wustrack, C. Curtis, M. Sirota and E. A. Sweet-Cordero (2024). "Osteosarcoma PDX-Derived Cell Line Models for

Preclinical Drug Evaluation Demonstrate Metastasis Inhibition by Dinaciclib through a Genome-Targeted Approach." Clin Cancer Res **30**(4): 849-864.

Shahar, N., S. Landman, I. Weiner, T. Elman, E. Dafni, Y. Feldman, T. Tuller and I. Yacoby (2020). "The Integration of Multiple Nuclear-Encoded Transgenes in the Green Al ga Chlamydomonas reinhardtii Results in Higher Transcription Levels." Frontiers in Plant Science **10**.

Takahashi, Y., T. Yasui, K. Tamari, K. Minami, K. Otani, F. Isohashi, Y. Seo, R. Kambe, M. Koizumi and K. Ogawa (2017). "Radiation enhanced the local and distant anti-tumor efficacy in dual immune checkpoint blockade therapy in osteosarcoma." PLoS One **12**(12): e0189697.

Tempany, J. C., J. H. S. Zhou, P. D. Hodgkin and V. L. Bryant (2017). "Superior properties of CellTrace Yellow™ as a division tracking dye fo r human and murine lymphocytes." Immunology & Cell Biology **96**(2): 149-159.

Uribe-Querol, E. and C. Rosales (2020). "Phagocytosis: Our Current Understanding of a Universal Biological Proc ess." Frontiers in Immunology **11**.

Wang, Y., X. Tian, W. Zhang, Z. Zhang, R. Lazcano, P. Hingorani, M. E. Roth, J. D. Gill, D. J. Harrison, Z. Xu, S. Jusu, S. Kannan, J. Wang, A. J. Lazar, E. J. Earley, S. W. Erickson, T. Gelb, P. Huxley, J. Lahdenranta, G. Mudd, R. T. Kurmasheva, P. J. Houghton, M. A. Smith, E. A. Kolb and R. Gorlick (2022). "Comprehensive Surfaceome Profiling to Identify and Validate Novel Cell -Surface Targets in Osteosarcoma." Molecular Cancer Therapeutics **21**(6): 903-913.

Wu, C. C., H. C. Beird, J. Andrew Livingston, S. Advani, A. Mitra, S. Cao, A. Reuben, D. Ingram, W. L. Wang, Z. Ju, C. Hong Leung, H. Lin, Y. Zheng, J. Roszik, W. Wang, S. Patel, R. S. Benjamin, N. Somaiah, A. P. Conley, G. B. Mills, P. Hwu, R. Gorlick, A. Lazar, N. C. Daw, V. Lewis and P. A. Futreal (2020). "Immuno-genomic landscape of osteosarcoma." Nat Commun **11**(1): 1008.

Yadav, R., S. Mahajan, H. Singh, N. K. Mehra, J. Madan, N. Doijad, P. K. Singh and S. K. Guru (2024). "Emerging In Vitro and In Vivo Models: Hope for the Better Understanding of Cancer Progression and Treatment." Adv Biol (Weinh) **8**(6): e2300487.

Zhang, Z., X. Tan, Z. Jiang, H. Wang and H. Yuan (2022). "Immune checkpoint inhibitors in osteosarcoma: A hopeful and challenging future." Front Pharmacol **13**: 1031527.

Supplemental Data

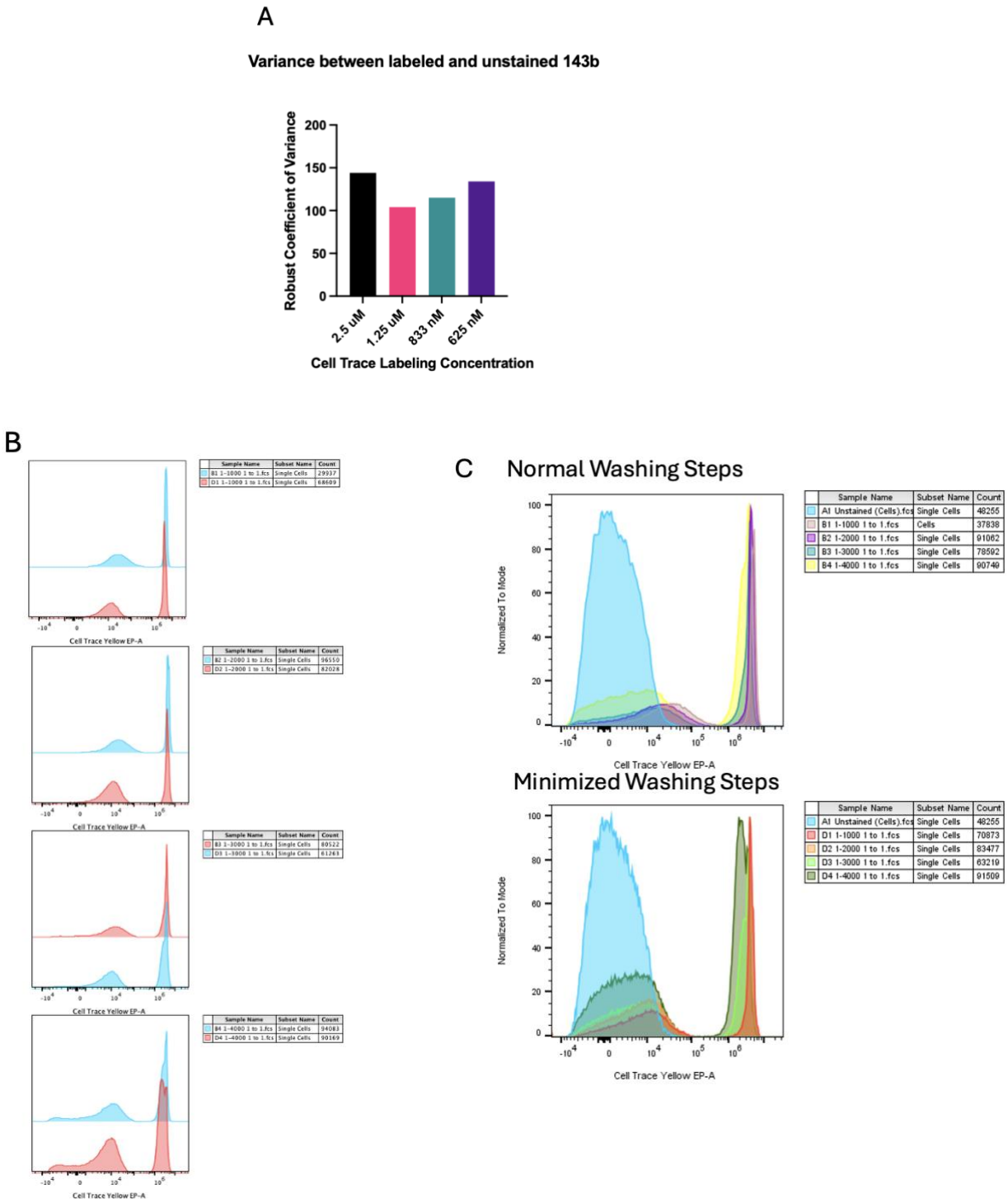

Supplementary Fig. 1 A) Bar graph depicting the robust coefficient of variance calculated from the histogram plots of Cell Trace 143b cells labeled at 4 concentrations (2.5 uM, 1.25 uM, 833 nM, 625 nM) and mixed with unstained 143b cells at a 1:1 mixture. **B)** Histograms comparing Cell Trace labeling at each concentration with or without all typical washing steps **C)** Histograms from Fig. 1E including unstained cells alone

Table 1

Marker For:	Target	Fluorophore
Viability	live/dead	**Zombie NIR**
leukocytes	CD45	**FITC**
endothelial cells	CD31 (PECAM-1)	**PerCP-eFluor 710**
fibroblasts	PDGFR (CD140a)	**BV421**
monocytes, monocyte-derived MOs, neutrophils, ILCs	CD11b	**PerCP**
dendritic cells, Alveolar macs	CD11c	**PE Cy7**

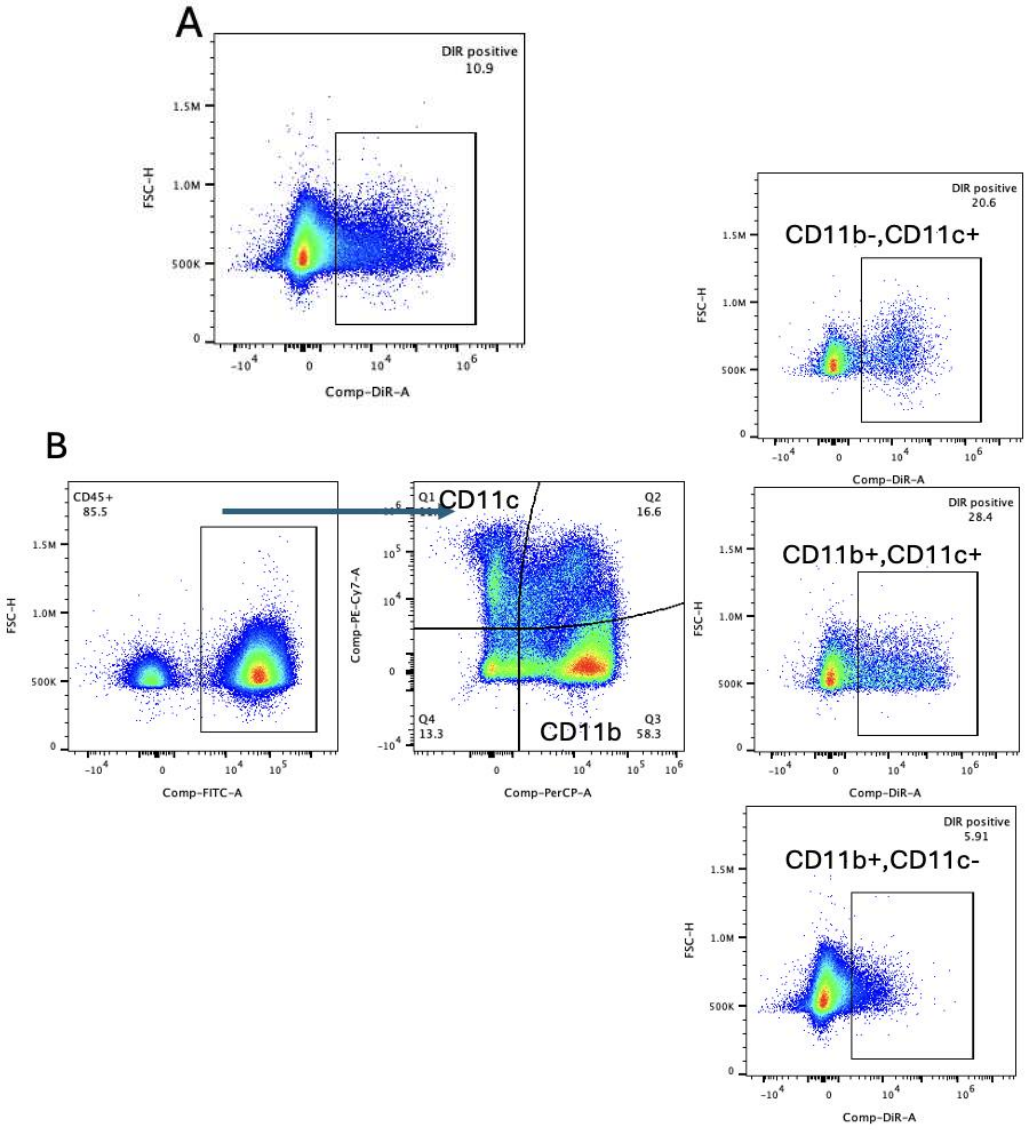

Supplementary Figure 2. Table 1) Antibody panel used for spectral flow cytometry **A)** Flow plot showing the gating strategy for selecting all live DIR+ cells. **B)** Flow plot shows gating of live, CD45+ then combinations of DIR+/CD45+/CD11b+/- and DIR+/CD45+/CD11c+/-

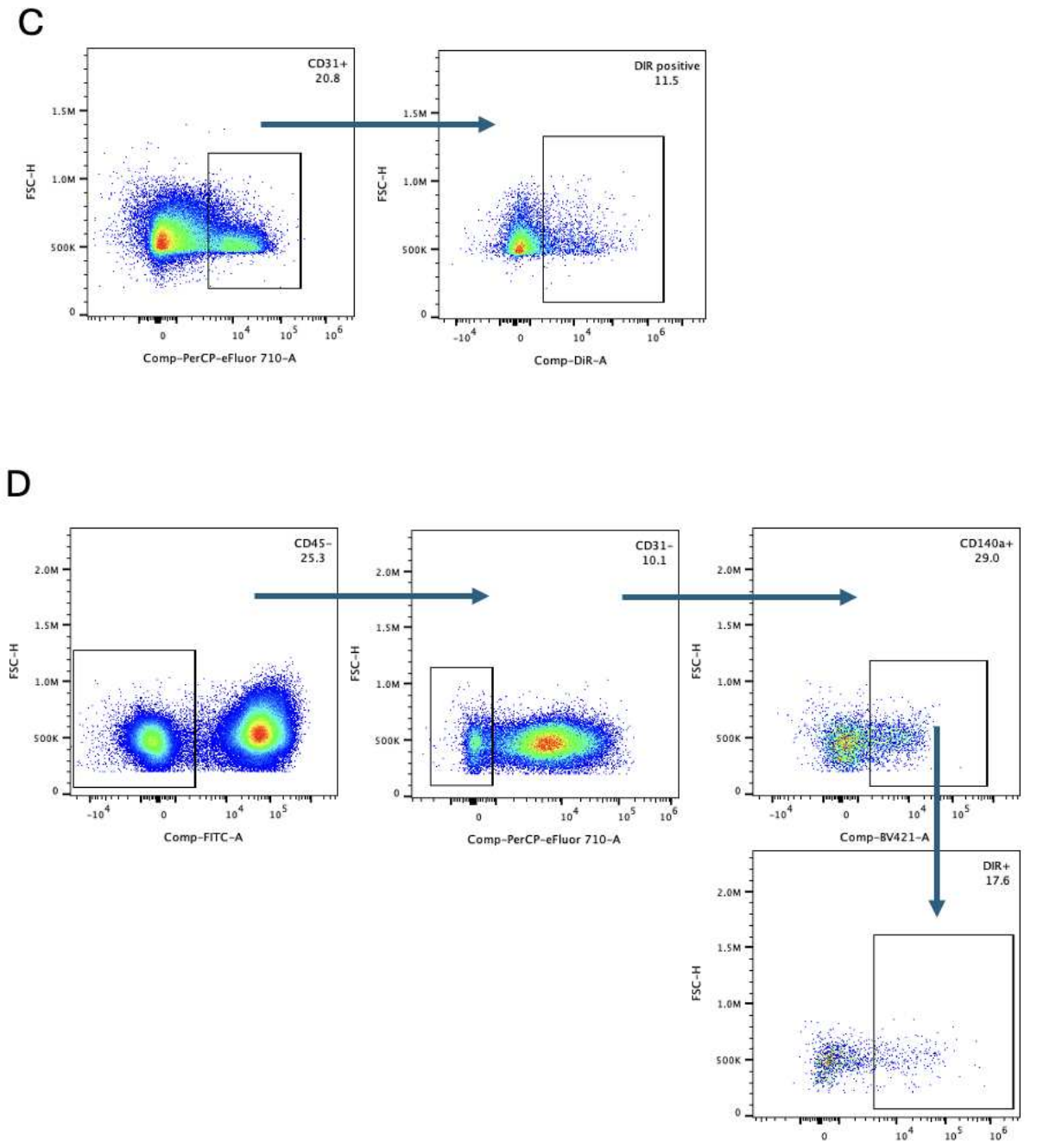

Supplementary Figure 2. C) Flow plot of live CD31+ and DIR+/CD31+ cells. **D)** Flow plots showing live CD45-/ CD31-/DIR+/CD140a+ cells

A

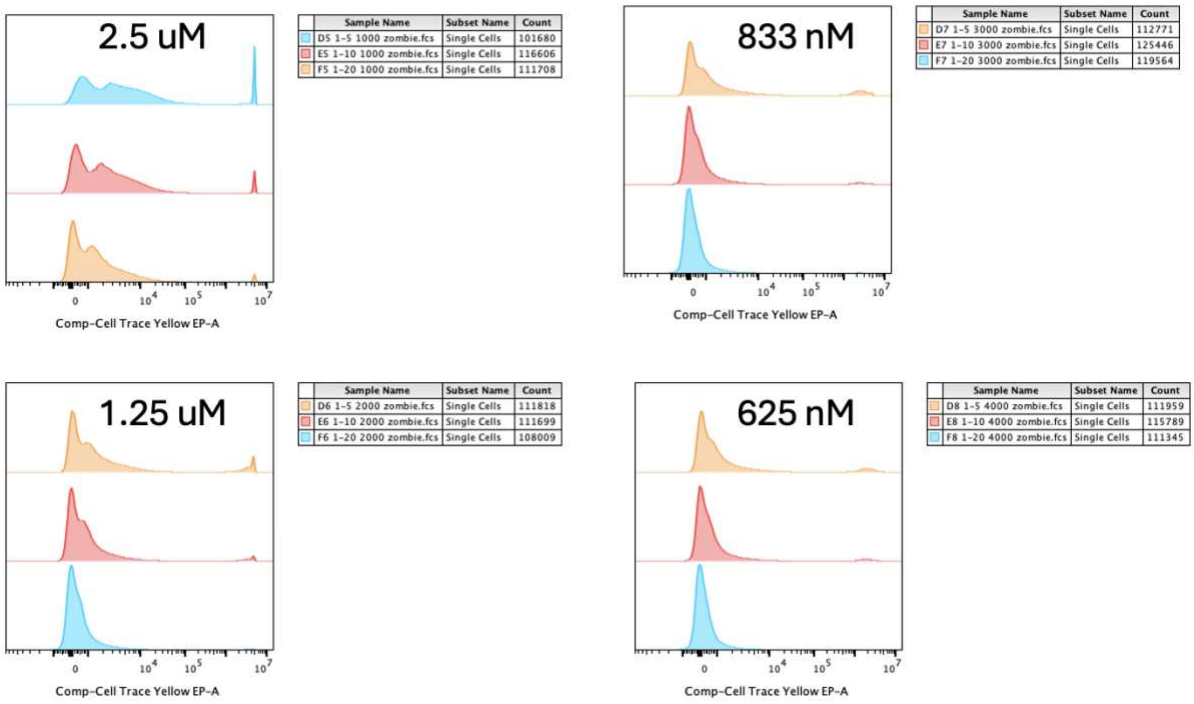

B

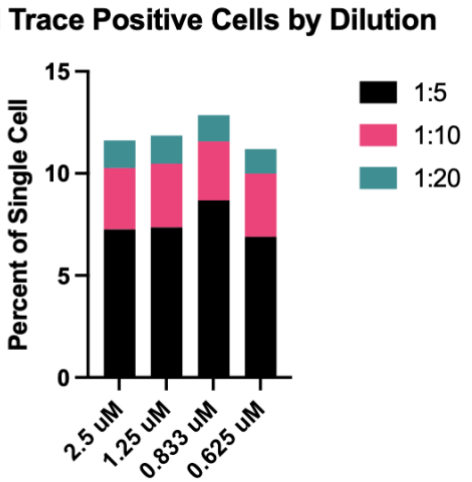

Supplementary Figure 2 A) Flow cytometry histograms showing results from Fig. 3A separated by Cell Trace labeling concentration. **B)** Bar graph showing the true ratio of Cell Trace labeled 143b cells from each labeling concentration as a percent of single cells analyzed

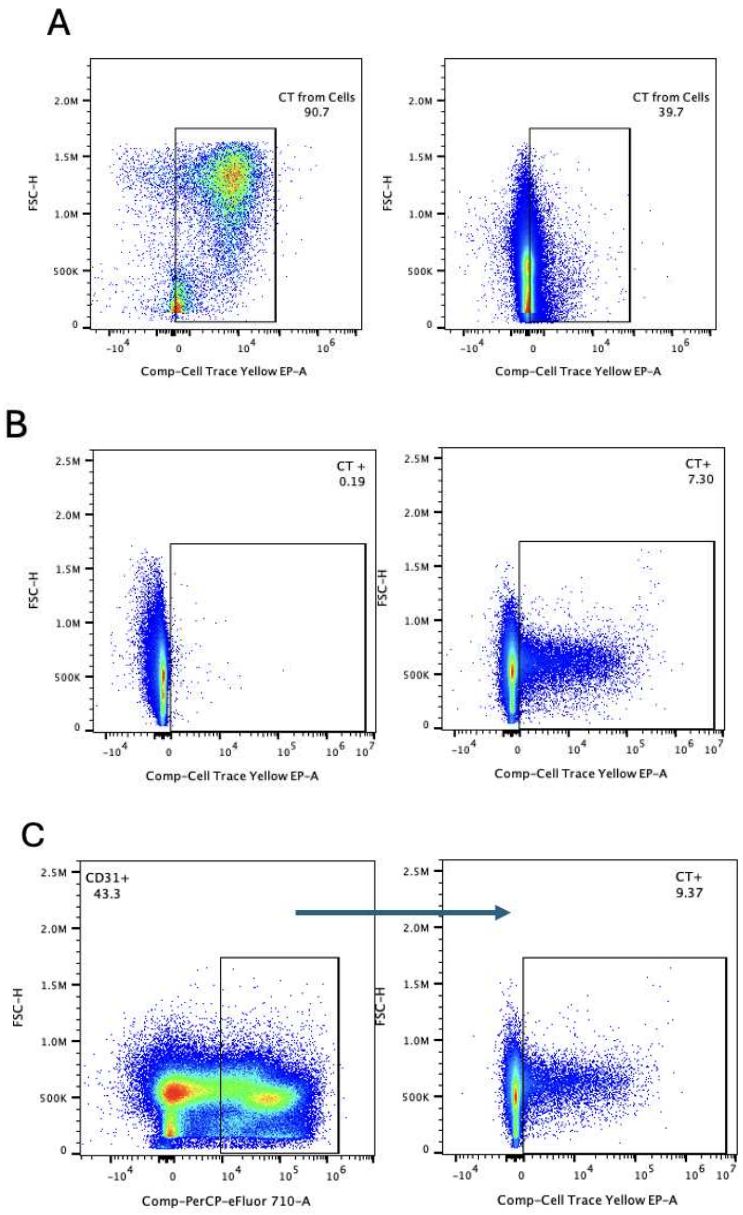

Supplementary Fig. 3 A) Flow Plots of Cell Trace labeled 143b-Luc cells spiked into naïve mouse lung cells ex vivo (Left) and tail vein injected mouse lungs 4-days post injection. **B)** flow plots of naïve, control mouse (Left) 143b-Luc cell injected mouse lungs (Right) gating all live, Cell Trace positive cells. **C)** Flow plots gating on live, CD31+ mouse lung cells (Left) and live, CD31+, Cell Trace+ mouse lung cells (Right).

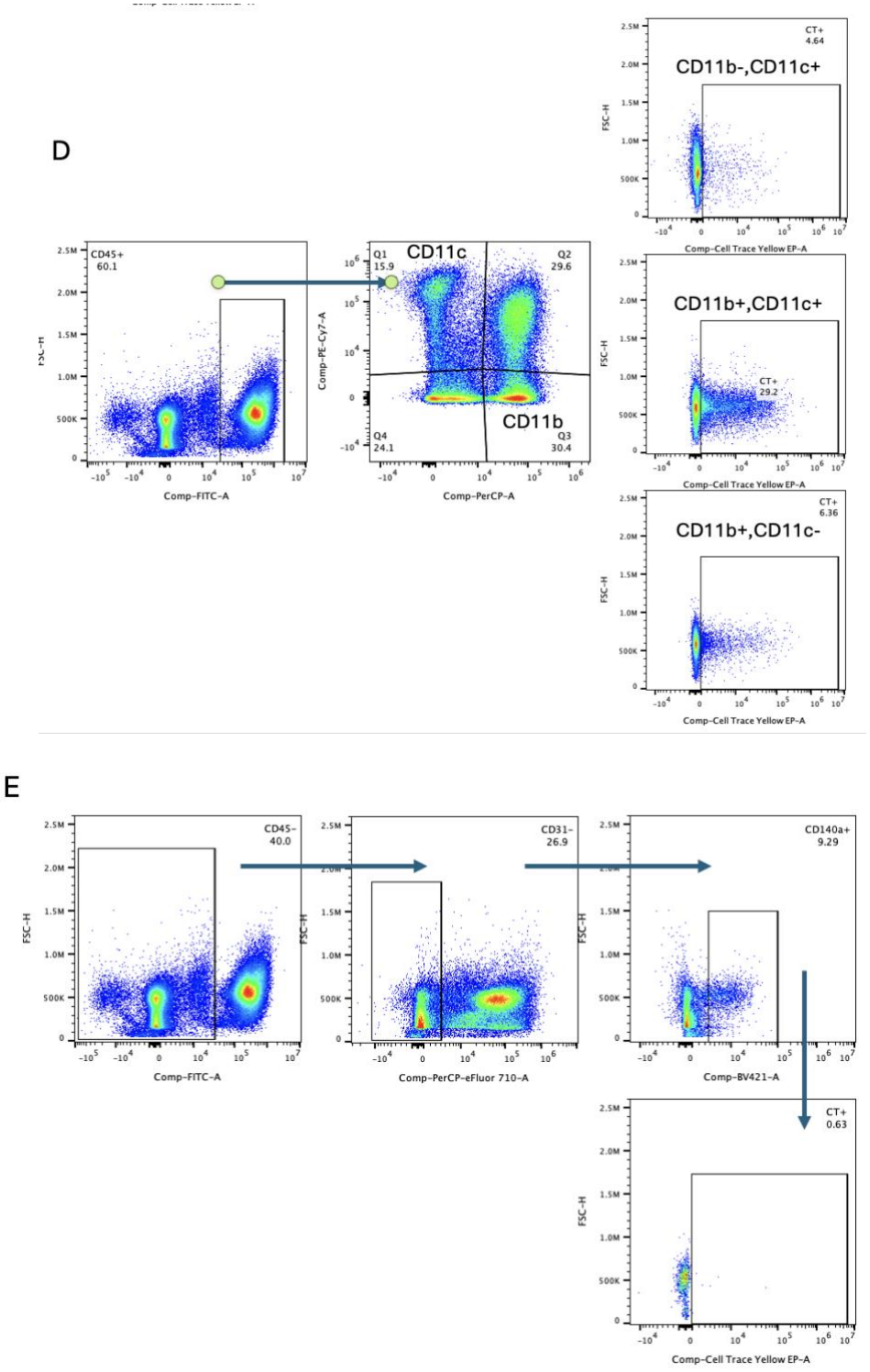

Supplementary Fig. 3 D) Flow plots of live, CD45+ mouse lung cells (Left), and cell trace positive cells among CD45+, CD11b/CD11c subsets (Right). **E)** Flow plots depicting gating of live, CD45-,CD31-, CD140a+ cells that are Cell Trace positive (Bottom Right).

A

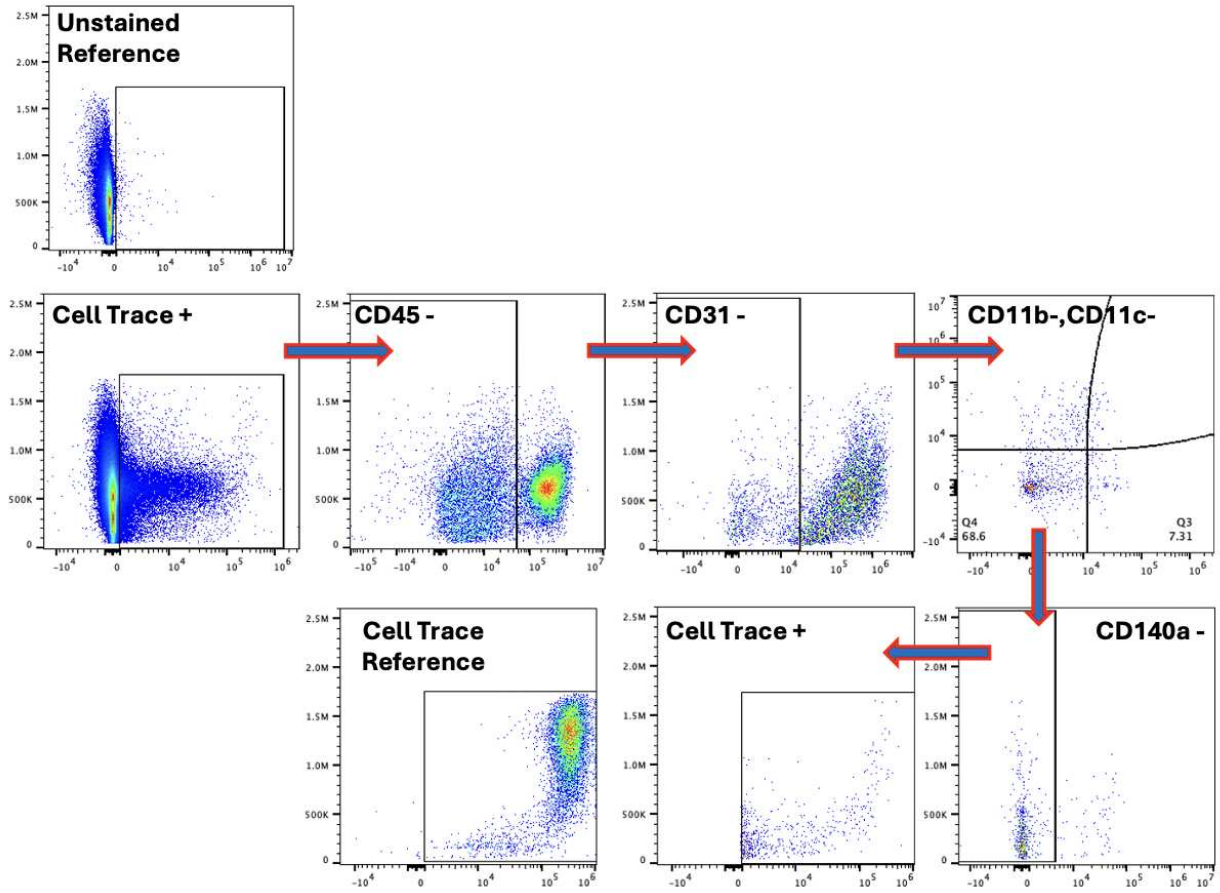

Supplementary Fig. 4 A) Gating strategy to exclude all live, cell trace+ cells by gating out CD45+, CD31+, CD11b/c+, and CD140a (PDGFRa)+ cells

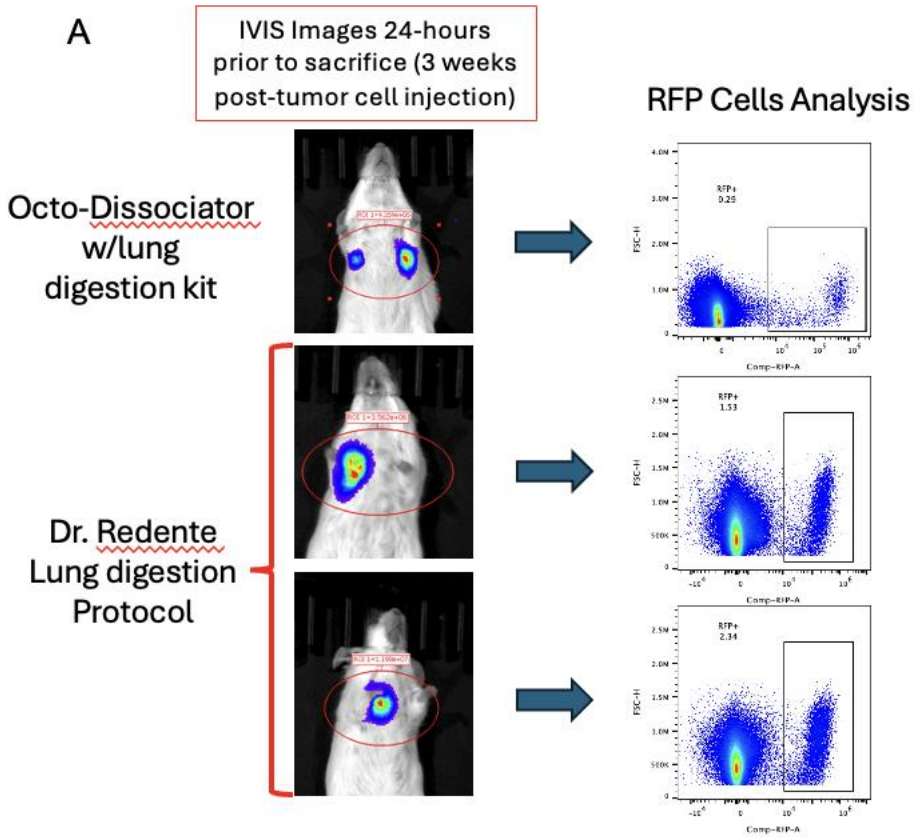

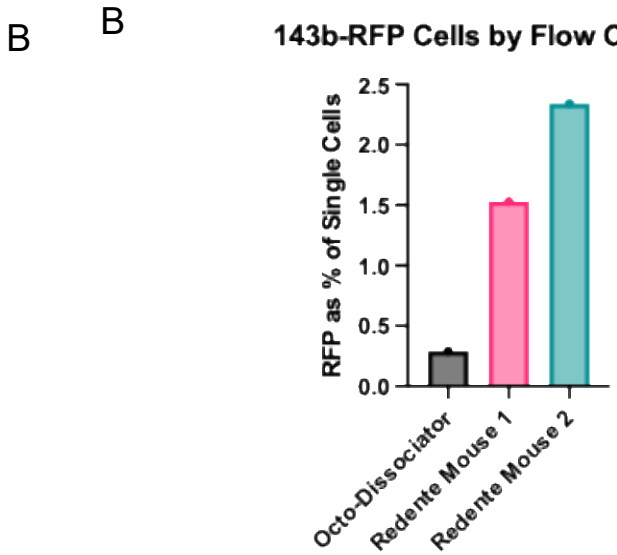

Supplementary Figure 5 A) Representative IVIS images of 143b-RFP-Luc cell injected mice (Left) 3-weeks post-tumor cell injection and flow plots of RFP+ cells detected in each mouse under 2 lung digestion protocols **B)** Bar graph depicting 143b-RFP-Luc detected in mouse lungs as a % of single cells comparing lung digestion protocols.

CHAPTER 4

Evaluating the influence of OS exosomes on metastatic colonization, overall survival, and resident lung cell population dynamics

Abstract

Osteosarcoma (OS) is a highly malignant cancer of the bone. Like many other cancers, addressing metastasis remains the greatest obstacle to improving survival outcomes. OS patients presenting with lung metastasis or those that develop recurrent disease have a dismal 5-year average survival rate of less than 20%, a clinical outcome that has not improved in nearly half a century. This is particularly disappointing as OS is typically observed in children and young adults, disproportionately impacting life years lost. OS displays a high predilection for the formation and outgrowth of secondary tumors in the lung, a phenomenon referred to as organotropism. For over 100 years, several theories attempting to explain the observation that cancer types prefer to metastasize to specific organs have been described. More recently, however, seminal work has identified several tumor-derived factors like cytokines, chemokines, growth factors, and extracellular vesicles, called exosomes, can influence the characteristics of distant organs in advance of metastatic colonization. Exosomes secreted by the primary tumor have been shown to traffic to specific organs where they are taken up by target cells, releasing their biological cargo, and reprogramming those cells to remodel the tissue toward a tumor-promoting phenotype, called the pre-metastatic niche (PMN). Our previous *in vitro* work has shown that OS-derived exosomes are capable of reprogramming primary donor-derived lung fibroblasts towards a cancer associated fibroblast-like phenotype characterized by transcriptional and functional alterations associated with a hallmark PMN. Specifically, among these alterations included enhanced fibroblast proliferation and significantly upregulated secretion of the tumor-promoting cytokines and chemokines, IL-6, IL-8, and CCL2. Furthermore, we demonstrated educations of OS exosomes induced phenotypic changes in lung fibroblasts that promote OS cell survival and proliferation in an *in vitro* co-culture model. Despite this, it is not clear if OS-derived exosomes will induce the same responses *in vivo*, thus promoting enhanced metastatic colonization of the lung. Here, we use *in vivo* and *ex vivo* bioluminescent imaging to show

exosomes derived from the human and mouse OS cell lines, 143b and K7M2, respectively, can promote the initial OS metastatic colonization of the lung. However, this observation was not associated with increased induction of the key cytokines/chemokines, IL-6 and CCL2 previously observed in our *in vitro* studies mentioned previously. Furthermore, we demonstrate optimizing lung digestion procedures substantially improves the viability of mouse lung cells and enhances the liberation of stromal cell populations from the lung matrix, making results from downstream analysis of these lung populations more reliable. Finally, although OS exosomes did not alter stromal cell populations in the lung when OS cells are excluded, we show the involvement of OS cells to exosome educated mice significantly increases lung fibroblast populations, suggesting OS exosomes paired with OS cell involvement may be required to induce significant alterations to the lung stromal compartment. Finally, we show exosome priming of mice prior to tail vein injections of OS cells does not significantly impact overall survival in this model. Taken together, we show OS-derived exosomes promote metastatic colonization of the lung in both a xenograft and syngeneic mouse models. However, mixed and often contradictory data regarding the influence of OS exosomes on resident lung cell population dynamics, cell signaling molecules typically associated with OS lung metastasis, and overall survival makes conclusively unraveling the mechanisms by which OS exosomes function *in vivo* difficult to ascertain.

Introduction

Osteosarcoma is a malignant cancer of the bone that displays a particularly high propensity for metastatic dissemination to the lung. (Mirabello, Troisi et al. 2009, Anderson, Meyers et al. 2014) Currently, metastasis remains the greatest obstacle for improving the clinical outcomes of OS patients. The nature of organ specific secondary tumor development, called organotropism, has been debated for over a century. Dr. Paget's seed and soil hypothesis suggests secondary organs possess inherent characteristics (fertile soil) that allow cells from the primary tumor (metastatic seeds) to successfully colonize and grow. (Paget 1989) More recently, investigators revisiting Dr. Paget's theory have begun to elucidate the mechanisms that may drive organotropism. Evidence from several seminal studies conducted in the last decade, suggest secondary, distal organs do not necessarily possess sufficient

intrinsic tumor promoting properties, but rather, tumor secreted factors are required to mediate the cellular and molecular alterations necessary for metastatic colonization. One of the key discoveries in this regard, identified tumor secreted extracellular vesicles, exosomes, as a potential signaling mechanism that can drive these organ specific changes. These effects were first observed in exosomes derived from pancreatic ductal adenocarcinoma (PDAC), melanoma, ovarian and breast cancer. These studies provided evidence that exosomes can traffic to specific organs where they release their biological cargo, and reprogram key, target cells within those organs, inducing phenotypes that substantially alter the tissue towards a favorable microenvironment for incoming tumor cells, deemed the pre-metastatic niche (PMN). (Peinado, Alečković et al. 2012, Costa-Silva, Aiello et al. 2015, Hoshino, Costa-Silva et al. 2015, Feng, Dean et al. 2019) More recently, studies evaluating the role of OS exosomes on tumor progression and metastasis, specifically, have shown OS exosome mediated signaling can enhance tumor cell proliferation, chemoresistance, epithelial to mesenchymal transition (EMT), angiogenesis, and extracellular matrix (ECM) remodeling. (Lagerweij, Pérez-Lanzón et al. 2018, Sha, Ma et al. 2020, Han, Pu et al. 2021, Li, Lin et al. 2021, Zhong, Liao et al. 2021) The results described in these works aligns with our own observations demonstrating OS derived exosomes were capable of reprogramming lung fibroblasts, a cell type increasingly recognized for their ability to orchestrate the cellular and molecular events characteristic of PMN formation. (Bussard, Mutkus et al. 2016, Asif, Longobardi et al. 2021) We observed OS exosomes induced pro-tumorigenic transcriptional and functional responses characterized by enrichment for gene sets associated with hallmark cancer associated fibroblast (CAF) phenotypes. This was also associated with significantly upregulated secretion of cytokines and chemokines heavily implicated in OS biology, and an enhanced ability to facilitate OS tumor cell survival and proliferation in an *in vitro* fibroblast-OS cell co-culture model.

This evidence led to our hypothesis that OS-derived exosomes could promote OS cell metastatic lung colonization *in vivo*. Additionally, the effects of OS exosomes on metastatic colonization would be associated with alterations to mouse lung resident cell population dynamics, upregulation of tumor-promoting cytokine and chemokine signaling, and reduced overall survival among tumor bearing mice. To test our hypothesis, we evaluated the impact of exosomes derived from the human OS cell line, 143b, and the mouse OS cell line, K7M2, on early metastatic colonization in immunocompromised and

immunocompetent syngeneic mouse models, respectively, as determined by bioluminescent IVIS imaging. We probed tumor bearing mouse lungs for changes to immune and stromal cell populations using spectral flow cytometry, as well as changes to IL-6, and CCL2 signaling in response to exosome educations. Finally, we set out to determine if exosomes derived from 143b OS cells could impact overall survival in tumor cell injected mice. Here, we show exosomes derived from 143b and K7M2 OS cells, could promote initial OS lung colonization and survival 4-days post tumor cell injection. We show modifications to lung digestion protocols improve the liberation of stromal cells from the lung for significantly improved detection and quantification of this lung cell population for flow cytometry analysis. We determine 143b exosomes significantly increase fibroblast populations in the lung in the presence of tumor cells, but no difference is observed when tumor cell involvement is excluded. This relationship was also observed as changes to IL-6 and CCL2 concentrations in the lung were influenced by the combination of exosome treatment and tumor cell involvement. However, we did not detect any significant exosome induced alterations to the CD45+ immune cell populations probed in our flow cytometry panel and exosome priming had no significant impact on overall survival in this model.

Materials and Methods

Mice

6–8-week-old, female BALB/cJ and BALB/c-severely compromised immuno-deficient (SCID) mice were purchased from Jackson Laboratory (Bar Harbor, Maine, #000651, #001803, respectively). All animals were housed in microisolator cages in groups of 5 in the Bay Laboratory Animal Facility at Colorado State University. All procedures were approved by the Institutional Animal Care and Use Committee (IACUC, protocol #4874) at Colorado State University, Fort Collins, CO.

Cell Lines

The human osteosarcoma (OS) cell line 143b was purchased from the American Type Culture Collection (ATCC, Manassas, VA USA). The murine OS cell line K7M2 was generously provided to our group by Dr. Dawn Duval (Flint Animal Cancer Center, Fort Collins, CO). All tumor cell lines were validated by short tandem repeat (STR) analysis and were routinely tested for mycoplasma contamination using a commercially available assay (Mycoalert, Lonza Inc.). Tumor cells were maintained in DMEM media (Gibco, Grand Island, NY USA) supplemented with 10% fetal bovine serum (FBS; Atlas Biologicals, Fort Collins, CO USA), penicillin (100 U/mL), and streptomycin (100 mg/mL) (All from Gibco). Cells were grown sterilely on standard plastic tissue culture flasks (Cell Treat, Shirley, MA), under standard conditions of 37 °C, 5% CO_2, and humidified air. For transduction using Luciferase (firefly 3) lentiviral constructs (GenTarget, San Diego, CA, #LVP674-PBS), 5k K7M2 or 143b cells were plated in 24-well, flat-bottom plates in 1 mL complete DMEM containing 10% fetal bovine serum and 1U/mL penicillin, 100 ug/mL streptomycin for 24 hours in an incubator at 37C, 5% CO2, 5% humidity, respectively. Media was removed from each well, and replaced with 1 mL complete DMEM media and 50 uL commercial lentiviral particle stock preparation. Cells were allowed to grow for 3 days in an incubator, then transduced wells were given a final concentration of 150 ug/mL D-Luciferin salt (200x was 30 mg/mL in DMSO, LUCK-1G, GoldBio, St. Louis, MO), and bioluminescent intensity was measured using the Spectrum Intravital Imaging System (IVIS) (Perkin Elmer, Waltham, MA). Media was removed and replaced with complete DMEM with 5 ug/mL Puromycin as antibiotic selection. Cells were monitored and grown in complete DMEM media under standard conditions.

Isolation and characterization of OS-derived exosomes

Cancer cell lines were seeded in 5-deck multi-flasks (Corning Falcon, cat# 353144) at ~20% confluence (roughly 1 million cells) in their respective media containing 10% FBS for 24 hours. Subsequently, media was removed and replaced with their respective base media containing only 2% exosome depleted FBS for 3 days before harvesting this tumor conditioned media (CM) for exosome isolation. Fetal bovine serum (FBS) was depleted of exosomes by differential ultracentrifugation (Optima

Max-XP ultracentrifuge (cat# 393315), MLA-55 rotor (cat# 393203), Beckman-Coulter) at 120,000 xg for 3 hours at 4°C and was confirmed to be depleted of exogenous exosomes by Qnano Gold (Izon) tunable-resistive pulse sensing particle analysis, as described below.(Chhoy, Brown et al. 2021) To isolate tumor-derived exosomes, tumor-CM was first centrifuged at 3,000 xg for 10 minutes at 4°C to remove cellular debris, and then was subjected to ultrafiltration using Amicon Ultra Centrifugal filters (Centricon Plus-70) with a 100 kDa molecular weight cut-off to concentrate EVs. To prepare the centricon plus-70 centrifugal filter (Sigma, cat# UFC710008) for concentration of tumor-CM, 35 mL of PBS was loaded and centrifuged at 3500 xg and 4°C for 10 minutes to remove glycerol from the filter. After discarding the PBS flow through, 70 mL of prepared tumor-CM was loaded onto the filter and centrifuged at 3500 xg for 45 minutes at 4°C. Flow through was discarded followed by addition of 35 mL of PBS to the filter and centrifuged at 3500 xg and 4°C for 15 minutes to wash the column. Flow through was once again discarded and the filters were flipped upside down, placed on the collection cup, and centrifuged at 1000 xg and 4°C for 2 minutes. This concentrated ultrafiltrate of tumor-CM collected from the centrifugal filters was then subjected to size exclusion chromatography to isolate a pure population of tumor-derived exosomes using QeV original 35 nm size exclusion chromatography columns and automatic fraction collector (Izon Scientific). Samples were eluted with 1x PBS and the void volume as well as all ten 0.5ml eluted fractions were collected and subjected to nanoparticle tracking analyses for quantification of extracellular vesicle and protein concentrations. Fractions 1-3, identified as the particle rich, protein-poor fractions, as reported in the QeV Original User Manual, were pooled and sterile filtered using 45 µm PES membrane syringe filters (Merck Millipore Ltd., Cat# SLGPR33S) prior to further characterization for exosome purity, as described below. Chromatography columns were reused no more than 5 times per manufacturer recommendation and were washed with PBS 3 times between uses.

Evaluating the impact of OS-derived exosomes on metastatic colonization *in vivo*

The 143b study used Balb/C-scid mice and the K7M2 study used Balb/C. For both studies, 9/20 mice received 2 weeks, daily retroorbital injections of 100 uL sterile 1x PBS, 10/20 received daily retroorbital injections of 1e11 exosomes per injection in 100 uL sterile 1x PBS, and 1/20 mice was used

as an untreated, uninjected naïve control mouse. Just prior to injections, 143b-Luc cells were exposed to a final concentration of 150 ug/mL D-Luciferin Salt solution. Following, 19/20 mice were tail vein injected with 1e6 143b-Luc cells in 50 uL PBS, each. Injected mice were then imaged for detection of bioluminescent signature using IVIS imaging (settings: bioluminescence, open filter, 2 min. exposure, medium binning) approx. 10 min. post-tumor cell injection under isoflurane anesthesia. Mice were then returned to cages and incubated for 96-hours. Mice were placed under isoflurane anesthesia, given ~ 100 uL, 30 mg/mL D-Luciferin Salt solution 10 minutes prior to *in vivo* IVIS imaging. Mice were then sacrificed immediately post *in vivo* imaging by cervical dislocation, lungs were removed, and imaged *ex vivo* using the IVIS. Day 4 *in vivo* and *ex vivo* signal intensities deemed as outliers using Graphpad Prism were excluded from further calculations. Colonization efficiency (% of cells remaining 4-days post tumor cell injection) was calculated by dividing day 4 by day 0 bioluminescent signal intensities.

Determining exosome induced changes to tumor-promoting signaling molecules and resident cell populations *in vivo*

Of 10, 8-week-old Balb/C-scid mice, 5/10 received 2 weeks, daily retroorbital injections of 100 uL 1x sterile PBS vehicle control, 5/10 received 100ul 1e11 143b-derived exosomes in 1x sterile PBS. Mice were sacrificed by cervical spine dislocation under isoflurane anesthesia and lungs were removed. Lungs were then placed in 1 mL ice cold 2x collagenase D (200 uL 10x per mL) and DNase (0.125 mg/mL or 80 U/mL) in serum free DMEM until all lungs were collected. Lungs were minced with ethanol-cleaned razor blades, then returned to collagenase/DNase media to incubate for 30 min. at 37C. 100 uL of 100 mM pH balanced EDTA is added to top the enzymatic reaction, partially digested lung homogenates were returned to ice, then triturated using 18-gauge needles to fully break up the tissue. Cell suspensions were run through 100 uM filter into 15 mL conical tubes before being centrifuged at 300xg for 5 min. at 4C. Supernatants were discarded, and cell pellets were resuspended in 1 mL of ACK lysis buffer for 5 min. to lyse red blood cells. 5 mL, ice cold complete DMEM is added to each 15 mL conical tube followed by another centrifugation step. Supernatants were again discarded, and the lung cell pellet was resuspended in 500 uL 1x sterile PBS prior to cell counting and evaluation of viability. Briefly, after lung cells from each mouse were plated in their respective wells in a 96-well, V-bottom plate, 100 uL of zombie NIR was

applied to cells at a 1:1000 dilution in 1X PBS + 5mM EDTA for 15 min. at room temp in a dark drawer. The plate was centrifuged at 300 xg for 5 min. at 4C, supernatants were discarded, and cells were resuspended in 150 uL FACS buffer. This was repeated 2x, then following centrifugation and supernatant removal, 10 uL mouse block was added to each well for 5 min. at room temperature to prevent non-specific binding of fluorescent antibodies. Then 50 uL of primary antibodies diluted to their respective concentrations in FACS buffer (Supplemental Table 1) were added on top of the mouse block, the plate was incubated at room temp. in a dark drawer for 15-20 min. then 100 uL FACS buffer was added directly to each well. The plate was washed 3x with FACS buffer as described previously before being brought to a final volume of 150 uL for flow cytometry analysis using a 4-laser Aurora cytometer (Cytek). Naïve mice were also sacrificed, and their lungs were processed for flow cytometry at the same time as the experimental mice. Lung cells from these mice are used for single stain unmixing and fluorescence minus one (FMO) controls used for informing gating strategies during down-stream data analysis using FlowJo.

Cytokine and Chemokine Analysis

Prior to digestion, ~30 mg lung tissue from each mouse was snap frozen in liquid nitrogen vapor for ~3 min. Frozen lung tissue samples were then digested in the gentleMACS octo dissociator (Miltenyi Biotech, Bergisch Gladback, Germany) using T-Per lysis buffer (Thermo) supplemented with phosphatase and protease inhibitors (Pierce), and protein concentration was measured by BCA (Pierce). Murine IL-6 and MCP-1/CCL2 ELISA duo-set kits (DY406, DY479, R&D Systems) and normalized to total protein determined previously by BCA.

Determining the impact of OS cell involvement using Stromal Cell Optimized Lung Digestion Protocol

9 Balb/C-scid mice were divided into 3 groups of 3 1) Received 2 weeks, daily retroorbital injections of PBS vehicle control only. 2) Received 2 weeks, daily retroorbital injections of 1e11 143b-derived exosomes with no tumor cell involvement. 3) Received 2 weeks, daily retroorbital injections of

1e11 143b-derived exosomes followed by tail vain injection of 1e6 143b cells in 50 uL 1x Sterile PBS. Following euthanasia by cervical dislocation under isoflurane anesthesia, a digestion solution comprised of 500 uL collagenase D (1 mg/mL in 1x PBS), 250 uL Dispase (5 U/mL in 1x PBS), 32 uL Elastase (4 U/mL in 1x PBS), and 500 uL sterile 0.9% saline was instilled in each mouse lung via the trachea. The trachea was tied off using surgical suture, lungs were removed and allowed to sit at room temp for 10 min. in a 12-well flat bottom plate. Lungs were then minced using ethanol-cleaned razor blades followed by incubation at 37C for 30 min. Partially digested lung homogenates were triturated using a P-1000 pipette with tips cut at the end. The lungs were transferred to a 15 mL conical tube and 5 mL complete DMEM media was added before centrifugation at 1500 rpm for 5 min. at 4C. Any floating tissue remaining was gently removed and returned to the cell culture plate. Supernatants were removed from each 15 mL conical tube and cell pellets were resuspended in 1 mL of trypsin solution comprised of 500 uL 0.25% trypsin, 500 uL saline, and 20 uL of DNAse solution per mL before incubation on a rotating plate at 37C for 30 min. Homogenates were again triturated using a P-1000 pipette, returned to a 15 mL conical tube where 3 mL complete DMEM media was added before centrifugation at 1500 rpm for 5 min at 4C. Supernatants were discarded, 5 mL sterile 0.9% saline was added, and using a 10 mL syringe attached to an 18-gauge needle, the pellet was pipetted in and out several times to form a single cell suspension prior to use of 100 um filters. Cells were then centrifuged at 1200 rpm for 5 min., supernatants were discarded, and cells were resuspended in 500 uL cold 1x sterile PBS. Cell suspensions were counted, and viability was determined before being plated in a 96-well V-bottom plate. Live/dead stain and fluorescently conjugated antibodies were applied as mentioned above prior to flow cytometry analysis.

Statistical analyses

Samples were not randomly assigned to experimental groups, and experimenters were not blind to group assignment and outcome assessment. For the comparison of mean values between three or more groups, a one-way ANOVA with Tukey's post-test was performed. For comparison of means between two groups, or comparison of repeated measures between two groups, a two-tailed, unpaired Students' *t* test or Wilcoxon matched-pairs t test was used, respectively. All statistical analyses were performed using Graph Pad Prism software, version 10 (La Jolla, CA, USA).

Results

Evaluating the impact of 143b-derived exosomes on metastatic colonization *in vivo*

Our previous *in vitro* work demonstrated OS exosomes can alter the transcriptional and functional characteristics of lung fibroblasts towards phenotypes associated with hallmark characteristics associated with pre-metastatic niche formation. Furthermore, OS exosome educated fibroblasts were observed to promote OS cell survival and proliferation in an *in vitro*, co-culture model. Based on these observations, we hypothesized OS exosomes could promote metastatic colonization *in vivo*. To determine this, we performed 2 weeks of daily retro-orbital intravenous injections of purified and concentrated exosomes derived from the highly metastatic human OS cell line, 143b, into Balb/C-scid mice depicted in the schematic (Fig. 4.1A). To visualize and quantify OS *cells in vivo* and *ex vivo*, 143b cells were transduced with a lentiviral construct containing a luciferase expression system capable of producing a bioluminescent signal detectable using an intravital imaging system (IVIS).

Following the 2-week exosome education period, $1e^6$ luciferase expressing 143b (143b-Luc) cells were tail vein injected into 19 Balb/C-scid mice. 10 mice had been subjected to the 2-week exosome treatment period, 9 mice had received daily injections of sterile PBS vehicle control, and 1 mouse from each group was used as a non-injected, naïve control. To determine injection efficiency, *in vivo* IVIS images were taken, and the bioluminescent signal intensity was measured 10 min. post-tumor cell injection. Initial analysis reveals a substantial degree of injection efficiency variability between exosome treated and PBS vehicle control mice, with a failure to measure a detectable bioluminescent signal above background in 1 mouse (Exosome educated mouse #7) as measured by Total Flux (photons/sec) and Average Radiance (photons/second/cm^2). Additionally, bioluminescent signal intensity was substantially higher among mice in the PBS vehicle control group (Fig. 4.1B). Following a 4-day incubation period, analysis of tumor bearing mice revealed a significant increase in the bioluminescent signal intensity among exosome treated mice *in vivo* (Fig. 4.1C*)*. Similarly, a substantial increase in signal intensity was observed among exosome treated mice *ex vivo*, however, this difference was not statistically significant (Fig. 4.1D). The detectable *in vivo* bioluminescent signal above background (total flux > 7.5e4) was observed among 67% (6/9) of mice in the PBS vehicle control group and 90% (9/10) of mice in the

exosome treatment group. *Ex vivo* imaging data demonstrates all mice in the PBS vehicle control group and 80% (8/10) of mice in the exosome treatment group displayed detectable bioluminescent signals above background (total flux > 1e4). The bioluminescent signal intensity measured 10 min. post-tumor cell injection is substantially higher than the *in vivo* signal measured 4-days post-tumor cell injection, indicating a significant number of tumor cells did not successfully colonize the lung (Fig. 4.1E). Taking this decrease into consideration, we developed a scaling metric describing the percent of initial tumor cells introduced into the mice capable of successfully colonizing the lung, deemed the colonization efficiency (Day 4 signal/Day 0 signal). We show colonization efficiency is significantly increased among the 143b exosome treated group, both *in vivo* and *ex vivo,* compared to mice in the PBS vehicle control group (Fig. 4.1F). In summary, we show IVIS imaging is capable of quantifying differences in metastatic burden during the earliest phases of lung colonization. Furthermore, imaging data from this xenograft model suggests OS exosomes derived from the highly metastatic OS cell line, 143b, can promote increased colonization efficiency of OS tumor cells *in vivo*.

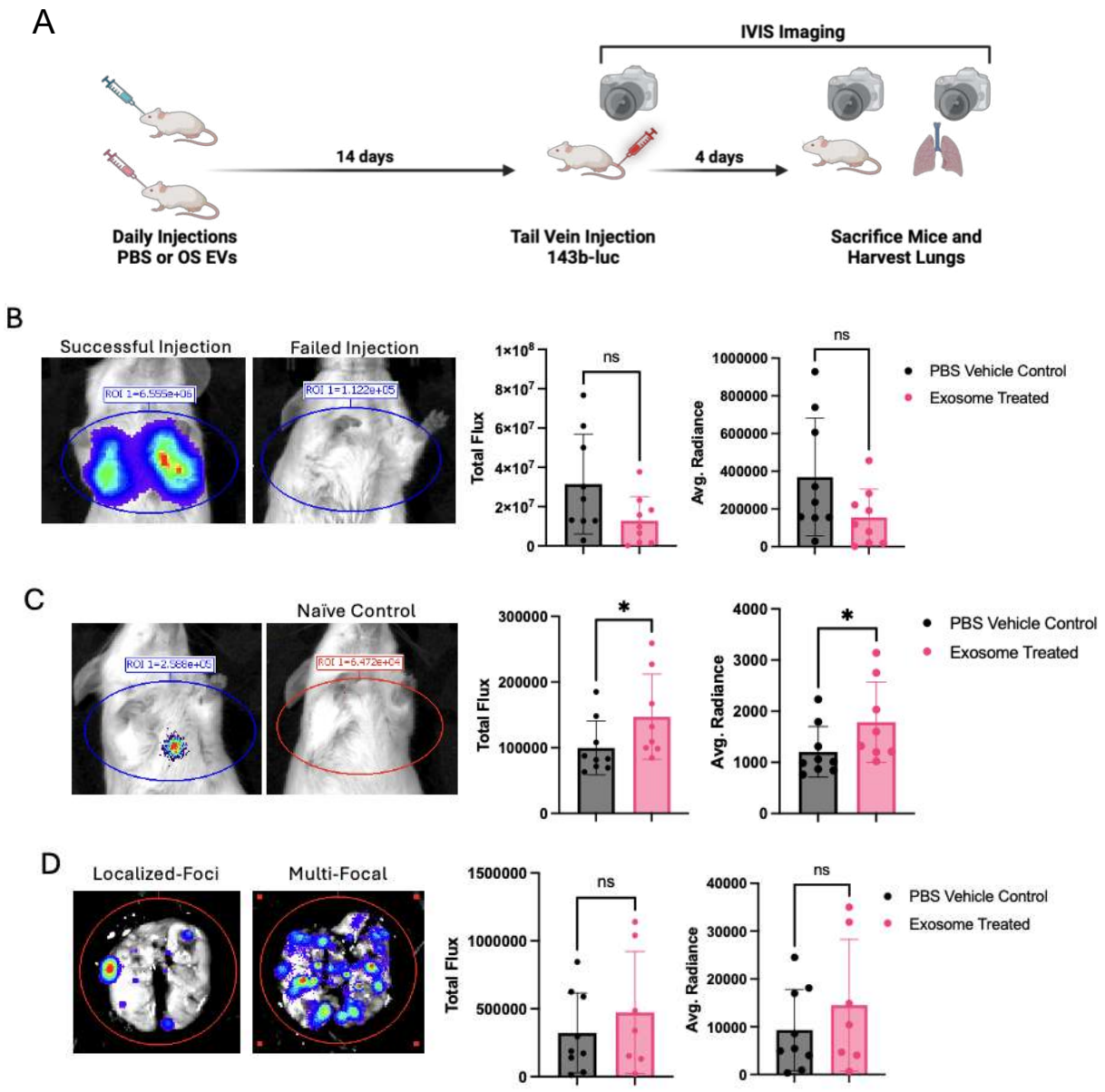

Figure 4.1 Evaluating the impact of 143b-derived exosomes on metastatic colonization *in vivo* A) Visual schematic of assay approach **B)** Representative *in vivo* IVIS images of mice with successful (Left) and failed (Right) injections and bar graphs quantifying luminescence measured as total flux and average radiance 10 min. post-143b-Luc injection **C)** Representative *in vivo* IVIS images of OS cell injected (Left) and Naïve control (Right) and bar graphs quantifying luminescence measured as total flux and average radiance 4-days post-143b-Luc injection **D)** Representative *ex vivo* IVIS images of mice with localized metastatic foci (Left) and dispersed colonization (Right) and bar graphs of luminescence measured as total flux and average radiance 4-days post-143b-Luc injection Outliers were identified and excluded using ROUT (Graphpad Prism) Mann-Whitney test * < 0.05

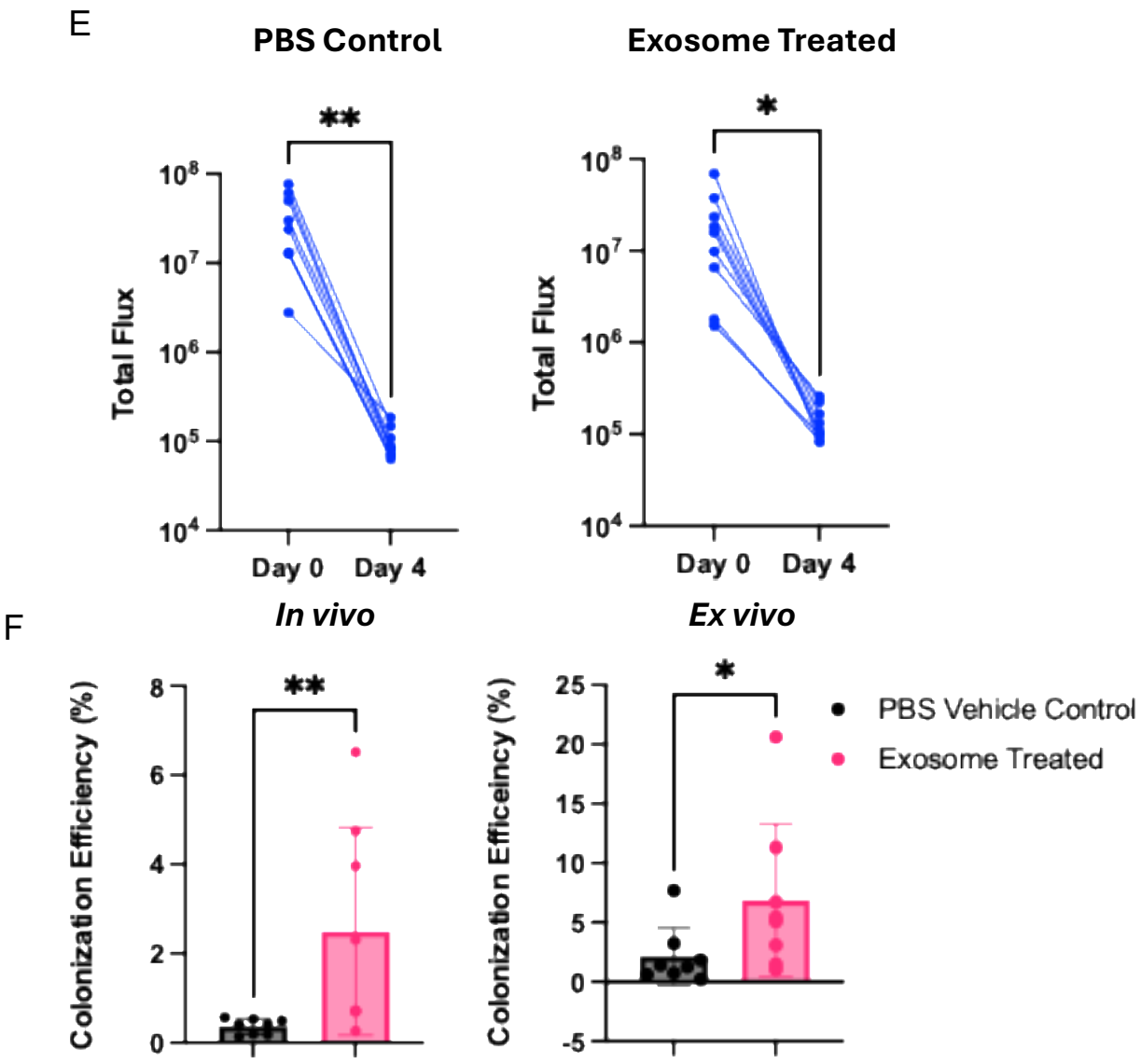

Figure 4.1 Evaluating the impact of 143b-derived exosomes on metastatic colonization *in vivo.* E) Dot plots of IVIS imaging data showing the decrease in luminescence from initial tumor cell injection to 4-days post-tumor cell injection between exosome treatment conditions as measured by total flux. **F)** Bar graphs depicting colonization efficiency among exosome treatment groups 4-days post-tumor cell injection Mann-Whitney test * < 0.05, ** < 0.01

Evaluating the impact K7M2-derived exosomes on metastatic colonization *in vivo*

To determine if the metastasis promoting effects observed in human OS exosome treated mice is conserved, we followed the same protocols discussed previously to evaluate the impact of OS exosomes derived from a metastatic mouse OS cell line, K7M2, in an immunocompetent syngeneic mouse model. Representative IVIS images depict bioluminescent detection of K7M2-Luc cells *in vivo*, and *ex vivo* 10 min. and 4-days post-tumor cell injection, respectively (Fig. 4.2A). Analysis of imaging data reveals variable injection efficiency among all mice, however, there is no significant difference in signal intensity between both treatment groups as measured by average radiance (Top) and total flux (Bottom) (Fig 4.2B). Imaging data gathered 4-days post-tumor cell injection reveals a significant increase in bioluminescent signal intensity among mice in the exosome treatment group *in vivo*, however, *ex vivo* imaging data shows conflicting results, with a significant increase in signal intensity detected among the PBS vehicle control treatment group (Fig 4.2C). K7M2 exosomes substantially increase colonization efficiency as measured by average radiance and significantly increase colonization efficiency as measured by total flux *in vivo*. However, these results conflict with *ex vivo* imaging data that show significantly enhanced colonization efficiency among PBS vehicle control treated mice as measured by average radiance and substantial enhancement as measured by total flux
(Fig. 4.2D). The discrepancy observed between *in vivo,* and *ex vivo* imaging data may be a function of limitations associated with the K7M2 cell line and the mouse model. For instance, we observed multiple log-fold differences in the signal intensity between 143b-Luc and K7M2-Luc cell lines 10 min. post tumor cell injection as measured by total flux and average radiance
(Fig. 4.2E). Furthermore, the *in vivo* and *ex vivo* signal intensity measured 4-days post tumor cell injection was highly correlative in the 143b model, but not in the K7M2 model (Fig. 4.2F). Taken together, these data suggest K7M2-derived exosomes may promote metastatic lung colonization *in vivo*. However, our data indicates several limitations with the use of this model, including the significantly reduced

bioluminescent signal amplitude compared to 143b-Luc cells and a lack of correlation between *in vivo* and *ex vivo* imaging data.

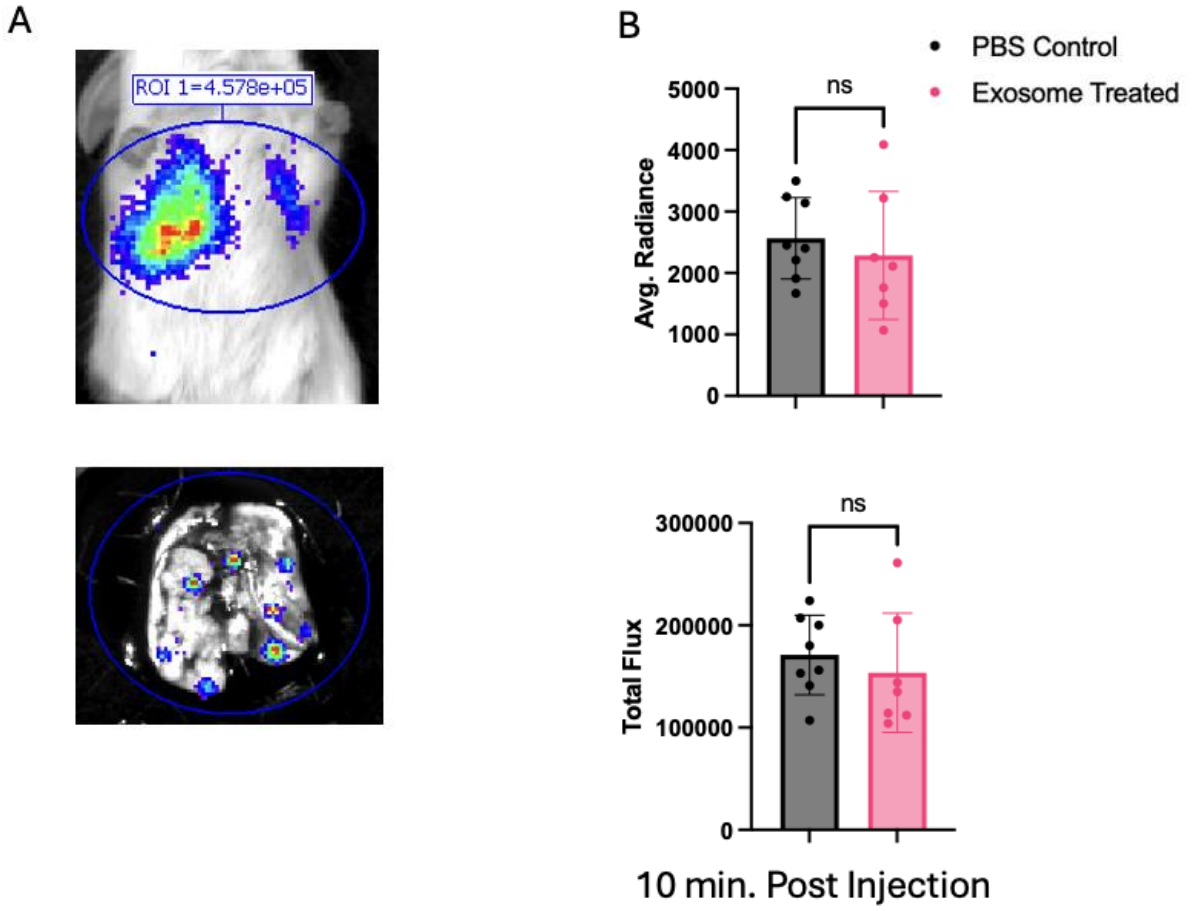

Figure 4.2 Evaluating the impact K7M2-derived exosomes on metastatic colonization *in vivo.* A) Representative IVIS images 4-days post-K7M2-Luc cell injection *in vivo (*Top) and *ex vivo* (bottom). **B)** Bar graphs depicting injection efficiency of tumor cell injected mice and comparing exosome treatment condition 10 min. post-injection as measured by Average Radiance (Top) and Total Flux (Bottom). Mann-Whitney test * < 0.05, ** < 0.01, *** < 0.001

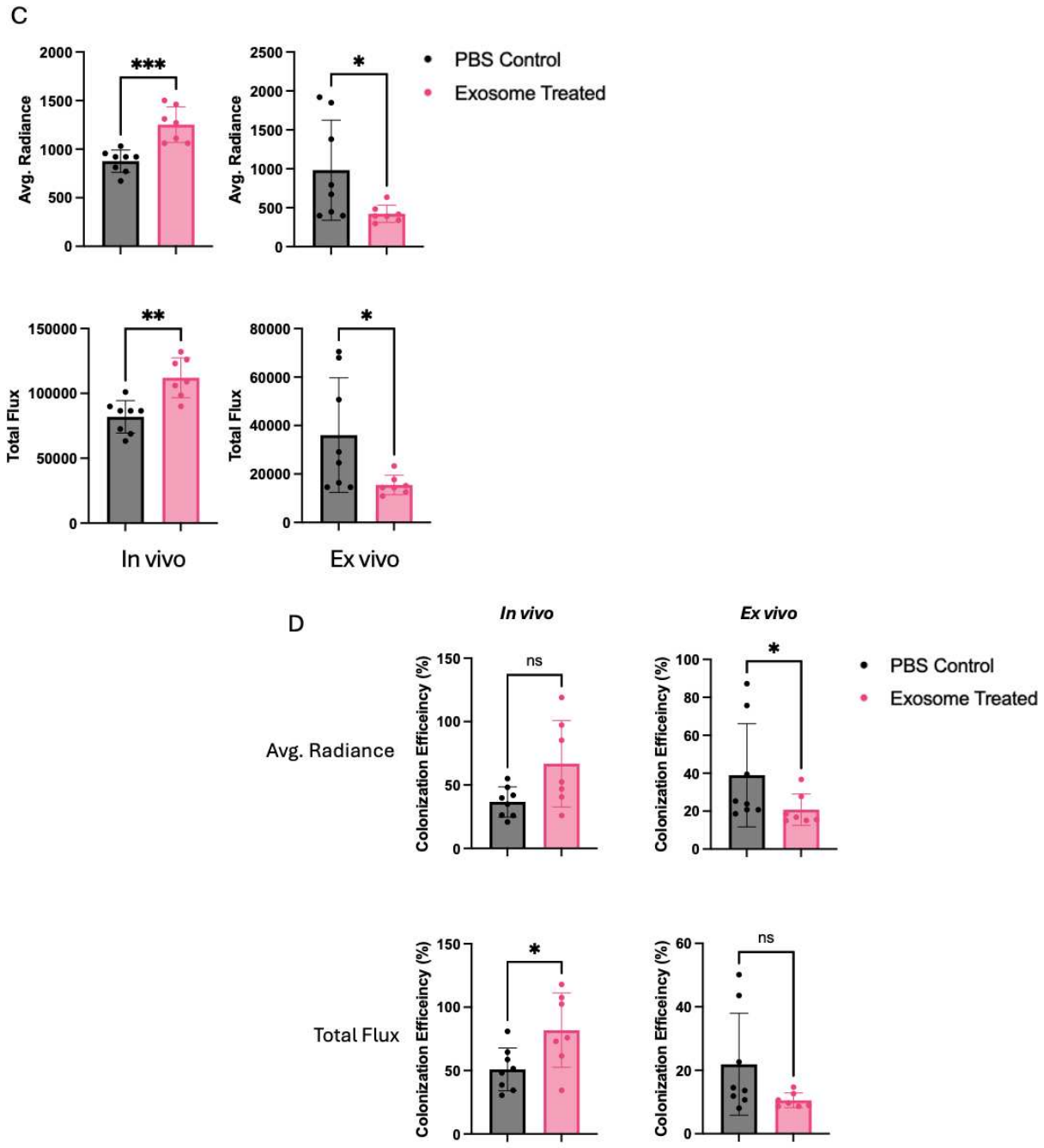

Figure 4.2 Evaluating the impact K7M2-derived exosomes on metastatic colonization *in vivo.* C)Bar graphs depicting in vivo (Left) and ex vivo (Right) IVIS detected luminescence under exosome treatment conditions as measured by Average Radiance (Top) and Total Flux (Bottom) 4-days post K7M2-Luc injection. **D)** Bar graphs depicting colonization efficiency among exosome treatment groups 4-days post-tumor cell injection Mann-Whitney test * < 0.05, ** < 0.01

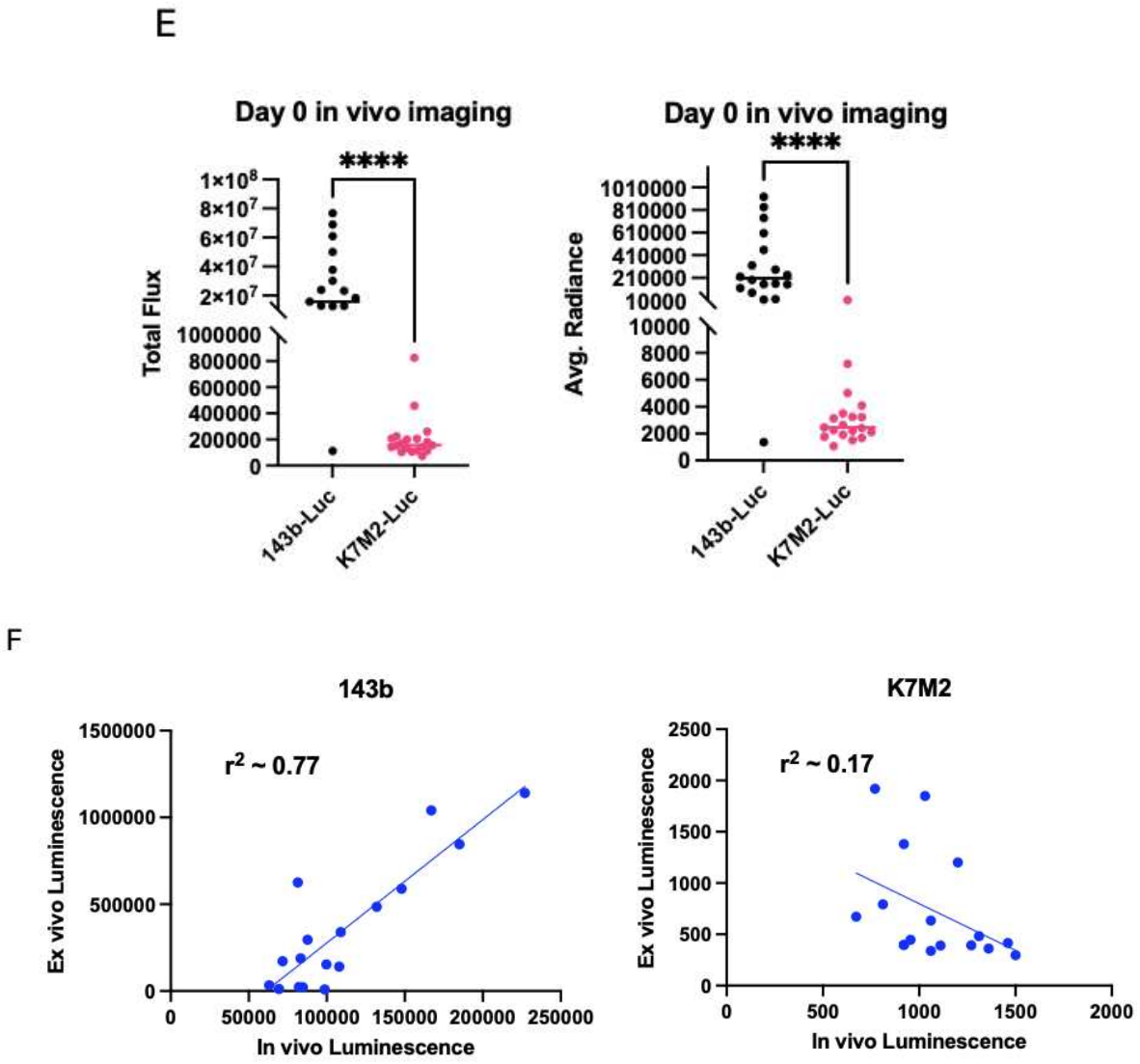

Figure 4.2 Evaluating the impact K7M2-derived exosomes on metastatic colonization *in vivo.* E) Dot plots comparing luminescent signal intensity between 143b-Luc and K7M2-Luc 10 min. post-tumor cell injection measured as Total Flux (Left) and Average Radiance (Right). **F)** Dot plots correlating in vivo and ex vivo signal intensities 4-days post tumor-cell injection of 143b-Luc (Left) and K7M2-Luc (Right). Mann-Whitney test **** < .0001

Optimization of tissue digestion and analytical methods to evaluate the influence of exosomes on lung resident cell populations

Our previous *in vitro* data demonstrated OS-derived exosomes were capable of inducing proliferation of lung fibroblasts. These observations, paired with data suggesting chronic treatments with 143b exosomes could promote metastatic lung colonization of OS cells *in vivo*, led to our hypothesis that OS exosomes may induce alterations to mouse resident lung immune and stromal cell populations *in vivo*. To determine this, we performed a 2-week, 143b exosome education study and evaluated lung cell population changes in the absence of OS cell injections. Flow plots depict the gating strategies used to inform our analysis of mouse resident lung cell populations in response to exosome treatments (Fig 4.3A) This analysis failed to identify significant differences between treatment conditions among the profiled immune cell populations as a percent of CD45+ cells (Fig. 4.3B). Furthermore, we did not identify significant differences in fibroblast or endothelial cell populations between treatment groups measured as a percent of live cells (Fig. 4.3C). Interestingly, analysis conducted on lung digests from the 20-mouse, 143b exosome metastasis study discussed previously, resulted in a significant increase in the lung fibroblast population among the exosome treatment group, but not to other CD45+ cell types probed in that study. (Fig 4.3D). This suggests treatments with exosomes alone may not be sufficient to induce alterations to the assessed cell populations *in vivo*, and tumor cell involvement may be required to promote the cell population changes we observed.

During flow cytometry analysis, it was identified that the lung fibroblast population as a percent of all live cells was substantially less than what was expected. It was later determined the commercial tissue dissociation instrument and associated proprietary enzyme cocktail used for the generation of lung digested, single cell suspensions recommended by the manufacturer, are optimized for liberating immune cell populations from the lung, and not necessarily stromal cells, which can be more embedded within the ECM. Because of this, we set out to validate a lung digestion protocol particularly suited for stromal cell flow cytometry analysis. Using our fibroblast specific antibody panel and gating strategy (Live, CD45-, CD31-, CD140a+ (PDGFRa)), we evaluated differences in the overall viability of all lung cells and fibroblast populations as a percent of live cells. Here, we show flow plots depicting the gating strategy employed to make this comparison, and visually represent the differences observed between digestion

methods (Fig. 4.3E). Furthermore, we show the stromal specific digestion protocol performs significantly better at preserving the viability of all cells (~65% vs. 40%) and increasing the number of fibroblasts identified as a percent of live cells (~12% vs. 3%) (Fig. 4.3F). Taken together, these data suggest immune and stromal resident lung cell populations do not significantly change in response to prolonged OS exosome treatments in the absence of OS cell involvement. In contrast, we show a significant increase in the fibroblast population among exosome treated mice when OS cells are introduced into the lung. However, the value of these results may be constrained by the limitations of our previously used lung digestion protocol, which we determined to be significantly improved upon by implementing a digestion method specific for liberating stromal cell populations from lung tissues.

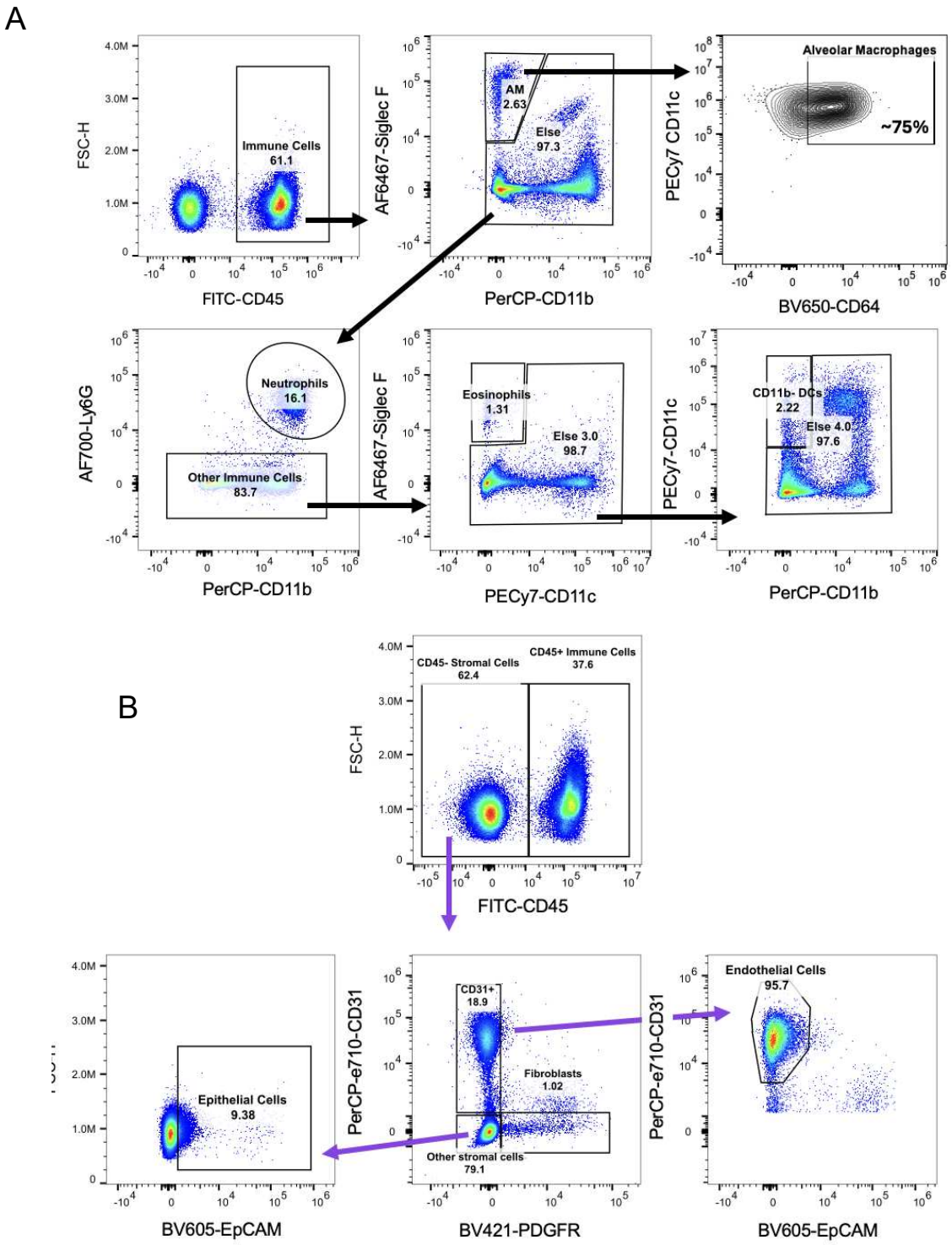

Figure 4.3 Optimization of tissue digestion and analytical methods to evaluate the influence of exosomes on lung resident cell populations A) Gating strategy used to identify CD45+ resident mouse lung populations **B)** Gating strategy used to identify PDGFR and CD31+ stomal resident lung populations

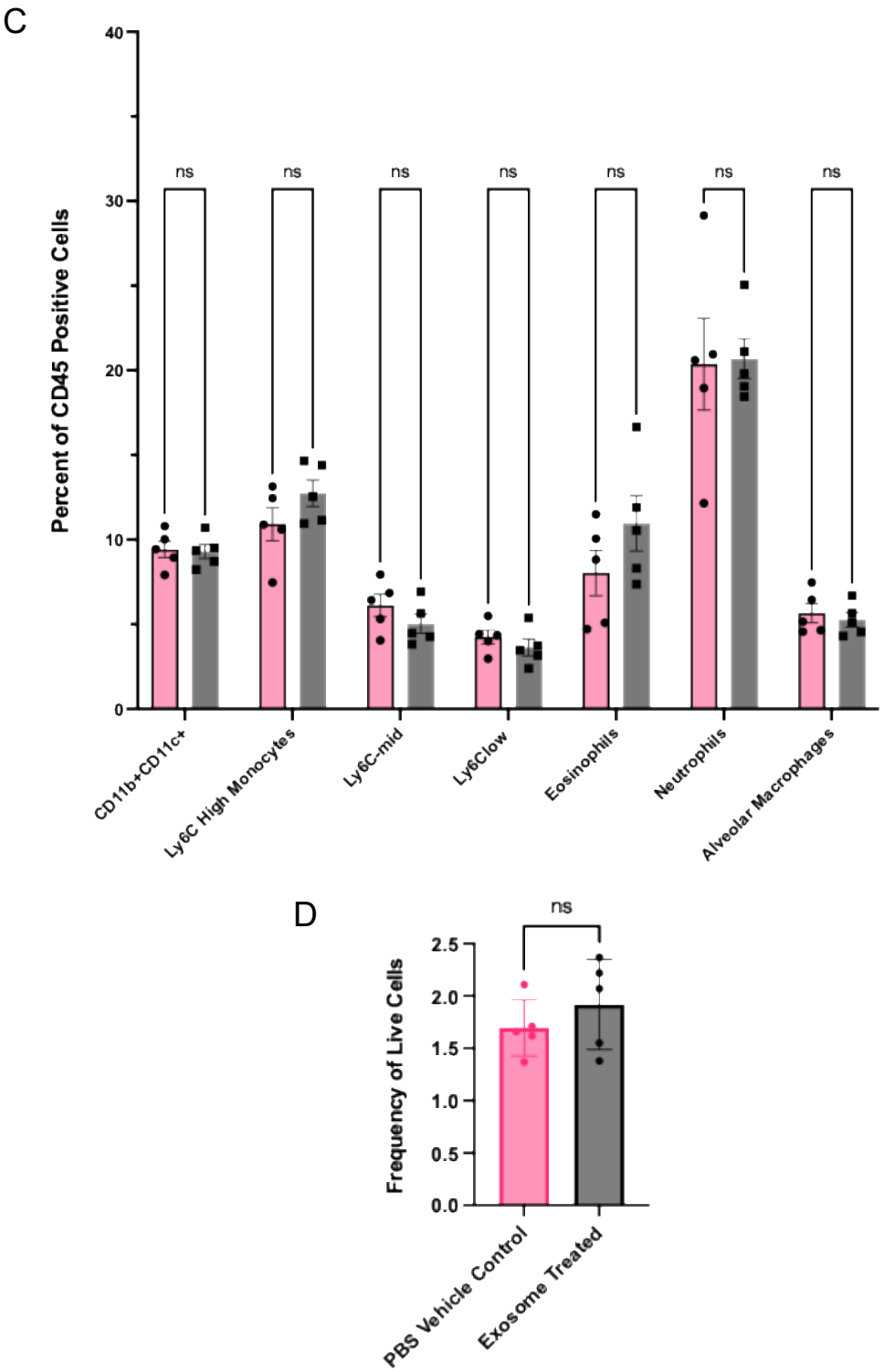

Figure 4.3 Optimization of tissue digestion and analytical methods to evaluate the influence of exosomes on lung resident cell populations C) Bar graphs depicting different CD45+ resident lung cell populations as % of live in response to exosome treatment condition. **D)** Bar graph depicting lung fibroblast population as % of live cells in response to exosome treatment conditions**.**

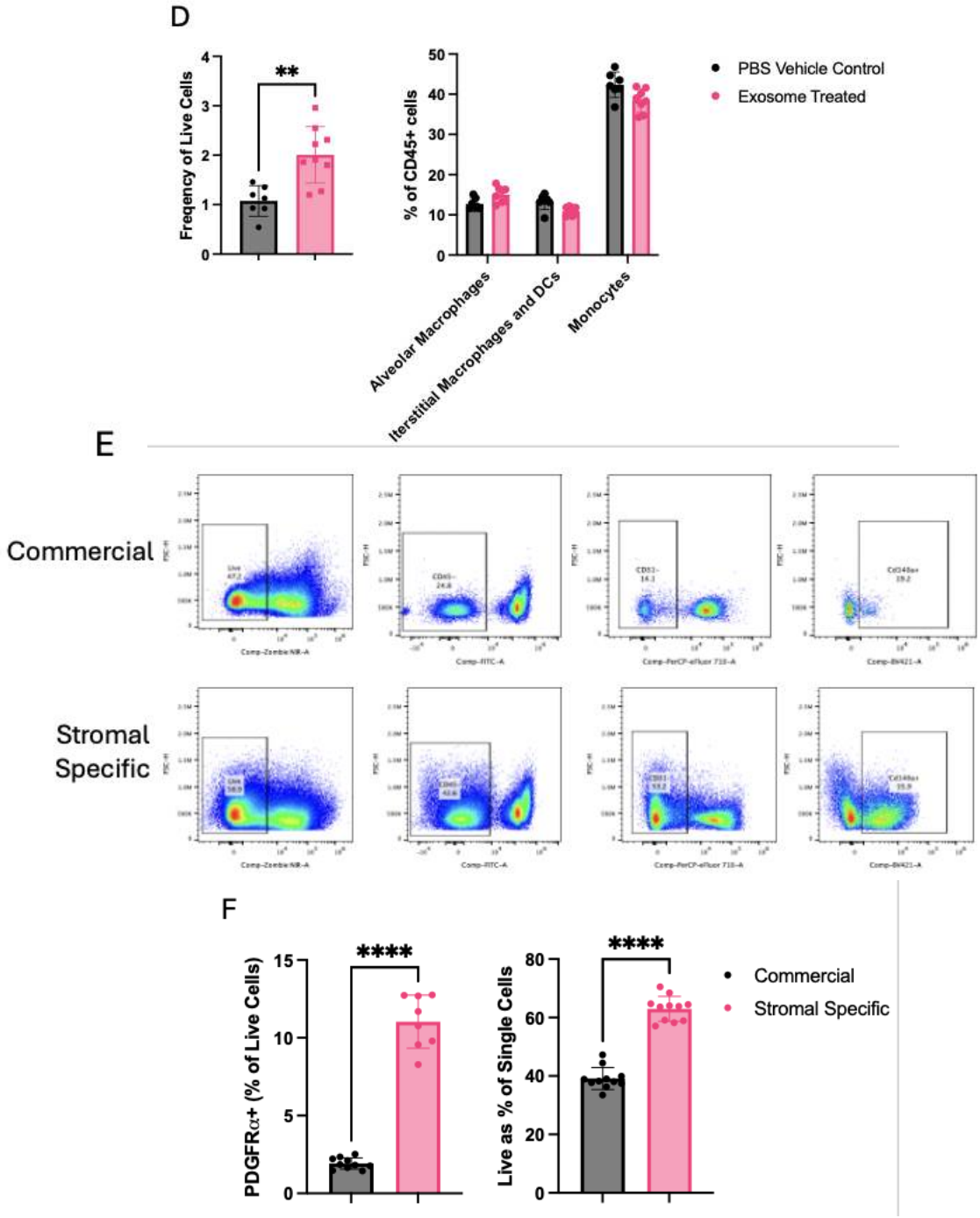

Figure 4.3 Optimization of tissue digestion and analytical methods to evaluate the influence of exosomes on lung resident cell populations D) Bar graphs depicting mouse lung fibroblast populations as % of live cells (Left) and mouse lung immune cell populations as a % of CD45+ cells under exosome treatment conditions **E)** Representative flow plots showing the gating strategy used to compare lung digestion protocols **F)** Bar graphs showing differences in lung PDGFR+ cells as a % of live cells and live cells as a % of single cells between lung digestion protocols ** < 0.01, *** < 0.001, **** < 0.0001

Evaluating the impact of exosomes and the influence of OS cell involvement on changes to stromal cell populations and cytokine signaling in exosome treated mice

Our previous *in vitro* work shows OS-derived exosomes can induce significantly upregulated secretion of known tumor promoting cytokines and chemokines, like IL-6 and CCL2, respectively. Additionally, because we observed OS exosome educations enhanced metastatic colonization *in vivo*, we set out to determine if these observations were associated with alterations to these key signaling molecules. Analysis of a 10-mouse, 2-week exosome education study that excluded tumor cell involvement revealed no significant differences in IL-6 concentrations between treatment groups. However, a significant increase in CCL2 signaling was measured in the lung among PBS vehicle control treated mice. (Fig. 4.4A). Previous analysis of exosome treated, and PBS vehicle control treated mice indicated a potentially important role for OS cell involvement in stimulating significant alterations to resident lung cell populations. To determine if this effect would also be observed in the context of intracellular signaling, we divided 9 mice into groups of 3. 1 group received exosomes followed by OS cell injections, 1 group received PBS vehicle control with OS cells injections, and 1 group received PBS vehicle control with no OS cell involvement. We then evaluated concentrations of IL-6 and CCL2 in the lung, as well as changes to fibroblast populations in each group. Interestingly, we see no significant differences in IL-6 or CCL2 expression between the 3 groups, however, we observe a trend suggesting OS cell involvement in addition to exosome treatments increases the concentrations of these signaling molecules in the lung (Fig. 4.4B). Interestingly, when evaluating alterations to the stromal cell compartment, we observed a significant increase in the fibroblast population as a percent of live cells among mice with OS cell involvement, regardless of exosome treatment condition (Fig. 4.4C).

These data suggest repeated treatments with human OS exosomes does not significantly alter lung concentrations of the key, tumor promoting signaling molecules, IL-6 and CCL2. However, the differences observed in resident lung stromal cell populations when tumor cell involvement was considered, led us to probe changes in these cytokines with, or without tumor cell injections. Although not statistically significant, the concentrations of IL-6 and CCL2 were substantially higher in the lungs of mice that had tumor cell involvement, and a trend hints that exosome educations prior to tumor cell injections may further promote this effect. Furthermore, we observed a significant increase in lung fibroblast populations when tumor cells were injected into mice regardless of exosome treatment condition. This suggests exosome signaling alone may not be sufficient to induce changes in the lung resident cell populations and signaling molecules we probed, but that host-tumor cell interactions may be required to further stimulate these responses.

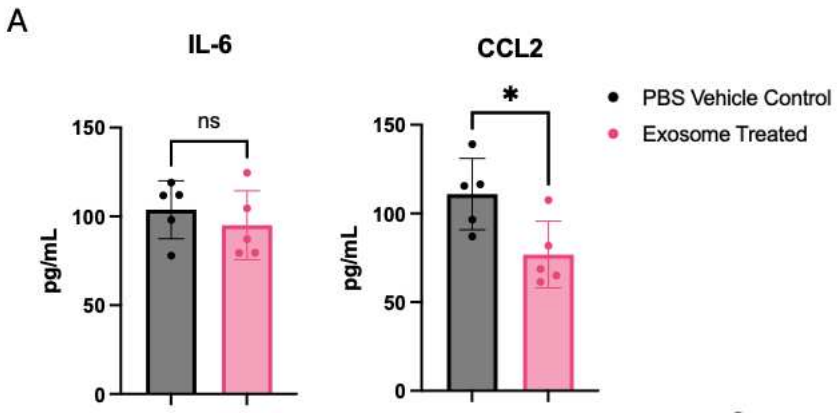

Figure 4.4 Evaluating the impact of exosomes and the influence of OS cell involvement on changes to stromal cell populations and cytokine signaling in exosome treated mice A) Concentrations of IL-6 and CCL2 in lung homogenate under exosome treatment condition as measured by commercial ELISA kit.

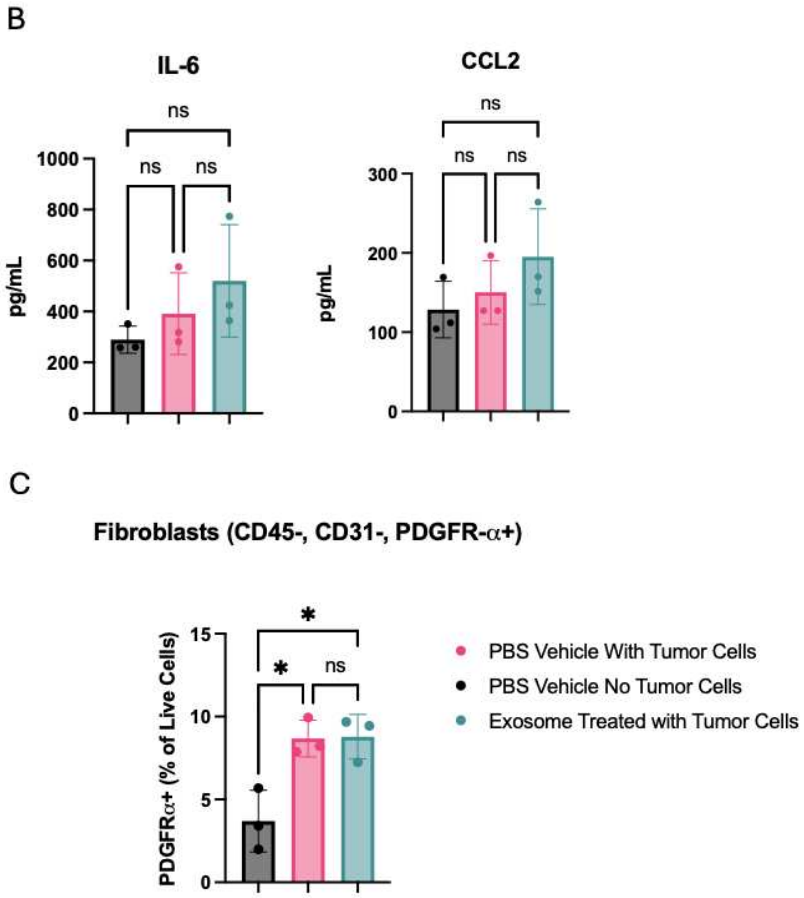

Figure 4.4 Evaluating the impact of exosomes and the influence of OS cell involvement on changes to stromal cell populations and cytokine signaling in exosome treated mice B) Bar graphs comparing IL-6 and CCL2 in mouse lung homogenates **C)** Bar graph of mouse resident lung fibroblast populations as a % of live cells. Both analyses were conducted on mice under the 3 conditions above. One-way ANOVA * < 0.05

Determining the effects of repeated exosome treatments on overall survival

Our data suggests exosomes derived from the highly metastatic human OS cell line, 143b, can enhance metastatic colonization efficiency of OS cells in the lung. Furthermore, we demonstrate exosome treatments in conjunction with OS tumor cell involvement significantly increases secretion of known tumor promoting signaling molecules and is associated with proliferation of lung fibroblasts, a key cell type recognized for their role in promoting tumorigenesis and metastasis. Because of this, we set out to determine if repeated exosome treatments prior to OS cell, tail vein injections can influence overall survival in a xenograft mouse model. To accomplish this required 2 separate studies. The first study was

conducted on 10 mice, with half receiving 2 weeks of daily retroorbital injections of PBS vehicle control, or 143b exosomes as depicted in the schematic (Fig. 4.5A). Circumstances prevented the validation of tumor cell injection efficiency or follow up imaging during the first weeks of the study. However, IVIS imaging conducted two weeks post-tumor cell injections revealed 100% (5/5) of mice in the PBS vehicle treated control group, and 60% (3/5) of mice in the exosome treatment group had a detectable *in vivo* bioluminescent signal (Fig. 4.5B) Among mice with a detectable bioluminescent signal after two weeks, there was no significant difference in overall survival observed between exosome treatment groups (Fig. 4.5C).

Because the initial survival study had a small sample size, a second survival study was conducted with 4 mice in the exosome treatment group and 2 mice in the PBS vehicle control group. IVIS images taken 10 min. post-tumor cell injection reveal successful injection efficiency among all mice in the study (Fig. 4.5D). Representative IVIS images and bioluminescent signal intensity as measured by total flux from all tumor-bearing mice shows the metastasis kinetics of mice in the second survival study over the first 2-weeks post-tumor cell injection. These data show substantial variability in the initial injection efficiency, a sharp drop in signal intensity in the first 2 days, followed by a steady increase in signal over the subsequent 2 weeks (Fig. 4.5E). Evaluating metastasis kinetics of individual mice in this study show variable colonization rates independent of exosome treatment condition (Fig. 4.5F). Pooling results from the two survival studies reveals no significant impact of exosome priming on overall survival in this model (Fig. 4.5G).

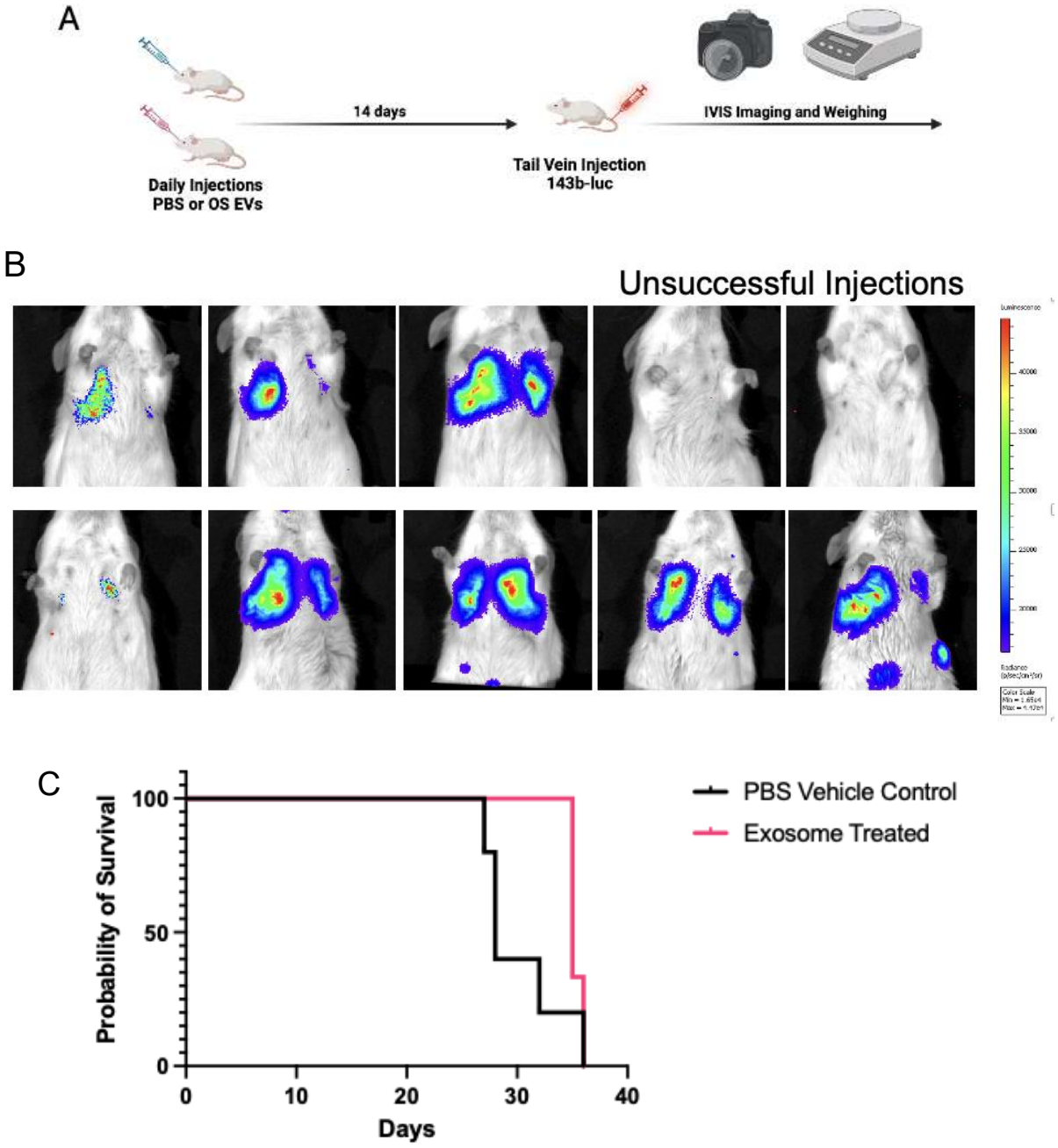

Figure 4.5 Determining the effects of repeated exosome treatments on overall survival

A) Schematic depicting assay approach **B)** IVIS images of mice from survival study 1, 14-days post tumor cell injection. **C)** Kaplan-Meier survival curve of survival study 1.

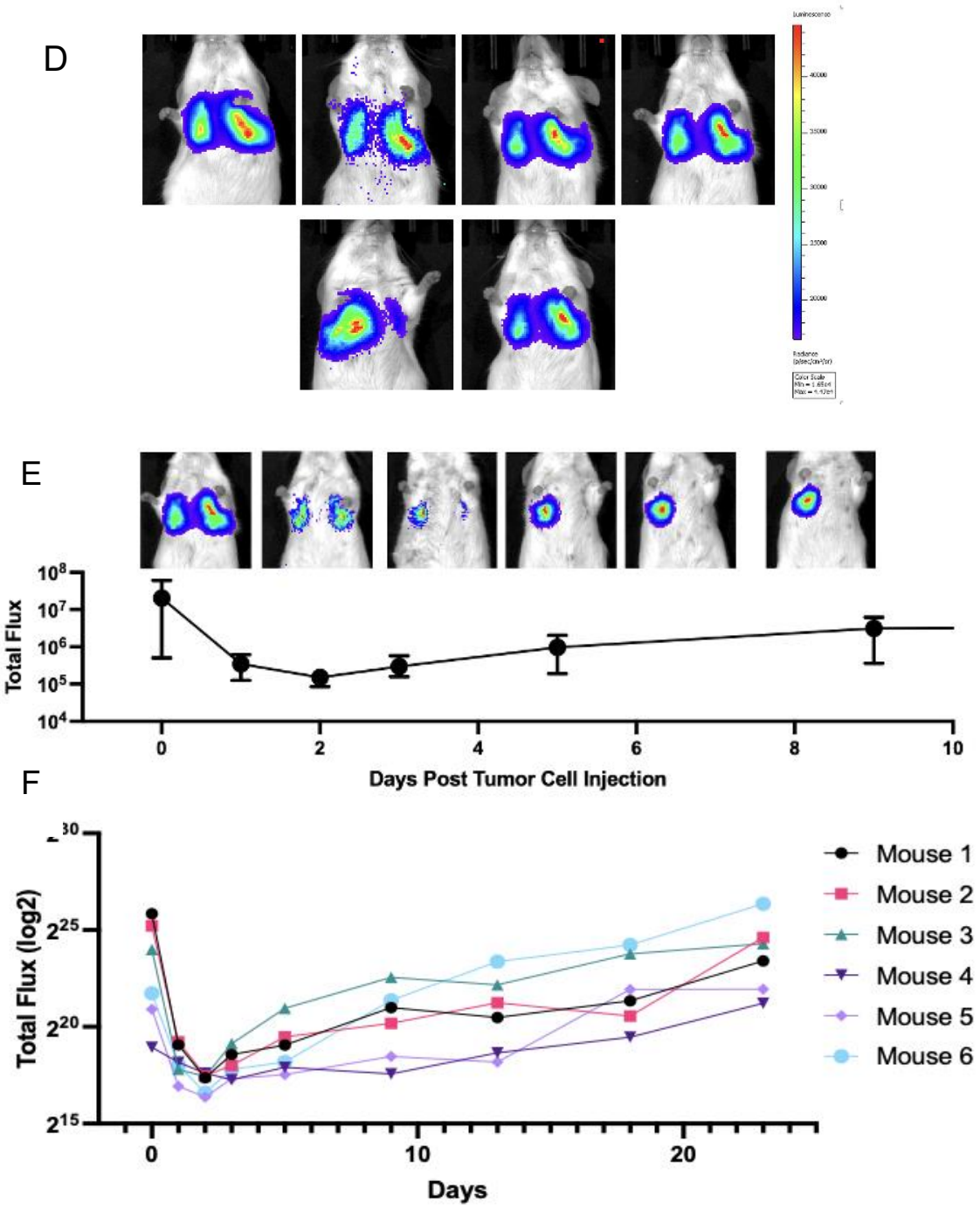

Figure 4.5 Determining the effects of repeated exosome treatments on overall survival
D) IVIS images of mice from survival study 2, 10 min. post tumor cell injection **E)** Representative images of a mouse over 10-days post-143b-luc cell injection and quantification of metastatic progression among mice in the second survival study as measured by Total Flux **F)** Metastatic colonization kinetics of each mouse in survival study 2 over the first 25 days post-tumor cell injection

G

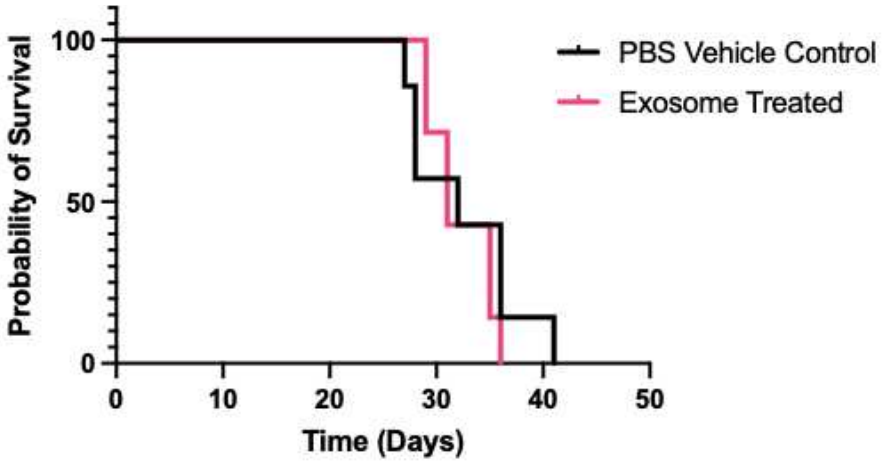

Figure 4.5 Determining the effects of repeated exosome treatments on overall survival
G) Kaplan-meier curve showing survival among exosome treatment groups pooling survival study 1 and 2 together.

Discussion

Recently, studies seeking to determine the mechanisms that drive the predilection for organ specific metastasis observed in pancreatic ductal adenocarcinoma, melanoma, ovarian and breast cancer, demonstrated tumor secreted extracellular vesicles called exosomes, could preferentially traffic to the organs most likely to develop secondary tumors for that cancer type. These seminal studies showed upon uptake of tumor-derived exosomes and subsequent delivery of their biological “cargoes, key cell types within those organs were reprogrammed towards phenotypes capable of orchestrating the molecular and cellular events responsible for creating a favorable microenvironment in advance of circulating tumor cell colonization, coined the pre-metastatic niche. (Peinado, Lavotshkin et al. 2011, Costa-Silva, Aiello et al. 2015, Hoshino, Costa-Silva et al. 2015) Osteosarcoma (OS) displays a particularly high affinity for the development of secondary tumors in the lung, which poses the greatest obstacle for improving clinical outcomes among patients diagnosed with OS. (Kempf-Bielack, Bielack et al. 2005, Ottaviani and Jaffe 2009) Additionally, an increasing body of evidence implicates exosomes derived from OS, specifically, in driving tumorigenesis through alterations to key cell types within the OS TME.(Macklin, Wang et al. 2016, Perut, Roncuzzi et al. 2019, Mazumdar, Urdinez et al. 2020) Because of this, we previously evaluated the impact of OS-derived exosomes on lung fibroblasts, a cell type

increasingly recognized for its tumor- and metastasis promoting characteristics. (Bussard, Mutkus et al. 2016, Kalluri 2016, Liu, Liu et al. 2016) We observed OS exosomes could reprogram lung fibroblasts *in vitro* toward phenotypes characterized by increased proliferation, and secretion of cytokines, chemokines, and growth factors heavily implicated in OS biology, such as IL-6, IL-8, and CCL2. (Chen, Sun et al. 2015, Gross, Cam et al. 2018, Itoh, Kadomatsu et al. 2018, Liu, Chen et al. 2020, Pausch, Aue et al. 2020) This exosome mediated response was associated with the promotion of OS cell survival and proliferation in a serum starved OS cell, exosome educated lung fibroblast co-culture model. Currently, studies investigating the effects of OS-derived exosomes have yet to demonstrate their role in promoting metastasis *in vivo,* particularly at the earliest stages of lung colonization.

Herein, we show mice undergoing treatments with exosomes derived from the highly metastatic human OS cell line, 143b, can significantly increase metastatic colonization efficiency of the lung among measured 4-days post-OS cell tail vain injection as measured by *in vivo* and *ex vivo* bioluminescent detection using IVIS imaging in an immunocompromised xenograft mouse model. We also show this effect may be conserved in an immune competent, syngeneic model, as K7M2-derived exosomes enhance lung colonization as measured by in vivo imaging. However, differences observed between *in vivo,* and *ex vivo* imaging data makes drawing concrete conclusions difficult. Spectral flow cytometry analysis of mouse lung single cell suspensions revealed no significant alterations to mouse resident immune and stomal cell populations. Similarly, no significant changes to the cytokine/chemokines we profiled in mouse lung homogenates were observed in response to 143b exosome priming. However, these studies were conducted with the exclusion of OS cell involvement. Previous analysis of cytokine signaling and stromal cell population changes in mice that received OS tumor cell injections hinted the changes observed in these cell populations may, in part, be due to the addition of tumor cell involvement. With the addition of a lung digestion protocol more specifically optimized to liberate stromal cell populations from the lung, we show injections of tumor cells significantly increases the population of fibroblasts and substantially increases the concentration of cytokine/chemokines we profiled in the lung, regardless of exosome education status. Finally, we determine OS derived exosomes have no significant impact on overall survival in this model.

Of the 6 OS cell lines we previously evaluated, 143b was selected for metastatic colonization studies, because they reliably produced the highest concentration of exosomes and consistently generated the tumor-promoting responses we observed in exosome treated fibroblasts *in vitro*. Furthermore, the 143b cell line was the product of the Fiddler selection method and displayed nearly 100% penetrance in other preclinical mouse models. (Luu, Kang et al. 2005, Uluçkan, Segaliny et al. 2015) To prime the lung pre-metastatic microenvironment prior to inoculation with 143b OS cells, immunocompromised Balb/c-scid mice were chronically exposed to 2 weeks of daily retroorbital injections. The two-week dosing period was chosen to emulate early studies investigating *in vivo* biological activity of luciferase expressing 143b cells injected intra-tibially, which were observed to form detectable, spontaneous lung metastases as early as 2 weeks post-tumor cell injection. (Garimella, Eskew et al. 2013) However, the exosome dosing strategy of daily injections may not be optimal to induce the responses we predicted, as recent studies suggest the biological half-life of exosomes *in vivo* ranges from 30 min. to 2 hours. (Takahashi, Nishikawa et al. 2013, Lai, Mardini et al. 2014) Additionally, it is likely that a spontaneous primary OS tumor is continuously releasing exosomes into circulation. Therefore, a more frequent dosing strategy, or a method to continuously administer exosomes may more accurately reflect conditions within spontaneous OS. Upon tail vein injection of 143b cells, mice were imaged 10 minutes post-injection. This allowed us to confirm the injections were successful and demonstrated that the number of cells entering the lungs was significantly variable. This also provided us with a method for normalizing the *in vivo* and *ex vivo* bioluminescent signal detected 4-days post-tumor cell injection. As our goal was to evaluate the effects of OS exosomes on initial lung colonization, we were able to derive a metric that describes the number of OS cells capable of initially seeding and colonizing the lung, deemed colonization efficiency. This baseline normalized metric showed 143b exosome educations significantly enhances the initial colonization of tail vein injected 143b-Luc cells in this model.

We next sought to determine if the metastasis promoting effects of OS cell-derived exosomes was conserved across models. The previous xenograft model lacked the full complement of immune cells shown to be influential in premetastatic niche formation and metastatic colonization (Patras, Shaashua et al. 2023) Therefore, we aimed to evaluate the role of exosomes derived from a murine OS cell line on metastatic colonization in a syngeneic mouse model. Numerous studies have taken advantage of an

immunocompetent mouse model to evaluate the biological activity of K7M2 murine OS cells *in vivo*, which have demonstrated a high likelihood to develop lung metastases. (Grisez, Ray et al. 2018) Although we observed a significant increase in colonization efficiency among exosome educated mice *in vivo* 4-days post-tumor cell injection, this is in contradiction to data from *ex vivo* imaging, thus making results difficult to interpret. However, the difference between *in vivo* and *ex vivo* imaging data may be due to differences between samples in the time variability from the administration of luciferase until the *ex vivo* images were taken. This was more carefully considered and avoided in the 143b mouse studies. Additionally, we observed a significantly higher luminescent signal among 143b-Luc cells compared K7M2-Luc cells, thus bioluminescent measurements at the lower limits of detection of the IVIS instrument may not be as reliable. The incubation period of 4 days post-tumor cell injection used for these studies was meant to measure OS cells that were capable of seeding in the lung at the earliest phases of colonization and still be detected by IVIS imaging. Later longitudinal studies would confirm this was the timepoint at which the bioluminescent signal intensity among 143b-Luc injected mice was at its lowest, suggesting any remaining OS cells were likely those to successfully colonize and outgrow within the lung. However, these metastatic dynamics may not have been optimized for the K7M2 model, as their growth rate and time to metastasis is substantially longer than that of 143b cells. (Miretti, Roato et al. 2008)

Next, we evaluated population dynamics of lung CD45+ leukocytes and, lung fibroblasts, as well as changes to IL-6 and CCL2 concentrations upon 143b exosome treatments using spectral flow cytometry and ELISAs, respectively. Interestingly, no significant changes were observed among the populations or signaling molecules we probed. Although, intravenous injections of OS derived exosomes are likely to be rapidly trafficked through circulation to the lungs, it is unclear if the metastasis promoting effects observed in 143b exosome educated mice can be directly attributed to functional responses among potential target resident cells of the lung. Although outside the scope of this study, determining the biodistribution and target cell types of 143b exosomes may provide insights into their observed metastatic promoting effects. Additionally, changes in lung cell population dynamics may not fully describe alterations to their functional state and follow up studies should consider characterizing the transcriptional alterations to these populations.

This study excluded the introduction of OS cells into the model. This data contrasts with evidence from previous studies showing that in the presence of OS cells, exosome treatments were associated with increased proliferation of resident stromal cells in the lung. Evidence supports tumor host interactions that occur during extravasation. For instance, adhesion molecules found among both tumor cells and resident lung cells like integrins, can stimulate activation of mitogenic pathways such as those downstream of focal adhesion kinase. Furthermore, this process requires interactions between CTCs and host immune cells like MDSCs and TAMs, that can release potent tumor promoting stimulatory molecules like TGFB1.(Qian, Deng et al. 2009, Labelle, Begum et al. 2011, Teo, Ankrum et al. 2012) Therefore, we set out to determine if tumor cell involvement was required to stimulate changes to lung fibroblast populations or cytokine/chemokine signaling in the lung following exosome priming. Interestingly, although there were no significant changes to the fibroblast populations between exosome treatment groups, the involvement of OS cells in the lungs appears to be associated with a significant increase in the fibroblast population as a percent of live cells. Additionally, IL-6 and CCL2 concentrations within the lung increase with tumor cell involvement and is substantially amplified among mice in the exosome treatment group. It should be noted that these studies had a small sample size of only 3 mice per group, and cytokine/chemokine concentrations were measured using commercial ELISA kits, which are limited in their sensitivity and dynamic range. These observations could be further validated with a larger sample size and other cell signaling measurement methods, such as PCR or bead-based multiplex cytokine panels.

Our observations demonstrated exosome educations improved the metastatic colonization efficiency of 143b cells in the lung, therefore, we set out to determine if this effect would translate into differences in overall survival. However, we observed no statistically significant differences in overall survival between exosome treatment groups. This may be due to several limitations that accompanied. these studies. First, it is unclear if the exosome treated mice in this study displayed enhanced metastatic colonization efficiency at the earliest phases of the study, as the IVIS instrument was not functional for imaging. Additionally, these studies had a small sample size, and therefore, it is difficult to determine the significance between small differences in survival outcomes. Furthermore, the route of tumor cell injection by tail vein is not typically used to determine effects on overall survival. Future studies investigating the

impact of exosome treatments on overall survival may be best served by using orthotopic, intra-tibial injections for the introduction of OS cells into mice, as these models more accurately reflect events that occur during spontaneous metastasis. (Luu, Kang et al. 2005, Garimella, Eskew et al. 2013, Fan, Roberts et al. 2020, Ko, Jeong et al. 2021, Beck, Ren et al. 2022) Interestingly, the metastatic colonization dynamics observed in the second phase of the survival study showed a high degree of variability among mice 10 min. after OS cell tail vein injections, which was then followed by a sharp drop in signal intensity among all mice, from which, remaining tumor cells then grow out at varying rates. These observed kinetics suggest mouse lungs may have a specific carrying capacity for supporting circulating tumor cells and facilitating tumor cell survival, regardless of exosome treatment status. However, the following differences in outgrowth may be the result of microenvironmental changes resulting from exosome priming, such as angiogenesis and immune suppression. This data hints that the role of exosomes in priming the pre-metastatic niche may be less important for the initial colonization of tumor cells in secondary organs, rather, the exosome induced microenvironmental alterations promote and allow for more rapid expansion of the tumor cells that successfully survive the initial colonization step.

References

Anderson, P. M., P. Meyers, E. Kleinerman, K. Venkatakrishnan, D. P. Hughes, C. Herzog, W. Huh, R. Sutphin, Y. M. Vyas, V. Shen, A. Warwick, N. Yeager, C. Oliva, B. Wang, Y. Liu and A. Chou (2014). "Mifamurtide in metastatic and recurrent osteosarcoma: a patient access study with pharmacokinetic, pharmacodynamic, and safety assessments." Pediatr Blood Cancer **61**(2): 238-244.

Asif, P. J., C. Longobardi, M. Hahne and J. P. Medema (2021). "The Role of Cancer-Associated Fibroblasts in Cancer Invasion and Metastasis." Cancers (Basel) **13**(18).

Beck, J., L. Ren, S. Huang, E. Berger, K. Bardales, J. Mannheimer, C. Mazcko and A. LeBlanc (2022). "Canine and murine models of osteosarcoma." Vet Pathol **59**(3): 399-414.

Bussard, K. M., L. Mutkus, K. Stumpf, C. Gomez-Manzano and F. C. Marini (2016). "Tumor-associated stromal cells as key contributors to the tumor microenvironment." Breast Cancer Res **18**(1): 84.

Chen, Q., W. Sun, Y. Liao, H. Zeng, L. Shan, F. Yin, Z. Wang, Z. Zhou, Y. Hua and Z. Cai (2015). "Monocyte chemotactic protein-1 promotes the proliferation and invasion of osteosarcoma cells and upregulates the expression of AKT." Mol Med Rep **12**(1): 219-225.

Chhoy, P., C. W. Brown, J. J. Amante and A. M. Mercurio (2021). "Protocol for the separation of extracellular vesicles by ultracentrifugation from in vitro cell culture models." STAR Protoc **2**(1): 100303.

Costa-Silva, B., N. M. Aiello, A. J. Ocean, S. Singh, H. Zhang, B. K. Thakur, A. Becker, A. Hoshino, M. T. Mark, H. Molina, J. Xiang, T. Zhang, T. M. Theilen, G. García-Santos, C. Williams, Y. Ararso, Y. Huang, G. Rodrigues, T. L. Shen, K. J. Labori, I. M. Lothe, E. H. Kure, J. Hernandez, A. Doussot, S. H. Ebbesen, P. M. Grandgenett, M. A. Hollingsworth, M. Jain, K. Mallya, S. K. Batra, W. R. Jarnagin, R. E. Schwartz, I. Matei, H. Peinado, B. Z. Stanger, J. Bromberg and D. Lyden (2015). "Pancreatic cancer exosomes initiate pre-metastatic niche formation in the liver." Nat Cell Biol **17**(6): 816-826.

Fan, T. M., R. D. Roberts and M. M. Lizardo (2020). "Understanding and Modeling Metastasis Biology to Improve Therapeutic Strategies for Combating Osteosarcoma Progression." Front Oncol **10**: 13.

Feng, W., D. C. Dean, F. J. Hornicek, H. Shi and Z. Duan (2019). "Exosomes promote pre-metastatic niche formation in ovarian cancer." Mol Cancer **18**(1): 124.

Garimella, R., J. Eskew, P. Bhamidi, G. Vielhauer, Y. Hong, H. C. Anderson, O. Tawfik and P. Rowe (2013). "Biological characterization of preclinical Bioluminescent Osteosarcoma Orthotopic Mouse (BOOM) model: A multi-modality approach." J Bone Oncol **2**(1): 11-21.

Grisez, B. T., J. J. Ray, P. A. Bostian, J. E. Markel and B. A. Lindsey (2018). "Highly metastatic K7M2 cell line: A novel murine model capable of in vivo imaging via luciferase vector transfection." J Orthop Res.

Gross, A. C., H. Cam, D. A. Phelps, A. J. Saraf, H. K. Bid, M. Cam, C. A. London, S. A. Winget, M. A. Arnold, L. Brandolini, X. Mo, J. M. Hinckley, P. J. Houghton and R. D. Roberts (2018). "IL-6 and CXCL8 mediate osteosarcoma-lung interactions critical to metastasis." JCI Insight **3**(16).

Han, F., P. Pu, C. Wang, X. Ding, Z. Zhu, W. Xiang and W. Wang (2021). "Osteosarcoma Cell-Derived Exosomal miR-1307 Promotes Tumorgenesis via Targeting AGAP1." Biomed Res Int **2021**: 7358153.

Hoshino, A., B. Costa-Silva, T. L. Shen, G. Rodrigues, A. Hashimoto, M. Tesic Mark, H. Molina, S. Kohsaka, A. Di Giannatale, S. Ceder, S. Singh, C. Williams, N. Soplop, K. Uryu, L. Pharmer, T. King, L. Bojmar, A. E. Davies, Y. Ararso, T. Zhang, H. Zhang, J. Hernandez, J. M. Weiss, V. D. Dumont-Cole, K. Kramer, L. H. Wexler, A. Narendran, G. K. Schwartz, J. H. Healey, P. Sandstrom, K. J. Labori, E. H. Kure, P. M. Grandgenett, M. A. Hollingsworth, M. de Sousa, S. Kaur, M. Jain, K. Mallya, S. K. Batra, W. R. Jarnagin, M. S. Brady, O. Fodstad, V. Muller, K. Pantel, A. J. Minn, M. J. Bissell, B. A. Garcia, Y. Kang, V. K. Rajasekhar, C. M. Ghajar, I. Matei, H. Peinado, J. Bromberg and D. Lyden (2015). "Tumour exosome integrins determine organotropic metastasis." Nature **527**(7578): integrins.

Itoh, H., T. Kadomatsu, H. Tanoue, M. Yugami, K. Miyata, M. Endo, J. Morinaga, E. Kobayashi, T. Miyamoto, R. Kurahashi, K. Terada, H. Mizuta and Y. Oike (2018). "TET2-dependent IL-6 induction mediated by the tumor microenvironment promotes tumor metastasis in osteosarcoma." Oncogene **37**(22): 2903-2920.

Kalluri, R. (2016). "The biology and function of fibroblasts in cancer." Nat Rev Cancer **16**(9): 582-598.

Kempf-Bielack, B., S. S. Bielack, H. Jürgens, D. Branscheid, W. E. Berdel, G. U. Exner, U. Göbel, K. Helmke, G. Jundt, H. Kabisch, M. Kevric, T. Klingebiel, R. Kotz, R. Maas, R. Schwarz, M. Semik, J. Treuner, A. Zoubek and K. Winkler (2005). "Osteosarcoma relapse after combined modality therapy: an analysis of unselected patients in the Cooperative Osteosarcoma Study Group (COSS)." J Clin Oncol **23**(3): 559-568.

Ko, Y., Y. H. Jeong, J. H. Seo and J. A. Lee (2021). "Development of a Bioluminescent Human Osteosarcoma Model in Humanized NSG Mice: A Pilot Study." In Vivo **35**(4): 2151-2157.

Labelle, M., S. Begum and R. O. Hynes (2011). "Direct signaling between platelets and cancer cells induces an epithelial-mesenchymal-like transition and promotes metastasis." Cancer Cell **20**(5): 576-590.

Lagerweij, T., M. Pérez-Lanzón and S. R. Baglio (2018). "A Preclinical Mouse Model of Osteosarcoma to Define the Extracellular Vesicle-mediated Communication Between Tumor and Mesenchymal Stem Cells." J Vis Exp(135).

Lai, C. P., O. Mardini, M. Ericsson, S. Prabhakar, C. Maguire, J. W. Chen, B. A. Tannous and X. O. Breakefield (2014). "Dynamic biodistribution of extracellular vesicles in vivo using a multimodal imaging reporter." ACS Nano **8**(1): 483-494.

Li, Y., S. Lin, X. Xie, H. Zhu, T. Fan and S. Wang (2021). "Highly enriched exosomal lncRNA OIP5-AS1 regulates osteosarcoma tumor angiogenesis and autophagy through miR-153 and ATG5." Am J Transl Res **13**(5): 4211-4223.

Liu, J. F., P. C. Chen, T. M. Chang and C. H. Hou (2020). "Monocyte Chemoattractant Protein-1 promotes cancer cell migration via c-Raf/MAPK/AP-1 pathway and MMP-9 production in osteosarcoma." J Exp Clin Cancer Res **39**(1): 254.

Liu, L., L. Liu, H. H. Yao, Z. Q. Zhu, Z. L. Ning and Q. Huang (2016). "Stromal Myofibroblasts Are Associated with Poor Prognosis in Solid Cancers: A Meta-Analysis of Published Studies." PLoS One **11**(7): e0159947.

Luu, H. H., Q. Kang, J. K. Park, W. Si, Q. Luo, W. Jiang, H. Yin, A. G. Montag, M. A. Simon, T. D. Peabody, R. C. Haydon, C. W. Rinker-Schaeffer and T. C. He (2005). "An orthotopic model of human osteosarcoma growth and spontaneous pulmonary metastasis." Clin Exp Metastasis **22**(4): 319-329.

Macklin, R., H. Wang, D. Loo, S. Martin, A. Cumming, N. Cai, R. Lane, N. S. Ponce, E. Topkas, K. Inder, N. A. Saunders and L. Endo-Munoz (2016). "Extracellular vesicles secreted by highly metastatic clonal variants of osteosarcoma preferentially localize to the lungs and induce metastatic behaviour in poorly metastatic clones." Oncotarget **7**(28): 43570-43587.

Mazumdar, A., J. Urdinez, A. Boro, J. Migliavacca, M. J. E. Arlt, R. Muff, B. Fuchs, J. G. Snedeker and A. Gvozdenovic (2020). "Osteosarcoma-Derived Extracellular Vesicles Induce Lung Fibroblast Reprogramming." Int J Mol Sci **21**(15).

Mirabello, L., R. J. Troisi and S. A. Savage (2009). "Osteosarcoma incidence and survival rates from 1973 to 2004: data from the Surveillance, Epidemiology, and End Results Program." Cancer **115**(7): 1531-1543.

Miretti, S., I. Roato, R. Taulli, C. Ponzetto, M. Cilli, M. Olivero, M. F. Di Renzo, L. Godio, A. Albini, P. Buracco and R. Ferracini (2008). "A mouse model of pulmonary metastasis from spontaneous osteosarcoma monitored in vivo by Luciferase imaging." PLoS One **3**(3): e1828.

Ottaviani, G. and N. Jaffe (2009). "The epidemiology of osteosarcoma." Cancer Treat Res **152**: 3-13.

Paget, S. (1989). "The distribution of secondary growths in cancer of the breast. 1889." Cancer Metastasis Rev **8**(2): 98-101.

Patras, L., L. Shaashua, I. Matei and D. Lyden (2023). "Immune determinants of the pre-metastatic niche." Cancer Cell **41**(3): 546-572.

Pausch, T. M., E. Aue, N. M. Wirsik, A. Freire Valls, Y. Shen, P. Radhakrishnan, T. Hackert, M. Schneider and T. Schmidt (2020). "Metastasis-associated fibroblasts promote angiogenesis in metastasized pancreatic cancer via the CXCL8 and the CCL2 axes." Sci Rep **10**(1): 5420.

Peinado, H., M. Alečković, S. Lavotshkin, I. Matei, B. Costa-Silva, G. Moreno-Bueno, M. Hergueta-Redondo, C. Williams, G. García-Santos, C. Ghajar, A. Nitadori-Hoshino, C. Hoffman, K. Badal, B. A. Garcia, M. K. Callahan, J. Yuan, V. R. Martins, J. Skog, R. N. Kaplan, M. S. Brady, J. D. Wolchok, P. B. Chapman, Y. Kang, J. Bromberg and D. Lyden (2012). "Melanoma exosomes educate bone marrow progenitor cells toward a pro-metastatic phenotype through MET." Nat Med **18**(6): 883-891.

Peinado, H., S. Lavotshkin and D. Lyden (2011). "The secreted factors responsible for pre-metastatic niche formation: old sayings and new thoughts." Semin Cancer Biol **21**(2): 139-146.

Perut, F., L. Roncuzzi, N. Zini, A. Massa and N. Baldini (2019). "Extracellular Nanovesicles Secreted by Human Osteosarcoma Cells Promote Angiogenesis." Cancers (Basel) **11**(6).

Qian, B., Y. Deng, J. H. Im, R. J. Muschel, Y. Zou, J. Li, R. A. Lang and J. W. Pollard (2009). "A distinct macrophage population mediates metastatic breast cancer cell extravasation, establishment and growth." PLoS One **4**(8): e6562.

Sha, L., D. Ma and C. Chen (2020). "Exosome-mediated Hic-5 regulates proliferation and apoptosis of osteosarcoma via Wnt/β-catenin signal pathway." Aging (Albany NY) **12**(23): 23598-23608.

Takahashi, Y., M. Nishikawa, H. Shinotsuka, Y. Matsui, S. Ohara, T. Imai and Y. Takakura (2013). "Visualization and in vivo tracking of the exosomes of murine melanoma B16-BL6 cells in mice after intravenous injection." J Biotechnol **165**(2): 77-84.

Teo, G. S., J. A. Ankrum, R. Martinelli, S. E. Boetto, K. Simms, T. E. Sciuto, A. M. Dvorak, J. M. Karp and C. V. Carman (2012). "Mesenchymal stem cells transmigrate between and directly through tumor necrosis factor-α-activated endothelial cells via both leukocyte-like and novel mechanisms." Stem Cells **30**(11): 2472-2486.

Uluçkan, Ö., A. Segaliny, S. Botter, J. M. Santiago and A. J. Mutsaers (2015). "Preclinical mouse models of osteosarcoma." Bonekey Rep **4**: 670.

Zhong, L., D. Liao, J. Li, W. Liu, J. Wang, C. Zeng, X. Wang, Z. Cao, R. Zhang, M. Li, K. Jiang, Y. X. Zeng, J. Sui and T. Kang (2021). "Rab22a-NeoF1 fusion protein promotes osteosarcoma lung metastasis through its secretion into exosomes." Signal Transduct Target Ther **6**(1): 59.

CHAPTER 5

Conclusions and Future Directions

Nearly 10 years ago, seminal studies identified tumor secreted extracellular vesicles called exosomes, as possible drivers of organ specific metastasis. (Peinado, Alečković et al. 2012, Costa-Silva, Aiello et al. 2015, Hoshino, Costa-Silva et al. 2015)Because OS displays a particularly high degree of lung specific metastasis, the broader goal of this dissertation was to characterize the role of exosomes in promoting OS lung metastasis with the hope of identifying insights into mechanisms that may one day be exploited for the development of novel, anti-metastatic therapeutic approaches.

In Ch.2, we characterized the role of OS exosomes in promoting phenotypic and transcriptional alterations in donor-derived lung fibroblasts *in vitro*. Initially, we identified 6 commercially available OS cell lines consisting of paired, WT or highly metastatic isogenic subclones of one another. Upon successful isolation and characterization of OS-derived exosomes, we evaluated their capacity to stimulate primary, donor-derived lung fibroblasts, a key cell type increasingly recognized for their tumor-promoting role within the tumor microenvironment and contributor to pre-metastatic niche formation in distant organs. (Bussard, Mutkus et al. 2016, Asif, Longobardi et al. 2021, Gong, Li et al. 2022) We hypothesized uptake of exosomes derived from highly metastatic subclones would induce a more robust response than their WT counterparts. Upon repeated educations with OS-derived exosomes under serum starved conditions, we discovered treated fibroblasts produced significantly elevated secretions of IL-6, IL-8, and CCL2, independent of metastatic subclone variant. This was a striking result, as these signaling molecules are heavily implicated in OS biology. (Chen, Sun et al. 2015, Gross, Cam et al. 2018, Karakasheva, Lin et al. 2018, Gok Yavuz, Gunaydin et al. 2019, Regan, Coy et al. 2019) Additionally, this was in comparison to exosomes derived from the normal osteoblast cell line, hFOB, and exosomes derived from other cancer types known to metastasize to the lung including breast, colorectal, transitional cell carcinoma and melanoma. This indicated something specific to OS exosomes was capable of driving such a potent secretory response of these signaling molecules and provided the first evidence that OS exosomes are highly functional in this context. Subsequently, using confocal fluorescent microscopy and spectral flow cytometry, we demonstrated the degree of fibroblast uptake of PKH26, fluorescently labeled, OS

exosomes occurred in an OS exosome donor cell line and fibroblast recipient cell line dependent manner, regardless of metastatic variant. Because we observed OS exosomes were efficiently taken up by lung fibroblasts, inducing a robust secretory response, this led us to evaluate possible intracellular signal transduction pathways driving this phenotype. Bead-based phospho-protein analysis of OS exosome treated fibroblasts revealed upregulation of Erk1/2-MAPK but not Akt/mTOR. Activation of this mitogenic signal transduction pathway was in line with our observations that OS exosomes can stimulate increased fibroblast proliferation.(Hayashi, Yamashita et al. 2000, Alspach, Flanagan et al. 2014) Less convincing results from several immunoblot phosphor-protein arrays of exosome treated fibroblasts indicated upregulation of STAT3, a kinase whose signaling has been shown to be associated with CAF functions in the OS TME. (Fossey, Liao et al. 2009, Wang, Zheng et al. 2011, Tu, Du et al. 2012, Karakasheva, Lin et al. 2018) Following, RNA-seq and subsequent analysis of exosome treated fibroblasts indicated nearly 500 DEGs, and confirmed our previous observations as gene sets were highly enriched for pathways associated with cytokine and chemokine signaling, specifically highlighting the signaling molecules discussed previously. Interestingly, other pathways that were highly enriched included those associated with a hallmark cancer associated fibroblast phenotype. Furthermore, gene sets hinted at induction of the recently described CAF subsets, inflammatory-CAF (iCAF) and myofibroblastic-CAF (myCAF). These subsets are characterized by secretion of tumor promoting, immunosuppressive signaling molecules, or ECM remodeling, wound-healing functional properties, respectively. Because we observed differential expression of genes associated with a myCAF phenotype, we hypothesized OS exosomes may induce the transition of fibroblasts from a quiescent phenotype, to an “activated” CAF-like phenotype. Therefore, we performed western blots to probe for proteins associated with a wound-healing, myCAF phenotype, alpha-smooth muscle actin and fibroblast activating protein. However, results indicated a high level of protein expression among fibroblasts in the untreated condition. These findings may be the result of repeated passages in tissue culture flasks, which subjectively alter the morphology of fibroblasts to a confirmation more indicative of a wound-healing state characterized by elongation and protruding spindles. This is in line with evidence indicating fibroblasts are highly responsive to the tensile forces of their culture conditions. Follow up studies may benefit by optimizing these conditions to include an artificial matrix that more accurately emulates the tensile forces fibroblasts would encounter during tissue

homeostasis. Finally, low-density seeding of RFP labeled OS cells onto exosome treated monolayers in serum starved conditions meant to recapitulate CTCs colonizing the lung, revealed priming of fibroblasts in advance of OS cell seeding significantly enhanced proliferation of OS cells in this model. Despite these results, no other analysis on the fibroblasts or OS cells in this model was conducted, therefore, it is difficult to say what specifically promoted the fibroblast mediated OS cell proliferation. Cell sorting of the RFP labeled OS cells from this model could be conducted to perform RNA-seq on the fibroblasts and OS cells to identify the transcriptional determinates of the tumor promoting phenotype we observed.

Studies investigating genomic alterations acquired by commercial OS cells lines during transformation towards highly metastatic variants have identified several differentially expressed genes that promote a metastatic phenotype. (Lauvrak, Munthe et al. 2013, Ren, Mendoza et al. 2015) Despite solid rationale for the comparison of functionality between exosomes derived from WT or metastatic OS subclones, no differences in the fibroblast responses were observed. Additionally, a heat map of the top 50 DEGs in exosome treated fibroblasts showed a striking similarity between subclone pairs. This suggests the acquired mutations among transformed cell lines may not be required for differences in response to exosome signaling, and the intrinsic genetic alterations that initiated tumorigenesis in these cell lines may be more important in this regard. Additionally, several limitations of using commercially available cell lines exist. This includes cell line gene expression profiles that often diverge from original tumor of origin, OS cell lines that lack complexity in cellular heterogeneity, and repeated passages that select for cells adapted to the tissue culture environment. More recently, there has been a shift towards investigating patient-derived (PDX) OS cell lines that are shown to more closely resemble the phenotypic and genetic characteristics of the original clinical samples. (Schott, Shah et al. 2020, Schott, Koehne et al. 2024)

The question of what drives the observed differential functional and transcriptional response of lung fibroblasts in response to exosomes derived from different OS cell lines or other cancer types remains unanswered. Several studies have evaluated the biological cargos contained within tumor derived EVs using mass spectrometry based proteomic profiling approaches. These studies typically identify miRNA, lncRNA, or proteins involved in cell signaling, along with the resulting influence of these molecules on various signal transduction pathways in target cells. (Han, Huo et al. 2019, Sha, Ma et al.

2020, Han, Pu et al. 2021, Li, Lin et al. 2021, Zhong, Liao et al. 2021, Xu, Fu et al. 2024) However, the shortcomings of these studies often result from the evaluation on the impact of the specific cargoes identified in exosomes derived from a single cell line, and therefore, lack the translational relevance of linking exosome cargo to the intrinsic, metastasis promoting genomic, translational, or functional characteristics of the cell lines in question. In other words, there remains a considerable knowledge gap in our understanding of how cargo loading during exosome biogenesis is influenced by the genetics, or functional state of the donor cancer cell.

To address the question of which tumor cell intrinsic properties influence the functional characteristics of exosomes, the use of mass spectrometry profiling approaches previously mentioned could be taken to screen for variations in exosome cargoes. For instance, EVs could be collected and sorted for proteomic analysis based on the perceived or documented metastatic behavior of the cell lines being evaluated or based on the functional response to their EVs in various target cell types as was demonstrated in Ch.2. This could be done between highly metastatic subclones we evaluated in Ch.2, or among exosomes derived from primary PDX OS cell lines whose patient outcomes are known. The likelihood of identifying a single exosomal cargo as a key driver of metastasis is unlikely. However, developing a panel of exosomal protein, miRNA, or lncRNA cargos derived from OS cell lines with specific genetic alterations associated with either a high or low likelihood of developing metastatic disease, could provide insights into the genetic or transcriptional drivers potentially influencing said exosomal cargo and their tumor-promoting effects. These data paired with studies describing improvements in capturing and identifying cancer specific exosomes from patient liquid biopsies, could then be used to develop an exosome cargo based molecular signature with the intention of stratifying patients based the potential to develop metastatic disease or therapy response. (Zhou, Xu et al. 2020, Zhu, Xing et al. 2022) Furthermore, this approach could be used as rationale to investigate the intrinsic characteristics that influence selective cargo sorting mechanisms during exosome biogenesis. Although the cellular machinery that produces exosomes has been increasingly characterized, there remains a substantial lack in understanding of the intrinsic cellular or functional state determinates of exosome cargo sorting.

As we successfully demonstrated uptake of labeled exosomes by lung fibroblasts using flow cytometry, the mechanisms by which exosomes are taken up by target cells surprisingly remains largely

unexplored. Limited evidence has shown exosomes can be taken up by target cells using several endocytic pathways, phagocytosis, and fusion. These studies conclude the mechanisms of exosome uptake is largely exosome donor and target cell type specific. (Feng, Zhao et al. 2010, Christianson, Svensson et al. 2013, Svensson, Christianson et al. 2013, Andreu and Yáñez-Mó 2014, Costa Verdera, Gitz-Francois et al. 2017, Gonda, Kabagwira et al. 2019, Cardeñes, Clares et al. 2021) These studies used approaches that broadly categorized the mechanisms of OS exosome uptake by target cells using compounds that selectively inhibited different endocytic pathways However, there remains a considerable knowledge gap in our understanding of specific molecular profiles that influence the trafficking of exosomes to specific organs as well as the docking and subsequent uptake of exosomes by target cells. Evidence from a seminal study used proteomic analysis to show exosomes can be trafficked to specific organs based on the repertoire of exosomal and target cell integrin receptors, however, follow up studies evaluating the role of integrins in exosome trafficking and uptake were not conducted. (Hoshino, Costa-Silva et al. 2015) More recently, studies characterizing all exosomal surface proteins and their post-translational modifications, identified specific phenotypes of the exosome donor cell types were associated with differences in exosome uptake by target cells due to specific differences between surface protein repertoires, and surfaceome profiling of exosomes paired with ligand-receptor analysis uncovered an interactome across 172 experimentally verified cognate binding partners whose enrichment was highest among cells of a specific organ. (Wu, Yan et al. 2019) (Meng, Chen et al. 2023) (Rai, Fang et al. 2021) Taking these studies into consideration, one could consider using these approaches to profile the surfaceome of exosomes derived from functionally or transcriptionally distinct commercial or PDX OS cell lines, and their uptake efficiency by various target cells, to determine the most significant ligand/receptor pairs associated with their uptake by target cell. This strategy may inform potential avenues for disrupting cancer specific exosome uptake mechanisms, thus inhibiting the functional response of target cells to exosome treatments. Additionally, surface profiling of exosomes allowed for pancreatic cancer exosome isolation in liquid biopsies, providing further rationale for characterizing the OS exosome surface protein repertoire as a potential prognostic indicator. (Castillo, Bernard et al. 2018)

RNA-seq and downstream analysis of exosome educated fibroblasts revealed pathway enrichment of gene sets associated with hallmark CAF phenotypes. Although changes in gene expression

observed in response to stimuli can provide valuable insights into important biological activity, it is difficult to assess the functional characteristics based on transcriptional changes alone. This is largely due to the numerous processes that regulate the activation state and abundance of proteins after translation. i.e. post-translational modifications, degradation, etc. (Vogel and Marcotte 2012) Furthermore, bead-based phospho-protein assays identified fibroblasts activate the Erk1/2/MAPKA signal transduction pathway in response to OS exosome treatments. However, the scope of this assay was narrow. To further characterize the activity of OS exosome induced signal transduction pathways in lung fibroblasts, follow up studies could employ the use of reverse phase protein arrays (RPPA) to identify changes in protein abundance and their activation states. This assay is complimentary of RNA-seq analysis and provides several advantages over bead-based or immunoblot protein profiling approaches. For instance, RPPA can detect low abundance regulatory proteins that can be difficult to measure using mass-spectrometry, can measure post-translational modifications, such as phosphorylation, measures nearly ~1000 proteins, and has been successfully employed as a discovery tool used to identify novel protein-signaling pathways and signatures in other cancer types. (Coarfa, Grimm et al. 2021, Signore and Manganelli 2022, Chen, Wang et al. 2024) Identifying the signal transduction pathways influenced by exosomes in target cells could provide valuable insights that could be exploited to develop novel anti-metastatic therapies targeting non-cancerous stromal cells in the TME or PMN.

In chapters 3 and 4, we sought to expand on observations that OS-derived exosomes induced CAF-like, tumor promoting phenotypes in donor-derived lung fibroblasts *in vitro* by developing a mouse model that could quantify the effects of exosome educations on the earliest phases of metastatic colonization in the lung, alterations to concentrations of key cytokines/chemokines, and changes to resident mouse lung cell population dynamics. Using *in vivo* bioluminescent imaging, we determined repeated intravenous treatments with OS exosomes significantly enhanced lung metastatic colonization efficiency of human 143b cells in an immunocompromised xenograft mouse model but cannot definitively conclude the same effect was observed in the syngeneic, K7M2 immunocompetent model. These findings were also not associated with significant changes to mouse resident lung cell populations or among the cytokines/chemokines we probed.

Although we observed enhanced metastatic colonization among exosome treated mice in a xenograft mouse model, it is difficult to ascertain specifically what about OS exosomes induced this response, as we did not observe correlative changes to cytokine/chemokine signaling or alterations to the mouse resident lung populations we probed. Studies run in parallel by my colleague have been used to characterize the biodistribution of OS exosomes within the resident lung cells of exosome treated mice with the goal of identifying the cells primarily taking them up. It should be noted, however, that a lack of changes among resident lung cell populations we observed may not necessarily indicate a lack of transcriptional or functional alterations that could influence metastatic colonization. Likewise, increased uptake by phagocytic cell types, such as dendritic cells and macrophages, may not induce the stimulatory response that could contribute to PMN formation. Therefore, follow up studies could employ several RNA sequencing approaches to probe for transcriptional changes to these cell populations in response to OS exosomes. First, bulk RNA sequencing of whole lung digested lysates could be used as a discovery-based approach, however, this method takes all cells within the lung into consideration and subtle changes occurring within individual populations may be masked or difficult to deconvolute. Another approach, though expensive, may be to use single-cell RNA sequencing (scRNA-seq) to identify transcriptional changes occurring within discrete cell populations of the lung. Pairing this approach with treatments of exosome derived from commercial or PDX OS cell lines with distinct genetic alterations, metastatic potential, or patient outcomes may provide valuable insights into the functional properties of a given donor cell type's exosomes, which resident lung cells are most influenced transcriptionally, and which transcriptional differences observed may be correlated to the intrinsic properties of the donor cell type.

Bioluminescent intravital imaging has been used as a non-invasive method to monitor *in vivo* tumor development and metastasis in OS for nearly 20 years. (Luu, Kang et al. 2005, Miretti, Roato et al. 2008) However, because we were seeking to evaluate the influence of OS exosomes on the earliest phases of lung colonization, we sought to pair IVIS imaging with a second, highly sensitive detection method using spectral flow cytometry. Using flow cytometry to detect OS cells in mouse lung, single cell digests presented challenges. For instance, several studies profiling the cell surface of OS cell lines and patient samples have been conducted to find OS specific cell surface markers; however, no single marker

has been found to be expressed across all samples that isn't also widely expressed among other host cell types, making these makers less useful for detecting OS cells *in vivo* using flow cytometry. (Batth, Meng et al. 2020, Wang, Tian et al. 2022) To sidestep this, we attempted to stain OS cells with fluorescent cell labeling dyes prior to tail vein injection into mice. This was largely a cautionary tale, as we discovered these dyes would likely not be useful for this application after it was determined the fluorescent signature associated with these labeling dyes were not restricted to the tumor compartment.

Ultimately, we were able to overcome these challenges to successfully develop a high-throughput, highly sensitive assay capable of detecting and quantifying 143b OS cells in mouse lungs within 24 hours of tumor cell tail vein injection. This model substantially improves upon previously described high-throughput *in vivo* models of metastatic colonization, which paired intravital imaging with semi-quantitative H&E staining of sectioned slides and required 10 days of metastatic growth post-tumor cell injection. (Speak, Swiatkowska et al. 2017) Furthermore, the approaches we developed could be rapidly deployed with minimal manpower and equipment requirements and could be broadly applied to study the rate-limiting step of metastatic colonization across other cancer types.

Future applications may take advantage of the high-throughput nature of this model to more rapidly screen tumor-cell-intrinsic factors for their role in promoting metastatic colonization *in vivo*. For instance, screening approaches using a library of guide RNAs cloned into lentiviral vectors could be used in conjunction with a CRISPR/Cas9 system to ablate genes in cancer cell lines and identify genes that most likely contribute to promoting metastasis. Studies using a discovery-based approach applied genome-wide CRSIPR/Caas9 screens that subsequently identified PHGDH as a driver of Sorafenib resistance in hepatocellular carcinoma and targeted CRISPR knockout of MT1-MMP in OS cell lines provided evidence for the gene's importance for promoting in metastasis in a xenograft mouse model. (Shalem, Sanjana et al. 2014, Wei, Lee et al. 2019, Ingvarsen, Gårdsvoll et al. 2020) Additionally, any genes identified for their contribution to lung colonization could be compared to a therapeutic targets database to develop and screen potential targeted, anti-metastatic therapies. (Kampmann 2017)

Another application of this model may be to evaluate the influence of the host specific cellular and molecular mediators contributing to metastatic colonization. Recently, *in vivo* studies employing a seemingly limitless number of genetically modified mouse models (GEMMs), engineered to lack specific

genes may be of interest in this context. Additionally, using a CRE-inducible diphtheria toxin receptor expressed on specific cell types allows for their ablation upon exposure to diphtheria toxin. This approach has been in use for 20 years and could provide concrete proof of host cell mediated promotion of metastatic colonization. (Buch, Heppner et al. 2005)

References

Alspach, E., K. C. Flanagan, X. Luo, M. K. Ruhland, H. Huang, E. Pazolli, M. J. Donlin, T. Marsh, D. Piwnica-Worms, J. Monahan, D. V. Novack, S. S. McAllister and S. A. Stewart (2014). "p38MAPK plays a crucial role in stromal-mediated tumorigenesis." Cancer Discov **4**(6): 716-729.

Andreu, Z. and M. Yáñez-Mó (2014). "Tetraspanins in extracellular vesicle formation and function." Front Immunol **5**: 442.

Asif, P. J., C. Longobardi, M. Hahne and J. P. Medema (2021). "The Role of Cancer-Associated Fibroblasts in Cancer Invasion and Metastasis." Cancers (Basel) **13**(18).

Batth, I. S., Q. Meng, Q. Wang, K. E. Torres, J. Burks, J. Wang, R. Gorlick and S. Li (2020). "Rare osteosarcoma cell subpopulation protein array and profiling using imaging mass cytometry and bioinformatics analysis." BMC Cancer **20**(1): 715.

Buch, T., F. L. Heppner, C. Tertilt, T. J. Heinen, M. Kremer, F. T. Wunderlich, S. Jung and A. Waisman (2005). "A Cre-inducible diphtheria toxin receptor mediates cell lineage ablation after toxin administration." Nat Methods **2**(6): 419-426.

Bussard, K. M., L. Mutkus, K. Stumpf, C. Gomez-Manzano and F. C. Marini (2016). "Tumor-associated stromal cells as key contributors to the tumor microenvironment." Breast Cancer Res **18**(1): 84.

Cardeñes, B., I. Clares, V. Toribio, L. Pascual, S. López-Martín, A. Torres-Gomez, R. Sainz de la Cuesta, E. M. Lafuente, M. López-Cabrera, M. Yáñez-Mó and C. Cabañas (2021). "Cellular Integrin α5β1 and Exosomal ADAM17 Mediate the Binding and Uptake of Exosomes Produced by Colorectal Carcinoma Cells." Int J Mol Sci **22**(18): integrin.

Castillo, J., V. Bernard, F. A. San Lucas, K. Allenson, M. Capello, D. U. Kim, P. Gascoyne, F. C. Mulu, B. M. Stephens, J. Huang, H. Wang, A. A. Momin, R. O. Jacamo, M. Katz, R. Wolff, M. Javle, G. Varadhachary, Wistuba, II, S. Hanash, A. Maitra and H. Alvarez (2018). "Surfaceome profiling enables isolation of cancer-specific exosomal cargo in liquid biopsies from pancreatic cancer patients." Ann Oncol **29**(1): 223-229.

Chen, Q., W. Sun, Y. Liao, H. Zeng, L. Shan, F. Yin, Z. Wang, Z. Zhou, Y. Hua and Z. Cai (2015). "Monocyte chemotactic protein-1 promotes the proliferation and invasion of osteosarcoma cells and upregulates the expression of AKT." Mol Med Rep **12**(1): 219-225.

Chen, S. F., L. Y. Wang, Y. S. Lin and C. Y. Chen (2024). "Novel protein-based prognostic signature linked to immunotherapeutic efficiency in ovarian cancer." J Ovarian Res **17**(1): 190.

Christianson, H. C., K. J. Svensson, T. H. van Kuppevelt, J. P. Li and M. Belting (2013). "Cancer cell exosomes depend on cell-surface heparan sulfate proteoglycans for their internalization and functional activity." Proc Natl Acad Sci U S A **110**(43): 17380-17385.

Coarfa, C., S. L. Grimm, K. Rajapakshe, D. Perera, H. Y. Lu, X. Wang, K. R. Christensen, Q. Mo, D. P. Edwards and S. Huang (2021). "Reverse-Phase Protein Array: Technology, Application, Data Processing, and Integration." J Biomol Tech **32**(1): 15-29.

Costa Verdera, H., J. J. Gitz-Francois, R. M. Schiffelers and P. Vader (2017). "Cellular uptake of extracellular vesicles is mediated by clathrin-independent endocytosis and macropinocytosis." J Control Release **266**: 100-108.

Costa-Silva, B., N. M. Aiello, A. J. Ocean, S. Singh, H. Zhang, B. K. Thakur, A. Becker, A. Hoshino, M. T. Mark, H. Molina, J. Xiang, T. Zhang, T. M. Theilen, G. García-Santos, C. Williams, Y. Ararso, Y. Huang, G. Rodrigues, T. L. Shen, K. J. Labori, I. M. Lothe, E. H. Kure, J. Hernandez, A. Doussot, S. H. Ebbesen, P. M. Grandgenett, M. A. Hollingsworth, M. Jain, K. Mallya, S. K. Batra, W. R. Jarnagin, R. E. Schwartz, I.

Matei, H. Peinado, B. Z. Stanger, J. Bromberg and D. Lyden (2015). "Pancreatic cancer exosomes initiate pre-metastatic niche formation in the liver." Nat Cell Biol **17**(6): 816-826.

Feng, D., W. L. Zhao, Y. Y. Ye, X. C. Bai, R. Q. Liu, L. F. Chang, Q. Zhou and S. F. Sui (2010). "Cellular internalization of exosomes occurs through phagocytosis." Traffic **11**(5): 675-687.

Fossey, S. L., A. T. Liao, J. K. McCleese, M. D. Bear, J. Lin, P. K. Li, W. C. Kisseberth and C. A. London (2009). "Characterization of STAT3 activation and expression in canine and human osteosarcoma." BMC Cancer **9**: 81.

Gok Yavuz, B., G. Gunaydin, M. E. Gedik, K. Kosemehmetoglu, D. Karakoc, F. Ozgur and D. Guc (2019). "Cancer associated fibroblasts sculpt tumour microenvironment by recruiting monocytes and inducing immunosuppressive PD-1(+) TAMs." Sci Rep **9**(1): 3172.

Gonda, A., J. Kabagwira, G. N. Senthil and N. R. Wall (2019). "Internalization of Exosomes through Receptor-Mediated Endocytosis." Mol Cancer Res **17**(2): 337-347.

Gong, Z., Q. Li, J. Shi, J. Wei, P. Li, C. H. Chang, L. D. Shultz and G. Ren (2022). "Lung fibroblasts facilitate pre-metastatic niche formation by remodeling the local immune microenvironment." Immunity **55**(8): 1483-1500.e1489.

Gross, A. C., H. Cam, D. A. Phelps, A. J. Saraf, H. K. Bid, M. Cam, C. A. London, S. A. Winget, M. A. Arnold, L. Brandolini, X. Mo, J. M. Hinckley, P. J. Houghton and R. D. Roberts (2018). "IL-6 and CXCL8 mediate osteosarcoma-lung interactions critical to metastasis." JCI Insight **3**(16).

Han, F., P. Pu, C. Wang, X. Ding, Z. Zhu, W. Xiang and W. Wang (2021). "Osteosarcoma Cell-Derived Exosomal miR-1307 Promotes Tumorgenesis via Targeting AGAP1." Biomed Res Int **2021**: 7358153.

Han, S., Z. Huo, K. Nguyen, F. Zhu, P. W. Underwood, K. B. G. Basso, T. J. George and S. J. Hughes (2019). "The Proteome of Pancreatic Cancer-Derived Exosomes Reveals Signatures Rich in Key Signaling Pathways." Proteomics **19**(13): e1800394.

Hayashi, R., N. Yamashita, S. Matsui, T. Fujita, J. Araya, K. Sassa, N. Arai, Y. Yoshida, T. Kashii, M. Maruyama, E. Sugiyama and M. Kobayashi (2000). "Bradykinin stimulates IL-6 and IL-8 production by human lung fibroblasts through ERK- and p38 MAPK-dependent mechanisms." Eur Respir J **16**(3): 452-458.

Hoshino, A., B. Costa-Silva, T. L. Shen, G. Rodrigues, A. Hashimoto, M. Tesic Mark, H. Molina, S. Kohsaka, A. Di Giannatale, S. Ceder, S. Singh, C. Williams, N. Soplop, K. Uryu, L. Pharmer, T. King, L. Bojmar, A. E. Davies, Y. Ararso, T. Zhang, H. Zhang, J. Hernandez, J. M. Weiss, V. D. Dumont-Cole, K. Kramer, L. H. Wexler, A. Narendran, G. K. Schwartz, J. H. Healey, P. Sandstrom, K. J. Labori, E. H. Kure, P. M. Grandgenett, M. A. Hollingsworth, M. de Sousa, S. Kaur, M. Jain, K. Mallya, S. K. Batra, W. R. Jarnagin, M. S. Brady, O. Fodstad, V. Muller, K. Pantel, A. J. Minn, M. J. Bissell, B. A. Garcia, Y. Kang, V. K. Rajasekhar, C. M. Ghajar, I. Matei, H. Peinado, J. Bromberg and D. Lyden (2015). "Tumour exosome integrins determine organotropic metastasis." Nature **527**(7578): integrins.

Ingvarsen, S. Z., H. Gårdsvoll, S. van Putten, K. S. Nørregaard, O. Krigslund, J. A. Meilstrup, C. Tran, H. J. Jürgensen, M. C. Melander, C. H. Nielsen, A. Kjaer, T. H. Bugge, L. H. Engelholm and N. Behrendt (2020). "Tumor cell MT1-MMP is dispensable for osteosarcoma tumor growth, bone degradation and lung metastasis." Sci Rep **10**(1): 19138.

Kampmann, M. (2017). "Elucidating drug targets and mechanisms of action by genetic screens in mammalian cells." Chem Commun (Camb) **53**(53): 7162-7167.

Karakasheva, T. A., E. W. Lin, Q. Tang, E. Qiao, T. J. Waldron, M. Soni, A. J. Klein-Szanto, V. Sahu, D. Basu, S. Ohashi, K. Baba, Z. T. Giaccone, S. R. Walker, D. A. Frank, E. P. Wileyto, Q. Long, M. C. Dunagin, A. Raj, J. A. Diehl, K. K. Wong, A. J. Bass and A. K. Rustgi (2018). "IL-6 Mediates Cross-Talk between Tumor Cells and Activated Fibroblasts in the Tumor Microenvironment." Cancer Res **78**(17): 4957-4970.

Lauvrak, S. U., E. Munthe, S. H. Kresse, E. W. Stratford, H. M. Namløs, L. A. Meza-Zepeda and O. Myklebost (2013). "Functional characterisation of osteosarcoma cell lines and identification of mRNAs and miRNAs associated with aggressive cancer phenotypes." Br J Cancer **109**(8): 2228-2236.

Li, Y., S. Lin, X. Xie, H. Zhu, T. Fan and S. Wang (2021). "Highly enriched exosomal lncRNA OIP5-AS1 regulates osteosarcoma tumor angiogenesis and autophagy through miR-153 and ATG5." Am J Transl Res **13**(5): 4211-4223.

Luu, H. H., Q. Kang, J. K. Park, W. Si, Q. Luo, W. Jiang, H. Yin, A. G. Montag, M. A. Simon, T. D. Peabody, R. C. Haydon, C. W. Rinker-Schaeffer and T. C. He (2005). "An orthotopic model of human osteosarcoma growth and spontaneous pulmonary metastasis." Clin Exp Metastasis **22**(4): 319-329.

Meng, Q., C. Chen, N. Yang, O. Gololobova, C. Shi, C. A. Dunn, M. Rossi, J. L. Martindale, N. Basisty, J. Ding, M. Delannoy, S. Basu, K. Mazan-Mamczarz, C. H. Shin, J. H. Yang, P. F. Johnson, K. W. Witwer, A. Biragyn, P. Sen, K. Abdelmohsen, S. De and M. Gorospe (2023). "Surfaceome analysis of extracellular vesicles from senescent cells uncovers uptake repressor DPP4." Proc Natl Acad Sci U S A **120**(43): e2219801120.

Miretti, S., I. Roato, R. Taulli, C. Ponzetto, M. Cilli, M. Olivero, M. F. Di Renzo, L. Godio, A. Albini, P. Buracco and R. Ferracini (2008). "A mouse model of pulmonary metastasis from spontaneous osteosarcoma monitored in vivo by Luciferase imaging." PLoS One **3**(3): e1828.

Peinado, H., M. Alečković, S. Lavotshkin, I. Matei, B. Costa-Silva, G. Moreno-Bueno, M. Hergueta-Redondo, C. Williams, G. García-Santos, C. Ghajar, A. Nitadori-Hoshino, C. Hoffman, K. Badal, B. A. Garcia, M. K. Callahan, J. Yuan, V. R. Martins, J. Skog, R. N. Kaplan, M. S. Brady, J. D. Wolchok, P. B. Chapman, Y. Kang, J. Bromberg and D. Lyden (2012). "Melanoma exosomes educate bone marrow progenitor cells toward a pro-metastatic phenotype through MET." Nat Med **18**(6): 883-891.

Rai, A., H. Fang, B. Claridge, R. J. Simpson and D. W. Greening (2021). "Proteomic dissection of large extracellular vesicle surfaceome unravels interactive surface platform." J Extracell Vesicles **10**(13): e12164.

Regan, D. P., J. W. Coy, K. K. Chahal, L. Chow, J. N. Kurihara, A. M. Guth, I. Kufareva and S. W. Dow (2019). "The Angiotensin Receptor Blocker Losartan Suppresses Growth of Pulmonary Metastases via AT1R-Independent Inhibition of CCR2 Signaling and Monocyte Recruitment." J Immunol **202**(10): 3087-3102.

Ren, L., A. Mendoza, J. Zhu, J. W. Briggs, C. Halsey, E. S. Hong, S. S. Burkett, J. Morrow, M. M. Lizardo, T. Osborne, S. Q. Li, H. H. Luu, P. Meltzer and C. Khanna (2015). "Characterization of the metastatic phenotype of a panel of established osteosarcoma cells." Oncotarget **6**(30): 29469-29481.

Schott, C., A. T. Shah and E. A. Sweet-Cordero (2020). Genomic Complexity of Osteosarcoma and Its Implication for Preclinical and Clinical Targeted Therapies. Advances in Experimental Medicine and Biology, Springer International Publishing**:** 1-19.

Schott, C. R., A. L. Koehne, L. C. Sayles, E. P. Young, C. Luck, K. Yu, A. G. Lee, M. R. Breese, S. G. Leung, H. Xu, A. T. Shah, H. Y. Liu, A. Spillinger, I. H. Behroozfard, K. D. Marini, P. T. Dinh, M. V. Pons Ventura, E. N. Vanderboon, F. K. Hazard, S. J. Cho, R. S. Avedian, D. G. Mohler, M. Zimel, R. Wustrack, C. Curtis, M. Sirota and E. A. Sweet-Cordero (2024). "Osteosarcoma PDX-Derived Cell Line Models for Preclinical Drug Evaluation Demonstrate Metastasis Inhibition by Dinaciclib through a Genome-Targeted Approach." Clin Cancer Res **30**(4): 849-864.

Sha, L., D. Ma and C. Chen (2020). "Exosome-mediated Hic-5 regulates proliferation and apoptosis of osteosarcoma via Wnt/β-catenin signal pathway." Aging (Albany NY) **12**(23): 23598-23608.

Shalem, O., N. E. Sanjana, E. Hartenian, X. Shi, D. A. Scott, T. Mikkelson, D. Heckl, B. L. Ebert, D. E. Root, J. G. Doench and F. Zhang (2014). "Genome-scale CRISPR-Cas9 knockout screening in human cells." Science **343**(6166): 84-87.

Signore, M. and V. Manganelli (2022). "Reverse Phase Protein Arrays in cancer stem cells." Methods Cell Biol **171**: 33-61.

Speak, A. O., A. Swiatkowska, N. A. Karp, M. J. Arends, D. J. Adams and L. van der Weyden (2017). "A high-throughput in vivo screening method in the mouse for identifying regulators of metastatic colonization." Nat Protoc **12**(12): 2465-2477.

Svensson, K. J., H. C. Christianson, A. Wittrup, E. Bourseau-Guilmain, E. Lindqvist, L. M. Svensson, M. Mörgelin and M. Belting (2013). "Exosome uptake depends on ERK1/2-heat shock protein 27 signaling and lipid Raft-mediated endocytosis negatively regulated by caveolin-1." J Biol Chem **288**(24): 17713-17724.

Tu, B., L. Du, Q. M. Fan, Z. Tang and T. T. Tang (2012). "STAT3 activation by IL-6 from mesenchymal stem cells promotes the proliferation and metastasis of osteosarcoma." Cancer Lett **325**(1): 80-88.

Vogel, C. and E. M. Marcotte (2012). "Insights into the regulation of protein abundance from proteomic and transcriptomic analyses." Nat Rev Genet **13**(4): 227-232.

Wang, Y., X. Tian, W. Zhang, Z. Zhang, R. Lazcano, P. Hingorani, M. E. Roth, J. D. Gill, D. J. Harrison, Z. Xu, S. Jusu, S. Kannan, J. Wang, A. J. Lazar, E. J. Earley, S. W. Erickson, T. Gelb, P. Huxley, J. Lahdenranta, G. Mudd, R. T. Kurmasheva, P. J. Houghton, M. A. Smith, E. A. Kolb and R. Gorlick (2022). "Comprehensive Surfaceome Profiling to Identify and Validate Novel Cell-Surface Targets in Osteosarcoma." Mol Cancer Ther **21**(6): 903-913.

Wang, Y. C., L. H. Zheng, B. A. Ma, Y. Zhou, M. H. Zhang, D. Z. Zhang and Q. Y. Fan (2011). "Clinical value of signal transducers and activators of transcription 3 (STAT3) gene expression in human osteosarcoma." Acta Histochem **113**(4): 402-408.

Wei, L., D. Lee, C. T. Law, M. S. Zhang, J. Shen, D. W. Chin, A. Zhang, F. H. Tsang, C. L. Wong, I. O. Ng, C. C. Wong and C. M. Wong (2019). "Genome-wide CRISPR/Cas9 library screening identified PHGDH as a critical driver for Sorafenib resistance in HCC." Nat Commun **10**(1): 4681.

Wu, D., J. Yan, X. Shen, Y. Sun, M. Thulin, Y. Cai, L. Wik, Q. Shen, J. Oelrich, X. Qian, K. L. Dubois, K. G. Ronquist, M. Nilsson, U. Landegren and M. Kamali-Moghaddam (2019). "Profiling surface proteins on individual exosomes using a proximity barcoding assay." Nat Commun **10**(1): 3854.

Xu, K., A. Fu, Z. Li, L. Miao, Z. Lou, K. Jiang, C. Lau, T. Su, T. Tong, J. Bao, A. Lyu and H. Y. Kwan (2024). "Elevated extracellular matrix protein 1 in circulating extracellular vesicles supports breast cancer progression under obesity conditions." Nat Commun **15**(1): 1685.

Zhong, L., D. Liao, J. Li, W. Liu, J. Wang, C. Zeng, X. Wang, Z. Cao, R. Zhang, M. Li, K. Jiang, Y. X. Zeng, J. Sui and T. Kang (2021). "Rab22a-NeoF1 fusion protein promotes osteosarcoma lung metastasis through its secretion into exosomes." Signal Transduct Target Ther **6**(1): 59.

Zhou, B., K. Xu, X. Zheng, T. Chen, J. Wang, Y. Song, Y. Shao and S. Zheng (2020). "Application of exosomes as liquid biopsy in clinical diagnosis." Signal Transduct Target Ther **5**(1): 144.

Zhu, S., C. Xing, R. Li, Z. Cheng, M. Deng, Y. Luo, H. Li, G. Zhang, Y. Sheng, H. Peng and Z. Wang (2022). "Proteomic profiling of plasma exosomes from patients with B-cell acute lymphoblastic leukemia." Sci Rep **12**(1): 11975.

APPENDIX

Pilot studies investigating K7M2 exosome treatments in an immune competent, syngeneic model were used to develop some methods and protocols used to evaluate the effects of exosome education treatments from human 143b OS cells on metastatic colonization in an immunocompromised xenograft model. These pilot studies initially evaluated the application of a dual reporter, RFP-luciferase expression system paired with flow cytometry to detect cells using IVIS imaging and flow cytometry. IVIS images show a detectable luminescent signal above background in 4/6 mice in vivo, and 6/6 mice ex vivo. (Appendix Fig. 1A, B) Despite this, RFP cells were difficult to detect as a discrete population of cells in the lung digest single cell suspensions (Appendix Fig. 1C) Furthermore, these two methods were not correlative (Appendix Fig. 1D).

Following, this model was used to evaluate DIR fluorescent labeling of K7M2-Luc cells. Due to the observation that 2/6 mice had undetectable luminescent signal, we began implementing IVIS imaging 10 min. post-tumor cell injection to confirm successful injection efficiency. IVIS images show luminescence 10 min. post injection in 7/8 mice (Appendix Fig. 1E). However, IVIS imaging 4-days post tumor cell injection reveal none of the mice have a signal substantially above background 4-days post injection in vivo, and only 4/8 mice have a detectable signal above background ex vivo (Appendix Fig. 1F). Ex vivo IVIS imaging used to detect fluorescence reveals all mice have a high level of signal associated with the fluorescent signature of DIR labeling dye (Appendix Fix. 1G). Analysis revealed these two measurement modalities were not correlated, indicating potential complications may exist with the use of this model (Appendix Fig. 1H). Flow cytometry analysis of the mouse lung single cell digests identified a substantial number of DIR positive cells in all the mice (Appendix Fig. 1I). However, this data was also not correlated to the ex vivo bioluminescent IVIS data (Appendix Fig. 1J). At this time, we suspected dye was being transferred to resident lung cell populations, and as a result, causing these two detection methods to have substantial differences between them. By employing a 6-marker antibody panel, we were able to exclude mouse resident lung cell populations that were also DIR positive as is depicted in the gating strategy we used to make this conclusion (Appendix Fig. 1K). Following the exclusion of DIR positive mouse resident lung cells, the correlation between the ex vivo bioluminescent signal and DIR+ cells (Appendix Fig. 1L).

A

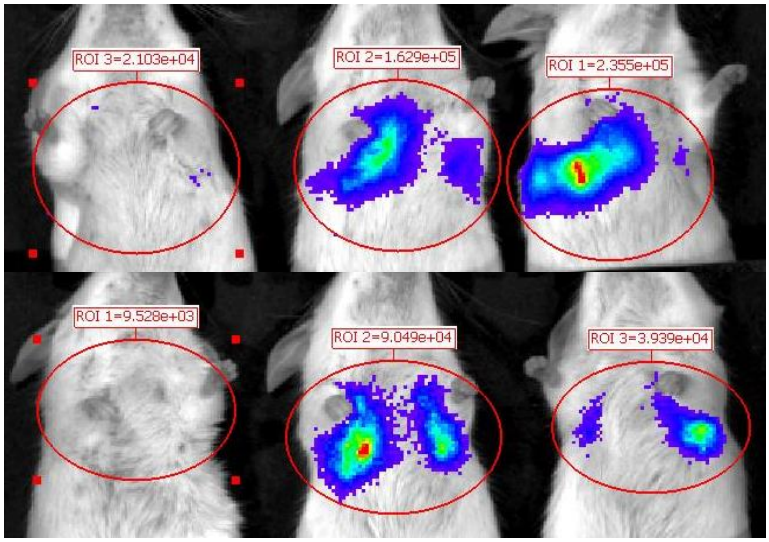

B

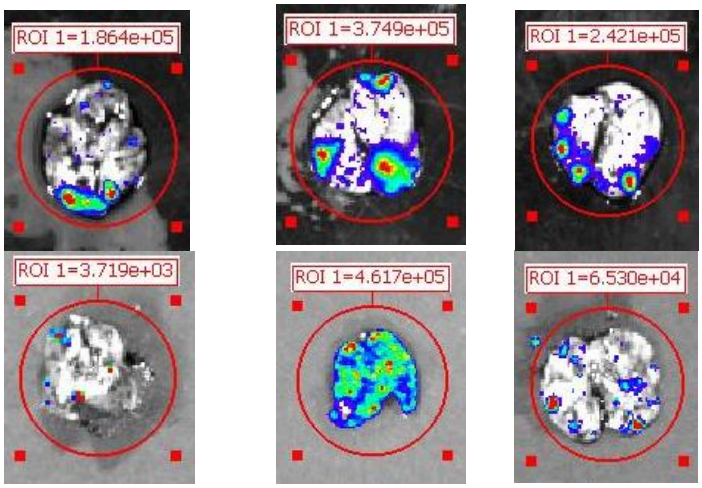

Appendix Fig. 1 A) In vivo IVIS images of K7M2-Luc injected mice 4-days post tumor cell injection. **B)** Ex vivo images of the same mice

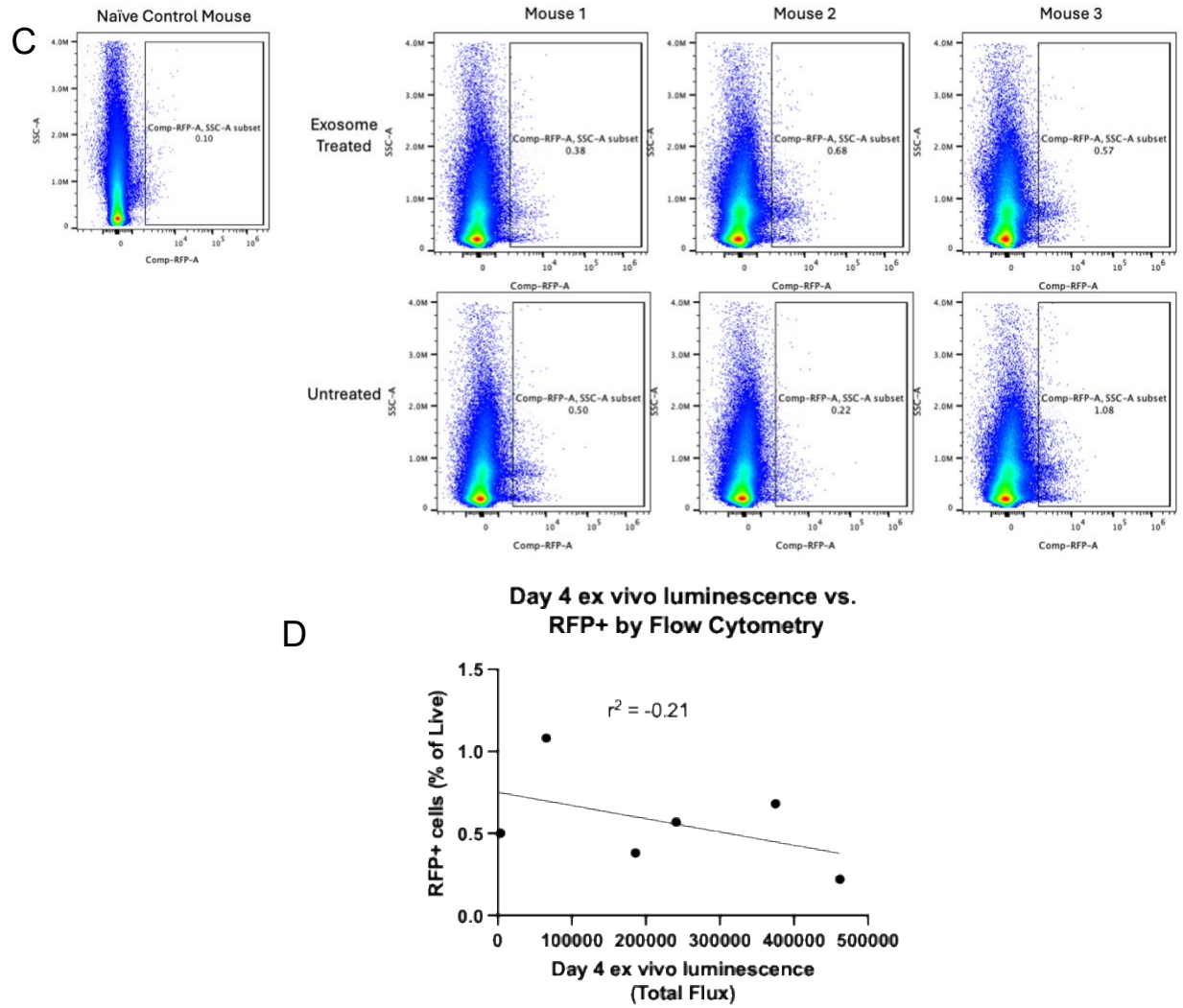

Appendix Fig. 1 C) Flow plots gating on RFP+ cells in K7M2-RFP injected mice. **D)** XY plot comparing RFP+ cells measured by flow cytometry and ex vivo luminescence as measured by Total Flux

E

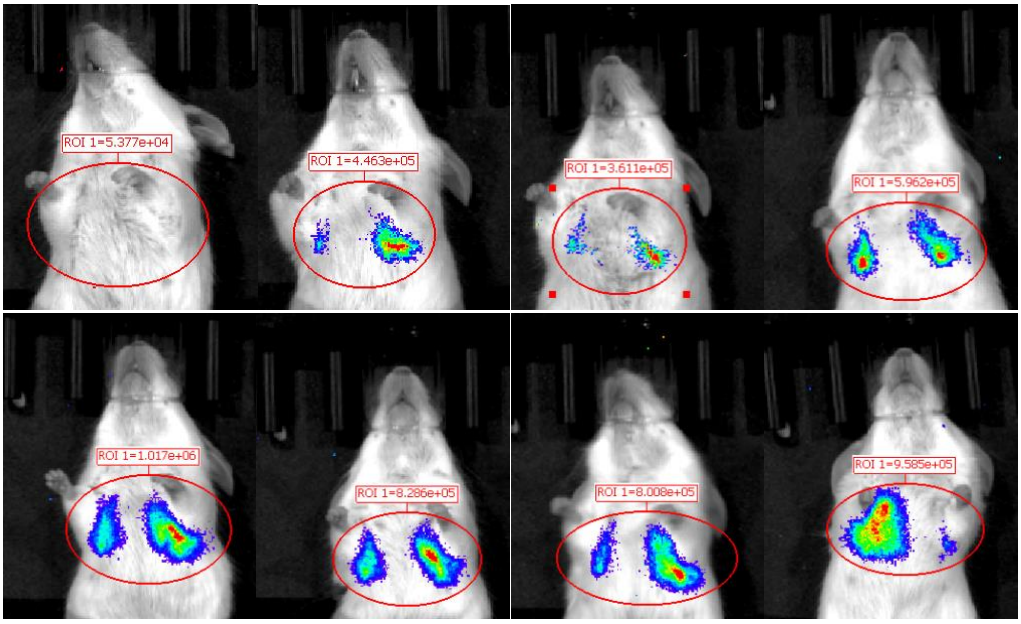

F

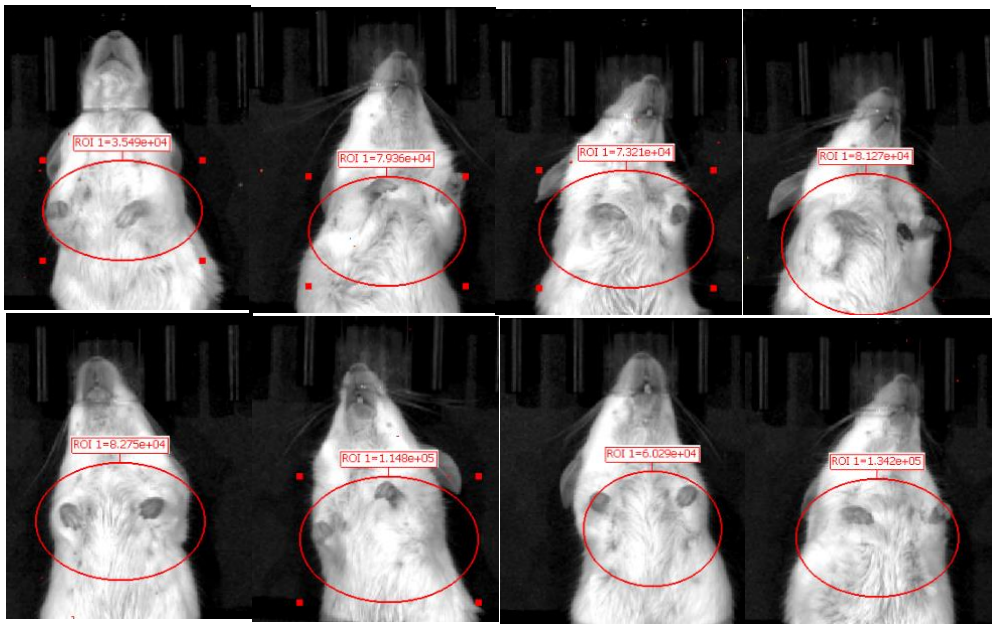

Appendix Fig. 1 E) In vivo IVIS images taken 10 min. post-K7M2-luc injection and **F)** 4-days post injection.

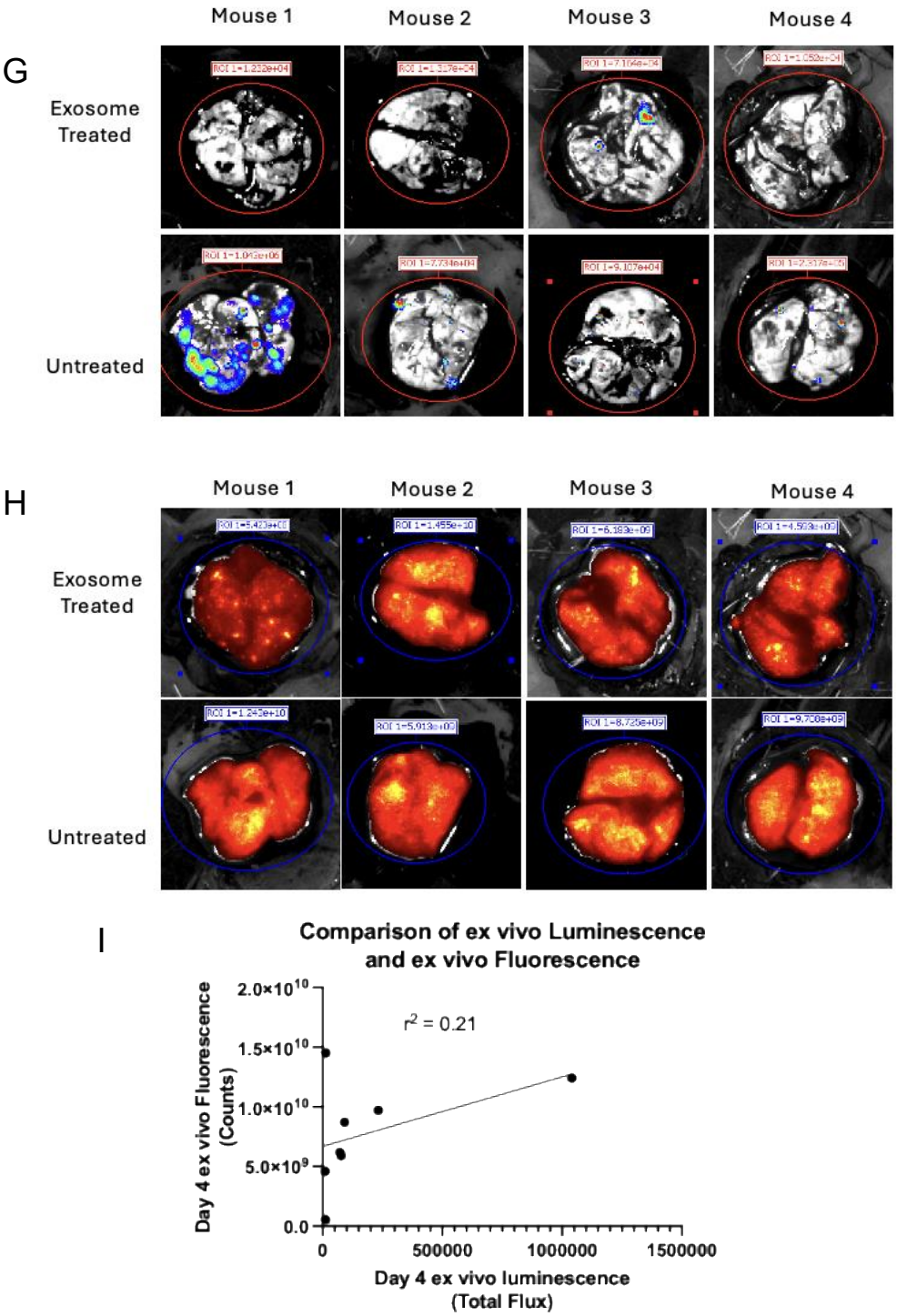

Appendix Fig. 1 G) ex vivo images of mouse lungs 4-days post K7M2-Luc injection measuring bioluminescence and **H)** DIR fluorescence **I)** XY plot comparing ex vivo fluorescence to ex vivo bioluminescence

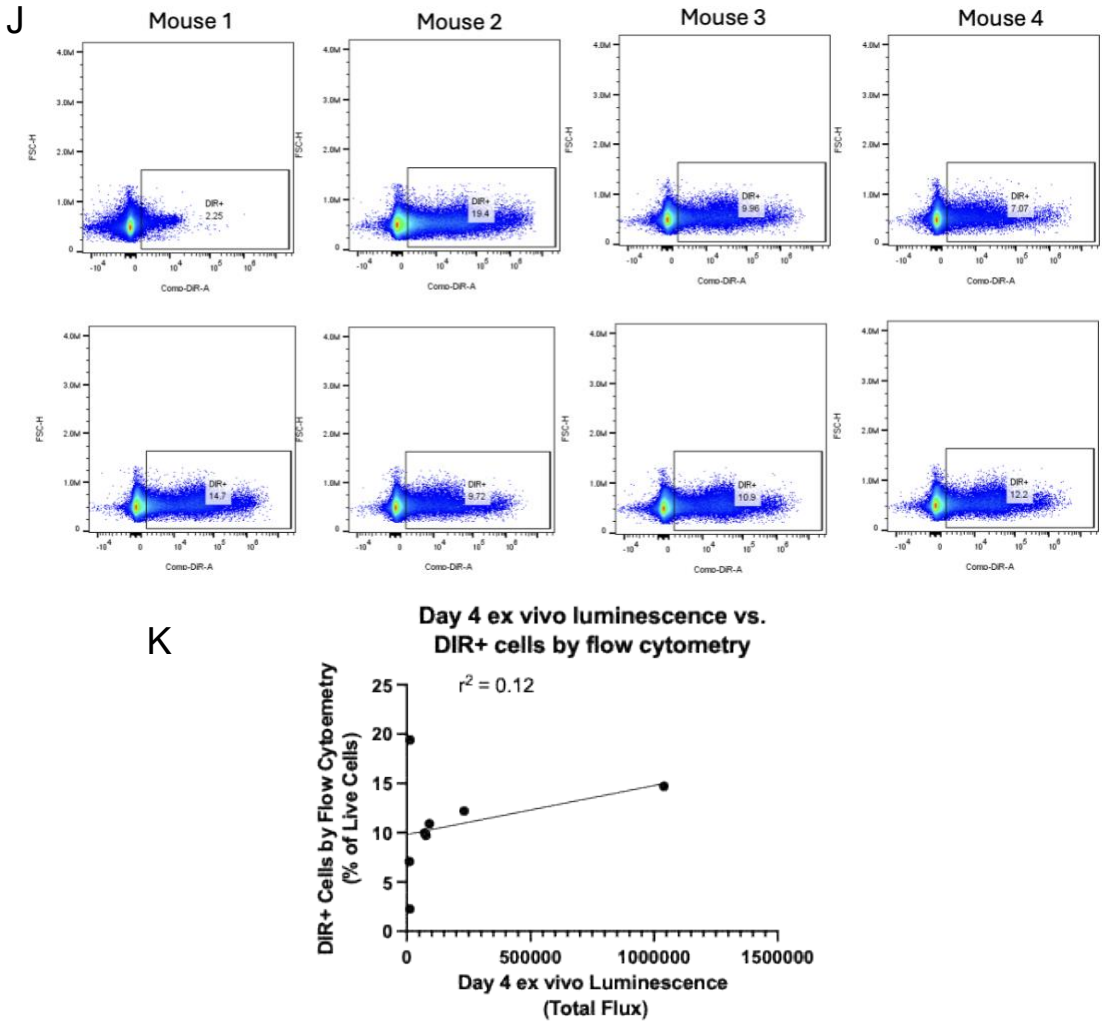

Appendix Fig. 1 J) Flow plots gating on DIR+ cells in K7M2-Luc injected mouse lungs **K)** XY plot comparing DIR+ cells as % of live cells measured using flow cytometry to Day-4 ex vivo bioluminescence as Total Flux

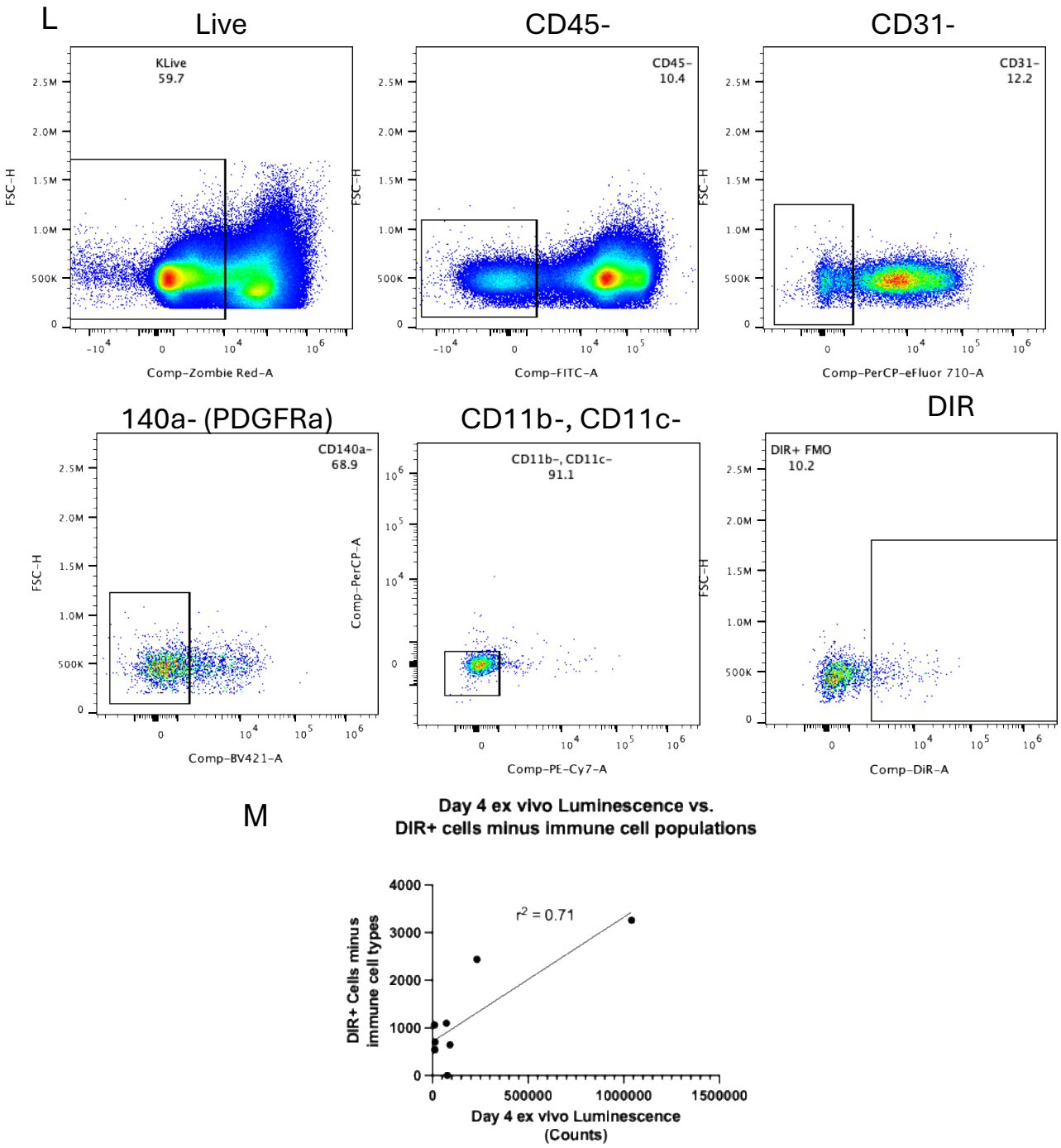

Appendix Fig. L) Progressive gating strategy used to exclude DIR+ resident lung cell populations **M)** XY plot comparing DIR+ cell left after exclusion of mouse lung cell populations to Day-4 ex vivo luminescence